Using real-time observations and land surface modelling for improved irrigation and water resources management in Mediterranean climate

Dissertation

zur

Erlangung des Doktorgrades (Dr. rer. nat.)

der

Mathematisch-Naturwissenschaftlichen Fakultät

der

Rheinischen Friedrich-Wilhelms-Universität Bonn

vorgelegt von

Olga Dombrowski

aus

Berlin

Bonn, November 2023

Angefertigt mit Genehmigung der Mathematisch-Naturwissenschaftlichen Fakultät

der Rheinischen Friedrich-Wilhelms-Universität Bonn

Erstgutachter: PD Dr. Heye Bogena

Zweitgutachter: Prof. Dr. Julian Klaus

Tag der Promotion: 28.03.2024

Erscheinungsjahr: 2024

Abstract

Irrigated agriculture is essential to sustain crop production and livelihoods of the rural population in semi-arid and arid regions such as the Mediterranean. Meanwhile, unsustainable irrigation practices, population growth, and climate change are increasing agricultural water demand while exacerbating water scarcity. Effective measures to reduce agricultural water consumption while sustaining a high level of crop production and securing environmental sustainability are therefore urgently needed.

This thesis aims at increasing the availability of environmental data and advancing the representation of agricultural systems in land surface models to improve local and regional scale irrigation and water resources management in the Mediterranean.

In the first part, the use of a low-cost weather station to deliver reliable and timely data for environmental monitoring, research, and modelling is assessed. Performance and data quality of multiple stations are examined in terms of inter-sensor variability and in comparison to a high-performance weather station.

The second part of this thesis focusses on improving the representation of typical Mediterranean crops in the Community Land Model version 5. A new sub-model to model deciduous fruit orchards is developed encompassing crop phenological stages, biomass growth and partitioning into different plant organs as well as typical management practices. The development is then tested using extensive field measurements from an apple orchard.

Finally, the new sub-model is used to assess irrigation and water management in a small Greek catchment dominated by irrigated apple orchards. First, simulated crop growth and soil moisture dynamics are examined in relation to irrigation and compared to observations from two monitored apple orchards. Thereby, further model improvements are made to represent the local irrigation practices. Subsequently, the model is applied at regional scale to determine irrigation requirements and examine the impact of different irrigation deficit scenarios on yield and crop water use efficiency as well as to assess the water saving potential in the catchment.

Zusammenfassung

Bewässerung sichert die landwirtschaftliche Produktion sowie die Lebensgrundlage der ländlichen Bevölkerung in semiariden und ariden Regionen wie dem Mittelmeerraum. Gleichzeitig erhöhen nicht nachhaltige Bewässerungspraktiken, Bevölkerungswachstum und der Klimawandel den landwirtschaftlichen Wasserbedarf und verschärfen die Wasserknappheit. Wirkungsvolle Maßnahmen zur Reduzierung des landwirtschaftlichen Wasserverbrauchs bei gleichzeitiger Erhaltung der Ernten und Gewährleistung ökologischer Nachhaltigkeit sind daher dringend erforderlich.

Die vorliegende Dissertation hat zum Ziel, die Verfügbarkeit von Umweltdaten zu erhöhen und die Darstellung landwirtschaftlicher Systeme in Landoberflächenmodellen weiterzuentwickeln, um Bewässerung und Wasserressourcenmanagement im Mittelmeerraum auf lokaler und regionaler Skala zu verbessern.

Im ersten Teil wird die Verwendung einer kosteneffektiven Wetterstation zur Bereitstellung zuverlässiger und aktueller Daten für Umweltmessungen, Forschung und Modellierung untersucht. Die Eignung und Datenqualität mehrerer Stationen werden hinsichtlich der Variabilität zwischen einzelnen Sensoren sowie im Vergleich zu einer hochwertigen Wetterstation bewertet.

Der zweite Teil dieser Dissertation befasst sich mit der Verbesserung der Darstellung typischer mediterraner Nutzpflanzen im Community Land Model Version 5. Ein neues Submodell zur Modellierung von sommergrünen Obstplantagen wird entwickelt, welches die phänologischen Entwicklungsphasen, das Wachstum und die Aufteilung der Biomasse auf verschiedene Pflanzenorgane sowie typische Bewirtschaftungspraktiken umfasst. Die Modellentwicklung wird anschließend anhand umfangreicher Feld-messungen von einer Apfelplantage getestet.

Schließlich wird das neue Submodell dazu verwendet, die Bewässerung und das Wasserressourcenmanagement in einem kleinen griechischen Einzugsgebiet zu untersuchen, in dem vorherrschend bewässerte Apfelplantagen gepflanzt sind. Dafür werden zuerst die Simulierung des Pflanzenwachstums und der Bodenfeuchtedynamik in

Bezug auf die Bewässerung untersucht und mit Messungen aus zwei Apfelplantagen verglichen. In dem Zusammenhang werden weitere Modellverbesserungen zur Darstellung lokaler Bewässerungspraktiken vorgenommen. Anschließend wird das Modell auf regionaler Skala angewendet, um den Bewässerungsbedarf zu bestimmen und die Auswirkungen unterschiedlicher Szenarien der Defizitbewässerung auf Ertrag und Wassernutzungseffizienz zu untersuchen sowie das Potenzial zur Wassereinsparung im Einzugsgebiet zu bewerten.

Acknowledgements

First of all, I want to thank my supervisors at Forschungszentrum Jülich Heye Bogena and Harrie-Jan Hendricks Franssen for their time, guidance, and fruitful discussions over the past years. I am grateful for the opportunities this has given me and for the scientific knowledge I have gained during my time at IBG-3. A big thanks also goes to Cosimo Brogi for his continuous support and readiness to share his experience, exchange thoughts, and provide helpful feedback throughout my time as a PhD student.

I also want to thank our project partners in Greece Andreas Panagopoulos, Vassilis Pisinaras, Anna Chatzi, Konstantinos Babakos, and Ioannis Tsakmakis. It has been a great pleasure working with them, in the field under the sizzling Greek sun or remotely. Thank you also to Stamatis and Nikos for working with us. Another thanks goes to Bernd Schilling and Ansgar Weuthen for their technical support and for teaching me to install SoilNet devices in the snow and mud as well as to Burkhard Neuwirth for sharing his knowledge about sapflow sensors.

Next, I would like to thank my fellow PhD students for helping each other out, for the useful exchange during group meetings, and relaxing lunch and coffee breaks. Thank you also to the administrative and other non-scientific staff at IBG-3. A special thanks to Chris for being a great teammate as PhD representatives and to Marie Ludwig for her work and motivation as scientific coordinator and for her constant support to the PhD students. Thanks also to Marius for many enjoyable car sharing rides.

Another thanks goes to Damiano Zanotelli from Bolzano University for a fruitful collaboration as well as to Sean Swenson and other folks at NCAR for their help, inspiring scientific exchange, and the wonderful time in Boulder.

Apart from everyone who has been part of my work life over the last years, I'm incredibly grateful for all the wonderful people in my life outside the PhD. A huge hug to Mia, Tschou, Caro, Lilith and the rest of the aerial silks crew for countless hours of training, having fun together, and taking my mind off of work when I needed it. Hugs to my lovely flatmates Anna, Alena, and Julian for sharing our lives, meals, laughs, kitchen hangouts,

and many joyful as well as difficult times. A big hug to Suse, Greta, Agata, Clara, Lotte, Inga, Caro, Vic, Leo, Max, Rhoda, Job, Albert, Sofi, Marina, and all the other old and new friends in Cologne and around the world for being in my life, doing remote co-working sessions together and staying connected. Thank you Antony for being the crazy human you are and for having been with me during part of this journey.

Hugs and kisses to Anna for being the best conversational partner, accepting me more than I accept myself, exploring our connection together, and for being just a wonderful person. I'm so happy to have you in my life.

Thank you to my parents, Eva and Tilman, for all your love, trust, support, open mindedness, and interest in anything I do. Thank you to my awesome sister Annah and to Jay for introducing me to EA and many mind-opening experiences. Thanks Sis for being such great company for festivals, travels, sports, and other adventures. You guys are the best family ever!

Finally, thank you Lorenz for becoming such an important part of my life in the final phase of my PhD. I love you for your endless enthusiasm and energy, your warmth, the best hugs in the world, for pushing me and supporting me, for not following the norm, and introducing me to a new world of music. Thank you for being a wonderful partner and for bringing a lot of glitter into my life. I'm excited to start a new chapter together ·–

Contents

List of Figures

List of Tables

List of Abbreviations

%bias	Percent bias
μ	Arithmetic mean
BDT	Broadleaf deciduous tree
BGC-crop	Biogeochemistry crop module
Biome-BGC	Biome BioGeochemical Cycles
C	Carbon
C1	Official ICOS climate station Selhausen
CLM	Community Land Model
CM	Crop model
CS	Climate station
CWUE	Crop water use efficiency
DI	Deficit irrigation
DSSAT	Decision Support System for Agrotechnology Transfer
EC	Eddy covariance
ESDB	European Soil Database
ET	Evapotranspiration
EU-DEM	European Digital Elevation Model
FI	Full irrigation
f_{max}	Maximum fractional saturated area
f_{thresh}	Tuning parameter in the CLM5 irrigation routine
G	Soil heat flux
GDD	Growing degree days
GDP	Gross domestic product
GPP	Gross primary productivity
H	Sensible heat
IAC	Institute of Atmospheric and Climate Science
IAV	Inter-annual variability
ICOS	Integrated Carbon Observation System

ICOS-bkp	Backup ICOS climate station Selhausen
IR	Infrared
LAI	Leaf area index
LE	Latent heat
LPJmL	Lund-Potsdam-Jena managed Land
LSM	Land surface model
LW_{in}	Incoming longwave radiation
MAE	Mean absolute error
MBE	Mean bias error
N	Nitrogen
NEE	Net ecosystem exchange
NPP	Net primary productivity
PE	Parameter effect
PFT	Plant functional type
PHO	Pinios Hydrologic Observatory
r	Pearson's coefficient of correlation
R^2	Coefficient of determination
R_a	Autotrophic respiration
R_{eco}	Ecosystem respiration
R_h	Heterotrophic respiration
RMSE	Root mean square error
R_n	Net radiation
R_s	Soil respiration
SM	Soil moisture
SMP	Soil matric potential
TAHMO	Trans-African Hydro-Meteorological Observatory
TERENO	TERrestrial ENvironmental Observatories
WMO	World Meteorological Organization
WSN	Wireless sensor network
ψ_{target}	Target soil matric potential in the CLM5 irrigation routine

1 Introduction

Agriculture has been and continues to be an essential component of human development, shaping our societies and sustaining the world's population. Although the global share of employment in agriculture, forestry, and fishing has been declining in recent years, it remains the second largest source of employment and currently provides roughly a quarter of the world's population with livelihood [*FAO*, 2022]. The agricultural sector currently accounts for 4.3% of the global gross domestic product (GDP) and for as much as 25% of GDP in low-income countries [*World Bank*, 2021]. As such, it is crucial to economic development and poverty reduction.

Practicing agriculture involves transforming the world's landscapes and utilizing natural resources to meet human needs. Agricultural land use has been expanding due to population growth, economic development, and advancements in technology. Simultaneously, crop breeding and the widespread use of fertilizers and pesticides have boosted agricultural productivity since the green revolution in the mid-20th century [*Perkins*, 1990]. As a result, croplands and pastures now are the largest land use worldwide and occupy 37% of the global land surface (excluding Antarctica and inland waters) [*FAO*, 2021b].

The growing demand for food and the expansion of agricultural land made it imperative to increase agricultural production in regions with insufficient or irregular rainfall. This led to significant increases and modernization of irrigation infrastructure, especially during the green revolution [*Angelakıs et al.*, 2020]. Irrigation is the process of artificially applying water to the soil to meet crop water requirements, thereby enabling or enhancing crop growth and yield. While most of the cropland continues to be rainfed, the importance of irrigated agriculture in terms of food security is ever growing. According to the *FAO* [2022], the global land area equipped for irrigation increased by 20% since 2000 and has more than doubled compared to the 1960s. Currently, ~40% of global food supply is produced on irrigated land, which covers one fifth of the total agricultural area [*WWAP*, 2019]. Irrigation, especially for crop production, accounts for 70% of total freshwater

withdrawals worldwide, making it the largest freshwater consumer [*Campbell et al.*, 2017].

Despite the apparent societal benefits of providing livelihood and supplying food, modern agriculture has profound and often negative impacts on the natural environment. Local and regional farming practices can lead to odour and sound pollution, contamination of soil and water bodies through the percolation or runoff of fertilizers and pesticides, or soil degradation through soil erosion processes [*Payraudeau and van der Werf*, 2005]. Other effects act on a global scale such as land use and -cover change, emission of greenhouse gases and biodiversity loss [*Ramankutty et al.*, 2018].

Irrigation practices also show strong environmental effects across scales, profoundly affecting the water cycle, surface energy budget, and climate [*Cook et al.*, 2015]. Irrigation directly influences soil water content through the addition of water from other sources, e.g. groundwater or surface water, which affects hydrological processes such as deep percolation and runoff. Intensive irrigation generally reduces river flows and drives groundwater depletion [*Thomas and Famiglietti*, 2019], thus exacerbating water scarcity with consequent risks to natural ecosystems. At the same time, more water is introduced into the atmosphere by evaporation from the soil and through crops that readily transpire the water supplied through irrigation practices, thereby impacting the climate [*Chen and Dirmeyer*, 2020]. These feedbacks can be observed in regard to temperature, humidity, and precipitation [*Cook et al.*, 2015; *Rappin et al.*, 2022]. Studies showed effects such as cooling of summer temperatures [*Chen and Dirmeyer*, 2020; *Lawston et al.*, 2020; *Lobell et al.*, 2008a; *Sacks et al.*, 2009], increases or changes in precipitation amount and location [*DeAngelis et al.*, 2010; *Devanand et al.*, 2019; *Tuinenburg et al.*, 2011; *Yang et al.*, 2019], and increased atmospheric moisture [*Xu et al.*, 2019] over various irrigated areas.

Apart from the environmental impact, poor management of irrigation can also negatively affect crop production and increase water use conflicts. Over-irrigation can lead to leaching of fertilizers and pesticides and increased risk for plant disease [*Irmak*, 2008; *Maharjan et al.*, 2014]. Moreover, the use of poor irrigation water quality can cause soil salinity problems [*Khan et al.*, 2006; *Zanchi and Cecchi*, 2010]. All of the above can limit crop growth with negative effects on crop yield. Excessive or inefficient irrigation can result in high conveyance or application water losses leading to poor crop water use efficiency (CWUE), referring to the amount of yield produced per unit volume of water

consumed, and potentially leaving insufficient water available to crops later in the season [*Akhtar et al.*, 2018]. This can also affect other water users downstream of the river network or as shared groundwater body. Indeed, this has caused national and international conflicts in the past, especially in semi-arid and arid regions [*Carkoglu and Eder*, 2001; *Houdret*, 2012; *Pacific Institute*, 2022; *Wiebe*, 2001].

The current issues of today's agriculture are numerous and will be exacerbated by continuing climate change. In the coming years, securing and sustaining freshwater availability for human activities and natural ecosystems will be one of our major challenges [*IPCC*, 2022]. Global water availability is projected to decrease, especially in regions already suffering from severe water scarcity i.e., South and East Asia, the Middle East, Mexico, the western US, and the Mediterranean [*Van Vliet et al.*, 2021]. This is driven by decreases in water quantity, that is the availability of surface and groundwater resources, and water quality, such as salinity levels, both of which constrain irrigation [*Van Vliet et al.*, 2021]. At the same time, global agricultural production will have to keep up with the needs of a growing population. Global food demand is projected to rise by up to 62% between 2010 and 2050 [*Van Dijk et al.*, 2021]. Consequently, water consumption for agriculture, including rainfed and irrigated production, is expected to increase by about 19% by 2050 [*WWAP*, 2012].

Irrigated agriculture will continue to play a key role in sustaining and increasing agricultural production in the future. At the same time, it needs to reconcile the conflicting trends in water availability and water use, and deal with the numerous present and future challenges as elaborated above. A sound understanding of the effects of irrigation is required to derive effective adaptation and mitigation measures. This is not only necessary to avoid the further depletion of water resources and detrimental impacts on aquatic and terrestrial ecosystems but also to sustain a high level of crop production [*Rosa*, 2022]. To accomplish this goal, there is a need to improve agricultural water management across spatial and temporal scales, ranging from individual agricultural fields and growing seasons to large catchments and long-term trends.

To improve irrigation management, information about the conditions in the irrigated area must be available through measurements and monitoring. This information can subsequently be used to directly guide irrigation decisions in the field [*Gu et al.*, 2020; *Hedley et al.*, 2012] and evaluate the performance of existing irrigation systems [*Akhtar*

et al., 2018] but also to better understand irrigation-climate interactions and inform modelling [*McDermid et al.*, 2023]. Unfortunately, irrigation practices are scarcely monitored and observations of irrigation, along with ancillary data such as meteorological data, soil moisture (SM), and other environmental variables are rarely available [*Dari et al.*, 2023; *Lawston et al.*, 2017; *Rappin et al.*, 2022].

Secondly, observations must be combined with the appropriate predictive tools, such as numerical models. These models should represent the agricultural system in interaction with other Earth-system processes to holistically study and understand irrigation impacts on crop growth and yield as well as on the surrounding environment, and to aid decision-making processes. This means that on one hand they need to provide an accurate representation of multiple crops and management options while, on the other hand, they should include aspects from a broader environmental context, for instance the impact of irrigation on regional climate or groundwater availability. Therefore, interactions and feedback mechanisms between land, water, and atmosphere including the hydrological and biogeochemical cycles within the Earth system must be captured [*Betts*, 2005; *Stehfest et al.*, 2007]. Current models are however associated with uncertainties and biases due to complex parameterizations, challenging physical representations, and spatial resolution [*Chen and Dirmeyer*, 2020; *de Vrese and Hagemann*, 2018; *Kueppers et al.*, 2008]. These aspects can lead to large errors in the estimation of irrigation water consumption or withdrawal, making it difficult to derive reliable recommendations for water resources management [*Felfelani et al.*, 2021; *Leng et al.*, 2017; *Pokhrel et al.*, 2015; *Zhang et al.*, 2020].

In essence, embracing a well-developed data and model-driven approach in irrigated agriculture can help to capitalize on the benefits irrigation is providing. At the same time, it has the potential to equip policymakers to take informed decisions for a better irrigation and water resources management. Ultimately, this can ensure economic viability and global food security, and improve environmental sustainability in the face of a changing climate.

1.1 Environmental data for irrigation and water resources management

1.1.1 Understanding the importance of environmental data

Access to comprehensive environmental data from different sources is paramount for agricultural and water resources management. Analysing this data can provide critical insights into the complex interplay between meteorological conditions, soil characteristics, and crop requirements. In this way, they are essential for decision-making and to develop, evaluate, and run models that simulate agricultural systems.

Among the most important environmental data are meteorological parameters such as air temperature, humidity, solar radiation, and precipitation. Meteorological parameters play a key role in determining plant growth, water requirements, and crop yields. Precipitation is a key factor in rainfed crop production, as it provides the water input without which crops cannot thrive. Air temperature and radiation influence the rate of photosynthesis which is directly linked to plant growth and yield [*Hall and Rao*, 1999]. Evapotranspiration (ET), a key parameter to define plant water requirements, is largely controlled by the presence of moisture in the air, which in turn is influenced by temperature, solar radiation, and wind speed [*Jensen*, 1968]. Moreover, meteorological data is one of the most important input data to initiate and run models used for agricultural applications [*Venäläinen and Heikinheimo*, 2002]. This requires precise and reliable measurements.

Furthermore, soil water is tightly linked to crop growth and irrigation management. It refers to the quantity of water within the upper layers of the soil that directly interacts with the atmosphere via ET, infiltration, and runoff [*De Lannoy et al.*, 2019]. The water content in the root zone must be maintained at a level that ensures optimal transpiration to realize the full yield potential of the crop. Soil water status can be expressed as SM content, indicating the amount of water present in the soil, or soil matric potential (SMP), which expresses the relative availability of the soil water for plant uptake. Both variables are commonly used in irrigation scheduling [*Blonquist Jr et al.*, 2006; *Dukes et al.*, 2007; *Gu et al.*, 2020; *Millán et al.*, 2019; *Miller et al.*, 2014; *Zotarelli et al.*, 2011] but are also valuable for model evaluation and improvement [*Devia et al.*, 2015; *Vereecken et al.*, 2008; *Zehe et al.*, 2005].

In addition, crop and agricultural management data are important factors influencing crop yield. These include crop-specific information such as crop phenology, leaf area index (LAI), and transpiration as well as data related to irrigation practices such as water withdrawal and quality, irrigation schedules and techniques, and other management information like fertilization or harvest practices [*Deryng et al.*, 2011; *Licker et al.*, 2010].

All of the above parameters can be highly variable in time and space. Meteorological phenomena for instance range from local microclimates over mesoscale events such as thunderstorms to global climate variations [*Steyn et al.*, 1981; *Tavakolifar et al.*, 2017]. Likewise, SM displays high spatial and temporal variability with a nonlinear effect on many environmental processes [*Vereecken et al.*, 2008; *Western et al.*, 2002]. Consequently, data acquisition must be tailored to different temporal and spatial scales depending on the application.

1.1.2 Scales of environmental data collection

Advancements in instrumentation and digital technology have diversified the possibilities for data acquisition across multiple scales [*NSF*, 2007]. These methods encompass a range of techniques, from satellite-based remote sensing to ground-based in-situ measurements (Figure 1.1).

At a large regional to global scale, environmental data can be gathered through a variety of space- and airborne remote sensing techniques. For instance, remote sensing, combined with subsequent downscaling techniques, is used to estimate rainfall. Rainfall products are available at spatial resolutions between 1 and ~27 km and temporal resolutions ranging from half hourly to weekly [*Kumar and Reshmidevi*, 2013; *Michaelides*, 2019]. Similarly, land surface temperature can be obtained starting from ~1 km resolution even though its correlation to air temperature is a topic of ongoing research [*Tomlinson et al.*, 2011]. Global meteorological datasets are usually based on a combination of satellite and ground station data with reanalyses (hybrid model-observational data sets) or numerical climate modelling, and interpolated to resolutions of 0.1° and coarser [*Davy and Kusch*, 2021; *Jiang et al.*, 2018; *Overpeck et al.*, 2011]. Comparisons of some currently available datasets showed large differences in magnitude and variability of the estimated variables [*Sun et al.*, 2018].

For SM retrieval, satellite-based optical, thermal infrared, and microwave sensors are being used [*Babaeian et al.*, 2019]. The spatial resolution of the resulting products is

typically coarse, in the range of 25 and 50 km, while the temporal resolution ranges from daily to weekly [*Brocca et al.*, 2017] [*Peng et al.*, 2021]. Currently, some satellite missions aim to retrieve SM at 0.1 to 1 km spatial resolution at the regional to continental scale [*Babaeian et al.*, 2019; *Mengen et al.*, 2021]. Additionally, unmanned aerial vehicles equipped with sensors deliver measurements of airborne SM at higher spatial resolution (1-100 m) but at the expense of spatial extent and temporal coverage as they are typically flown over specific regions for a limited time only [*Kumar and Reshmidevi*, 2013].

The above techniques are based on an indirect linkage of the measured signal to SM and suffer from interference with clouds and vegetation resulting in relatively low accuracy when compared to ground based reference data [*Gruber et al.*, 2020]. Additionally, they usually yield information on near-surface SM (up to ~5 cm soil depth), which is insufficient for many agricultural applications that rely on root zone SM [*Montzka et al.*, 2017]. Other remote sensing products include estimates of crop ET or vegetation greenness (normalized difference vegetation index), crop classification or the mapping of irrigated areas. Despite their great potential, they are often limited in the amount of distinguished crop types and spatial coverage, and come with relatively high uncertainties [*He et al.*, 2023; *Portmann et al.*, 2010]. Although remote sensing products can deliver spatially continuous information over large areas, their limitations become apparent when addressing microscale variability. Downscaling or interpolation techniques are frequently used to infer regional or local information from these global data sets, which can be associated with great uncertainty and low skill in reproducing local conditions [*Maurer and Hidalgo*, 2008; *Schoof*, 2013]. Hence, ground-based measurements remain indispensable for investigating individual fields and small catchments due to the high spatial and temporal heterogeneity of e.g. meteorological variables and SM.

Locally, meteorological data can be obtained from the nearest ground-based weather station. These often belong to networks run by national meteorological services or research infrastructures. Such networks are typically well developed in high-income countries, but station coverage is often limited in rural areas, difficult terrain, or lower income countries requiring additional non-conventional stations to better observe the local climate [*Mendelsohn et al.*, 2007; *Nsabagwa et al.*, 2019; *WMO*, 2016].

For SM measurements, various techniques are available at the field or intermediate scale. These include non- or minimally invasive techniques such as electromagnetic induction [*Sheets and Hendrickx*, 1995] and electrical resistivity tomography [*Brunet et al.*, 2010] or emerging techniques such as cosmic ray neutron sensing [*Zreda et al.*, 2008] among others. The accurate determination of SM from the received signal can however be quite complex and sensitive to soil and vegetation properties [*Brogi et al.*, 2019; *Brunet et al.*, 2010; *Jakobi et al.*, 2018]. Also, the investigated soil depth can be limited and thus not represent the entire root zone depending on SM conditions [*Köhli et al.*, 2015] or on the measurement methodology [*Bernard*, 2003; *Koyama et al.*, 2017]. At the point-scale, in-situ sensors based on different electromagnetic principles are used to continuously measure SM [*Bogena et al.*, 2017]. In order to obtain representative measurements for a given area, a large number of in-situ sensors must be installed in multiple locations and at different depths within the soil profile [*Bogena et al.*, 2010]. However, applying such a high number of sensors requires cost effectiveness and automated solutions.

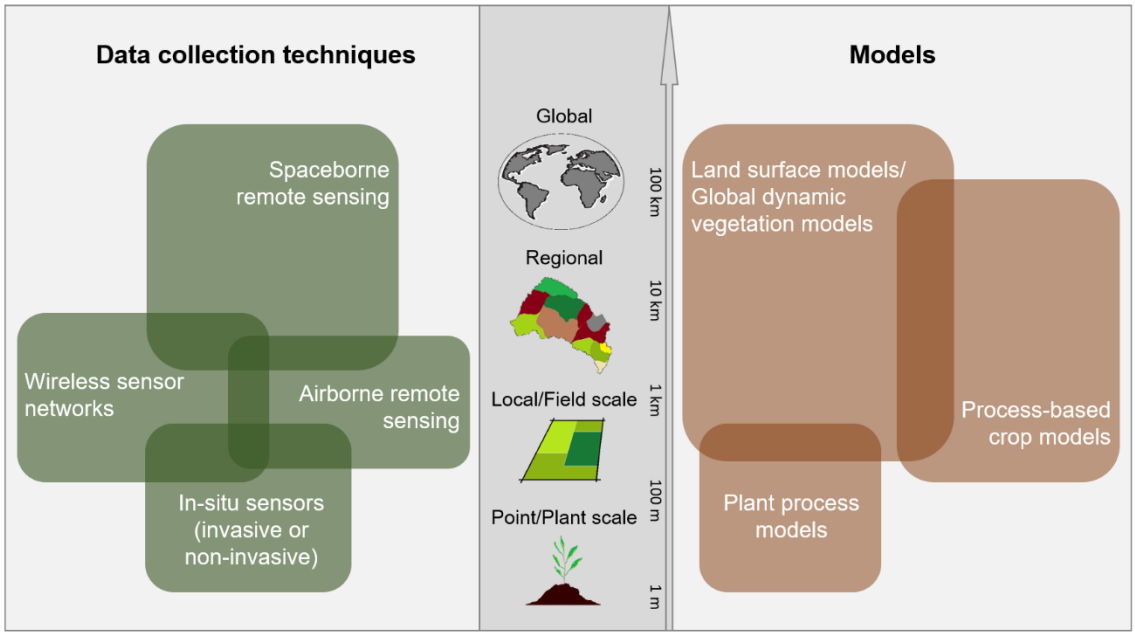

Figure 1.1 Typical spatial scales for the measurement and modelling of agricultural systems.

1.1.3 Low-cost sensors for wireless sensor networks

The rising demand for automated measurement systems has led to a range of low-cost sensors available from various manufacturers. Furthermore, recent advancements in electronics and communication technology have facilitated the integration of these sensors into wireless sensor networks (WSNs) for continuous environmental monitoring [*Martinez et al.*, 2004]. In WSNs, individual sensing devices communicate with one or

multiple base stations from where data is forwarded to a central server with remote access via a communication protocol [*Hart and Martinez*, 2006]. Commonly used protocols include ZigBee, Long Range (LoRa), and Narrow Band Internet of Things (NB-IoT). They make use of the low-power wide-area technology that enables wireless communication at relatively low cost and power consumption [*Bogena et al.*, 2022].

To gather meteorological variables, low-cost all-in-one weather stations have recently gained popularity. They offer a compact and easy way to collect meteorological data at a given location. Due to their ease of use and cost efficiency, they are becoming widely used for field-scale applications [*de la Concepcion et al.*, 2015; *Tenzin et al.*, 2017; *Watthanawisuth et al.*, 2009] and larger monitoring networks [*van de Giesen et al.*, 2014]. For SM measurements, one type of suitable sensor is based on the capacitance method [*Blonquist Jr et al.*, 2005], whereby the soil is incorporated as dielectric medium and the resultant output voltage is related to SM content [*Bogena et al.*, 2007]. Other commonly used sensors are time domain reflectometry probes that determine the dielectric constant by wave propagation transmitted by two parallel metal probes [*Tilse et al.*, 2023]. For SMP measurements, tensiometers are common though they are generally unsuitable for agricultural studies when crops grow under water-limited conditions. Instead, wettable porous media such as gypsum with embedded electrodes can be used for these applications [*Brogi et al.*, 2022].

With the widespread use of low-cost sensors, concerns regarding their accuracy, reliability, and performance have been raised. These must be addressed as there can be trade-offs between low-cost and traditional sensors with the former potentially being less precise and less sensitive to the variable of interest [*Okafor et al.*, 2020; *Rai et al.*, 2017; *Schwamback et al.*, 2023]. Hence, proper testing and calibration is indispensable to ensure suitability of these sensors for different applications, and to determine the factors that influence data quality for a given measurement [*Bogena et al.*, 2017; *Ioannou et al.*, 2021; *Nsabagwa et al.*, 2019; *Okafor et al.*, 2020]. If reliable, low-cost sensors in combination with WSNs offer diverse opportunities for data collection and monitoring at high spatiotemporal resolution complementary to more traditional monitoring and existing datasets.

1.1.4 Applications of wireless sensor networks

WSNs have found diverse applications across various fields and aspects of agricultural and water resources management and monitoring. Nowadays, they are widely used to directly support farmers in various management decisions. This recent data driven approach is called smart farming and is seen as a key component for sustainable agricultural management [*Bach and Mauser*, 2018; *Lytos et al.*, 2020]. It aims to increase resource efficiency through precise input application, optimize yield, and generate high-resolution data to guide decision-making processes [*Dhanaraju et al.*, 2022; *Walter et al.*, 2017].

Due to its crucial role in modern agriculture, especially in arid and semi-arid regions, irrigation water management has become one of the main areas of application in smart farming. Different smart irrigation practices are explored to achieve more efficient and sustainable water use [*Moysiadis et al.*, 2021; *Touil et al.*, 2022]. Additionally, more effective irrigation systems like the use of drip and micro-irrigation, whereby water is delivered more directly to the plant root zone, have become more widespread [*Hla and Scherer*, 2003]. These systems minimize water loss due to evaporation and runoff, increase CWUE and improve crop yield [*Obaideen et al.*, 2022]. Traditional irrigation practices, based on farmer experience and standard schedules are increasingly being replaced by automated irrigation systems. These systems integrate real-time data from various sources to remotely control, monitor, and adjust irrigation timing, duration, and intensity. These decisions are based on a variety of approaches from simple irrigation triggers (e.g., lower limit or threshold of SM or SMP), to regression algorithms and various machine-learning techniques, to more complex physically-based models [*Gu et al.*, 2020].

Despite the benefits of smart farming, the high cost and advanced knowledge and skill needed to make proper use of such technologies pose a significant challenge for many small-scale farmers, especially in low-income countries [*Walter et al.*, 2017]. To extend the focus beyond the scale of individual fields and single crop growing seasons, the installed WSNs can be integrated into a larger monitoring network. This is necessary as water management decisions are often taken at regional or catchment scale and need to be informed by an accurate understanding of the interacting processes occurring at this scale over time [*Jensen and Illangasekare*, 2011].

Recognizing this necessity has led to the establishment of hydrological observatories that intend to cover whole catchments with a dense observational network. One aim of these observatories is to collect long-term hydrological measurements to predict the consequences of climate and land use changes, and to take a holistic approach to water resources management [*Bogena et al.*, 2018; *Jensen and Illangasekare*, 2011]. Several of such observatories across the world investigate the impact of agricultural systems on the environment. The Hyderabad Observatory in India for instance looks at various components of the water cycle in intensely irrigated areas [*Maréchal et al.*, 2018]. The Northeast German Lowland Observatory as part of the German TErrestrial ENvironmental Observatories network (TERENO) includes several intensely managed agricultural sites [*Heinrich et al.*, 2018] and the Dutch Hupsel Brook catchment was established with the aim to improve agricultural water management [*Brauer et al.*, 2018]. Observatories with a focus on the Mediterranean area where established in France and Tunisia [*Molénat et al.*, 2018], Italy [*Romano et al.*, 2018], and Greece [*Pisinaras et al.*, 2018] and put an emphasis on sustainable water management among others.

Notably, the importance of environmental data to further improve agricultural and water resources management cannot be overstated. Low-cost sensors in combination with WSNs offer new opportunities to increase data availability and to better capture the heterogeneity and spatiotemporal variability of e.g. SM across larger areas [*Vereecken et al.*, 2019]. The sensors, though cost-effective, should however undergo rigorous testing and calibration to address data quality concerns and make them suitable for various applications. If leveraged correctly, WSNs integrated into hydrological observatories can greatly contribute to not only providing a holistic understanding of local and regional scale processes relevant for irrigation and water resources management but also to developing, calibrating and validating various models used in this context.

1.2 Modelling agricultural systems

Modelling is an essential tool not only for farm-scale crop yield prediction and irrigation management but also to guide decision-making at regional or catchment scale and beyond for improved agricultural and water resources management. A multitude of models is available for the simulation of agricultural systems at different scales (Figure 1.1). These models can vary greatly in their degree of process representation, physical basis, and input requirements.

1.2.1 Crop modelling approaches

Generally, crop modelling can be used to simulate crop growth and yield in agricultural systems. Available approaches include empirical or process-based models that were developed for field-scale applications or for global dynamic vegetation and land-surface modelling [*Elliott et al.*, 2015; *White et al.*, 2011]. Empirical or statistical models estimate climate-yield relationships based on observed datasets of yield and climate variables, and are mainly applied for agricultural climate impact assessments [*Gornott and Wechsung*, 2015; *Lobell et al.*, 2008b]. However, as their equations are solely fitted based on available observations, they do not explain the underlying mechanisms of yield variation and have limited applicability under climatic or environmental conditions beyond the observed ones [*Holzkämper*, 2017].

Other models are based on a mechanistic understanding of biophysical processes and therefore provide a good basis to assess management or climate change impacts on crops and their interactions in different agroecosystems [*Kephe et al.*, 2021]. Certain models represent specific biophysical processes such as photosynthesis [*Farquhar et al.*, 1980; *Wang et al.*, 2014], respiration [*Sweetlove et al.*, 2013], or crop growth and development [*Prusinkiewicz and Runions*, 2012]. They typically operate at narrow spatiotemporal scales to assess how a process is affected by environmental parameters for a particular crop type [*Marshall-Colon et al.*, 2017].

Beyond individual processes or plants, dynamic process-based crop models (CMs) were developed to simulate crop development and yield in relation to environmental conditions (e.g., SM, air temperature, CO_2 concentration) and management practices (e.g., irrigation, nitrogen fertilization) at the field scale [*Muller and Martre*, 2019]. Compared to empirical models, they require a larger amount of input data (e.g. soil and crop parameters) due to

their greater complexity [*Manivasagam and Rozenstein*, 2020]. Some of the early, widely known CMs are the CERES model for maize [*Jones et al.*, 1986] and wheat [*Ritchie and Otter*, 1985], SUCROS for spring wheat [*Van Laar et al.*, 1997], and SOYGRO for soybeans [*Wilkerson et al.*, 1983].

The above mentioned CMs were later incorporated into the decision support system for agrotechnology transfer (DSSAT) for better compatibility and application [*Jones et al.*, 2003]. This suite of CMs currently includes models for various annual crops e.g. grains, legumes, and vegetables as well as perennial forage crops [*Pereira et al.*, 2020]. DSSAT can be used to simulate crop growth, development, and yield and to investigate crop management decisions over single or multiple seasons under the consideration of soil, crop phenotype, and weather [*Jones et al.*, 2003]. Other widely used multi-crop models include EPIC [*Williams et al.*, 1989], CropSyst [*Stöckle et al.*, 2003], AquaCrop [*Steduto et al.*, 2009], or the APSIM suite of CMs [*Keating et al.*, 2003] and can simulate a variety of annual and perennial crops and management options similarly to DSSAT. Apart from biophysical processes, APSIM can also simulate economic and ecological outcomes of specific crop management practices under changing climatic conditions [*Keating et al.*, 2003].

The models differ in terms of complexity, i.e. AquaCrop focusses on simulating the effect of water limitation on potential crop yield while the DSSAT model family integrates crop responses to soil water, nutrients, and soil carbon (C). EPIC and CropSyst additionally integrate climate and management effects on soil erosion while APSIM is more detailed in representing crop growth processes and differentiates between individual plant components [*Holzkämper*, 2017].

Most CMs were designed for field-scale simulations with one exception being the regional-scale crop model GLAM [*Challinor et al.*, 2004], but are often applied at regional or even global scale [*Challinor et al.*, 2018; *Holzkämper*, 2017]. This however can lead to computational challenges and may impact their ability to accurately represent the spatial heterogeneity of climate variability on yield [*Doering and Otto*, 2002]. Additionally, because of their development as standalone CMs, they typically lack a more detailed description of the soil profile including soil hydraulic properties that are key to adequately simulate soil water status and irrigation requirements [*Vereecken et al.*, 2016]. Other approaches therefore combine CMs with transient state models, e.g. the crop

growth model WOFOST and the hydrologic model HYDRUS-1D [*Zhou et al.*, 2012] or the agro-hydrological model SWAP and the crop growth model EPIC [*Xu et al.*, 2013] to improve the representation of water dynamics in the soil. Moreover, CMs neglect the wider interactions of crop and environment [*Levis et al.*, 2012]. For instance, climate change will affect water resources with consequent impact on water availability for irrigation [*Arnell*, 1999; *Döll*, 2002].

As croplands cover substantial areas of land and greatly impact the Earth system, there has been increasing interest and need to model these interactions of crop production and management with local climate, hydrology, and land surface processes. This has led to the inclusion of agricultural systems into spatially distributed models with broader scopes such as dynamic global vegetation models, e.g. the Lund-Potsdam-Jena managed Land model (LPJmL) [*Bondeau et al.*, 2007], river basin models such as SWAT/SWIM [*Arnold et al.*, 1998; *Krysanova et al.*, 2000], or different land surface models (LSMs) [*Fisher and Koven*, 2020] that can be coupled to climate models and are typically used for regional to global scale modelling. Due to their large-scale application and their origin from other disciplines (e.g. hydrology, terrestrial ecosystem or climate sciences), crop and management representations in these models are often comparatively simpler than those of field-scale CMs [*Holzkämper*, 2017; *Manivasagam and Rozenstein*, 2020]. However, LSMs represent hydrology, surface energy balance, and biogeochemical cycles and could thus appear more suitable to evaluate the environmental impacts of agriculture in the Earth system in a more holistic way [*Blyth et al.*, 2021; *Peng et al.*, 2020].

1.2.2 Land surface models

LSMs form the land component of earth system models and depict all terrestrial ecosystem processes. They require meteorological, land cover, and soil data to simulate the interactions between land, vegetation, water, and the atmosphere at large regional, continental, or global scales [*Bonan*, 2019]. LSMs originated from the climate modelling community where their primary purpose was to deliver the physical boundary conditions at the land-atmosphere interface to study the influence of land on weather and climate. However, the role of the terrestrial biosphere and land surface itself with the related biogeophysical and biogeochemical processes has since gained greater attention and has led to many further developments of LSMs across a broad range of spatial and temporal scales [*Buechel*, 2021; *Fisher and Koven*, 2020]. Their application has thus expanded to

a wide variety of contexts including the effects and potential risks of land use and change on climate, terrestrial and aquatic ecosystems as well as human societies [*Blyth et al.*, 2021; *Fisher and Koven*, 2020]. As a result, LSMs have greatly evolved in the representation of processes to include SM dynamics, land surface hydrological processes, C and nitrogen cycling, land cover, and human land management such as crop production [*Lawrence et al.*, 2019].

1.2.3 Crop representations in LSMs

Initially, crops were represented by a generic crop type similar to grasses in many LSMs [*Lombardozzi et al.*, 2020]. Various LSMs, such as ORCHIDEE, the Community Land Model (CLM), JULES and Noah-MP have since incorporated process-based CMs to dynamically model crops and crop management [*Levis et al.*, 2012; *Liu et al.*, 2016; *Osborne et al.*, 2014; *Wu et al.*, 2016]. Crop representations typically include a description of crop phenology, partitioning of dry matter, and management practices such as sowing, fertilization, and harvest. Similar to classical CMs, crop growth is governed by crop phenological phases that are triggered by growing degree-day thresholds [*Liu et al.*, 2016]. In CLM version 5 (CLM5), planting, leaf emergence, grain fill, and harvest are distinguished while other LSMs may use additional or fewer phenological phases. During the growing season, C and N are allocated based on C:N ratios of the individual plant organs (leaf, stem, fine roots, grain), whereby N is supplied by the soil mineral N pool. At harvest, the grain pool is transferred to a grain product pool and exported as yield [*Lombardozzi et al.*, 2020]. The integration of crops into LSMs has significantly improved the simulation of the seasonal evolution of LAI [*Osborne et al.*, 2014; *Wu et al.*, 2016], gross primary productivity [*Drewniak et al.*, 2013; *Osborne et al.*, 2014], net ecosystem exchange and latent heat [*Levis et al.*, 2012; *Lokupitiya et al.*, 2016].

However, the diversity of crop types, cultivars, and management practices is still greatly simplified in these models [*Lombardozzi et al.*, 2020]. This has resulted in inaccurate representations of phenology and crop yield [*Chen et al.*, 2018; *Lombardozzi et al.*, 2020; *Sheng et al.*, 2018]. Besides a limited number of major annual crop types (e.g., wheat, soy, corn, rice) descriptions of other crops such as perennials or less common grains or tuber crops are still scarce, partially due to a lack of comprehensive datasets to parameterize these crops. Recently, some efforts have been made to improve crop growth and management processes or to include additional crop types and cropping systems into

LSMs and other global modelling environments. For instance, *Peng et al.* [2018] developed a new maize model in CLM4.5 and *Boas et al.* [2021] implemented a subroutine for winter wheat and new parameters for sugar beet, potatoes, and winter wheat in CLM5. Bioenergy crops [*Schaphoff et al.*, 2018] and agricultural trees [*Fader et al.*, 2015] were included in the LPJmL model. Moreover, *Fan et al.* [2015] parameterized oil palms, as a perennial evergreen crop within CLM4.5 and *Cheng et al.* [2020] included two perennial grasses for energy production in CLM5. These extensions improved the simulation of crop phenology, yield, and the surface energy and C fluxes [*Boas et al.*, 2021; *Peng et al.*, 2018], and continue to increase the ability of LSMs to represent a greater diversity of agricultural systems.

1.2.4 Irrigation in LSMs

Irrigation has only recently been acknowledged as an important driver of Earth system processes to be included in LSMs. Consequently, irrigation is still largely underrepresented or implemented in a rather simplistic way in many LSMs [*McDermid et al.*, 2023; *Pokhrel et al.*, 2016].

De Rosnay et al. [2003] incorporated an irrigation scheme in ORCHIDEE to examine the regional impacts of irrigation on energy partitioning. In their study, daily irrigation requirements were calculated based on the difference between potential evaporation multiplied by a crop coefficient and precipitation. Actual irrigation was then determined depending on water availability in the river system and aquifer as simulated by a routing scheme. Other authors prescribed a fixed irrigation rate or implemented dynamic irrigation schemes based on defined SM thresholds in the root zone to trigger irrigation in JSBACH, NoahMP and CLM4 using satellite-derived data to identify irrigated areas [*de Vrese et al.*, 2016; *Levis and Sacks*, 2011; *Ozdogan et al.*, 2010; *Sacks et al.*, 2009]. Using this approach, irrigation is driven by soil water status independent of management techniques or water availability. Consequently, irrigation and irrigation-induced impacts simulated in these studies have shown various issues including overestimation of irrigation amounts and duration or runoff, and underestimation of the change in latent heat [*Kueppers and Snyder*, 2012; *Lawston et al.*, 2017; *Sacks et al.*, 2009].

More recently, model developments added new capabilities such as distinguishing different irrigation techniques (i.e. sprinkler, surface, drip irrigation) [*Leng et al.*, 2017; *Pokhrel et al.*, 2015; *Yao et al.*, 2022] or including different sources for irrigation water

withdrawal including groundwater pumping [*Leng et al.*, 2017; *Xia et al.*, 2022] in CLM5, NoahMP, ACME or HiGWMAT. Others added water regulation modules accounting for other water uses next to irrigation [*Pokhrel et al.*, 2012], and limitations on water availability [*Yin et al.*, 2020] to MATSIRO and ORCHIDEE, respectively. These developments improved the performance of the models when compared to observed river discharge, irrigation water withdrawals, and groundwater depletion. However, given the various approaches to model irrigation, simulated irrigation exhibits considerable discrepancies especially at local and regional scales [*Haddeland et al.*, 2014; *McDermid et al.*, 2023; *Pokhrel et al.*, 2016]. The coarse scales (10–100 km) at which the mentioned irrigation studies were performed and the lack of local irrigation data further contribute to these uncertainties [*Lawston et al.*, 2017; *McDermid et al.*, 2023]. As more irrigation data become available at higher resolution, they can be used to better evaluate and improve existing irrigation schemes. This can give further insight into the effects of irrigation and its current representations in LSMs down to the field scale [*Huang et al.*, 2022; *Lawston et al.*, 2017].

Clearly, efforts are ongoing to improve the simulation of human land and water management in terms of crop and irrigation representations in LSMs. While noteworthy progress has been made in both areas, this work needs to be continued to include missing crop types, e.g. perennial crops, and to more realistically represent local irrigation practices. This will allow to better account for regions with a more diverse agricultural landscape, e.g. mixed annual or perennial cropping systems.

1.3 The Mediterranean context

Although most of the work in this thesis aims to be applicable across the world, the focus is put on the Mediterranean. This region combines a rich history and biodiversity, a wide range of traditional and modern agricultural activities, a highly variable climate, different degrees of economic development, chronic water scarcity and high environmental vulnerability [*Tramblay et al.*, 2020]. All of these factors create a unique environment and necessity for research and policy development for sustainable irrigation practices and water resources management. Moreover, the lessons learned from this region can have a broader applicability and offer valuable insights to address challenges related to agriculture, water, and climate change globally.

1.3.1 Characteristics of the region

The Mediterranean region spans over southern Europe, Northern Africa, and the Middle East. Its climate falls in the transitional zone between the subtropical and temperate zones and is characterized by hot and dry summers and cool wet winter periods with high intra- and inter-annual variability in rainfall [*Joffre and Rambal*, 2001; *Lionello et al.*, 2006]. The region has a diverse geography and rich biodiversity with a large number of endemic plant species, while at the same time conditions in the area are suitable to grow a wide variety of crops [*Myers et al.*, 2000].

The Mediterranean has been a cradle of agriculture dating back millennia [*Aguilera et al.*, 2020]. Agricultural practices have shaped the landscape, cultural identity, and economic growth of the region. Until today, agricultural production is of high economic value employing more than a fifth of the population and contributing > 10% of GDP in some Mediterranean countries [*CIHEAM*, 2009]. Next to annual crops including cereals and pulses, the cultivation of perennial crops, like olive trees, vineyards, and various fruit and nut trees, is an integral part of the region's agricultural landscape. Farm sizes are generally small compared to other agricultural areas, which creates a fragmented, diverse landscape, and a challenge to farmers who often struggle to provide sufficient income to adequately support their families [*Lobianco and Roberto*, 2006]. Considering the semi-arid conditions and irregular rainfall patterns, irrigation has been a cornerstone of agriculture in the Mediterranean to achieve adequate crop growth and yield [*Semple*, 1929]. As a result, irrigated land has been expanding continuously, facilitating food production and securing livelihoods for a growing population [*Daccache et al.*, 2014].

Presently, irrigated agriculture is responsible for around 50% of total water withdrawal, with strong sub-regional differences ranging from 11% in Croatia and France to > 80% in Egypt, Greece, and Syria [*FAO*, 2022].

1.3.2 Environmental pressures

The Mediterranean region faces mounting pressure on its water resources due to the dependence on irrigation combined with other factors including rapid population growth, urbanization, and climate change [*Fader et al.*, 2016]. Together with poor water governance and inefficient irrigation practices, this has repeatedly led to over extraction of water, decline of groundwater quality, soil degradation, and environmental pollution [*Aureli et al.*, 2008; *Daccache et al.*, 2014; *Kurunc et al.*, 2016; *Pisinaras et al.*, 2010]. Additionally, the Mediterranean has been declared one of the climate change hotspots and is likely to experience more frequent and intense heat waves and prolonged periods of drought [*Diffenbaugh and Giorgi*, 2012; *IPCC*, 2012]. Consequently, certain areas could see up to 40% decrease in winter precipitation under RCP8.5 scenario (the Representative Concentration Pathway that would lead to 4 °C of global warming) [*Tuel and Eltahir*, 2020].

The effects of climate change on Mediterranean agriculture are manifold. Higher temperatures together with changes in the amount and distribution of rainfall will result in increased competition for the already limited water supplies in many Mediterranean countries [*Cramer et al.*, 2018; *Iglesias and Garrote*, 2015; *IPCC*, 2022; *Tuel and Eltahir*, 2020]. Additionally, yield reduction and increased crop water demand are expected for various spring-grown crops. While the increases in CO_2 may reduce these negative effects partially, the yield loss will hardly be recovered entirely [*Skuras and Psaltopoulos*, 2012]. The changes in temperature and precipitation might render some crops unsuitable for production in the Mediterranean [*Ceglar et al.*, 2019; *Zagaria et al.*, 2023]. Moreover, crop phenological development will likely shift to earlier in the year which can result in yield decline for certain crops [*Moriondo and Bindi*, 2007; *Zagaria et al.*, 2023]. Furthermore, irrigation water requirements will be strongly affected, for example, the southern and eastern Mediterranean is expected to see an increase of up to 35% [*Fader et al.*, 2016].

1.3.3 Need for adaptation measures

Water scarcity, poor irrigation management, and progressing climate change have raised concerns about the sustainability and resilience of Mediterranean agriculture and have emphasized the need for adaptation measures [*Fader et al.*, 2016]. These measures include the switch to more efficient irrigation systems, adjustment of irrigation schedules, diversification of water resources, storage and harvesting of rainwater, or water pricing [*García-Tejero et al.*, 2014; *Harmanny and Malek*, 2019]. In addition to measures focussed on alternative water resources and improved irrigation efficiency, crop selection and management can be effective measures to mitigate climate change impacts. The FAO, for instance, has emphasized the role of perennial agriculture in protecting and improving soil ecosystem health and enhancing food security [*Batello et al.*, 2014; *Glover et al.*, 2010].

Supporting sustainable agricultural and water resources management will require a holistic understanding of the state and potential developments of Mediterranean crop production and the role of irrigation in water resources. The high diversity and distinctive characteristics of Mediterranean agricultural systems pose a challenge to establishing a comprehensive data base as well as to the development of modelling tools that can accurately represent these systems. Modern data observation networks and cost effective sensors can help leverage data availability of e.g., weather, soil, crop, and irrigation, which unfortunately is often limited, especially in southern Mediterranean countries [*Fader et al.*, 2015]. In addition, the continued development of process representations in LSMs can equip these models to guide decisions in crop production, irrigation, and water resources management at different scales to secure environmental sustainability as well as economic viability of Mediterranean agriculture.

1.4 Research objectives and thesis outline

The overall aim of this thesis is to improve the representation of crops and irrigation in LSMs and combine them with local observational data to assess crop water requirements and derive management recommendations that can ultimately lead to reduced irrigation water consumption while sustaining agricultural yield in the context of the Mediterranean region. The following sub-objectives were defined to achieve this goal.

The first objective is to examine the use of low-cost weather sensors to deliver accurate data and improve overall data availability for field-scale crop and water management as well as regional agricultural, hydrologic, or climate research and modelling. These sensors should be robust, reliable, easy to use and maintain, and should not deviate strongly from high-end sensors in order to be adequate for use in single site monitoring or as components of larger environmental observatories.

The second sub-objective is to improve the representation of perennial crop types within LSMs by including deciduous fruit trees in CLM5. To achieve this, the current model descriptions of annual crops and natural vegetation must be expanded to include new features that are unique to fruit trees and orchards. This should result in more reliable simulations of crop growth and water requirements, and reduce the existing bias in the representation of the biogeophysical and biogeochemical processes in regions where this type of cultivation is prevalent.

The third sub-objective addresses the critical role of irrigation in global food production, especially in semi-arid regions, and its impact on yield, land surface processes, and water resources. Despite its critical importance, irrigation is not yet accurately accounted for in most LSMs. It is therefore necessary to assess and improve the existing model capabilities, demonstrate how these improvements are relevant in advancing the incorporation of human land-water management into global LSMs, and illustrate how they can contribute to more sustainable irrigation and water resources management.

To address these objectives, the thesis is structured into five parts. Chapter 1 provided a general introduction and background to the following three chapters that are based on two peer-reviewed and published papers and one submitted paper.

In Chapter 2, the performance of the ATMOS41 all-in-one weather station (METER Group Inc.) is evaluated and its potential use in the context of microclimate monitoring for various user applications as well as research activities is discussed. This cost-effective and easy-to-use station can increase the availability of data, especially in remote regions and low-income countries. However, adequate calibration and testing should be performed to ensure sufficiently high data quality. Under this objective, three ATMOS41 were installed next to a high-performance reference station at an experimental site in Germany. Meteorological data was collected over a three-month period at a 10-min interval. Collected data of solar radiation, precipitation, air temperature, relative humidity, atmospheric pressure, wind speed, and wind direction was analysed using graphical and statistical techniques. The inter-sensor variability between the three stations and the overall quality of the weather data from the ATMOS41 compared to the reference station was assessed. Moreover, systematic and random errors were determined and potential limitations for the deployment of the ATMOS41 were discussed.

In Chapter 3, CLM5-FruitTree, a new sub-model for perennial deciduous fruit trees, is presented, which improves the representation of agricultural systems within the LSM CLM5. The development encompassed (1) a new perennial crop phenology description, (2) an adapted C and nitrogen allocation scheme, considering both storage and photosynthetic growth of annual and perennial plant organs, (3) typical management practices associated with fruit orchards, and (4) the parameterization of an apple plant functional type (PFT). Extensive field measurements from an apple orchard in South Tyrol, Italy were available to develop and test the sub-model. Measurements of biomass and C and nitrogen ratios of the individual plant organs, root distribution as well as literature values were used to parameterize the apple PFT. Additionally, a simple one-by-one sensitivity analysis was performed to further tune model parameters and assess the influence of newly added parameters on the simulation results. Finally, the simulation results were compared to observed LAI, yield, C, energy, and water fluxes from an eddy covariance station, and SM measurements.

Chapter 4 focusses on the representation of irrigation in CLM5. The new CLM5-FruitTree sub-model, as presented in Chapter 3, was used to assess irrigation practices and water consumption in a small Greek catchment dominated by apple orchards. First, the representation of local irrigation practices and resulting SM dynamics and crop

growth was evaluated at the point-scale. An irrigation data stream was implemented that allows to directly read in measured irrigation data. The simulations were compared to data collected from WSNs in two highly instrumented apple orchards and were forced with atmospheric data obtained from two ATMOS41 weather stations evaluated in Chapter 2. Subsequently, a regional modelling case was set up to compute irrigation requirements for the entire catchment. Based on these modelling results and using the irrigation stream, different irrigation deficit scenarios were created and their effect on yield and CWUE was examined to derive recommendations for regional irrigation management.

Finally, the thesis concludes with Chapter 5, in which a synthesis of this work is provided and directions for future research and applications are discussed.

2 Performance of the ATMOS41 All-in-One Weather Station for Weather Monitoring

This chapter is based on the following journal article:

Dombrowski, O., Hendricks Franssen, H. J., Brogi, C., & Bogena, H. R. (2021). Performance of the ATMOS41 All-in-One Weather Station for Weather Monitoring. Sensors, 21(3), 741. https://doi.org/10.3390/s21030741

Abstract

Affordable and accurate weather monitoring systems are essential in low-income and developing countries and, more recently, are needed in small-scale research such as precision agriculture and urban climate studies. A variety of low-cost solutions are available on the market, but the use of non-standard technologies raises concerns for data quality. Research-grade all-in-one weather stations could present a reliable, cost effective solution while being robust and easy to use. This study evaluates the performance of the commercially available ATMOS41 all-in-one weather station. Three stations were deployed next to a high-performance reference station over a three-month period. The ATMOS41 stations showed good performance compared to the reference, and close agreement among the three stations for most standard weather variables. However, measured atmospheric pressure showed uncertainties > 0.6 hPa and solar radiation was underestimated by 3%, which could be corrected with a locally obtained linear regression function. Furthermore, precipitation measurements showed considerable variability, with observed differences of ±7.5% compared to the reference gauge, which suggests relatively high susceptibility to wind-induced errors. Overall, the station is well suited for private user applications such as farming, while the use in research should consider the limitations of the station, especially regarding precise precipitation measurements.

2.1 Introduction

Weather monitoring plays a central role in the understanding of the hydrological cycle, weather forecasting, risk assessment and management as well as agricultural planning, the administration of natural resources, climate change studies and other public and private interests. Despite the fact that modern automatic weather station networks are typically well developed in high-income countries, data quality and station coverage are often limited in low-income countries due to high instrumentation and maintenance costs [*Nsabagwa et al.*, 2019; *Pietrosemoli et al.*, 2019; *WMO*, 2016]. Consequently, resources and trained personnel to set up and maintain a sufficient number of stations are lacking to adequately cover the spatiotemporal variability of meteorological variables [*Sabatini*, 2017; *WMO*, 2009]. Additionally, growing interest in microclimate monitoring for precision agriculture [*de la Concepcion et al.*, 2015; *Tenzin et al.*, 2017; *Watthanawisuth et al.*, 2009] or urban climate and heat island studies [*Gaitani et al.*, 2011; *Tomlinson et al.*, 2013] requires weather stations that are inexpensive, efficient, and provide local and reliable data for modelling applications. Ideally, the design of such weather stations meets the following criteria: (i) robustness to reduce calibration frequency; (ii) compact design for ease of handling and to minimize sensor damage; (iii) low maintenance; (iv) low power requirements; (v) low cost; (vi) compatibility with different logger systems; (vii) wireless communication.

With the increasing use of wireless sensor networks [*Yick et al.*, 2008], various non-standard low-cost weather monitoring systems have been developed in the past few years using a wide range of sensor hardware and different microcontroller architectures, such as Arduino [*Katyal et al.*, 2016; *Lopez and Villaruz*, 2015; *Saini et al.*, 2016] or Raspberry Pi [7,15,16]. These stations can be very cost effective, with prices of several hundred Euros [*Pietrosemoli et al.*, 2019], but they often lack adequate calibration and testing, raising concerns about the accuracy, precision, and reliability of the collected data [*Gunawardena et al.*, 2018]. However, information on data quality in terms of both the accuracy and repeatability of such low-cost weather stations is crucial for modelling applications and decision-making [*Aponte-Roa et al.*, 2018; *Muller et al.*, 2015]. Furthermore, designing these non-standard devices requires sufficient knowledge of the associated hardware and software for installation and maintenance, while the moving parts may be susceptible to failure. Commercial all-in-one weather stations, e.g., [*Environmental XPRT*, 2020; *Gill Instruments Limited*, 2023; *Met One Instruments Inc.*,

2023], that incorporate multiple sensors in a single unit can be a viable alternative as they are easily deployable, generally cheaper than standard weather stations composed of individual sensors, and include manufacturer reported accuracy, precision, and calibration details. On the downside, they are less flexible in terms of adding or exchanging sensors and may suffer from interference between sensors due to their compact architecture [*Warne*, 2017]. Nonetheless, their plug-and-play principle and the compact design are clear advantages since they facilitate non-expert use and make them suitable for continuous deployment in rural or remote areas.

This study focuses on the assessment of the ATMOS41 all-in-one weather station that holds 12 embedded sensors, developed and produced by METER Group, Inc. The station is currently used in sub-Saharan Africa to improve crop production of maize [*Mutuku et al.*, 2020] and to build the Trans-African Hydro-Meteorological Observatory (TAHMO) network [*TAHMO*, 2020]. TAHMO aims at installing 20,000 hydro-meteorological stations across sub-Saharan Africa and collected data will be used for educational purposes at local schools as well as aid in scientific modelling, early warning systems, and the analysis of water availability [*van de Giesen et al.*, 2014]. Furthermore, the ATMOS41 has recently found applications in crop research and private sector sensor networks of various industrialized countries. In Portugal, the station is being used in the development of a forest monitoring system for fire detection [*Brito et al.*, 2020] and in the field of smart agriculture to improve vineyard management practices [*Valente et al.*, 2020]. In addition, the ATMOS41 is part of the Montana Mesonet monitoring stations in the Upper Missouri River Basin, where collected data are used for drought detection and natural resource management, amongst others [*Jencso et al.*, 2019]. Further applications include the investigation of crop water stress in apple orchards at Washington State University [*Mohamed et al.*, 2019] and the estimation of the plant growth status of paddy rice in Japan [*Xie et al.*, 2020].

METER and partners provide reports of calibration and sensor performance tests for the complete weather station or for individual components performed in the lab or in outdoor testbeds of the METER Pullman campus [*METER Group*, 2018]. Furthermore, [*Anand and Molnar*, 2018] conducted a first-order performance analysis of the early version of the station. The study compared 6 months of data recorded in 2017/2018 by the ATMOS41 station against a weather station of the Institute of Atmospheric and Climate Science (IAC) of ETH Zurich and a SwissMetNet solar radiation station located at 2.5

km distance from the test site. Overall, the ATMOS41 showed similar performance to the IAC station, but the authors suggested that further tests are needed.

Since its first release in 2017, several improvements of the ATMOS41 station were developed, some of which directly affect the measurement of certain variables and the overall performance of the station [*Ayman*]. These changes include: (i) improved sensor geometry to avoid adverse effects on wind measurements caused by heavy rain, (ii) improved sensor firmware and wind sensing algorithm, (iii) upgraded sensors and the addition of a secondary calibration for relative humidity and atmospheric pressure.

Considering the wide use of the ATMOS41 weather station for small- and large-scale weather monitoring in sub-Saharan Africa [*Mutuku et al.*, 2020; *TAHMO*, 2020; *van de Giesen et al.*, 2014] as well as industrialized countries [*Brito et al.*, 2020; *Jencso et al.*, 2019; *Mohamed et al.*, 2019; *Valente et al.*, 2020; *Xie et al.*, 2020], independent testing under "out of the lab" conditions can provide further insight and eventually identify possible limitations of the ATMOS41 station. In this way, a thorough performance assessment can inform private costumers and research organizations regarding the potential fields of application and provide impulses for further hardware or software developments. Therefore, the aim of this study is to carry out such in-depth assessment through direct comparison to an independent, high-performance weather station as well as the inter-comparison of multiple ATMOS41 stations. Within this context, the following questions will be addressed:

- What is the quality of weather data from the ATMOS41 weather station?
- What systematic or random errors affect the ATMOS41 station?
- How well does the ATMOS41 station perform compared to a high precision, high quality weather station?
- What are the limitations of the ATMOS41 station?

2.2 Materials and Methods

2.2.1 ATMOS41 all-in-one weather station

The ATMOS41 is an all-in-one weather station developed by METER Group, Inc. (Pullman, WA, USA). The device is rather inexpensive for developed countries (below EUR 2000), has a compact design with no moving parts, and can be mounted with minimal effort to ensure easy deployment in a variety of terrains and locations. The station has 12 embedded sensors that measure standard weather variables, namely solar radiation, precipitation, air temperature, relative humidity, atmospheric pressure, wind speed and direction, plus additional parameters such as lightning strike count or compass heading. Further characteristics of the station are summarized in Table 2.1.

Table 2.1 Characteristics of the ATMOS41 all-in-one weather station.

Characteristic	**ATMOS41**
Manufacturer	METER Group, Inc.
Cost	EUR 1750
Dimensions	Height: 34 cm, Ø = 10 cm
Warranty	1 year
Installation	Mount on pole, stand, or tripod; orient to true North; level the weather station
Maintenance	Recalibration: every 2 years; Cleaning: check for bird droppings and insect debris
Power requirements	Supply Voltage: 3.6 to 15 V Current draw: 8.0 mA during measurement, 0.3 mA while asleep
Operating temperature	−40 to +50 °C
Communication protocol	SDI-12
Additional equipment	Pole, stand or tripod and a data logger (third party loggers are compatible too)

2.2.2 Reference weather station

The performance of the ATMOS41 weather station was evaluated through a comparison with measurements from a meteorological station that serves as a backup station for the official Selhausen (C1) measurement site [*Schmidt et al.*, 2012], which is part of the Integrated Carbon Observation System (ICOS) [*ICOS*]. The backup station, hereafter referred to as ICOS-bkp, consists of individual, high-quality sensors that fully comply with the ICOS standard. This standard specifies minimum requirements for sensor selection as recommended by the World Meteorological Organization (WMO) [*WMO*, 2008] and includes detailed descriptions for measurement and calibration processes as well as regular maintenance [*Laurent*, 2017]. ICOS measurement uncertainty requirements are based on the “achievable uncertainty” that can be expected in

operational practice, as specified in the WMO Guide N° 8 [*WMO*, 2008]. The total equipment costs for an ICOS level one station are estimated at EUR 10,000 [*Brus et al.*, 2013], including the costs of logger and tripod (ca. EUR 1800 for the Selhausen station). The cost of weather sensors used at an ICOS station is hence more than four times the cost of an ATMOS41 device. The ICOS-bkp station records instantaneous values for solar radiation, temperature, and relative humidity at an interval of 20 s and an installation height of 2.5 m. Precipitation is recorded at a height of 1 m above ground, and a 10 min accumulated value recorded at a separate data logger was used for the comparison with the ATMOS41 stations.

Atmospheric pressure, wind speed, and wind direction are only recorded at the main ICOS station but are not recorded at the backup station. For the comparison of wind speed and direction, data recorded by a Vaisala WXT520 weather transmitter (Vaisala Corporation, Helsinki, Finland) were used. This instrument is installed at a height of 2 m above ground next to the ICOS-bkp station and records data for the SE_BDK_002 station of the TErrestrial ENvironmental Observatories network (TERENO) [*TERENO*, 2020] at a 10 min interval. The Vaisala WXT520 meets the high accuracy and precision standards specified by ICOS for wind speed and direction but has a measurement uncertainty of ±0.5 hPa for atmospheric pressure instead of the ±0.3 hPa required by ICOS standards. Therefore, the atmospheric pressure sensor at the main ICOS was used as a reference to the ATMOS41 stations.

2.2.3 Experimental setup

Data were collected from 23 April to 5 July 2020 (73 days) in Selhausen, Germany (50.87 N 6.45 E) at an altitude of 103 m a.s.l. The area is characterized by a temperate maritime climate with a mean annual air temperature of 10 °C and annual precipitation of 700 mm. The site is located in an agricultural area with the dominant crops being sugar beet, winter wheat, and winter barley [*ICOS*, 2020].

Three ATMOS41 weather stations (hereafter referred to as Atmos1, Atmos2 and Atmos3) were set up next to the Vaisala and ICOS-bkp stations. Atmos1 is the first generation of the station, purchased in 2017, and was previously deployed for a period of less than 6 months. Atmos2 and Atmos3 are the latest versions of the station, purchased in 2020, and used for the first time in this study. All three ATMOS41 stations were mounted in a row and installed at 2 m above ground (Figure 2.1). The stations were oriented north and

levelled according to the user manual [*METER Group*, 2017] to ensure accurate measurements of wind direction, precipitation, and solar radiation. Cumulative or instantaneous data were recorded at a 10 min interval for precipitation and all other variables, respectively. The ATMOS41 stations were connected to a CR1000X data logger (Campbell Scientific Ltd., Logan, UT, USA) which was powered via a 12 V battery connected to a battery charger.

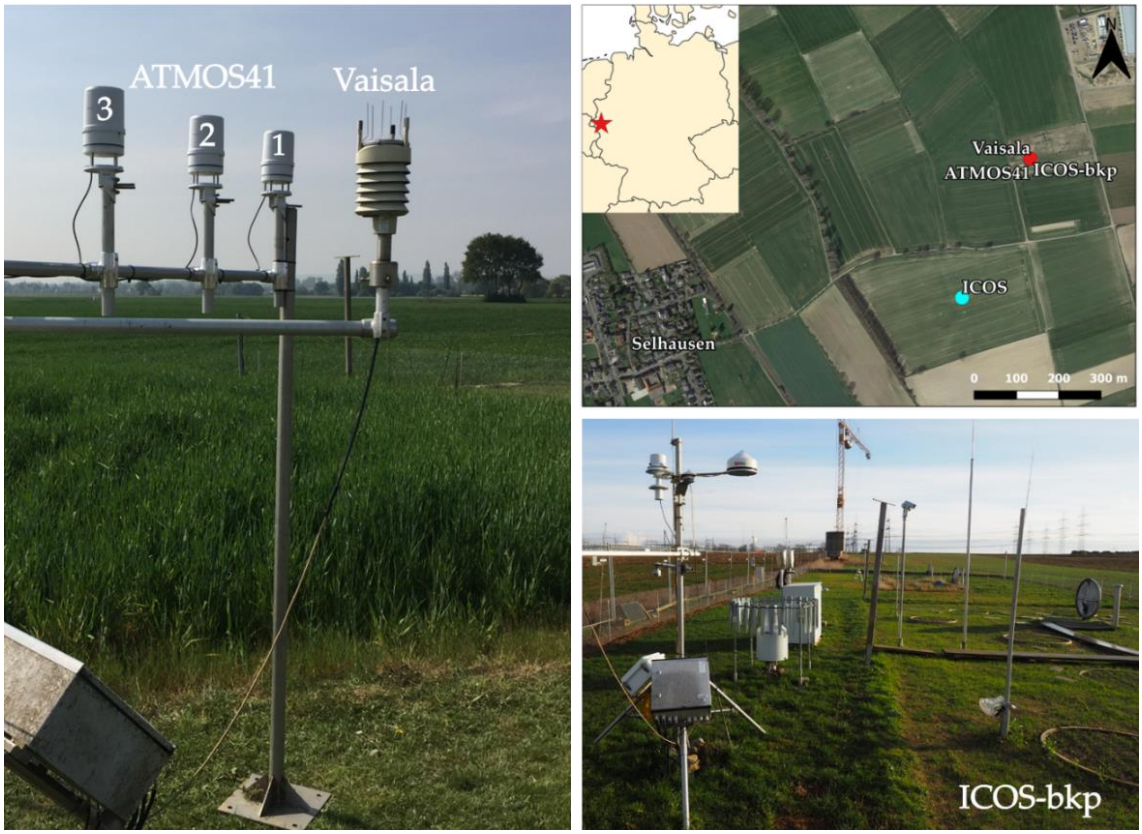

Figure 2.1 Experimental site with the three ATMOS41 stations, the Vaisala weather transmitter and the ICOS-bkp station.

Details on the sensors that measured each variable for the ATMOS41 and for the ICOS-bkp, ICOS or Vaisala stations, including approximate costs for individual sensors used at the reference stations, are listed in Table 2.2. The accuracy of most weather sensors used in the ATMOS41 station, as stated by the manufacturer, is compliant with the "achievable uncertainty" standard used by ICOS, with the exception of the air temperature and atmospheric pressure sensor (ICOS standard of ±0.1 °C and ±0.3 hPa, respectively).

Table 2.2 Sensor details for the ATMOS41 weather station as well as the ICOS-bkp, Integrated Carbon Observation System (ICOS) or Vaisala station.

Parameter	ATMOS41	ICOS-bkp, ICOS or Vaisala
Radiation	Miniature pyranometer with silicon-cell (Apogee Instruments, Logan, USA) Resolution: 1 W/m^2 Accuracy: ±5%	Pyranometer with permanent ventilation/heating (CMP21, Kipp & Zonen, Delft, Netherlands; EUR 900) Resolution: 1 W/m^2 Accuracy: ±1%
Precipitation	Optical sensor rain gauge with 68 cm^2 catch area (METER Group Inc., Pullman, USA) Resolution: 0.017 mm Accuracy: ±5% (up to 50 mm/h)	Weighing rain gauge with 200 cm^2 catch area (Pluvio^2, Ott HydroMet, Kempten, Germany; EUR 5000) Resolution: 0.05 mm within an hour Accuracy: ±1 mm
Temperature	Thermistor, non-aspirated (METER Group Inc., Pullman, USA) Resolution: 0.1 °C Accuracy: ±0.6 °C	Resistance thermometer PT100 1/3 Class B (HC2S3, Rotronic, Bassersdorf, Germany; EUR 900) Resolution: 0.01 °C Accuracy: ±0.1 °C
Relative humidity	(METER Group Inc., Pullman, USA) Resolution: 0.1% Accuracy: ±3% (varies with temperature and humidity)	ROTRONIC® Hygromer IN-1 (HC2S3, Rotronic, Bassersdorf, Germany) Resolution: 0.02% Accuracy: ±0.8%
Pressure	Barometric pressure sensor (METER Group Inc., Pullman, USA) Resolution: 0.1 hPa Accuracy: ±1.0 hPa	BAROCAP® sensor (PTB110, Vaisala Inc., Helsinki, Finland; EUR 730) Resolution: 0.1 hPa Accuracy: ±0.3 hPa (at +20 °C)
Wind speed	Ultrasonic anemometer (METER Group Inc., Pullman, USA) Resolution: 0.01 m/s Accuracy: the greater of 0.3 m/s or 3%	WINDCAP® ultrasonic transducer (WXT520, Vaisala Inc., Helsinki, Finland; EUR 2350) Resolution: 0.1 m/s Accuracy: ±3% at 10 m/s
Wind direction	Ultrasonic anemometer (METER Group Inc., Pullman, USA) Resolution: 1° Accuracy: ±5°	WINDCAP® ultrasonic transducer (WXT520, Vaisala Inc., Helsinki, Finland) Resolution: 1° Accuracy: ±3°

2.2.4 Performance analysis

Python software (version 3.7.6, Python Software Foundation) was used for the graphical and statistical evaluation of the data quality and performance of the ATMOS41 weather station. Data were checked for consistency and erroneous measurements were removed manually. Wind speed and relative humidity were computed according to the procedure described in the ATMOS41 user manual [*METER Group*, 2017]. Data from the ICOS-bkp and ICOS station were resampled to 10 min instantaneous data for comparison to the ATMOS41 data. Measured atmospheric pressure was corrected for the difference of 3.7

m in observation height (combination of elevation and sensor installation height) between the instrument locations using the barometric formula, while the effect of the distance of 350 m between the stations was considered negligible. Graphical evaluation included time series plots and scatterplots for each parameter. Additionally, residual plots and correlation matrices were obtained and analysed. Residuals were calculated by subtracting the value obtained at the ATMOS41 stations from the value measured at the reference station using hourly mean values (hourly sums for precipitation).

The statistical analysis of solar radiation only considered daytime values as measured nighttime solar radiation was zero. For the evaluation of measured precipitation, all time steps without precipitation were discarded. Statistical analysis of precipitation additionally included an event-based approach using a minimum rainfall amount of ≥ 0.2 mm/event and a minimum inter-event time of 1 h.

For statistical comparison, the Arithmetic Mean (μ) of the measured variables was calculated. Other metrics included the Coefficient of Determination (R^2, Eq. (2.1)) as a measure of agreement between two stations. The Root Mean Square Error (RMSE, Eq. (2.2)) was used as a measure of the difference between two stations. The RMSE is sensible to outliers since higher weights are given to larger deviations between two stations [*Walther and Moore*, 2005]. The Mean Bias Error (MBE, Eq. (2.3)) was used as a measure of the average error between a station and the reference, with positive values indicating an overestimation and negative values indicating an underestimation. The MBE should be used in combination with other metrics as it is subject to cancellation errors since the sum of positive and negative values may result in a smaller MBE [*Ruiz and Bandera*, 2017]. Lastly, the Mean Absolute Error (MAE, Eq. (2.4)) was used as a measure of the absolute difference of a measurement compared to the reference measurement. It is not subject to cancellation errors and is less sensitive to outliers compared to the RMSE [*Walther and Moore*, 2005].

$$R^2 = 1 - \frac{\sum_{i=1}^{N}(y_i - \hat{y}_i)^2}{\sum_{i=1}^{N}(\hat{y}_i - \bar{y})^2} \tag{2.1}$$

$$RMSE = \sqrt{\frac{1}{N}\sum_{i=1}^{N}(y_i - \hat{y}_i)^2} \tag{2.2}$$

$$MBE = \frac{\sum_{i=1}^{N}(y_i - \hat{y}_i)}{N} \tag{2.3}$$

$$MAE = \frac{1}{N}\sum_{i=1}^{N}|y_i - \hat{y}_i| \quad (2.4)$$

where y is the reference value, $\hat{y}$ is the measured value, $\bar{y}$ is the mean of the reference value, and N is the number of measurements.

2.3 Results and Discussion

2.3.1 ATMOS41 inter-sensor variability

Instrument orientation data were recorded in the X- and Y-orientation for all three ATMOS41 stations to identify undesired rotation or tilt. Orientation data (Figure 2.2) showed that all stations remained stable within ±2 degrees of dead level in X- and Y-direction as recommended for accurate measurements in the user manual [*METER Group*, 2017]. A few larger tilts that exceed the ±2 degrees mark are observed in Figure 2.2, which mostly coincide with wind speeds > 6 m/s (data not shown). However, only ~0.3% of measurements were affected for Atmos2 and Atmos3 and large tilts were never sustained for more than a few measured time steps. For Atmos1, a larger 2.6% of measurements were affected due to a small, temporary change in orientation between 24 and 29 April 2020, which was likely caused by a movement of the whole mounting structure. In addition, Atmos1 showed a slight misalignment of 0.5 to 1.0 degrees compared to Atmos2 and Atmos3, which was not considered significant.

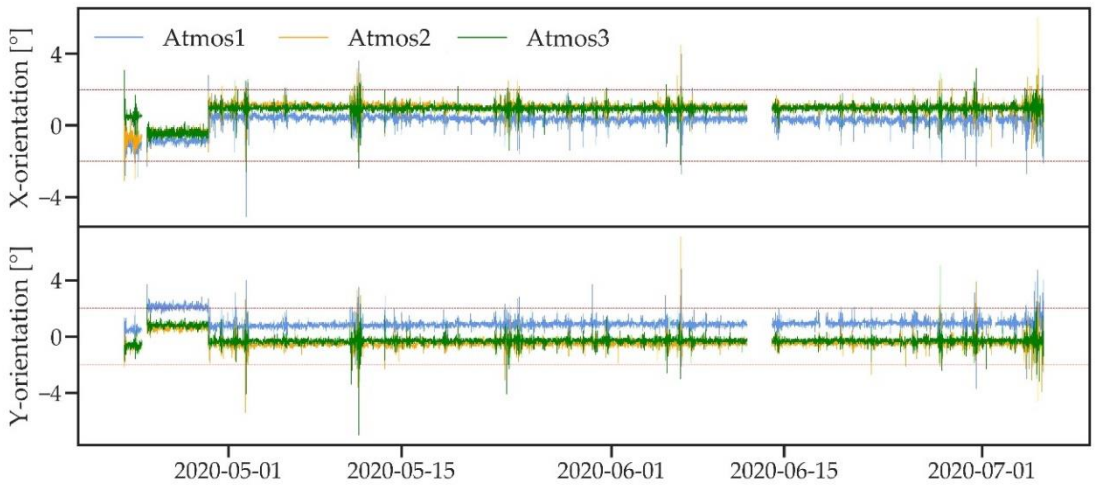

Figure 2.2 *X*- and *Y*-orientation for the three ATMOS41 weather stations. The red dotted line indicates ±2 degrees from dead level.

The inter-sensor variability of the three ATMOS41 stations was analysed for the entire observation period (23 April to 5 July 2020) for all standard weather variables by examining 10 min instantaneous data. Figure 2.3 shows a pairwise comparison of the three stations using scatterplots, histograms with probability density functions, and the R^2 value arranged in a matrix. The scatterplots show good agreement and no apparent bias between stations, with most of the data points lying in the proximity of the identity line. Some scattering effect can be observed for solar radiation (Figure 2.3a), which may have been caused by temporal shading of a single sensor or differences in response time to changing radiation. Relatively strong scatter can be observed in the wind speed measurements (Figure 2.3f), which was likely caused by other external effects such as small-scale turbulences around the stations. This scatter is reduced considerably when the data are aggregated to a larger time step (data not shown). The histograms and probability density functions of all measured variables generally show very similar distributions. Only in the case of relative humidity (Figure 2.3e) does Atmos1 show small differences in the distribution of values compared to the histograms of Atmos2 and Atmos3.

The comparison of all variables shows an $R^2 \geq 0.96$ except for wind speed, for which the R^2 ranges between 0.72 and 0.74. R^2 values increase when hourly averages are considered (data not shown), especially in the case of wind speed (R^2 increases to 0.91 for Atmos1 vs. Atmos2, 0.92 for Atmos1 vs. Atmos3, and 0.90 for Atmos2 vs. Atmos3). Despite most comparisons being rather satisfactory, there is slightly better agreement between Atmos2 and Atmos3 when compared to Atmos1 for solar radiation, atmospheric pressure, and relative humidity.

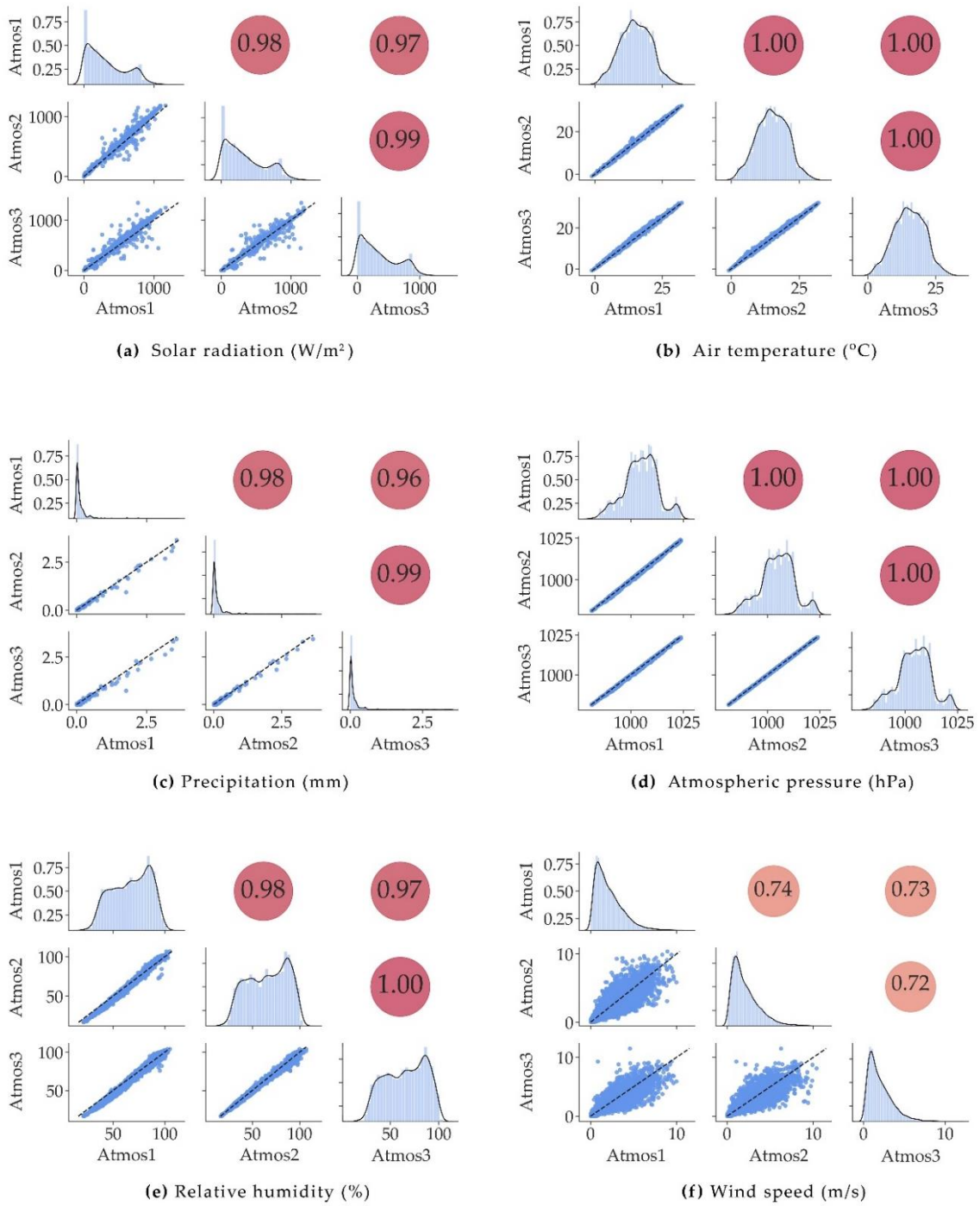

Figure 2.3 (a–f) Correlation matrices for all weather variables measured by the three ATMOS41 stations. Subplots in the lower left show scatterplots of station pairs with the dashed line indicating the 1:1 identity line, the diagonal shows histograms of measured values with probability density functions, upper right shows the coefficient of determination R^2.

A statistical summary with a pairwise assessment of all three ATMOS41 stations is given in Table 2.3. There is generally close agreement between all stations for most parameters with low RMSE and small MBE. Larger variability within the three stations was observed for wind speed and precipitation measurements. RMSE for wind speed is ~0.76 m/s at an average wind speed between 2.02 and 2.11 m/s. Atmos1 and Atmos2 measured on

average slightly higher wind speed compared to Atmos3 as shown by the mean and MBE. Precipitation measurements show a RMSE of ~0.06 mm at an average precipitation between 0.17 and 0.20 mm. The variability in precipitation measurements becomes more apparent when comparing the total precipitation amounts, which were unusually low for the observed months from late April to early July. The total amounts are 82.21 mm (Atmos1), 75.92 mm (Atmos2), and 70.79 mm (Atmos3), while long-term monthly means (1981–2010) are between 47 and 77 mm for the same months [*DWD*, 2021]. The difference between the three stations is considerable given the relatively short observation period and low total rainfall and stands in contrast to the test measurements performed by METER, where a difference of < 20 mm was observed within three ATMOS41 stations for a total of ~800 mm of rainfall over a period of 4 months [*METER Group*, 2018]. The results suggest that wind-induced random errors such as the deflection of air flow and the formation of eddies and turbulences around the gauges [*Sieck et al.*, 2007] had an important effect on the measurements. Atmos1 was positioned west-southwest of the other two stations, which was identified as the prominent wind direction during rainfall (data not shown). The three stations may have perturbed each other due to their alignment with respect to the wind direction and the relatively small distance between the stations, thus increasing the above-mentioned wind effects for Atmos2 and even more for Atmos3. This could explain the consistently lower amounts of rainfall measured by Atmos2 and Atmos3 compared to Atmos1. Low rainfall rates, as observed for most of the measurement period, show a high volumetric fraction of smaller drops (diameter < 1 mm), which are particularly prone to wind induced errors [*Nešpor and Sevruk*, 1999]. This may have caused the large observed variability despite the relatively low wind speeds observed during rainfall events and throughout the measurement period (~2 m/s).

Generally, somewhat lower RMSE and MBE were observed between Atmos2 and Atmos3 as opposed to Atmos1 for solar radiation, atmospheric pressure, and relative humidity. The greater similarity between the newer ATMOS41 variants with regard to the latter two variables is most likely a result of the sensor improvements implemented after 2017, as mentioned above. However, the most pronounced difference was observed for solar radiation, where a bias of ~−25 W/m^2 was found between the older Atmos1 (2017 version) and the newer ATMOS41 stations. In comparison, the bias between Atmos2 and Atmos3 was only −0.39 W/m^2 (Table 2.3).

Table 2.3 Statistical summary of the inter-sensor comparison for all standard weather variables measured by three ATMOS41 weather stations. Colours give an evaluation of the comparison, with red indicating the lowest and green the highest performance.

	μ			RMSE			MBE		
Parameter \ **Station °N**	**1**	**2**	**3**	**1 vs. 2**	**1 vs. 3**	**2 vs. 3**	**1 vs. 2**	**1 vs. 3**	**2 vs. 3**
Solar radiation [W/m^2]	320.26	345.21	345.6	38.34	47.37	32.76	−24.96	−25.35	−0.39
Precipitation [mm]	0.20 (82.21) *	0.18 (75.92) *	0.17 (70.79) *	0.06	0.08	0.05	0.015	0.027	0.012
Air temperature [°C]	15.05	15.11	15.26	0.22	0.38	0.34	−0.07	−0.22	−0.15
Atmospheric pressure [hPa]	1004.92	1004.70	1004.53	0.42	0.51	0.23	0.22	0.39	0.17
Relative Humidity [%]	67.35	66.18	65.56	3.26	3.49	1.38	1.17	1.79	0.62
Wind speed [m/s]	2.1	2.11	2.02	0.77	0.75	0.76	−0.009	0.089	0.098

* values in parentheses refer to the total precipitation amount during the observation period.

At first, the ageing of the pyranometer was considered as a possible explanation for the better agreement between the two newer ATMOS41 stations. This assumption was tested using previous data from the older Atmos1 (2017 version). Between 12 December 2017 and 24 May 2018 (164 days), the station was set up next to the ICOS site in Selhausen, 350 m from the ICOS-bkp station (Figure 2.1). Graphical and statistical analysis showed minor differences in the performance of the station between the two periods (data not shown), which is more likely a result of the different seasons and lengths of the two observation periods. The results suggest a stable performance of the Atmos1 over the 3-year period, even though calibration or maintenance were not performed. However, Atmos1 did not operate continuously throughout this period and hence it was not exposed to adverse weather conditions, such as strong solar radiation or heavy wind and precipitation. Therefore, sensor ageing or deterioration should be further studied, especially when continuous deployment of the station as part of a large monitoring network such as TAHMO is intended. A long-term assessment could include field visits, calibration checks and the establishment of statistical validation procedures as proposed in [*Estévez et al.*, 2011] or, if possible, comparison with a nearby reference station over an extended period.

Communication with the manufacturer allowed us to identify another possible issue related to the pyranometer provided by Apogee Instruments. A problem in the production of the early pyranometers was identified, which affected some of the earlier weather

stations and was solved at a later stage. This most likely explains the observed difference in performance between the older Atmos1 (2017 version) and the more recent Atmos2 and Atmos3 stations.

2.3.2 Comparison of ATMOS41 with ICOS backup station

In the following, data collected over the 73-day period that includes late spring and early summer months with a small data gap of two days in mid-June are compared. The first three weeks of radiation data for Atmos3 were missing due to a defect funnel that was later replaced. To better visualize the comparison of the different stations, only a period of eight days from 30 May to 6 June (23 April to 5 July for precipitation) is shown in this section. The full time series can be found in the Appendix (Figure A.1).

Table 2.4 shows a summary of the statistical performance analysis of the three ATMOS41 stations compared to the reference station. Overall, $R^2 > 0.90$ and relatively low RMSE, MBE and MAE were found for most variables except precipitation, wind speed, atmospheric pressure and solar radiation (only Atmos1). In the following, each variable is assessed in more detail.

Table 2.4 Statistical summary of the performance of three ATMOS41 stations compared to the ICOS-bkp or Vaisala reference station. Colours give an evaluation of the comparison, with red indicating the lowest and green the highest performance.

	R^2			RMSE			MBE			MAE		
Variable \ **Station °N**	**1**	**2**	**3**	**1**	**2**	**3**	**1**	**2**	**3**	**1**	**2**	**3**
Solar radiation (W/m^2)	0.96	0.99	0.99	56.46	31.88	32.28	−35.22	−9.03	−10.06	38.14	18.40	17.14
Precipitation (mm/10min)	0.92	0.93	0.93	0.13	0.13	0.13	0.02	−0.01	−0.02	0.08	0.09	0.08
Precipitation (mm/event)	0.99	0.99	0.99	0.19	0.24	0.30	0.06	−0.05	−0.17	0.11	0.15	0.21
Temperature (°C)	0.99	0.99	0.99	0.53	0.49	0.45	−0.37	−0.31	−0.16	0.42	0.38	0.33
Atmospheric Pressure (hPa)	0.98	0.99	1.00	1.17	0.89	0.75	1.01	0.79	0.63	1.02	0.80	0.64
Relative Humidity (%)	0.95	0.97	0.97	4.33	3.36	3.39	1.37	0.25	−0.36	3.47	2.50	2.55
Wind speed (m/s)	0.62	0.58	0.63	0.84	0.88	0.82	0.17	0.18	0.09	0.55	0.59	0.55

2.3.2.1 Solar radiation

Figure 2.4a shows an 8-day period of solar radiation as measured by the four weather stations. The timing and variability of radiation during the day are well captured by the ATMOS41 stations. However, the maximum measured solar radiation is slightly lower than that of the reference station, especially for Atmos1. On a clear day, Atmos3 shows a recurring small drop in solar radiation in the early morning, suggesting a shadow cast from a surrounding sensor. On overcast days such as 4 June, the four stations show almost identical measurements.

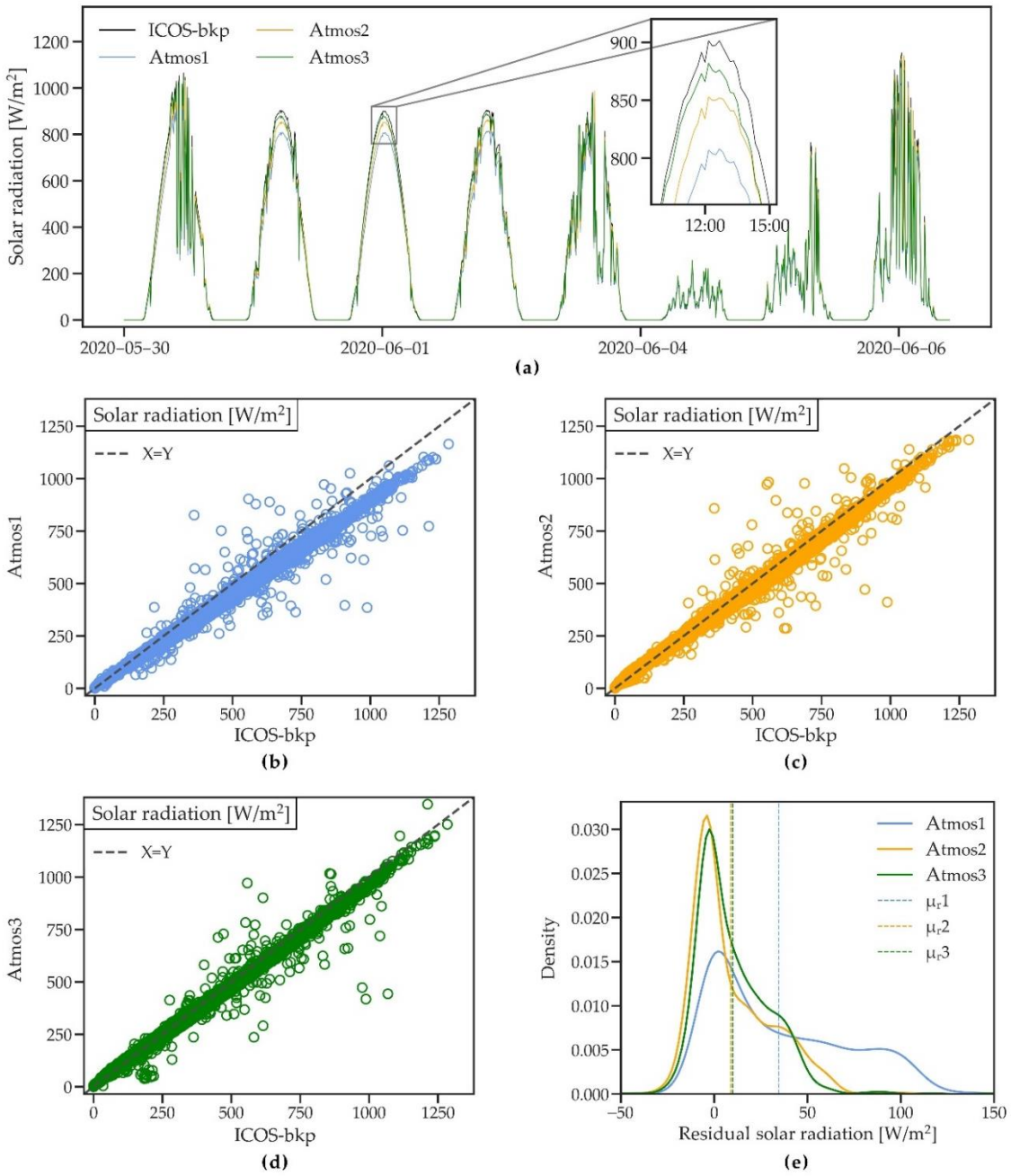

Figure 2.4 (a) A short time series of solar radiation measured by three ATMOS41 weather stations and the ICOS-bkp station from 30 May to 6 June 2020. (b–d) Scatterplots of 10 min solar radiation for the three ATMOS41 stations vs. the reference station. (e) Probability density functions of the residual mean hourly solar radiation. Dashed lines show the mean of residuals (μ_r).

The scatterplots of the ATMOS41 station vs. the ICOS-bkp (Figure 2.4b–d) confirm the overall good agreement of the stations, with an R^2 between 0.96 and 0.99 (Table 2.4). The plots show little scatter and RMSE is ~32 W/m^2 for Atmos2 and Atmos3 and somewhat higher for Atmos1 (56.46 W/m^2) (Table 2.4). Solar radiation values > 400 W/m^2 show a small underestimation by the ATMOS41 (Figure 2.4b–d).

Figure 2.4e depicts the deviation between the three ATMOS41 stations and the ICOS-bkp station through a probability density plot of the residuals from hourly average data, which considers only daytime solar radiation. The peaks of the distributions show a small tendency of the ATMOS41 stations to measure higher values (negative residuals), which occurs at lower solar radiation as suggested by the scatterplots (Figure 2.4b–d). The underestimation of high solar radiation is represented in the right tail of the distribution (positive residuals), with a mean bias of −35.22 W/m^2 for Atmos1 and mean biases of −9.03 and −10.06 W/m^2 for Atmos2 and Atmos3, respectively (Table 2.4).

The presented results for the Atmos1 generally agree well with the analysis by [*Anand and Molnar,* 2018], which compared the 2017 version of the ATMOS41 station with a SwissMetNet station. In their study, a lower bias of 8.9% was found compared to the one in this comparison (9.9%). This may be attributed to the overall lower radiation during the winter period studied by [*Anand and Molnar*, 2018] as opposed to the early summer period of this study that included many sunny days. Despite the 2 km distance between pyranometers, the authors observed a lower MAE and RMSE (13.57 and 39.40 W/m^2) than what was found in this study, which may again be related to the characteristics of the observation period since the ATMOS41 measures more accurately in the lower radiation range.

Despite the small systematic deviation from the reference ICOS-bkp station, the quality of the radiation measurements provided by the ATMOS41 was satisfactory. The newer stations show considerable improvement compared to the 2017 version of the station (Atmos1) and confirm the comparison test performed by the manufacturer, where a linear regression (y = 1.0323x) showed ~3% underestimation [*METER Group,* 2018]. Linear regressions for Atmos2 (y = 1.0372x) and Atmos3 (y = 1.0336) were similar to the one found by METER (Figure A.2). Granting that this bias persists in other climates and locations and compared to other high-performance pyranometers, a simple linear correction function may be developed and used to adjust the measurements.

2.3.2.2 Precipitation

Figure 2.5a shows an 8-day period with several precipitation events between 28 April and 4 May. The timing of the events agrees well for all four stations, but there are some differences in magnitude and the effect of the different measurement resolutions (0.017 mm for the ATMOS41 and 0.05 mm within an hour for the Pluvio^2 that is used at the

ICOS-bkp station) is visible. A direct comparison of the rainfall measured by the two gauges is complicated given the difference in measurement resolution, gauge size and shape, and installation height, as well as the use of a windshield with the Pluvio^2. The difference in resolution caused a greater scatter for small rainfall amounts in the 10 min time series (Figure 2.5b), with an R^2 ~0.9, RMSE ~0.15, and MAE ~0.10 mm for the three stations. The event-based analysis compared 46 rainfall events with rainfall amounts ranging between 0.2 and 19.5 mm and showed more coherent results with R^2 ~0.99 (Figure 2.5c). On average, Atmos1 measured higher precipitation, Atmos3 measured somewhat lower precipitation, while Atmos2 showed the least bias compared to the reference station (Table 2.4).

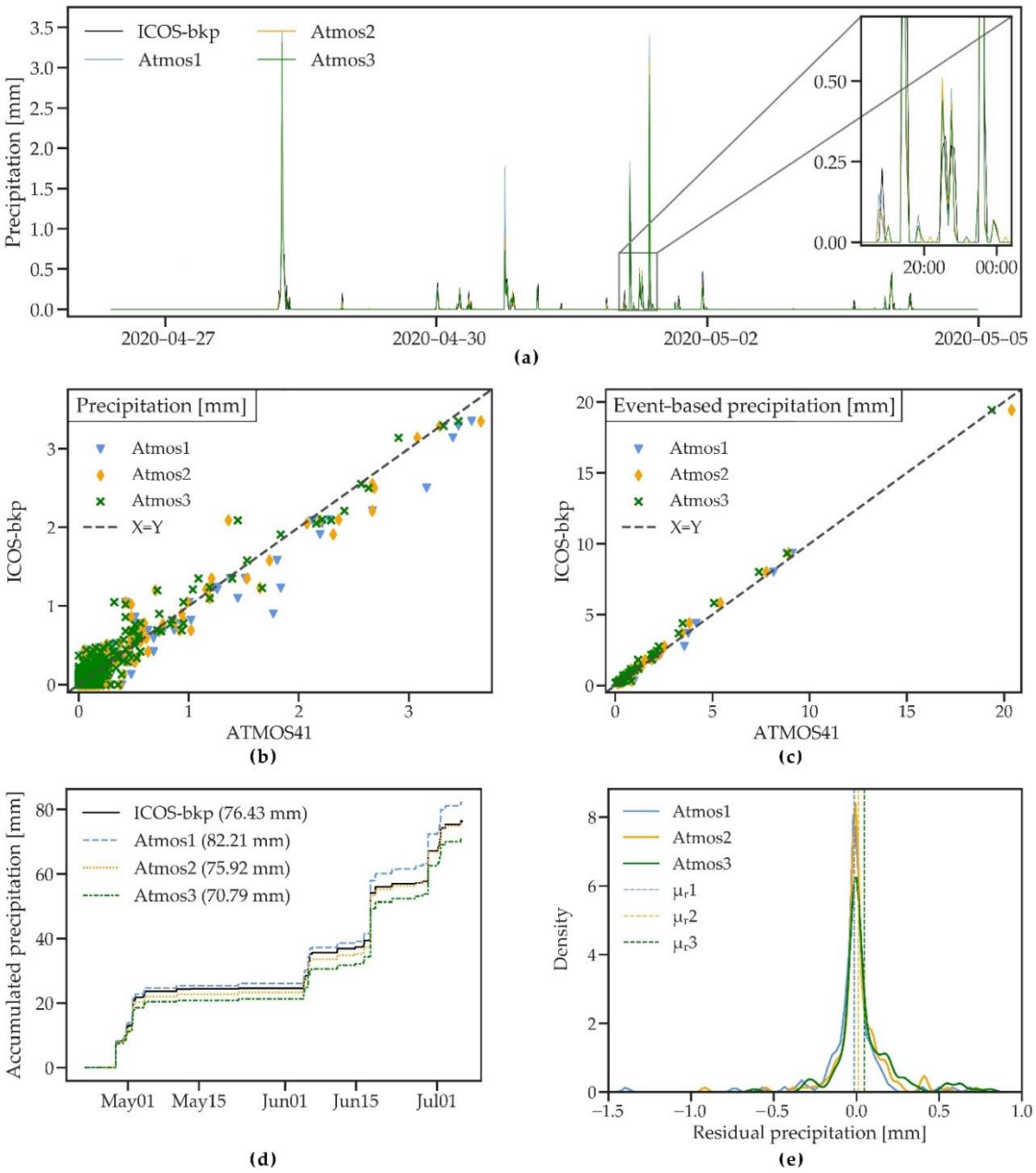

Figure 2.5 (a) A short time series of precipitation measured by three ATMOS41 weather stations and the ICOS-bkp station from 28 April to 4 May 2020. (b,c) Scatterplots of 10 min precipitation and event-based precipitation sum for the three ATMOS41 stations vs. the reference station. (d) Cumulative precipitation measured by the three ATMOS41 weather stations and the reference station for the whole time series (numbers in parentheses refer to total precipitation amount). (e) Probability density functions of the residual hourly precipitation sum. Dashed lines show the mean of residuals (μ_r).

Differences between the stations are more apparent when the cumulative precipitation for the observation period is analysed (Figure 2.5d). Total differences in precipitation compared to the reference are 5.78 mm (7.56%), −0.51 mm (−0.67%), and −5.64 mm (−7.38%) for Atmos1, Atmos2, and Atmos3. The difference to the reference rain gauge and between the ATMOS41 stations (as discussed in Section 2.3.1) is considerable and shows higher discrepancies than what is reported by the manufacturer (within 3% of the

average of three tipping-spoon rain gauges) [*METER Group*, 2018]. Surprisingly, *Anand and Molnar* [2018] found an underestimation of only 8.7%, even though their observation period included the entire winter season with several snowfall events. Since the ATMOS41 rain gauge is not heated and solid precipitation first needs to melt before it can be measured, higher errors could be expected during that period. This could not be further investigated, since snow was not observed during the measurement period of the present study. However, many applications such as agricultural monitoring or the use of the station in snow free climates do not rely on accurate measurements of the volume of solid precipitation.

As previously discussed in Section 2.3.1, wind-induced errors have likely played an important role in the measurement of rainfall, leading to significant errors considering the relatively small total precipitation amount and low rainfall intensities that were characteristic for the observed period. Additionally, gauge size and shape influence the deformation of the wind field at the gauge and minor changes in installation height can cause differences of up to 10% in precipitation measurements, as comparison studies of different rainfall gauges have shown [*Nešpor and Sevruk*, 1999; *Sevruk and Klemm*, 1989]. A higher wind-induced under catch could therefore be expected for the ATMOS41 stations that were installed at an approximate height of 2 m compared to the Pluvio^2 that is installed at a height of 1 m and uses an Alter windshield which has shown to improve the performance of the gauge [*Colli et al.*, 2016; *Kochendorfer et al.*, 2017]. The higher precipitation amount measured by the Atmos1 could be a result of the frequent detection of very small rainfall amounts, since the Pluvio^2 does not measure fine precipitation below a threshold of 0.05 mm within an hour.

Rainfall intensity during the observation period rarely exceeded 10 mm/h, a commonly used threshold for heavy rainfall [*DWD*, 2020]. Those events did not show lower accuracy of the ATMOS41 station, but a longer observation period with higher rainfall intensities is needed to accurately assess the performance of the station during extreme events.

2.3.2.3 Air temperature

Figure 2.6a shows air temperature data of the four stations during an 8-day period. Temperature dynamics are well captured by all ATMOS41 stations. However, daily maximum temperature and temperature during rainfall (5 June) are slightly lower and show a higher noise level for the ATMOS41 stations. The latter could be a result of a wet,

exposed temperature sensor or its immediate surroundings, making it more prone to evaporative cooling compared to the shielded ICOS-bkp sensor. In comparison, *Anand and Molnar* [2018] found that night-time lows measured by the ATMOS41 were generally lower compared to the IAC instrument, while showing high relative humidity. The authors observed temperatures ranging from −13 to 23 °C with a mean temperature of 4.5 °C, as opposed to the mean temperature of 15 °C measured during the present study. The scatterplots (Figure 2.6b–d) and statistical analysis (Table 2.4) show very good performance of the ATMOS41 with values close to the identity line, little scatter, and R^2 close to 1. RMSE and MAE are between 0.33 and 0.53 °C for all stations, nearly 50% lower than the RMSE and MAE reported in *Anand and Molnar* [2018].

Similar to the findings of *Anand and Molnar* [2018], there is a small mean bias towards lower temperature measured by the ATMOS41 (MBE between −0.16 and −0.37 °C), as also reflected in the probability density plot of the hourly residuals (Figure 2.6e). The temperature sensor of the ATMOS41 is exposed to solar heating, which is why an energy balance correction is used to calculate the actual temperature. The correction factor is proportional to solar radiation and inversely proportional to wind speed. Since errors in the measurement of those two variables may propagate to the temperature measurement, the overestimation of wind speed may explain the small bias in the measurement (Table 2.4). However, most values lie within 0.5 °C difference. Additionally, no tendency to lower accuracy with temperatures > 30 °C was identified, which suggests that the ATMOS41 measurements are reliable within the observed range of −1.1 to 32.2 °C. Even though the accuracy of ±0.6 °C, as stated by the manufacturer, does not meet the "achievable uncertainty" standard of ±0.2 °C used by ICOS, air temperature measurements with the ATMOS41 were reliable and consistent.

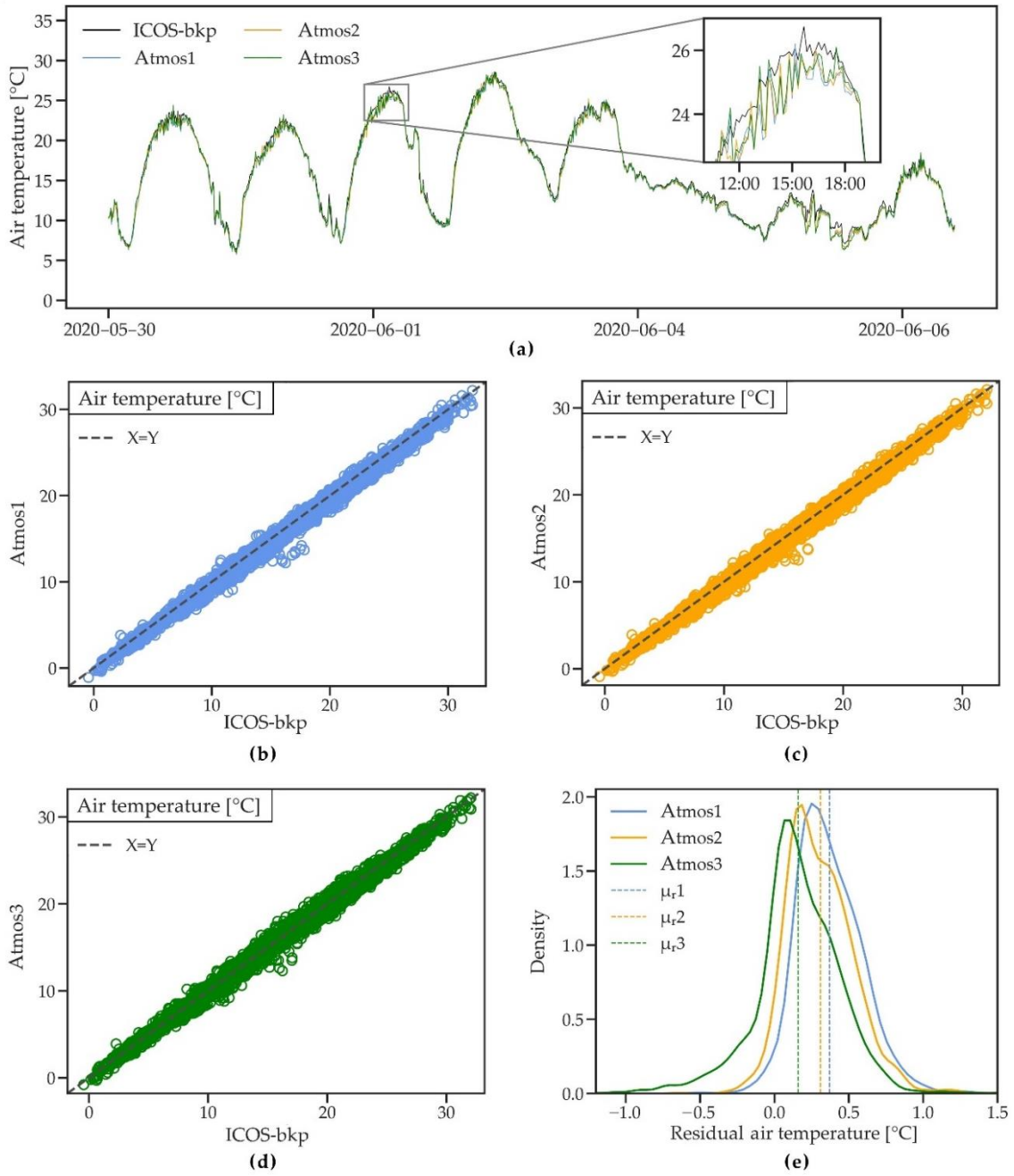

Figure 2.6 (a) A short time series of air temperature measured by three ATMOS41 weather stations and the ICOS-bkp station from 30 May to 6 June 2020. (b–d) Scatterplots of 10 min air temperature for the three ATMOS41 stations vs. the reference station. (e) Probability density functions of the residual mean hourly air temperature. Dashed lines show the mean of residuals (μ_r).

2.3.2.4 Atmospheric pressure

Figure 2.7a shows atmospheric pressure measured by the four stations during an 8-day period. The ATMOS41 stations closely follow the reference station with small differences that are consistently found during daily peaks and at lower pressures, which generally coincide with rainfall. The high $R^2 \geq 0.97$ indicates good agreement of the measurements. However, RMSE and MAE are relatively large, ranging between 0.75 and 1.17 hPa and

0.64 and 1.02 hPa, respectively. In agreement with *Anand and Molnar* [2018], the scatterplots (Figure 2.7b–d) and the probability density plot (Figure 2.7e) show a small bias towards higher values measured by the ATMOS41 compared to the reference station (MBE between 0.63 and 1.01 hPa). Atmos1 shows slightly lower overall performance, which was likely improved as a consequence of the secondary calibration added for the newer stations (see Section 2.1). While the ATMOS41 performs satisfactorily within the manufacturer stated accuracy of ±1 hPa, the pressure sensor does not meet the "achievable uncertainty" requirement of 0.3 hPa as commissioned by the WMO [*WMO*, 2008]. Therefore, the ATMOS41 shows only moderate performance in measuring atmospheric pressure compared to the reference station.

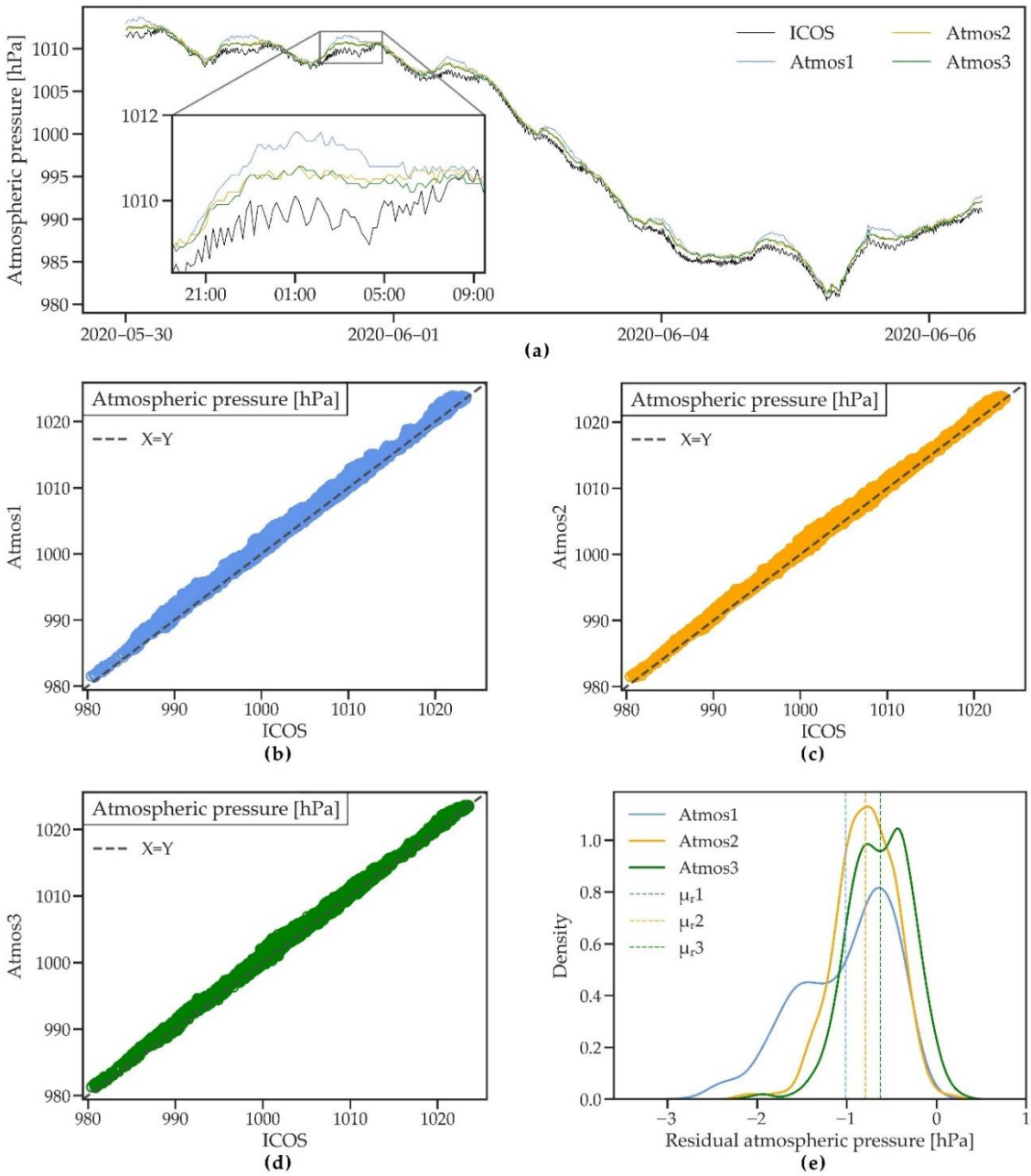

Figure 2.7 (a) A short time series of atmospheric pressure measured by three ATMOS41 weather stations and the ICOS-bkp station from 30 May to 6 June 2020. (b–d) Scatterplots of 10 min atmospheric pressure for the three ATMOS41 stations vs. the reference station. (e) Probability density functions of the residual mean hourly atmospheric pressure. Dashed lines show the mean of residuals (μ_r).

2.3.2.5 Relative humidity

Figure 2.8a shows relative humidity as measured by all four stations during an 8-day period of the measured time series. Relative humidity is captured well by the ATMOS41, with slightly higher humidity measured only during rain events such as 5 June for all ATMOS41 stations. This matches the observed small underestimation of temperature during rain events, as discussed in Section 2.3.2.3. Atmos1 additionally shows higher values during the daytime minimum humidity. The statistical summary (Table 2.4) shows $R^2 \geq 0.95$ for all stations and RMSE and MAE range from 3.4 to 4.3% and 2.5 to 3.5%, respectively, with Atmos1 showing slightly poorer performance than Atmos2 and Atmos3.

The scatterplot for Atmos1 (Figure 2.8b) confirms a small bias towards higher values for lower relative humidity and towards lower values when humidity is high. As a result, the Atmos1 shows a relatively higher MBE of 1.37% compared to Atmos2 and Atmos3 (MBE of 0.25 and −0.36%, respectively). This indicates that the manufacturer's adaptation of the calibration function (see Section 2.3.1) for the newer stations resulted in an improvement compared to the older Atmos1 (2017 version). The probability density plot of the residuals (Figure 2.8e) confirms the improved performance of the newer stations.

The ATMOS41 stations tend to saturate at 100% relative humidity more frequently than the reference station, which seems to verify the observation of *Anand and Molnar* [2018] and which may also be related to the underestimation of air temperature, as discussed in Section 2.3.2.3.

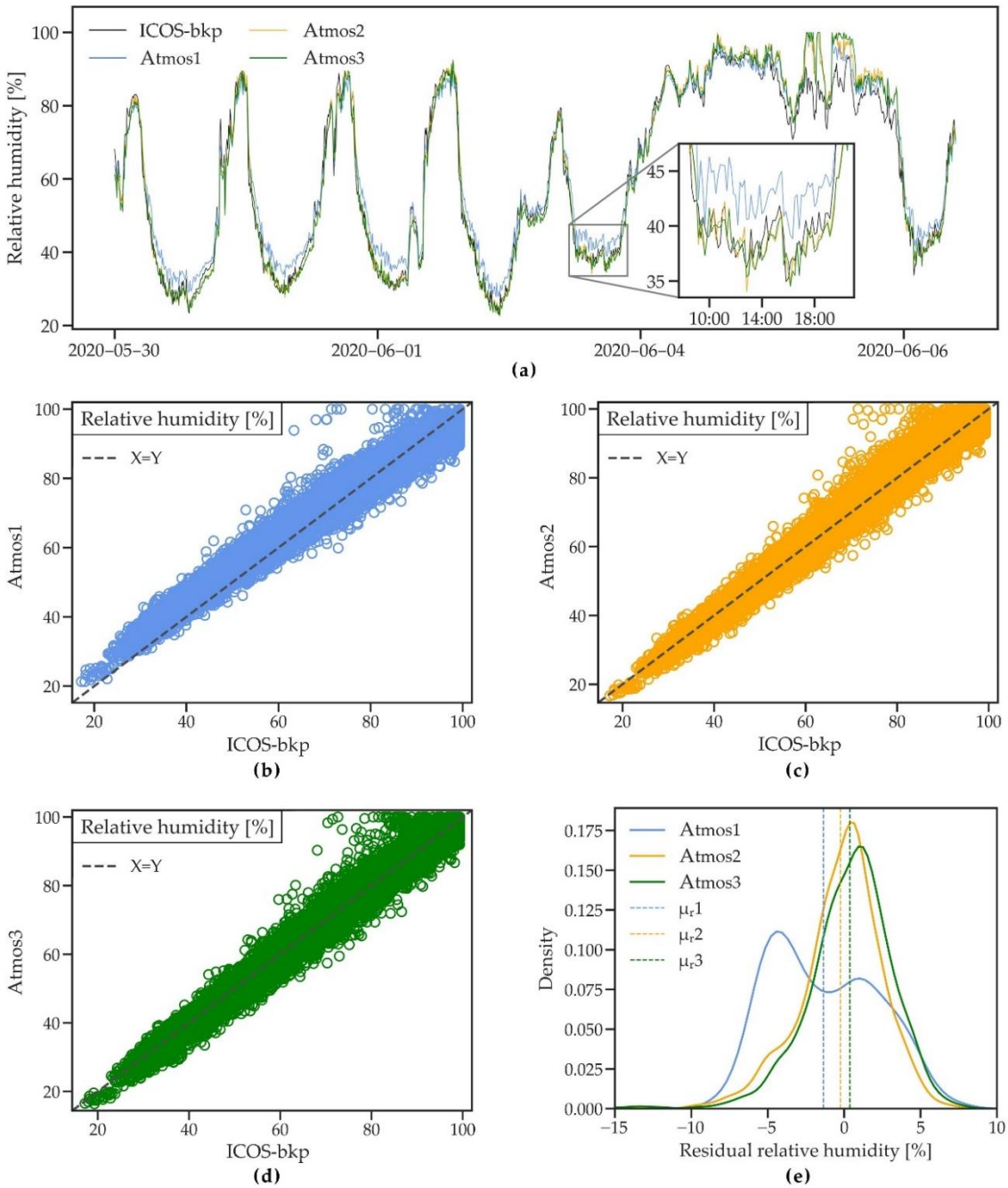

Figure 2.8 (a) A short time series of relative humidity measured by three ATMOS41 weather stations and the ICOS-bkp station from 30 May to 6 June 2020. (b–d) Scatterplots of 10 min relative humidity for the three ATMOS41 stations vs. the reference station. (e) Probability density functions of the residual mean hourly relative humidity. Dashed lines show the mean of residuals (μ_r).

2.3.2.6 Wind speed and direction

Figure 2.9a shows wind speed measured by the four stations during an 8-day period. Daily wind dynamics measured by the three ATMOS41 stations match well with the measurements of the Vaisala station. However, measurements by the ATMOS41 show higher peak values and a larger variability compared to the Vaisala station, which can be explained by the finer resolution of the anemometer of the ATMOS41.

The scatterplots (Figure 2.9b–d) show relatively large scatter around the identity line, with an R^2 between 0.58 and 0.63. The wide spread in wind measurements is likely a result of small-scale turbulence caused by surrounding instruments, as discussed in the context of the precipitation measurements in Section 2.3.2.2 and which are captured due to the rapid response of ultrasonic anemometers to sudden changes in wind speed [*Ammann*, 1994]. R^2 increases up to 0.89 when hourly averages are considered, suggesting that the scatter can be reduced when small-scale differences average out over larger periods. RMSE and MAE are ~0.9 and ~0.6 m/s, respectively (Table 2.4). The probability density plot of the residuals (Figure 2.9e) shows a small mean overestimation of wind speed (negative residuals) with MBE between 0.09 and 0.18 m/s, with Atmos3 showing the best performance. Both station types used in this comparison use ultrasonic anemometers, which can measure very low wind speeds. Therefore, the agreement found in this comparison was higher than that of *Anand and Molnar* [2018], where the ATMOS41 was compared to a cup anemometer that records zero wind speed values more frequently.

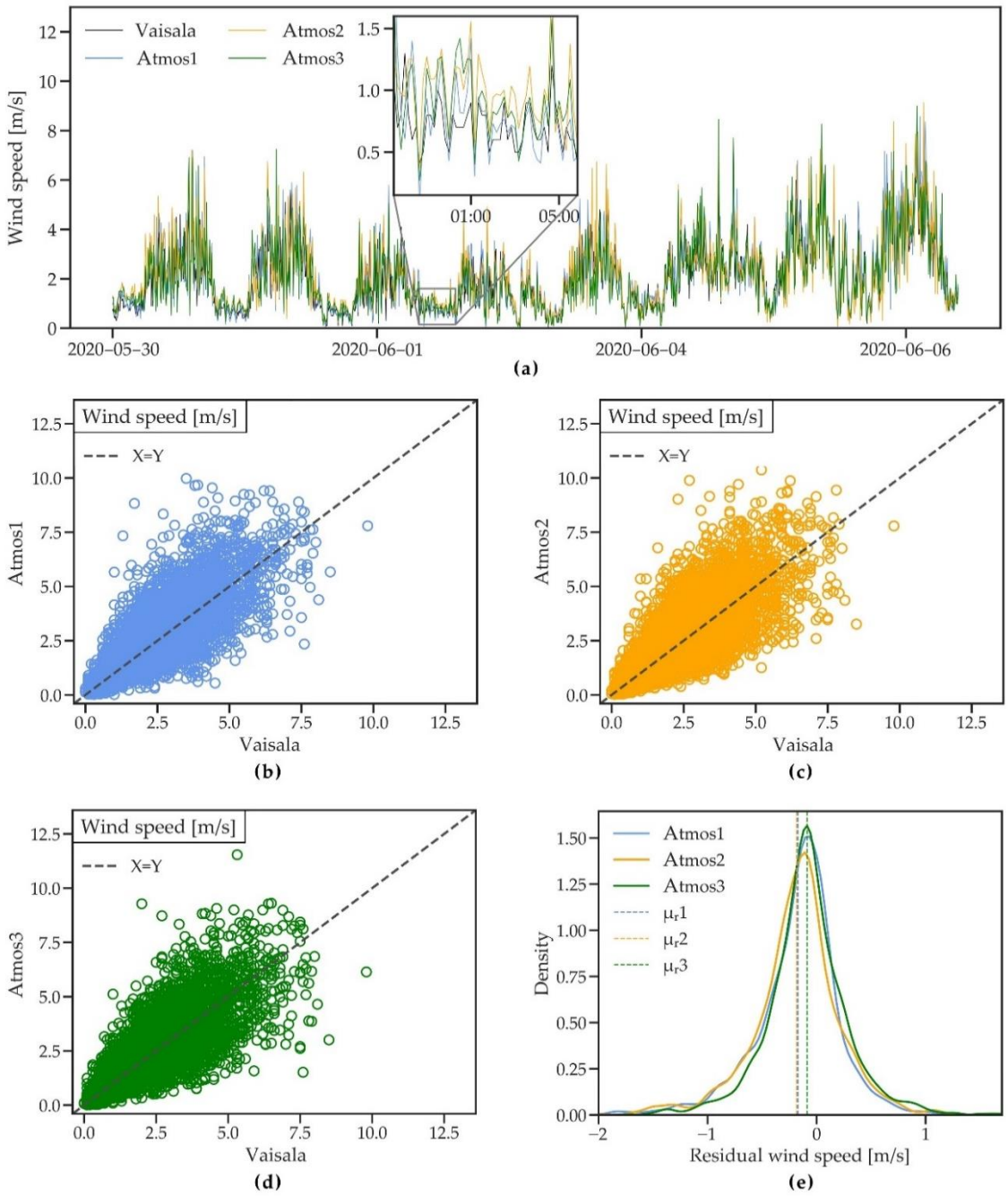

Figure 2.9 (a) A short time series of wind speed measured by three ATMOS41 weather stations and the ICOS-bkp station from 30 May to 6 June 2020. (b–d) Scatterplots of 10 min wind speed for the three ATMOS41 stations vs. the reference station. (e) Probability density functions of the residual mean hourly wind speed. Dashed lines show the mean of residuals (μ_r).

Wind direction was compared by drawing wind roses for each station (Figure 2.10a–d), where the length of the bins represents the frequency of the observed direction in percent, while colours indicate the magnitude of wind speed. West to South-West and East are dominant wind directions that occur, in total, ~40% of the time with a top frequency of around 7.5% for West/South-West, while wind from the North is observed in total ~13% of the time. The measurements from the Vaisala station agree well with the commonly

observed wind direction at the Selhausen site [*Schmidt et al.*, 2012]. Strong winds were mainly observed from West and South-West and sometimes from the North, while East winds were considerably weaker. Wind roses from the ATMOS41 stations agree in the main wind directions and speed with the reference station. Atmos1 more frequently recorded northerly winds with a top frequency of ~7%, while Atmos2 and Atmos3 recorded West/South-West winds with a higher frequency of ~10% as compared to the reference station. Wind roses for the newer ATMOS41 stations differ somewhat from that of Atmos1 likely due to adjustments made by the manufacturer (Section 2.3.1). Although our results do not show a significant improvement of the measurement from the older Atmos1 (2017 version) to the newer ATMOS41 stations, wind direction is still measured reasonably well by the ATMOS41.

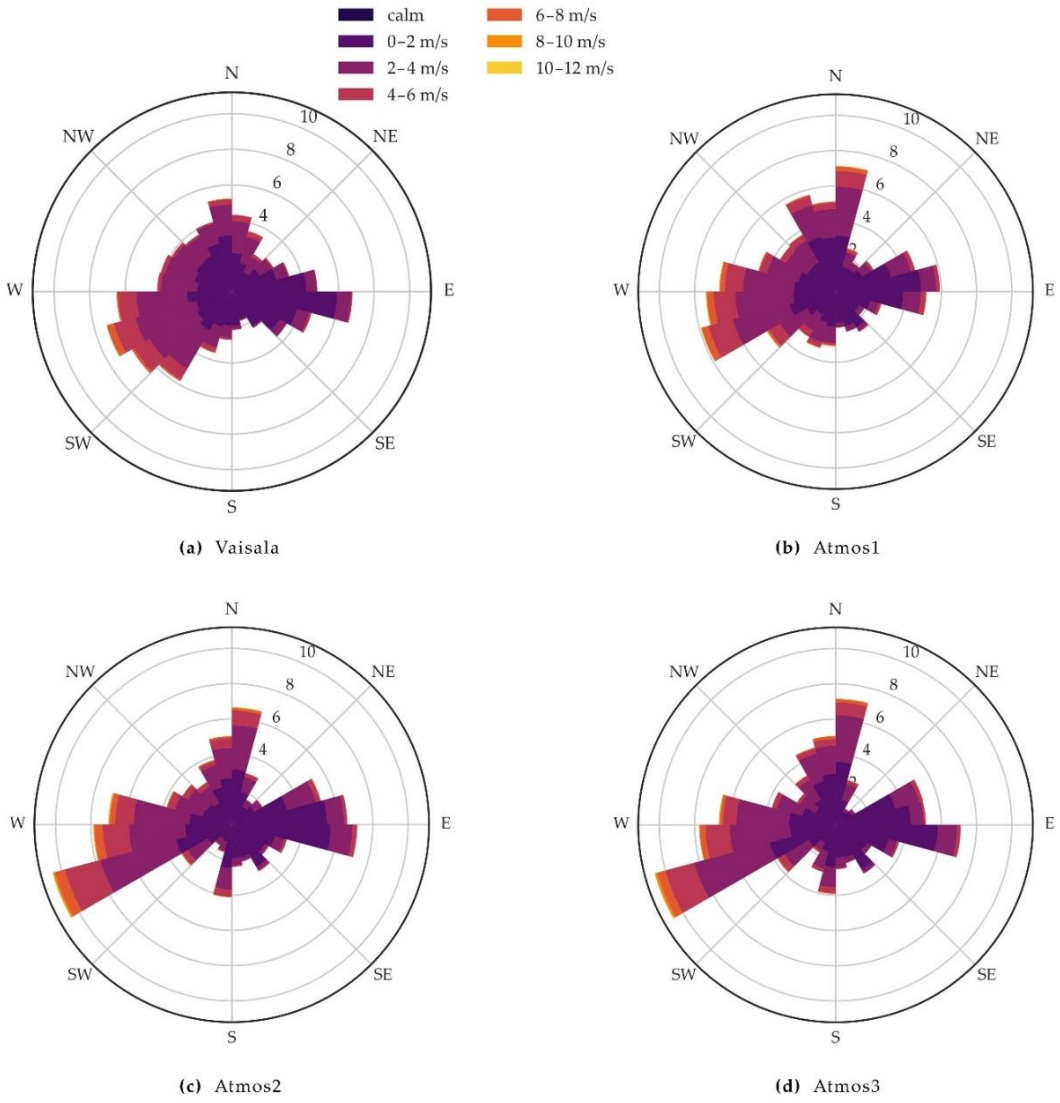

Figure 2.10 Wind roses showing the frequency of observed wind direction at a 10 min interval measured by (a) the Vaisala reference station. (b–d) the three ATMOS41 weather stations, for the period from 23 April to 5 July 2020.

2.4 Conclusions

This study evaluated the performance of the ATMOS41 all-in-one weather station over a period of 73 days by assessing the inter-sensor variability of three stations and by comparison against high quality, highly standardized reference meteorological stations. Inter-sensor comparison of the three ATMOS41 stations showed overall close agreement for most variables, while the newer Atmos2 and Atmos3 stations performed better in measuring atmospheric pressure, relative humidity and solar radiation compared to the older Atmos1 (2017 version). Solar radiation showed the greatest improvement, where the bias was reduced from 35.22 W/m^2 to ~9.55 W/m^2. Generally good agreement with $R^2 > 0.95$ and small biases were observed for most of the examined weather variables when compared to the reference station. If reference solar radiation data are locally available, a simple linear correction function was proposed to account for the 3% systematic bias that remained in solar radiation measured by the ATMOS41. The atmospheric pressure sensor of the ATMOS41 showed only moderate performance compared to the ICOS station, showing greater uncertainty in the measurements than recommended by the "achievable uncertainty" standard commissioned by the WMO. The measurement of wind speed by the ATMOS41 was slightly overestimated and showed relatively large scatter. Better results are achieved with hourly or half-hourly averages, which are suitable for most modelling applications. The largest variability between the stations was found in the measurement of precipitation, where total precipitation measured by the ATMOS41 showed differences around ±7.5% compared to the reference. This was attributed mainly to wind-induced errors that may have been exacerbated due to the close proximity of the three ATMOS41 stations as well as differences in the measurement resolution and architecture of the compared rain gauges.

The results of this study showed similar or improved performance of the ATMOS41 compared to the early performance test, but also revealed its limitations. Further work should focus on the performance assessment of the ATMOS41 during extreme precipitation and wind speed as well as the long-term durability and accuracy of the station. The station seems to be well suited for private users. In particular, farmers in high-income countries can benefit from its compact design and limited maintenance requirements. Developing countries may similarly benefit from the ATMOS41 station when costs are jointly carried by multiple actors that use the collected data to market data products to private and governmental institutions. This strategy is applied within the

TAHMO project. Due to the higher uncertainty related to atmospheric pressure and precipitation measurements, and the non-heated gauge, the use of the ATMOS41 station in research appears to be better suited for studies where the amount of solid precipitation is not relevant, where precise rainfall or atmospheric pressure is not a key parameter or when multiple gauges can be deployed to calculate average values for a given location. Overall, the ATMOS41 is a good compromise between measurement accuracy and cost effectiveness, making it an attractive component of wireless sensor networks as well as an expansion tool for weather monitoring networks in remote areas or under limited financial resources.

3 CLM5-FruitTree: A new sub-model for deciduous fruit trees in the Community Land Model (CLM5)

This chapter is based on the following journal article:

Dombrowski, O., Brogi, C., Hendricks Franssen, H.-J., Zanotelli, D., & Bogena, H. (2022). CLM5-FruitTree: a new sub-model for deciduous fruit trees in the Community Land Model (CLM5). Geoscientific Model Development, 15(13), 5167-5193. https://doi.org/10.5194/gmd-15-5167-2022

Abstract

The inclusion of perennial, woody crops in land surface models (LSMs) is crucial for addressing their role in carbon (C) sequestration, food production, and water requirements under climate change. To help quantify the biogeochemical and biogeophysical processes associated with these agroecosystems, we developed and tested a new sub-model, CLM5-FruitTree, for deciduous fruit orchards within the framework of the Community Land Model version 5 (CLM5). The model development included (1) a new perennial crop phenology description, (2) an adapted C and nitrogen allocation scheme, considering both storage and photosynthetic growth of annual and perennial plant organs, (3) typical management practices associated with fruit orchards, and (4) the parameterization of an apple plant functional type. CLM5-FruitTree was tested using extensive field measurements from an apple orchard in South Tyrol, Italy. Growth and partitioning of biomass to the individual plant components were well represented by CLM5-FruitTree, and average yield was predicted within 2.3% of the observed values despite low simulated inter-annual variability compared to observations. The simulated seasonal course of C, energy, and water fluxes was in good agreement with the eddy covariance (EC) measurements owing to the accurate representation of the prolonged growing season and typical leaf area development of the orchard. We found that gross primary production, net radiation, and latent heat flux were highly correlated ($r > 0.94$) with EC measurements and showed little bias ($< \pm 5\%$). Simulated respiration components, sensible heat, and soil heat flux were less consistent with observations. This was attributed to simplifications in

the orchard structure and to the presence of additional management practices that are not yet represented in CLM5-FruitTree. Finally, the results suggested that the representation of microbial and autotrophic respiration and energy partitioning in complex, discontinuous canopies in CLM5 requires further attention. The new CLM5-FruitTree sub-model improved the representation of agricultural systems in CLM5 and can be used to study land surface processes in fruit orchards at the local, regional, or larger scale.

3.1 Introduction

Orchards and other perennial fruit crops are a major component of the global agricultural production with significant coverage and yield in China, the United States, south-western Africa, and some parts of Europe [*FAO*, 2021a]. In the European region, perennial crops are a key economic element of Mediterranean agro-ecosystems as they provide 45% of the local agricultural output [*Lobianco and Roberto*, 2006]. Apples are the most important fruit tree crop as one third of European orchards is devoted to their production. With a coverage of 984,509 ha, they provide a yearly harvest of over 17 million tons which is one fifth of the overall European fruit production in terms of output value [*FAO*, 2021a].

In contrast to annual crops, fruit trees can be productive for several decades before rotation is needed. Their prolonged growing season, standing biomass, and low respiratory losses can support carbon (C) storage and promote higher C use efficiencies [*Wünsche and Lakso*, 2000; *Zanotelli et al.*, 2013]. The transport of C stored in biomass into the soil in addition to reduced soil tillage and disturbances under fruit orchards compared to annual crops further promote C sequestration [*Bwalya*, 2012; *Ledo et al.*, 2020; *Wu et al.*, 2012]. The FAO has therefore suggested perennial agriculture as a possible measure to mitigate climate change and enhance food security [*Glover et al.*, 2010], and many studies have recently investigated this potential for various fruit orchards [*Hammad et al.*, 2020; *Scandellari et al.*, 2016; *Wu et al.*, 2012; *Yasin et al.*, 2021]. The study of water and irrigation requirements in fruit orchards has become another field of intense research due to the need for a more resilient agriculture in the context of climate change and water supply shortages [*El Jaouhari et al.*, 2018; *Maestre-Valero et al.*, 2017; *O'Connell and Scalisi*, 2019; *Segovia-Cardozo et al.*, 2022]. In order to answer questions related to C sequestration, water requirements, and sustainable food

production of fruit orchards, a better understanding of the related ecosystem processes is vital [*Fader et al.*, 2015].

Models with a comprehensive description of the carbon, water, and energy fluxes, such as global land surface models (LSMs), are a powerful tool to explore complex ecosystems like the abovementioned fruit orchards. The use of LSMs was recently extended to not only model the processes at the land–atmosphere interface, but also to study the response of ecosystems and water resources to climate change [*Blyth et al.*, 2021; *Fisher and Koven*, 2020; *Prentice et al.*, 2015]. To quantify these effects, LSMs need to represent a wide range of land use and vegetation types. However, most LSMs consider only perennials such as deciduous and coniferous trees, as well as major annual crops such as wheat, soy, or maize [*Lawrence et al.*, 2018]. Recently, some LSMs additionally included bioenergy crops [*Schaphoff et al.*, 2018], while others group crops into a few generic crop types [*Balsamo et al.*, 2009; *Krinner et al.*, 2005; *Noilhan and Mahfouf*, 1996]. Despite their significance, perennial crops, such as fruit trees, are rarely considered in LSMs and attempts of including them in global and regional modelling environments are scarce [*Cheng et al.*, 2020; *Fader et al.*, 2015]. An example of such an attempt is the inclusion of agricultural trees (e.g., grapes, cotton, and apple trees) in the Lund-Potsdam-Jena managed Land (LPJmL) model to improve the representation of Mediterranean agro-ecosystems [*Fader et al.*, 2015]. Here, agricultural trees were modelled as small trees and fruit harvest was determined as the product of a plant specific harvest index and the net primary productivity (NPP). Other authors parameterized oil palm trees, a perennial evergreen crop, in the Community Land Model (CLM) version 4.5 [*Fan et al.*, 2015]. Palm trees were represented by a new phenology where large palm leaves with fruit bunches emerge successively, leaves are pruned regularly, and harvest occurs once a month. Recently, two perennial grasses for energy production were parameterized in the latest version of the model, CLM5 [*Cheng et al.*, 2020]. Parameters for bioenergy crops were tuned using sensitivity analysis and observations, while harvest was represented by removing around 70% of the aboveground biomass.

While the abovementioned studies describe some common features of perennial plants, they do not, or only partially, represent the seasonal deciduous phenology of fruit trees or the explicit modelling of fruit growth. Furthermore, key aspects such as C reserve accumulation and mobilization in the following spring are generally not considered, possibly due to necessary simplifications or because the drivers of these processes are

still not fully understood [*Le Roux et al.*, 2001; *Neumann*, 2020]. The absence of perennial crops in land surface models introduces a significant bias in the representation of biogeophysical and biogeochemical processes in agro-ecosystems where this type of cultivation is prevalent. As a result, the response to climate change in terms of C sequestration, water requirements, or food production cannot be assessed adequately in regions such as the Mediterranean, where perennial, woody crops are very common and play a vital role for food security and economy [*Fader et al.*, 2015; *Lobianco and Roberto*, 2006].

Although deciduous fruit trees share certain characteristics with natural vegetation and annual crops in LSMs such as CLM5, several particularities in their growth dynamics and management practices still prevent a meaningful simulation using currently available representations of vegetation. In this study, we therefore provide CLM5 with the ability to model perennial fruit trees and the associated processes. For this purpose, we developed a new sub-model named CLM5-FruitTree within the existing model framework of CLM5. CLM5-FruitTree combines elements of the broadleaf deciduous tree subroutine such as growth and C turnover of woody components, with distinctive phenological stages and a harvestable organ similar to the annual crop subroutine. We first describe the model conceptualization including the new phenology, carbon and nitrogen (CN) allocation, and management options. We further demonstrate the applicability of CLM5-FruitTree by parameterizing a new apple plant functional type (PFT). Finally we evaluate and discuss the model performance using extensive field data from an apple orchard in South Tyrol, Italy.

3.2 Methods

3.2.1 Vegetation characterizations in CLM5

The latest version of the Community Land Model, CLM5, simulates the exchange of water, energy, C, and nitrogen (N) between land and atmosphere as well as their storage and transport on the land surface and in the subsurface, driven by climate variability and modulated by soil and vegetation states and characteristics. The land surface in CLM5 is characterized by one of five land units namely glacier, lake, urban, vegetated, and crop. These units are further divided to capture the variability in soil, vegetation, and

management options (i.e., irrigated or non-irrigated). Compared to previous model versions, CLM5 features various improvements in the representation of land use and vegetation modelling such as plant CN cycling, soil and plant hydrology and crop modelling [*Lawrence et al.*, 2018; *Lombardozzi et al.*, 2020].

Many of the C and N cycle components of CLM5 were originally derived from the Biome BioGeochemical Cycles (Biome-BGC) model [*Thornton et al.*, 2002]. Here, vegetation is represented conceptually by three different plant C and N pools that are maintained separately for the individual plant organs (leaf, live/dead stem, fine root, live/dead coarse root, and grain). The storage pools represent C and N reserves, the transfer pools serve as intermediate pools to separate fluxes in and out of the storage pools, and the display pools represent the actual growth of a given organ (Figure 3.1). C made available through photosynthesis is first used to support maintenance respiration of live organs based on organ N content, temperature, and a constant base rate as proposed by *Atkin et al.* [2015]. Dead stem and dead coarse root components are assumed to consist of dead xylem cells, without metabolic function (no C cost for maintenance). The remaining C can then be allocated to the growth of new tissue considering associated growth respiration costs. Maintenance respiration, growth respiration and C cost of N uptake from the soil comprise the autotrophic respiration component (R_a) in CLM5. Plant material reaching the end of its lifespan feeds into different litter pools from where it progressively decomposes to soil organic matter under C losses through heterotrophic respiration (R_h).

For the simulation of fruit orchards, a module for perennial deciduous crops is needed which is currently missing in CLM5. Such a module must account for the perennial deciduous nature of fruit trees, which is similar to the existing representation of broadleaf deciduous trees (BDTs) included in Biome-BGC but with differences in phenological triggers, vegetation structure, and C partitioning. In addition, it must represent growth and harvest of the fruits and typical management practices, of which some are already conceptualized in the prognostic Biogeochemistry Crop Module (BGC-crop), while others are not yet implemented. The algorithm for the seasonal phenology of BDT controls initial leaf development and senescence that mark the beginning and end of a growing season based on temperature and day length thresholds. Once a new growth period is initiated, C and corresponding N fluxes accumulated in the previous season, occur out of the storage pools into the transfer pools, from where they are gradually sent to the display pools (Figure 3.1). During the active growth period, C and corresponding

N storage pools are replenished based on specified C:N ratios of each plant organ. During leaf senescence, C and N pools feed the litter or coarse woody debris pool except for live stem and live coarse roots that are mostly retained as structural woody tissue (dead stem and dead coarse roots).

BGC-crop, adopted from the prognostic crop module of the Agro-Ecosystem Integrated Biosphere Simulator (Agro-IBIS), currently features eight different annual crop species with interactive crop management options (i.e., irrigation and fertilization). Another 23 currently inactive crop types can be defined but have not been provided with specific crop parameters [*Lombardozzi et al.*, 2020]. Crop phenology and CN allocation follow three phenological phases: (1) from planting to leaf emergence, (2) from leaf emergence to the start of grain fill, and (3) from grain fill to grain maturity and harvest, which are controlled by temperature and growing degree-day (GDD) thresholds. Different to natural vegetation, crops have a grain pool representing the harvestable organ but no structural woody tissue. Furthermore, all assimilates are directed to the displayed pools while the storage pools remain unused. At harvest, C and N from the grain pool are transferred to a grain product pool while a small amount is kept to reseed the crop in the following year. All remaining plant parts feed the litter cycle (Figure 3.1). The reader is referred to *Lombardozzi et al.* [2020] and the technical documentation of CLM5 for a more detailed description of the BDT and crop representation [*Lawrence et al.*, 2018].

From the above description of the existing vegetation modules, the following limitations for the application of CLM5 to deciduous fruit trees arise. (1) The current BGC-crop algorithm does not allow the simulation of perennial and/or woody crops. (2) The BDT phenology algorithm although describing some characteristics common to fruit trees, lacks the capability to simulate a harvestable organ, individual development of different plant parts, and the separation of growth from C reserves of the previous year and photosynthetic growth of the current season. (3) Typical management practices of fruit orchards such as transplanting of tree seedlings and pruning are currently not represented in CLM5. (4) There is no parameterized fruit tree PFT in the default parameter set of CLM5.

3.2.2 Model conceptualization and technical implementation

To resolve the model limitations discussed in Section 3.2.1, we developed a new sub-model CLM5-FruitTree to model the ecosystem processes and exchanges of energy and

matter of deciduous fruit trees grown in commercial orchards with a focus on the simulation of biomass growth and yield. More specifically, for the implementation of CLM5-FruitTree, we introduced a new phenology subroutine that describes the main phenological development of fruit trees and includes triggers for seasonal orchard management practices typical under organic or conventional production. In addition, the CN allocation module as well as corresponding modules (C and N state and flux updates) were modified to reproduce the growth dynamics of fruit trees and to model the fates of C and N in the orchard system. The sub-model development does not include any changes to the existing calculation schemes for radiative transfer or momentum, heat, and water fluxes to explicitly account for the discontinuous canopy structure of tree rows and vegetated or non-vegetated alleys in fruit orchards. In-row and between-row planting distances and alley vegetation are not defined directly. Instead, the orchard structure and the area covered by the canopy are accounted for through parameterization of the leaf and stem area indices, the planting density, maximum canopy height, and aerodynamic parameters, similar to the implementation of crops and forest in CLM5.

CLM5-FruitTree combines characteristics of both BDT and annual crops to simulate a perennial woody crop with a harvestable organ making use of the existing concepts of storage, transfer, and display vegetation pools described in Section 3.2.1 (Figure 3.1). Similar to the existing BDT phenology algorithm in CLM5, the fruit tree algorithm uses a perennial deciduous phenology with standing woody biomass and annual leaf shedding. During the active growth period however, the phenology and CN allocation of vegetative and harvestable organs are described by distinct growth phases and are driven by a GDD summation similar to the crop phenology.

An orchard is established by transplanting small tree seedlings from a nursery, a typical planting method for this type of cultivation [*Corelli-Grappadelli and Marini*, 2008; *Wheaton et al.*, 1990]. Once planted, the orchard remains productive according to a user-defined lifespan which, depending on fruit tree type and production system, typically ranges between 10 and 30 years [*Cerutti et al.*, 2014; *Demestihas et al.*, 2017]. The sub-model makes no specific assumptions about the rootstock, but the effect of different rootstocks in terms of tree height and rooting depth can be set by the user via the respective parameters, *ztopmx* and *root_dmx* (Table A.2). In CLM5-FruitTree, both stored C and current photosynthesis contribute to the growth of the fruit tree, as leaf and shoot development at the beginning of a growing season utilizes carbohydrate reserves and

nitrogenous compounds that were accumulated during the previous season [*Loescher et al.*, 1990; *Oliveira and Priestley*, 1988; *Tromp*, 1983]. Deciduous fruit trees are dormant in winter and resume growth in spring after meeting species- and cultivar-specific chilling and heat requirements [*Anderson et al.*, 1985; *Faust et al.*, 1997; *Zavalloni et al.*, 2006], which is represented in CLM5-FruitTree using the chilling and forcing model proposed by *Cesaraccio et al.* [2004]. Early in the season, the canopy develops rapidly until it reaches maturity typically by midsummer, while leaf shedding occurs when temperatures drop in autumn [*Kozlowski*, 1992; *Lakso et al.*, 1999; *Loescher et al.*, 1990]. Fruit trees usually start flowering 3–4 weeks after bud break, which is not specifically represented by CLM5-FruitTree which instead assumes that fruit growth begins at the end of flowering [*Lakso et al.*, 1999]. The implementation of flowering to include effects of non-optimal pollination, frost during flowering, or hormonal processes affecting fruit set and development is outside of the scope of this development and of minor importance for large-scale simulations and processes at ecosystem level that are typically the focus of LSMs such as CLM5. Consequently, CLM5-FruitTree does not produce information on fruit size or number but only on total yield which we consider adequate for most applications of the sub-model development. Fruit growth is described by two stages, cell division and cell expansion that together form a sigmoid growth curve observed for many fruit tree species such as apple, pear, and orange [*Corelli-Grappadelli and Lakso*, 2002; *Jackson*, 2011].

In the following, the new developments to account for the distinct phenology, CN allocation, and management practices of a fruit orchard are described in more detail. Other biochemical and biophysical processes such as photosynthesis, water and litter cycles, and fixation and uptake of N were not modified except for minor adaptations to the re-translocation of N and respiration to enable the use of certain parts of these scripts for the fruit tree PFT. The technical implementation of some features of the new phenology routine (transplanting, pruning, harvest, and final rotation) was based on CLM-Palm, a previous model development for palm trees in CLM4.5 (*Fan et al.* [2015] and unpublished code). References where code elements were directly reused or modified based on CLM-Palm are made in the published source code of CLM5-FruitTree [*Dombrowski*, 2022]. Along with the new sub-model, an apple PFT was parameterized using one of the existing but thus far inactive crop types in CLM5, types 35 and 36 (rainfed and irrigated citrus).

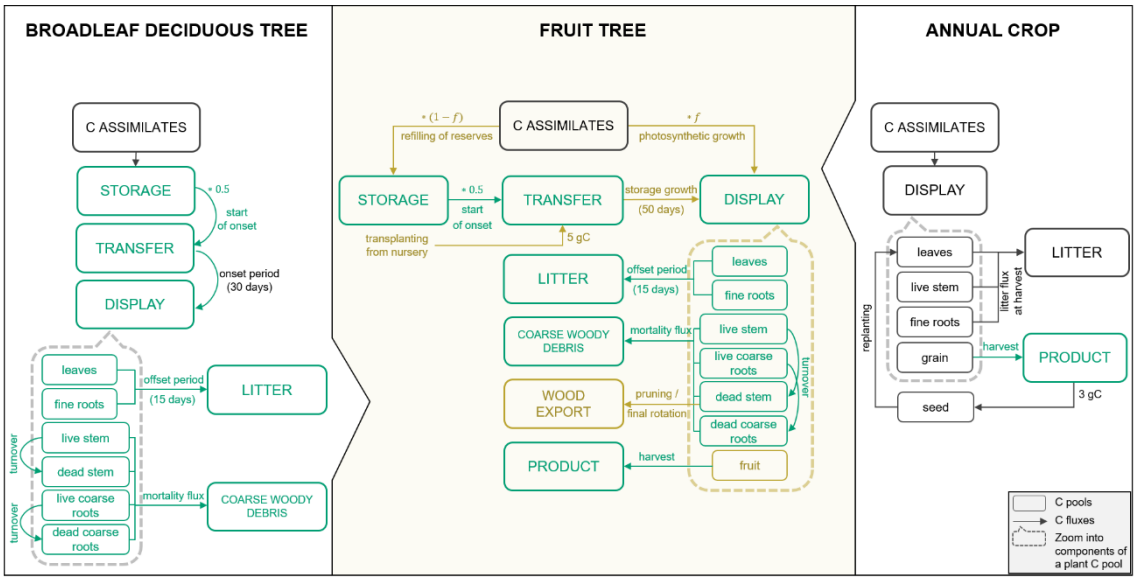

Figure 3.1 Schematic of the main phenology and C allocation features of the broadleaf deciduous tree and annual crop representations in CLM5 as well as the new sub-model CLM5-FruitTree. C pools within the dashed boxes are the individual components that make up the displayed C pool (the same components can be found for the other main plant pools: storage and transfer pools respectively). Carbon pools and fluxes in green were reused for CLM5-FruitTree while pools and fluxes in brown were modified or newly added.

3.2.2.1 Phenology

A new orchard life cycle is initialized by transplanting seedlings at the beginning of the year during dormancy. Tree growth thereafter is described by six post-planting phenological stages, namely: (1) bud break, (2) fruit growth, (3) fruit ripening, (4) canopy maturity, (5) fruit maturity and harvest, and (6) start of leaf senescence (Figure 3.2).

Bud break is predicted by a sequential model that first accumulates chill days followed by anti-chill days based on a predefined temperature threshold and chilling requirement [*Cesaraccio et al.*, 2004]. More information on the sequential model and the calibration of model parameters can be found in Appendix III. Outside the dormant period, leaf and fruit development occurs in parallel but with a time shift as fruit growth typically starts 4–5 weeks after bud break while canopy development continues until mid-season and leaf senescence does not occur until after the fruits are harvested [*Goldschmidt and Lakso*, 2005; *Wünsche and Lakso*, 2000] (Figure 3.2).

The thermal thresholds to reach phases (2)–(5) are defined as accumulated GDDs since bud break and can be adjusted by the user via the parameter file which applies to all parameters listed in Table A.2 of the Appendix. GDDs are determined as the difference between the average daily air temperature and a base temperature of 4 °C with a maximum daily increment of 26 degree days (Eq. (3.1)). Different to the existing deciduous phenology, leaf senescence is triggered not by day length but by the drop of the daily

mean temperature below a critical temperature threshold, in this case the base temperature. This approach was selected since many fruit trees that belong to the Rosaceae family (e.g., apple, pear, plum, and cherry) are unaffected by photoperiod and instead controlled by temperature [*Heide and Prestrud*, 2005]. The last day of the leaf senescence period marks the beginning of dormancy. The new phenology subroutine of CLM5-FruitTree also controls C reserve dynamics, stem and root turnover, and final rotation, which involves removing and replanting trees when the maximum orchard lifespan is reached.

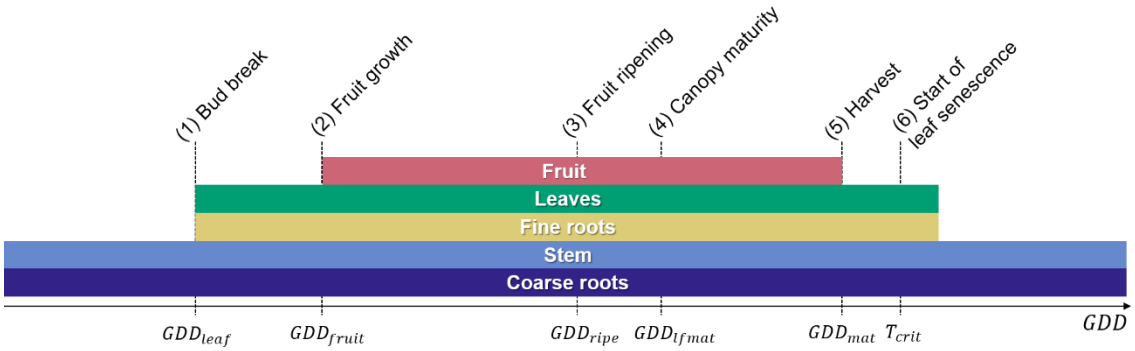

Figure 3.2 Fruit tree phenological stages of (1) bud break at the end of dormancy, (2) the start of fruit growth, (3) fruit ripening, (4) canopy maturity, (5) harvest, and (6) the start of leaf senescence. The lengths of phenological stages (2)-(5) are determined by their respective growing degree-day thresholds (GDD) starting from bud break (GDD_{leaf}=0), while stage (6) is determined by a critical temperature threshold (T_{crit}). Coloured bars correspond to the time any plant organ is present on the field throughout a year.

3.2.2.2 Carbon and nitrogen allocation

CN allocation to the growth of new tissue (display pools) and to storage pools follows the phenological stages described in Section 3.2.2.1 (Figure 3.2). A coupled CN allocation subroutine determines the fate of newly assimilated C from photosynthesis. A user-defined initial biomass can be assigned to leaf and fine root transfer pools via the *transplant* parameter (Table A.2), while additionally 10% of this biomass is assigned to the dead stem pool to define an initial stem area index > 0. Each pool is also assigned the corresponding amount of N. Adjustments to this parameter have only little effect on the biomass growth and yield of the adult trees as the trees reach their maximum canopy height and develop their full leaf area index (LAI) within the first couple of years after transplanting. Thereafter, the potential allocation to the different plant components is based on allocation coefficients and allometric relationships between dead and live parts of stem and coarse root. Throughout the growing period until harvest, 5% of the newly assimilated C is allocated to the storage pools, as defined by the *fcur* parameter, except for fruits where all allocated C is assigned to the displayed pool. For all other organs, the

remaining C is also allocated to the displayed C pools. At bud break, a fraction of the C in the storage pool of all plant components, except fruits, is transferred to the actively growing C pools over a period that can be specified by the newly added parameter *ndays_stor*. This is based on the assumption that resources are partially mobilized to support growth of new tissue [*Loescher et al.*, 1990; *Oliveira and Priestley*, 1988]. Lacking more specific knowledge of the exact fraction, the default of 0.5 used by the seasonal deciduous phenology in CLM5 is adopted for fruit trees.

Before the start of fruit growth, phase (1), newly assimilated C and corresponding N are partitioned between leaf, stem, and root pools. The allocation coefficients are calculated according to a set of equations that were adapted from the AgroIBIS crop phenology algorithm used in CLM5-BGC-crop [*Lawrence et al.*, 2018]:

$$GDD_{T2m} = GDD_{T2m} + T_{2m} - T_f - 4 \quad \text{where} \quad 0 \leq T_{2m} - T_f - 4 \leq 26\,°days\,, \tag{3.1}$$

$$a_{repr} = 0\,, \tag{3.2}$$

$$a_{froot} = a^i_{froot} - \left(a^i_{froot} - a^f_{froot}\right) * \frac{GDD_{T2m} - GDD_{leaf}}{GDD_{fruit} - GDD_{leaf}}\,, \tag{3.3}$$

$$a_{leaf} = \left(1 - a_{froot}\right) * \frac{a^i_{leaf} * (e^{-b} - e^{-b * \frac{GDD_{T2m} - GDD_{leaf}}{GDD_{lfmat} - GDD_{leaf}}})}{e^{-b} - 1}\,, \tag{3.4}$$

$$a_{livestem} = 1 - a_{repr} - a_{froot} - a_{leaf}\,, \tag{3.5}$$

where GDD_{T2m} are the accumulated growing degree days for the 2 m air temperature with maximum increments of 26 degree days; T_{2m} is the simulated 2 m air temperature in K; T_f is the freezing temperature of water and equals 273.15 K; GDD_{leaf}, GDD_{fruit}, and GDD_{lfmat} are thermal thresholds for bud break, start of fruit growth, and canopy maturity, respectively; b is an exponential factor; a^i_{leaf}, a^i_{froot}, and a^f_{froot} are initial and final values for the allocation coefficients to leaf (a_{leaf}) and fine root (a_{froot}), respectively; and a_{repr} and $a_{livestem}$ are the allocation coefficients to fruit and live stem, respectively.

Once fruit growth begins in phase (2), an increasing proportion of the assimilated C and corresponding N is allocated to this organ, causing leaf allocation to decline and fruit

allocation to plateau at a high value once canopy maturity is reached. Allocation to fine roots and stem continues to decline and then settles at a constant value until harvest:

$$a_{livestem} = a_{livestem} * \left(1 - \frac{(GDD_{T2m} - GDD_{leaf}) - (GDD_{fruit} - GDD_{leaf})}{(GDD_{mat} - GDD_{leaf})^{d_L - (GDD_{fruit} - GDD_{leaf})}}\right)^{d_{alloc}^{stem}}, \quad (3.6)$$

$$a_{repr} = 1 - a_{froot} - a_{livestem} - a_{leaf}, \quad (3.7)$$

where GDD_{mat} is the thermal threshold for fruit maturity and harvest, while d_L and d_{alloc}^{stem} are stem allocation decline factors.

After harvest and until the start of dormancy, all of the newly assimilated C is sent to the storage pools following the notion that late in the season, assimilates are used mostly to fill up reserves that can be mobilized to resume growth in the following spring [*Le Roux et al.*, 2001]. Fruit trees store C in the perennial woody parts of the tree, from where it is re-mobilized to support the growth of new shoots, leaves, and fine roots [*Le Roux et al.*, 2001; *Millard*, 1996; *Oliveira and Priestley*, 1988]. Since in CLM5 separate storage pools are assigned to each plant organ, the newly added *aleafstor* parameter (Table A.2) defines the fraction of allocatable C going to the leaf storage pool, while the remainder is split equally between roots and stem.

Fruit trees, similar to other deciduous species, have been observed to translocate N out of senescent leaves to be reused by other tree organs [*Malaguti et al.*, 2001; *Millard*, 1996; *Millard et al.*, 2006]. Therefore, CLM5-FruitTree adopts the same N re-translocation strategy as used in the BDT phenology during which N is removed from falling litter based on leaf and litter C:N ratios and the available C to pay for the extraction of N from increasingly recalcitrant litter pools. Subsequently it is transferred to the plant N pool from where it can be used for the growth of new plant tissue [*Lawrence et al.*, 2018].

3.2.2.3 Representation of management practices

Furthermore, management practices such as fertilization and stem pruning are represented in the new sub-model. Fertilization is performed on a yearly basis after the occurrence of bud break, as N fertilization in early spring is still the most common practice in fruit orchards even though autumn fertilization or multiple applications via fertigation are also in use to increase fertilizer N use efficiency and reduce N losses [*Carranca et al.*, 2018; *Sanchez et al.*, 1995]. We use the existing fertilization scheme of the crop phenology that

adds fertilizer directly to the soil mineral N pool. A user-defined fertilization rate or amount can be applied as synthetic fertilizer or manure respectively, although there currently is no difference in model behaviour for these two fertilizer types [*Lawrence et al.*, 2018].

Winter pruning is a common practice in fruit orchards and may be performed throughout the winter to control the shape and size of fruit trees, and partially to manage crop load [*Grechi et al.*, 2008]. In many intensive orchard production systems, pruning residues are mulched into the soil, possibly increasing C sequestration [*Aguilera et al.*, 2015; *Montanaro et al.*, 2010]. Alternatively, residues may also be exported and treated as waste [*Benyei et al.*, 2018] or utilized for energy production [*Kazimierski et al.*, 2021]. In CLM5-FruitTree, pruning is performed as the tree enters dormancy by removing a user-defined fraction, *prune_fr* (Table A.2), of the dead stem from both storage and displayed C pools. We remove C from the dead stem pool instead of the live stem pool since the former is the main wood pool in CLM5 that receives 85% of the C allocated to total new wood. Furthermore, the implemented live wood turnover in CLM5 converts live stem to dead stem at the end of the growing season to account for differences in maintenance respiration and C:N ratios between these tissue types [*Lawrence et al.*, 2018]. Hence the live stem C pool remains rather small and stable over the years, so that applying pruning to this pool would have little effect on total tree biomass. The pruning implemented in CLM5-FruitTree affects only the tree biomass and height that are calculated based on this biomass pool, which in turn affects the calculation of turbulent fluxes of sensible and latent heat. However, this effect is small, and since turbulent fluxes are generally low in winter, the exact timing of pruning does not play a significant role in the magnitudes of these fluxes. During the first three years after planting, trees are not pruned to allow some initial stem biomass to grow. The sub-model treats pruning residues in one of two ways to account for their possible difference in fate: (1) residues are added to the wood harvest pool and exported from the field or (2) residues are added to the woody debris pool thus feeding the litter cycle.

When the orchard reaches the end of its lifespan, C of all biomass pools (storage, transfer, and display) is sent to either the litter pool for leaves and fine roots, or the wood harvest pool for live and dead stem and coarse roots, while any remaining C in the fruit pool is harvested. The orchard can then be replanted in the following year. Lastly, the standard

irrigation routine implemented in CLM5 can be used for irrigated orchards by selecting the irrigated crop PFT.

3.2.3 Model implementation and testing

3.2.3.1 Site data

Extensive field measurements from an apple-growing region in the Adige River valley, South Tyrol, Italy (46°21' N, 11°16' E; 240 m a.s.l.) were used to parameterize and test the new CLM5-FruitTree sub-model along with the new apple PFT [*Zanotelli et al.*, 2019; *Zanotelli et al.*, 2015; *Zanotelli et al.*, 2013]. Measurements were obtained from an approximately 0.5 ha irrigated apple orchard planted in 2000 with the Fuji apple cultivar grafted on M9 dwarfing rootstock. The apple trees were planted at a row and tree spacing of 3x1 m (3333 trees per hectare). A 1.8 m wide grass strip was grown between the tree rows, which was mowed three times a year. Other management practices included regular pruning, spring fertilization of 7.5 gN m^{-2} yr^{-1}, and tillage of the soil directly underneath the trees [*Zanotelli et al.*, 2013]. Stand-related data included general stand characteristics and phenology observations, LAI, C:N ratios, rooting distribution at three depth ranges (0–20, 20–40, and 40–60 cm), measurements of the biomass growth of different tree organs at a monthly or seasonal interval, and fruit harvest information (Table 3.1). Furthermore, daily soil respiration measurements from a control and a trenching plot (with (R_s) and without (R_h) root respiration, respectively) were performed in 2010. Additionally, an eddy covariance (EC) station provided measurements of the turbulent exchange of trace gases and energy at the studied apple orchard between 2013 and 2015. The quality check, gap filling, and flux partitioning of collected data followed the procedure outlined in *Reichstein et al.* [2005]. The average closure of the energy balance was 60%. To correct for the closure failure, the missing energy was assigned to the latent (LE) and sensible (H) heat fluxes based on the daily Bowen ratio [*Zanotelli et al.*, 2019]. Measured or derived fluxes included net ecosystem CO_2 exchange (NEE), ecosystem respiration (R_{eco}), gross primary production (GPP), LE, H, and evapotranspiration (ET) at half-hourly intervals. Furthermore, soil heat flux (G) measured at 5cm depth as well as soil moisture (SM) measurements up to a depth of 60 cm of soil are available. Table 3.1 gives a summary of the available data and measurement periods. A complete description of the measurement procedures and instruments can be found in *Zanotelli et al.* [2013], *Zanotelli et al.* [2015], and *Zanotelli et al.* [2019].

Meteorological data, recorded partly at the EC tower and at the Laimburg meteorological station located 4 km from the site (46°23' N, 11°17' E; 224 m a.s.l.), were used at an hourly time step to force the model. Measured data included precipitation, solar radiation, net radiation (R_n, only at the EC tower), air temperature, air pressure (only at Laimburg), relative humidity, and wind speed. Measurements of incoming longwave radiation (LW_{in}) were available for 2010 only, but additional calculations following *Konzelmann et al.* [1994] and *Sedlar and Hock* [2009] were produced and used as forcing for the remaining years 2011–2019 (Appendix IV). This was necessary since the use of the internally calculated LW_{in} in CLM5 resulted in unrealistic underestimations compared to the available measurements of LW_{in} leading to a significant bias in R_n.

Table 3.1 Summary of available data from an apple orchard in the Adige River valley, South Tyrol, Italy between 2010 and 2019. Solid lines represent continuous and dotted lines monthly measurements, while diamonds represent single measurements.

Data	**2010**	**2011**	**2012**	**2013**	**2014**	**2015**	**2016**	**2017**	**2018**	**2019**
Weather data EC tower	▬			▬	▬	▬				
Weather data Laimburg	▬	▬	▬	▬	▬	▬	▬	▬	▬	▬
Biomass (NPP) components	▪▪▪	♦	♦							
C:N ratios of biomass components	▪▪▪									
Leaf area index (LAI)	▪▪▪	▪▪▪	▪▪▪							
Fruit production (yield)	♦	♦	♦	♦	♦	♦				
Root distribution (0-60 cm)	♦									
Soil respiration (R_s, R_h)	▬									
Soil heat flux (G)				▬	▬	▬				
Soil moisture (SM, 0-60 cm)				▬	▬	▬				
EC data: carbon (GPP, R_{eco}, NEE), energy (R_n, LE, H), water (ET)				▬	▬	▬				

3.2.3.2 Model set-up

The model was set up in point mode to simulate the apple orchard in the Adige valley using available sand, clay, and organic matter fractions. The model was spun-up for 200 years, first in accelerated decomposition and then in normal decomposition mode, until all state variables, such as total ecosystem soil C and soil water, reached equilibrium

[*Lawrence et al.*, 2018]. For the model spin-up, the CRUNCEPv7 atmospheric forcing data set from 1986 to 2016 was used [*Viovy*, 2018]. The apple orchard was then initiated using the newly developed sub-model and the apple PFT selecting the site-specific management (i.e., fertilization with 7.5 gN m^{-2} yr^{-1}, irrigation, mulching of pruning material). Simulations were performed for a period of 10 years to mirror the time from orchard establishment in 2000 up to the start of the measurements in 2010 using 10 years (2010–2019) of the available meteorological data from Laimburg meteorological station. Simulations were then extended for another 6 years from 2010 to 2015 for model parameterization and performance evaluation purposes.

3.2.3.3 Parameterization

Key parameters of the new sub-model as well as other PFT-specific parameters were parameterized using the first 3 years of simulations between 2010 and 2012. The lengths of phenological stages and associated parameters were determined based on field observations of bud break, full bloom, and harvest as well as non-cultivar specific apple phenology descriptions that were found in the literature (Appendix V). The length of the period where growth is supported out of reserves (*ndays_stor*) was calibrated based on the biomass measurements and the estimate by *Zanotelli et al.* [2013] that apple trees use stored carbohydrates in the first two months after bud break. C allocation coefficients were calculated based on the monthly measurements in 2010 by dividing the biomass growth of the individual plant organs by the total biomass increment. Subsequently, model parameters associated with the CN allocation subroutine (Eq. (3.2) – (3,7)) were calibrated manually to match the coefficients obtained from the observations and the overall biomass partitioning on a yearly basis. Parameter values for C:N ratios of all plant organs and maximum LAI were based on field observations in 2010 and 2010–2012, respectively. The specific leaf area (*slatop*) was calculated by dividing monthly measurements of LAI by leaf biomass and taking the average of the obtained values. Structural and morphological parameters such as maximum tree height (*ztopmx*), planting density (*nstem*), the ratio of stem height to radius at breast height (*taper*), or rooting depth (*root_dmx*) were adjusted based on site-specific information [*Zanotelli et al.*, 2013]. Initial biomass at transplanting was assumed 5 gC m^{-2}, resulting in an initial tree height of around 100 cm and a stem diameter of 16 mm. As seedlings are dormant at the time of transplanting, their LAI is 0. The CLM5 root distribution parameter (*rootprof_beta*), which sets the root ratios at different depths, was calibrated by least squares regression of

the measured root ratios at 0–20, 20–40, and 40–60 cm depths and the calculated ratios. Optical parameters for leaf transmittance and reflectance in the visible and near-infrared (IR) were set to average values reported for apple by *Bastías and Corelli-Grappadelli* [2012]. Stem reflectance and transmittance were assumed to be similar to other woody species and therefore set to the values used for BDT in CLM5, similar to the assumptions made by *Fan et al.* [2015] for the palm tree development in CLM4.5. The ratio of momentum roughness length to canopy top height (*z0mr*) was set to the average value of the ranges reported for apple and citrus orchards to account for the differences in canopy structure compared to annual crops and forest [*la Fuente-Sáiz et al.*, 2017; *Tanny and Cohen*, 2003]. No specific values could be found for the ratio of displacement to top of canopy height (*displar*), the leaf orientation index (*xl*), or the intercept to calculate the top of canopy maintenance respiration base rate (*lmr_intercept_atkin*). These values were assumed to be comparable to other deciduous trees and thus set to the values used for BDT in CLM5. Parameters related to C reserve dynamics (e.g., *fcur*) and photosynthesis (e.g., the slope of the relationship between leaf N per unit area and the maximum rate of carboxylation at 25 °C, *s_vcad*) were adjusted to match observed LAI and productivity data. All parameters with their values and references to the literature are summarized in Table A.2 of the Appendix.

3.2.3.4 Sensitivity analysis

A simple one-by-one sensitivity analysis was performed to further tune model parameters and assess the influence of newly added parameters on the simulation results. As a complete sensitivity analysis of all PFT-related parameters would have exceeded the scope of this study, the analysis focused on key parameters of the new phenology and CN allocation subroutines. Other potentially influential parameters were selected based on previously performed sensitivity analyses by *Göhler et al.* [2013] for CLM3.5, and by *Cheng et al.* [2020] and *Dagon et al.* [2020] for CLM5, taking into account differences between previous and current model versions. Parameters selected for the analysis were perturbed by varying a parameter by ±30%, ±20%, and ±10% while keeping the others fixed to the value of the control simulation (after initial parameterization). The goal here was not to perform an in-depth analysis covering the full range of possible parameter values, but rather to provide a first indication of influential parameters in the new sub-model similar to the approach of *Fan et al.* [2015]. As a measure of sensitivity, the parameter effect (PE) was calculated using the average of three years of simulations

between 2013 and 2015 of the control and the perturbed simulations for selected output variables and the following formula adjusted from *Luo et al.* [2020]:

$$\Delta X_{i,j} = \sum_{k=1}^{n} \frac{\left|\overline{X_{\iota,j,k}} - \overline{X_{\iota,control}}\right|}{\left|\overline{X_{\iota,control}}\right|} , \tag{3.8}$$

$$PE_{i,j} = \frac{\Delta X_{i,j}}{max\left[\left(\Delta X_{i,j}\right)_{1\le i\le n;1\le j\le m}\right]} , \tag{3.9}$$

where X is a simulated value of the control or a perturbation run, ΔX is the summed absolute difference between the control and the perturbation run across all perturbations, k is the parameter perturbation factor, i is the i[th] variable across $n = 6$ selected output variables including: GPP, NEE, R_a, LE, maximum LAI, and yield, and j is the j[th] parameter across m selected parameters. $PE_{i,j}$ is a number between 0 and 1 that represents the sensitivity of an output variable i to the parameter j, with 1 meaning high and 0 meaning low sensitivity. The parameters selected for sensitivity analysis are indicated in Table A.2 of the Appendix.

3.2.3.5 Model performance evaluation

Modelling results are compared to observed biomass, yield, and LAI data as well as ecosystem fluxes retrieved from the EC measurements. Statistical indices for model performance evaluation include the Pearson coefficient of correlation (r), the root mean square error (RMSE) and the percent bias (%bias):

$$r = \frac{\left(\frac{1}{n}\sum_{i=1}^{n}(X_i^o - \mu^o) * (X_i - \mu)\right)}{\sigma * \sigma^o}, \tag{3.10}$$

$$RMSE = \sqrt{\frac{1}{n}\sum_{i=1}^{n}(X_i - X_i^o)^2} , \tag{3.11}$$

$$\%bias = \frac{\sum_{i=1}^{n}(X_i - X_i^o)}{\sum_{i=1}^{n}(X_i^o)}, \tag{3.12}$$

where i is the time step, n is the total number of time steps, and X_i and X_i^o are simulated and observed values at each time step respectively, μ and μ^o are simulated and observed mean values, respectively, and σ and σ^o are simulated and observed standard deviations.

3.3 Results and Discussion

3.3.1 Sensitivity analysis

A total of 34 parameters were initially considered for the sensitivity analysis of which the 13 most influential parameters (PE > 0.1 for at least one of the selected output variables) are shown in Figure 3.3. GPP, NEE, R_a, and yield have similar sensitivity patterns and are most sensitive to the leaf C:N ratio (*leafcn*) and the relationship between leaf N and the maximum rate of carboxylation at 25 °C (*s_vcad*). Together with *slatop* and other constants, they control the maximum photosynthetic capacity in the photosynthesis calculation and thus largely influence total C assimilation. As expected, LAI is most influenced by parameters that control the CN allocation to leaves such as the initial leaf allocation coefficient (*fleafi*), the GDDs needed to reach canopy maturity (*lfmat*), the maximum LAI (*laimx*), photosynthetic parameters, and, to a smaller extent, the fraction of C allocated to the leaf storage pool to refill C reserves (*aleafstor*). The first three parameters influence leaf biomass and thus show a considerable effect on GPP, NEE, R_a, and yield. The same output variables are affected in a similar fashion by the GDDs needed until fruit harvest (*hybgdd*) that control the amount of C allocated to fruits. LE is influenced largely by the parameter controlling stomatal conductance (*medlynslope*), and the photosynthetic parameters (*leafcn*, *s_vcad*).

Overall, photosynthetic parameters play a key role in determining the magnitude of the studied output variables with an average PE value close to 0.7 across all six variables. Phenological parameters (top seven parameters in Figure 3.3) are generally less influential for the same output variables with average PE values up to 0.43. These findings are largely consistent with earlier studies of parameter sensitivity [*Cheng et al.*, 2020; *Dagon et al.*, 2020; *Göhler et al.*, 2013; *Luo et al.*, 2020]. In contrast to *Luo et al.* [2020], we did not find a strong effect of the root distribution parameter (*rootprof_beta*) on LE, which can be attributed to the low water stress due to the irrigation management of the studied orchard.

While the one-at-a-time sensitivity analysis provides some insight into model sensitivity, the ranking of influential parameters is strongly influenced by the choice of parameters and output variables, the parameter perturbation strategy (i.e. percent change, linear sampling), and the index chosen as the sensitivity measure. Parameter tuning based on this analysis is further complicated since this approach does not consider parameter covariation that is particularly strong for plant parameters that influence photosynthesis [*Göhler et al.*, 2013]. Selecting parameter values based on the individual best simulation hence does not necessarily yield the best overall result [*Luo et al.*, 2020]. We therefore decided to first adjust *s_vcad* to best match the observed average GPP. In the following, we further adjusted *fleafi*, *hybgdd* and *medlynslope* to improve the simulated biomass components as well as the LE flux, respectively.

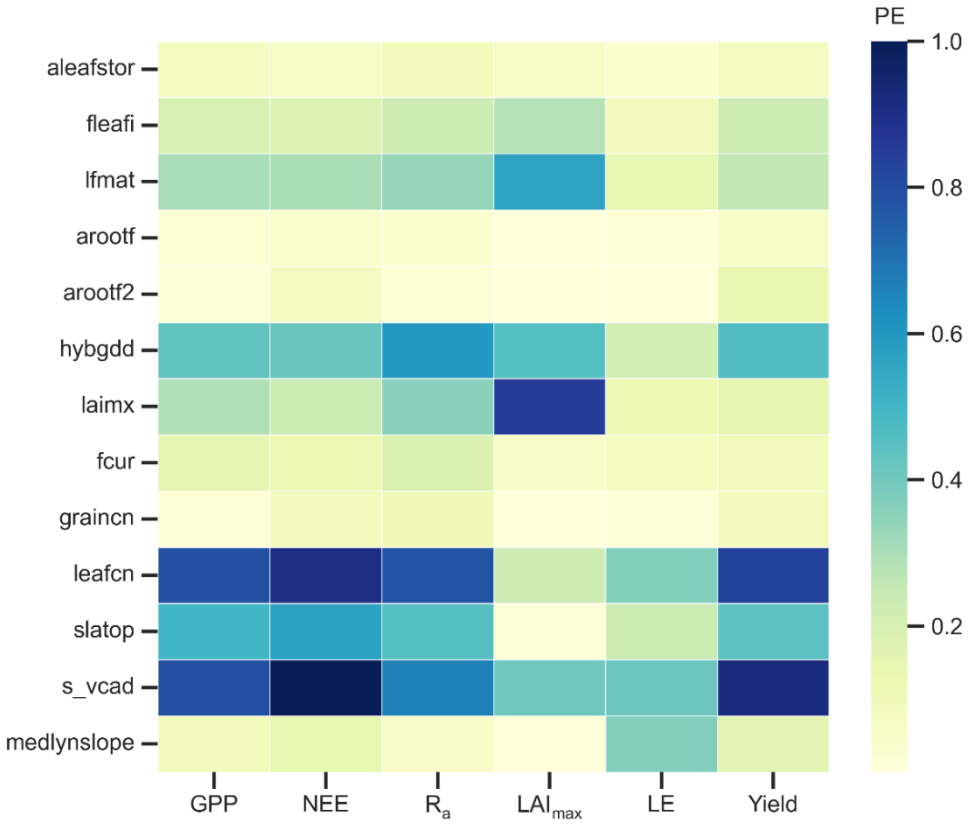

Figure 3.3 Parameter effect (PE) as a measure of sensitivity of selected output variables to the most influential model parameters. Output variables include gross primary production (GPP), net ecosystem exchange (NEE), autotrophic respiration (R_a), maximum leaf area index (LAI_{max}), latent heat flux (LE) and yield. Parameters are: Post-harvest leaf allocation coefficient to storage (aleafstor), initial leaf allocation coefficient (fleafi), GDD to canopy maturity (lfmat), root allocation coefficients at the start of fruit development (arootf) and until harvest (arootf2), GDD needed until harvest (hybgdd), maximum LAI (laimx), fraction of allocation that goes to currently displayed growth (fcur), C:N ratios of fruits (graincn) and leaves (leafcn), specific leaf area at top of canopy (slatop), slope of the relationship between leaf N per unit area and the maximum rate of carboxylation at 25 °C (s_vcad), and the medlyn slope of the conductance–photosynthesis relationship (medlynslope). For more details on the parameters, see Appendix V.

3.3.2 Modelling results

In the following, we present the modelling results according to the initial parameterization and the updated parameter values from the sensitivity analysis. Daily simulations or yearly sums are compared to observed biomass, yield, and LAI data as well as ecosystem fluxes retrieved from the EC measurements and the SM measurements aggregated to daily mean values.

3.3.2.1 Biomass growth and yield

The patterns in seasonal biomass allocation simulated by CLM5-FruitTree show good agreement with the monthly observations from 2010 (Figure 3.4a). The beginning and end of the growing season are well captured. After bud break at the beginning of March, biomass is allocated to the vegetative organs of leaves, fine roots, and woody organs, and growth is supported by C and N reserves until the start of fruit growth in early May (50 days according to the *ndays_stor* parameter). In the following months, fruit biomass grows rapidly until harvest takes place in mid-October, following the typical sigmoidal growth curve that is well captured by the new phenology and CN allocation. Simulated leaf biomass peaks in mid-June and remains constant thereafter, with leaf senescence starting later October when temperatures drop below 4 °C. Pruning is performed when the tree enters dormancy by removing 85% of the stem biomass assimilated over the season according to the observed pruning amounts in the studied apple orchard [*Zanotelli et al.*, 2015; *Zanotelli et al.*, 2013]. From 2010 to 2012, the modelled percentage of biomass allocation to plant organs was generally in agreement with the observations [*Zanotelli et al.*, 2015], with differences ranging between 1 and 5% for fruits, leaves, aboveground wood, and roots (Figure 3.4b). *Penzel et al.* [2020] stated that different studies reported biomass allocation to fruits ranging from 50 to 85% depending on apple cultivar, suggesting considerable variability in allocation coefficients. This emphasizes the benefit of a cultivar specific calibration in order to obtain realistic modelling results. On the other hand, it suggests that a more general parameterization, that reflects an average apple tree, may be necessary to apply CLM5-FruitTree at larger scales and across multiple cultivars.

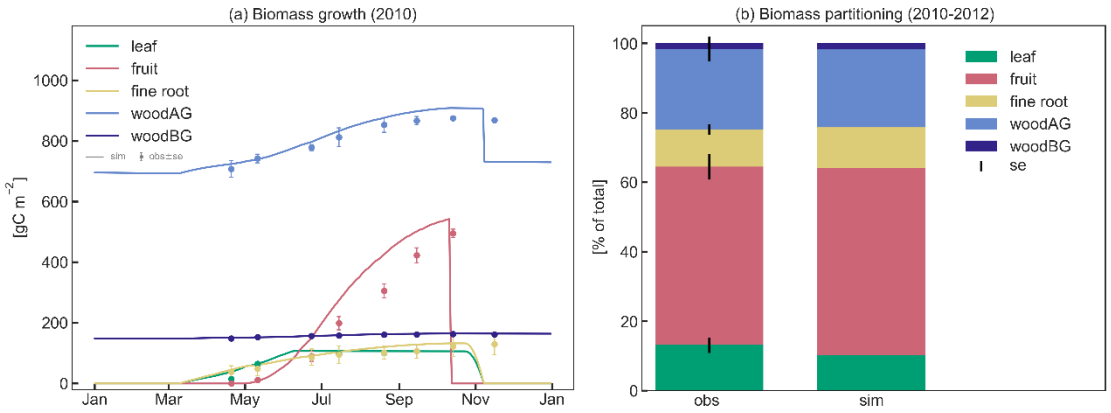

Figure 3.4 (a) Observed and simulated growth of leaves, fruits, fine roots, aboveground (live and dead stem), and belowground biomass (live and dead coarse roots) during 2010. (b) Observed and simulated biomass components between 2010 and 2012 as percentage of total biomass.

The timing for initial leaf development in spring and leaf senescence in late autumn are sufficiently well captured by the implemented bud break prediction algorithm and the simple temperature threshold for leaf abscission, respectively (Figure 3.5). Observed maximum LAI varied between 2.8 and 3.3 m^2 m^{-2} and occurred during the first half of July. The simulations reached similar values in 2010 and 2012, matching the observations, while the simulated LAI in 2011 underestimated the measurements due to a smaller C transfer from storage and lower solar radiation early in the growing season. The discrepancy between the low simulated LAI and the high observed LAI in 2011 could have been further exacerbated by a lighter pruning performed in the previous winter compared to other years [*Zanotelli et al.*, 2013]. Such practice is sometimes performed in an attempt to counteract the strong alternate bearing behaviour of the Fuji variety, which causes a substantial drop in yield following a high yielding year [*Atay et al.*, 2013; *Belleggia et al.*, 2009; *Pasa et al.*, 2021]. As a consequence of the light pruning, a larger number of vegetative and flower buds remained on the tree, leading to more growth and possibly contributing to the larger discrepancy between relatively high observed LAI and relatively low simulated LAI. The adjusted pruning is however based on a somewhat subjective assessment of the farmer and information about the exact amount is hardly available. Thus, CLM5-FruitTree currently adopts a simplified pruning practice based on the removal of a fixed portion of the seasonal stem growth which manages tree size and total woody biomass without affecting LAI.

Measured LAI showed a slow decline soon after maximum LAI was reached, while simulated values in contrast are assumed to remain constant until leaf senescence is initiated. The observed early decline may be an artefact of the sampling strategy used to

determine LAI that extrapolated individual leaf area measurements to the whole tree, assuming a constant leaf distribution within the tree [*Zanotelli et al.*, 2013]. Another reason could be some premature leaf fall in the summer at the expense of the inner shadowed leaves, as observed during field sampling. Other studies suggest that the LAI of fruit trees generally stays constant until a rapid decline with the start of senescence [*Lakso et al.*, 1999; *Pallas et al.*, 2016], supporting the simulated LAI dynamic.

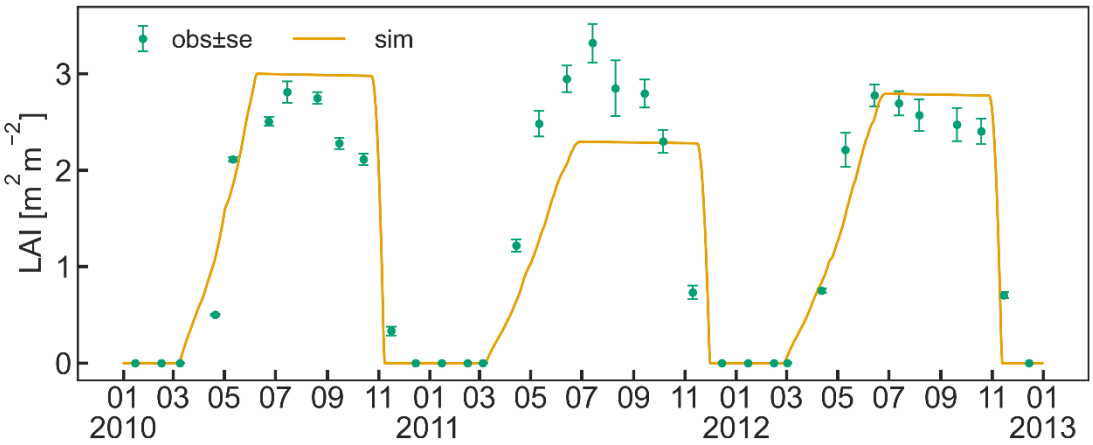

Figure 3.5 Simulated daily leaf area index (LAI) between 2010 and 2012 together with observations (±standard error) of LAI that were made once a month for the same period. Ticks on the x-axis refer to the beginning of the month.

Simulated yield averaged 70 t ha^{-1} between 2010 and 2015 and was within 2.3% of the observed average yield. While simulated yield varied between 61 and 76 t ha^{-1}, the observations showed a greater inter-annual variability (IAV), as exemplified in the case of the years 2012 (low yield of 51 t ha^{-1}) and 2015 (high yield of 101 t ha^{-1}) (Figure 3.6). Low IAV of yield has also been observed in previous crop simulations with CLM5 for winter wheat [*Boas et al.*, 2021] suggesting that certain drivers of IAV such as extreme environmental conditions (e.g., frost, heat, and hail) or plant pests and diseases and the resulting plant physiological responses (e.g., stress-induced leaf shedding or failure to flower) [*Charrier et al.*, 2021] are missing or not represented with sufficient detail in CLM5. In the case of apple trees, yield is also tightly linked to the number of flowers and early fruit growth, which in turn depend on a complex interaction of the environmental conditions during winter dormancy and the start of the new growing season [*Chmielewski et al.*, 2012; *Corelli-Grappadelli and Lakso*, 2002]. Additionally, C reserves accumulated in the previous year [*Greer et al.*, 2002], and crop load management play an important role in determining the final harvest [*Penzel et al.*, 2020]. The latter includes pruning or fruit thinning to ensure optimal fruit growth and to reduce the effect of alternate bearing.

The low observed yield in 2012 may be a result of such behaviour. This phenomenon and the processes involved are not universal, so that different fruit trees may be bearing regularly, irregularly, or biannually [*Hoblyn et al.*, 1937; *Monselise and Goldschmidt*, 1982]. As such, alternate bearing and its treatment through pruning or fruit thinning cannot easily be generalized and are thus not currently implemented in CLM5-FruitTree, which could have further reduced simulated IAV. Storage growth is considered in CLM5-FruitTree and exhibited an impact on the final yield of the following season, as shown by the sensitivity analysis of the *aleafstor* and *fcur* parameters (Figure 3.3). However, its effect on fruit growth in CLM5-FruitTree is indirect since it supports leaf development in the early growth stage but does not directly contribute to fruit growth. Identifying the driving forces of reserve deposition and mobilization and their quantification remains an unsolved issue, and there is yet no consistent formulation of this process in tree modelling [*Allen et al.*, 2005; *Le Roux et al.*, 2001]. Predicting final yield in fruit orchards is further complicated by the fact that harvest is usually based on certain fruit quality traits such as firmness or soluble solids and can occur successively as fruits may not mature at the same time [*Corelli-Grappadelli and Lakso*, 2002; *Musacchi and Serra*, 2018]. Within this context, the proposed simplifications of the C reserve dynamics and fruit harvest are likely contributing to the difference in observed and simulated yields. Considering the many specific challenges in modelling this apple cultivar, we believe that the yield predictions are satisfactory enough in the context of the sub-model development.

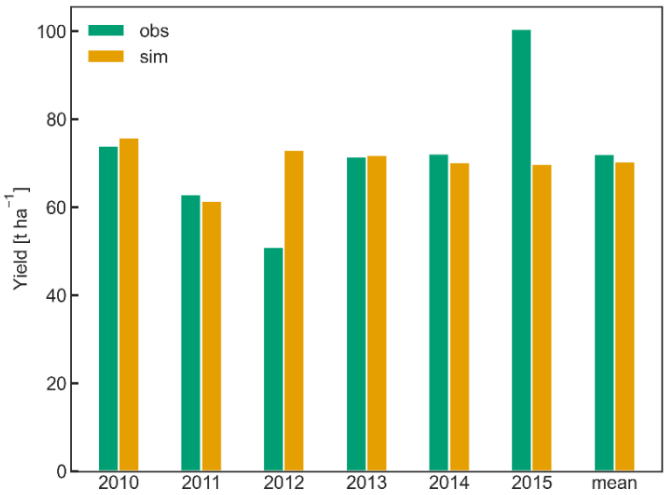

Figure 3.6 Annual yields from 2010 to 2015 and their mean in tons of fresh weight per hectare. For the conversion of simulated fruit biomass in gram carbon per square metre to tons per hectare, fruit C content was assumed 42% of total dry weight, harvest efficiency was assumed 95%, and fruit water content 83% according to *Zanotelli et al.* [2013].

3.3.2.2 Ecosystem fluxes and soil moisture variation

Carbon fluxes

As shown in Figure 3.7, CLM5-FruitTree was able to capture the overall patterns of GPP, NEE, and R_{eco}, particularly during the transition between dormancy periods and growing seasons (April to November). Simulated C fluxes are highly correlated with observations ($r \geq 0.84$) while the RMSE ranges between 1.12 and 1.53 gC m^{-2} d^{-1}. Observed and simulated peak C fixation occurred in mid-June (Figure 3.7a), corresponding to the maximum (negative) NEE (Figure 3.7c) and maximum LAI (Figure 3.5). Simulated NEE becomes negative (net carbon sink) around April and returns to positive (net carbon source) around November, in agreement with the observed dynamic (Figure 3.7c). Observed yearly sums of GPP (NEE) were 1.60 (–0.49), 1.43 (–0.48), and 1.65 (–0.76) kgC m^{-2} yr^{-1} for 2013, 2014, and 2015, respectively. Simulated yearly sums of GPP (NEE) were 1.58 (–0.53), 1.56 (–0.51), and 1.53 (–0.57) kgC m^{-2} yr^{-1} for the same years, showing a negligible positive bias of on average 0.17% for GPP (Figure 3.7b) and a small underestimation (less negative) of on average 3.8% for NEE (Figure 3.7d). Simulated and observed R_{eco} (Figure 3.7e) generally increased until July because of the increase in air temperature and respiratory costs of the developing canopy, and declined thereafter as air temperature started to drop. Simulations of R_{eco} tend to slightly underestimate observations between April and late August and to overestimate observations during winter, although discrepancies are relatively small. Observed yearly sums of R_{eco} were 1.13 (2013), 0.98 (2014), and 0.94 (2015) kgC m^{-2} yr^{-1}, while simulated values were 1.08, 1.08, and 0.99 kgC m^{-2} yr^{-1}, respectively. CLM5-FruitTree overestimated yearly R_{eco} by on average 3.3%, explaining most of the difference in observed and simulated NEE in 2013, while differences in 2014 and 2015 are due to a combination of small biases in both GPP and R_{eco}. Measured R_{eco} showed irregular fluctuations in the early part of the growing season 2013 and mid to late season 2014 and 2015 that are not reproduced well by the model. These fluctuations mostly correspond to the observed temperature dynamics (not shown) as a result of the applied gap filling that is based on an air (or soil) temperature-R_{eco} relationship [*Reichstein et al.*, 2005]. Such discrepancies between observed and simulated dynamics could be further explained by the occurrence of field management practices such as mowing of the grassed alleys or soil tillage under the tree rows, which are currently not represented in CLM5-FruitTree. Such practices could have led to a temporary rise in soil respiration (R_s) due to increased heterotrophic respiration

(R_h) as discussed in *Zanotelli et al.* [2013]. Indeed, soil tillage experiments performed in an apple orchard located in a Loess plateau in Shaanxi Province in China were found to increase R_s 14–57% depending on the tillage method [*Hou et al.*, 2021].

Zanotelli et al. [2013] measured a total R_s of 801±95 gC m^{-2} in 2010, contributing around 90% to R_{eco}, based on soil chamber measurements within the orchard (total soil respiration). The comparison to parallel measurements in a trenched plot produced a high ratio R_h/R_s of 0.77 for the apple orchard. In contrast, simulated R_s was 510 gC m^{-2}, contributing merely 45% to R_{eco} for the same year with a ratio R_h/R_s of 0.87. Simulated R_{eco} was instead dominated by autotrophic respiration (R_a) due to high C costs for maintenance, mainly of leaf biomass (data not shown). Other studies found that R_s contributed 56–67% to R_{eco} in irrigated citrus orchards of different ages that share common management practices (i.e., use of heavy machinery, irrigation, fertilization, tree pruning, and mulching) as well as structural similarities (e.g. planting in tree rows) with the studied apple orchard. Both aspects have a strong influence on soil respiration components in orchards [*Martin-Gorriz et al.*, 2020]. In forest ecosystems, where the magnitude of ecosystem fluxes was found to be somewhat comparable to orchards, R_s contributed > 60% to R_{eco} [*Lasslop et al.*, 2012; *Zanotelli et al.*, 2013].

In addition to the missing representation of certain management practices, CLM5-FruitTree currently does not account for an active ground cover in the orchard, which has shown to enhance R_s in an Italian olive orchard through increased fine root and microbial biomass [*Turrini et al.*, 2017]. Furthermore, the simplified representation of microbial activity in CLM5, through fixed respiration fractions for litter and soil organic matter pools, may limit the ability of CLM5-FruitTree to accurately represent soil respiration processes. Not accounting for mycorrhizal respiration may fail to adequately represent R_{eco} of the orchard, as measurements suggested a substantial contribution of 11±6% to total R_s in an apple orchard [*Tomè et al.*, 2016]. Lastly, biases in simulated soil temperature, SM content, and fine root density could further contribute to explaining the above discussed differences, as these factors have a major effect on R_s in apple orchards [*Ceccon et al.*, 2011].

In contrast to the underestimation of R_s in the model, the simulated R_a of 693 gC m^{-2} was almost twice the measured value of 372±195 gC m^{-2}. In our simulations, maintenance respiration comprised the main part of R_a, with on average 78%. The calculation of

maintenance respiration in CLM5 (see Section 3.2.1) does not account for a lower or varying maintenance cost observed in mature apple orchard canopies compared to annual crops [*Bepete and Lakso*, 1996; *Lakso et al.*, 1999]. It therefore seems likely that the tissue maintenance costs in the orchard are overestimated in CLM5-FruitTree, accounting for on average 45% of R_a (28% of R_{eco}). This could also explain the lower simulated carbon use efficiency (NPP/GPP) of 0.59 compared to 0.71 found by *Zanotelli et al.* [2013]. Further work and more experimental data are needed to better understand the differences in modelled and observed respiration partitioning and to improve the performance of CLM5-FruitTree to adequately simulate the respiration components in fruit orchards.

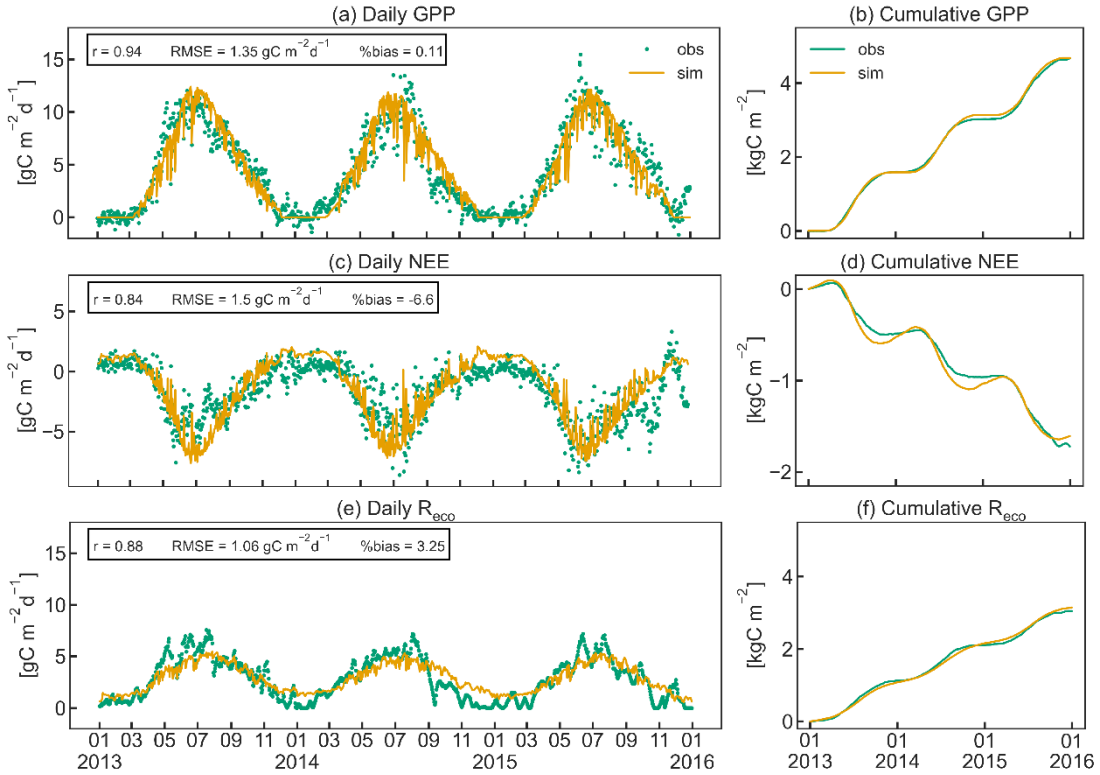

Figure 3.7 Daily instantaneous (a, c, e) and cumulative (b, d, f) observed and simulated fluxes of gross primary productivity (GPP), net ecosystem exchange (NEE), and ecosystem respiration (R_{eco}) for the studied apple orchard between 2013 and 2015. Pearson's coefficient of correlation (r), the root mean square error (RMSE) and the percent bias (%bias) are displayed as statistical indices.

Energy and water fluxes

The simulated seasonal course of the energy balance components R_n, G, LE, and H agrees well with observed dynamics in the orchard (Figure 3.8). CLM5-FruitTree shows a high performance in reproducing R_n and LE with $r \geq 0.97$ and RMSE of 15.98 and 17.85 W m^{-2}, respectively (Figure 3.8a and c). Due to the lack of LW_{in} measurements, the CLM5 internal LW_{in} calculation based on a clear-sky parameterization after *Idso* [1981] was used initially. This resulted in a significant underestimation of 5% (511 MJ) for LW_{in} and

18% (471 MJ) for R_n compared to the observations in 2010. The R_n bias could be reduced by 14% for the observed time series when LW_{in} was calculated by considering cloud cover as described in Appendix IV. This stresses the necessity of accounting for cloud cover, ideally combined with locally calibrated parameters, for an accurate calculation of LW_{in}. The remaining small negative bias of 4.48% in R_n is due to negative simulated R_n during the winter months (Figure 3.8b), which may be a result of the higher reflectance of solar radiation from bare soil compared to a grass surface [*Bryś et al.*, 2019]. The model assumes a bare soil (except for stem area) during the dormancy period, as the grass-covered alleys in the orchard are not considered explicitly.

The simulated LE (Figure 3.8c) shows similar dynamics and variability to the observations following the increase and decrease in GPP (Figure 3.7a) and LAI (Figure 3.5). Similarly to LE, modelled ET shows a high correlation coefficient of 0.97 and a small RMSE of 0.62 mm d^{-1} (Figure 3.8i). Simulated ET exceeds observed ET by 1.1 mm d^{-1} on average during its peak in July, but the overall bias is almost negligible (Figure 3.8j). Total observed ET is 901 (2013), 858 (2014), and 883 (2015) mm, while the corresponding simulated values are 916, 877, and 925 mm, respectively. When examining the order of magnitudes of the ET components, canopy transpiration takes up around 85% of ET, followed by soil evaporation and canopy evaporation (data not shown). Typically, apple orchard ET represents a combined flux from the apple trees and the grassed alley system, which is not explicitly represented in CLM5-FruitTree since CLM5 currently does not consider inter-row grass coverage or intercropping. *Ntshidi et al.* [2021] found that the contribution of understory transpiration is high in young, non-bearing apple orchards but contributes less than 10% to whole-orchard ET in mature orchards with high canopy cover, which may explain the good model performance despite not considering the grass cover.

Simulated H and G are less consistent with the observations with r values of 0.54 and 0.64, respectively, and large percent bias (Figure 3.8e and g), which is partially due to the much smaller magnitudes of the two fluxes compared to R_n and LE. A possible reason for the lower amplitude of observed G (Figure 3.8h) compared to simulated values may be the dampening effect of the grass cover providing additional shading during summer and insolation during winter [*Bryś et al.*, 2019; *Oorthuis et al.*, 2021]. Observed H was rather constant throughout the year, with slightly higher values at the start and end of the growing season when the canopy was not yet fully developed or leaves were shedding.

CLM5-FruitTree simulated a clear rise of H until April, closely following the observations, but H thereafter declined steeply in May, with negative values in August 2013 and 2015. Negative H during August corresponds to maximum LE and the main simulated irrigation season (June to September) that added 357 (2013), 281 (2014), and 517 mm (2015) of water to the orchard (Figure 3.9a). In a study conducted with CLM4.5, intense irrigation was found to strongly influence the convective heat fluxes by increasing LE and decreasing H [*Zeng et al.*, 2017]. Although precise measurements of the irrigation amount in the orchard are not available for the studied period, the average yearly irrigation was estimated around 200 mm, with no irrigation in 2014 due to sufficient rainfall [*Montagnani et al.*, 2018]. The difference in irrigation amounts may in part explain why the described phenomenon is not observed in the measurements. Indeed, negative simulated H in the summer months occurred as a result of strong evaporative cooling of ground and vegetation temperature through energy absorption by LE following irrigation that caused simulated LE to exceed simulated R_n. This behaviour was not observed in the measurements where LE rarely exceeded R_n and was mostly due to an overestimation of simulated LE compared to the measurements. Persisting model weaknesses in the partitioning of the energy balance were pointed out by a recent study examining land surface processes over a tropical rainforest using CLM4.5 and CLM5, and were linked to missing detail in the representation of the canopy and an oversensitivity of vegetation temperature to incoming solar radiation, among others [*Song et al.*, 2020]. As a result, the authors observed an overestimation of LE and unrealistically high day-to-night changes in G, which was also observed in this study when examining the model output at an hourly time step (results not shown).

Energy partitioning in orchards is strongly influenced by the positioning and pruning of branches to optimize tree architecture for higher productivity, planting density, tree height, and LAI distribution [*López-Olivari et al.*, 2016]. Consequently, the contribution of H and LE can significantly differ in the discontinuous orchard canopy (grass-covered alleys between tree rows) compared to the closed canopies of annual crops [*la Fuente-Sáiz et al.*, 2017]. Currently CLM5 is still limited to the assumption of a closed canopy structure that is uniform in space, and hence biases are likely to arise from this model limitation. Future developments towards integrating multi-layer schemes for canopy processes and the explicit representation of the canopy to improve the related processes are desirable for a more realistic representation of the orchard canopy structure.

Soil moisture variation

Simulated mean SM at 5 cm depth was within 1.6%vol of the observed value during the three observed growing seasons, despite the higher simulated irrigation amount (Figure 3.9b). Simulated daily values show a greater variability than the measured data in response to precipitation and to frequent irrigation (Figure 3.9a–b). In contrast, observed SM in the deeper soils (30–60 cm), was 3–11%vol higher during the growing season compared to simulated values (Figure 3.9c–d). Considering the total investigated soil depth, simulations exhibit a larger variability in SM throughout the year, with a general overestimation in winter and underestimation during the growing season (especially in the deeper soils). However, the collected SM data were limited to a single soil profile that may not adequately reflect the average SM of the apple orchard, which should be considered when comparing measurements and simulations. Even though the measurements are incomplete, the constant high observed SM in the deeper soils suggests an ample supply of water due to capillary rise from the shallow groundwater table that typically ranges between 1.2 and 1.85 m in the area [*Montagnani et al.*, 2018]. This process replenishes the water removed by ET processes and may explain the reduced need for irrigation compared to the simulations. Despite the shallow simulated ground water table (generally 1.2 m depth), groundwater could not be used for root water uptake in the simulation as the rooting depth of the orchard was restricted to 0.8 m according to local measurements, and capillary rise is currently not implemented in CLM5.

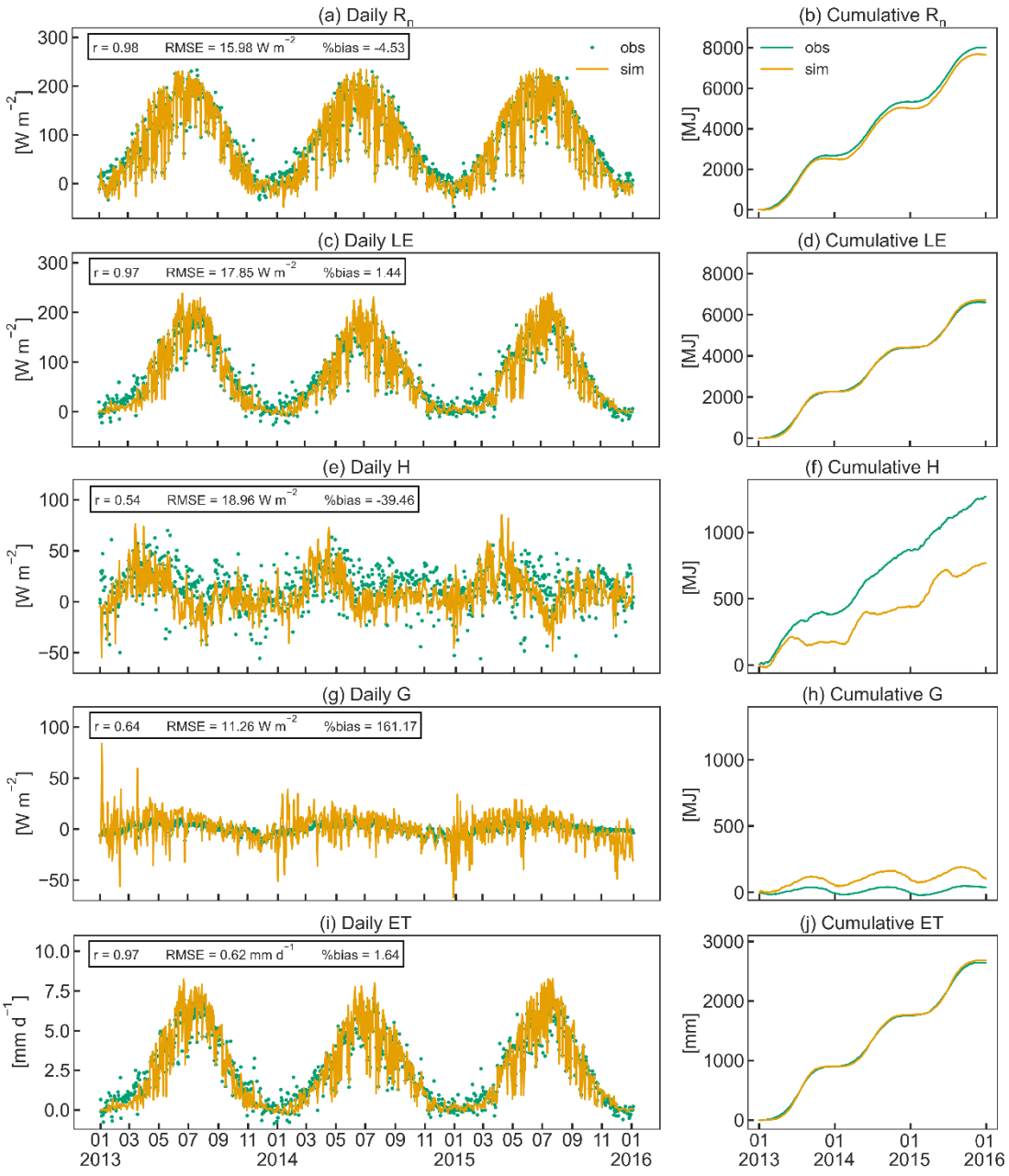

Figure 3.8 Daily and cumulative observed and simulated fluxes of net radiation (R_n), ground heat (G), latent heat (H), sensible heat (LE) and evapotranspiration (ET) for the studied apple orchard between 2013 and

2015. The coefficient of determination (r), the root mean square error (RMSE) and the percent bias (%bias) are displayed as statistical indices.

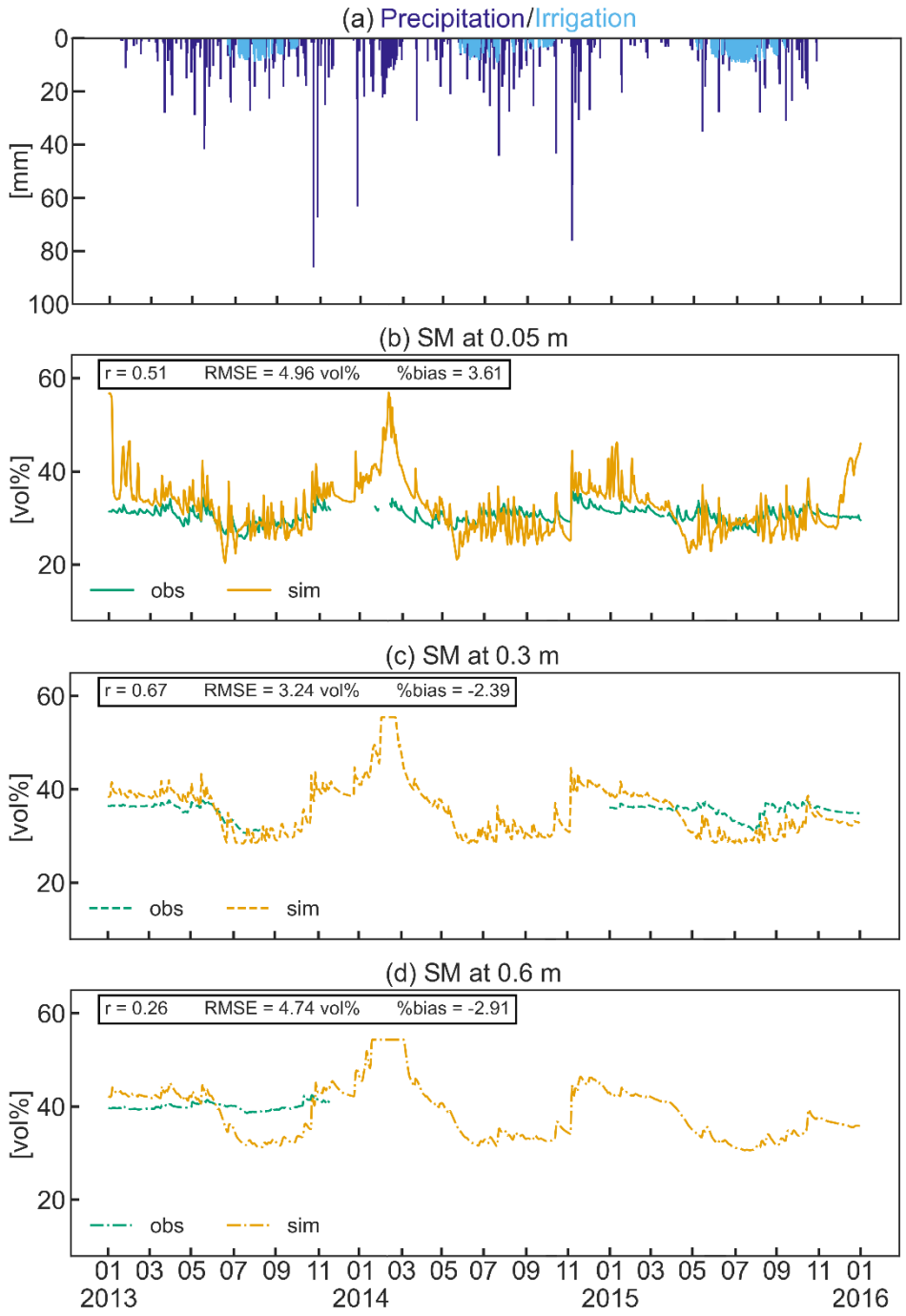

Figure 3.9 Precipitation and simulated irrigation (a), and observed and simulated soil moisture (SM) at 0.05 m (b), 0.3 m (c), and 0.6 m (d) depth from 2013-2015.

3.4 Conclusions

The novel CLM5-FruitTree was developed to model perennial deciduous fruit orchards and thus extended the representation of agricultural systems in CLM5. The development included a new phenology subroutine to account for the perennial nature, prolonged growing season, and distinct phenological development of fruit trees compared to annual crops. Furthermore, C reserve dynamics of perennial deciduous trees were considered by adapting the CN allocation and typical management practices associated with fruit orchards were represented, such as transplanting of seedlings and winter pruning. To evaluate the development, a new apple PFT was parameterized, and the model was set up and tested using extensive site data of a mature apple orchard in northern Italy.

One-by-one parameter sensitivity analysis revealed that photosynthetic parameters and parameters associated with canopy conductance have the highest influence on GPP, NEE, LE, and yield, while phenological parameters were more influential in biomass partitioning to the different plant organs. Due to the high number of model parameters and parameter covariation, future studies could propose a more comprehensive sensitivity analysis with a training data set consisting of multiple sites, which would give more insight into model sensitivity and could further improve the parameterization.

CLM5-FruitTree was able to capture the seasonal biomass development as well as the average relative partitioning of the total biomass into the different plant organs. The inclusion of C reserves next to photosynthetic growth was imperative to enable regrowth at the end of a dormancy period and influenced LAI development, total seasonal biomass, and yield. Average simulated yield was within 2.3% of the observation even though CLM5-FruitTree showed a lower IAV likely due to the simplification of C reserve dynamics, specific management practices, and the alternate bearing behaviour exhibited by the Fuji apple cultivar.

The new phenology and CN allocation algorithms well represented the seasonal course of carbon, water, and energy fluxes of the orchard. The magnitude of ecosystem fluxes was particularly well captured for GPP, R_n, LE, and ET, with correlation coefficients > 0.94 and percent bias < ±5%. The model exhibited small biases in NEE and R_{eco} that were most likely caused by the overestimation of R_a, especially leaf maintenance respiration, and an underestimation of R_s. Possible reasons for the smaller simulated contribution of R_s to R_{eco} could be the missing representation of the grass-covered alleys, differences in

simulated and actual soil temperature or organic matter content, and oversimplification of microbial respiration processes. Additionally, large negative biases in simulated H were found over most of the main irrigation season during summer as the model simulated a strong evaporative cooling of the surface temperature.

Further model developments should consider the improvement of canopy processes related to energy partitioning and the inclusion of an active ground cover in the orchard representation to improve the yearly energy budget calculations and possibly soil respiration. An explicit representation of the microbial community and a more flexible calculation of R_a, i.e. considering tissue age, should also be the focus of future model improvements. While the particular alternate bearing of the Fuji variety posed a challenge in this specific study, the pruning routine that is currently implemented may be sufficient for most other apple cultivars and fruit tree species for which this behaviour is less pronounced or not exhibited. However, future developments could be envisioned once the model is further tested and applied. In addition, management practices such as mowing or soil tillage could further enhance the model capability of capturing the dynamics and fate of assimilated C. Fruit thinning is another common practice in orchards, but its implementation would be more challenging, as the current model structure does not represent individual fruits. This process could however be implicitly accounted for through parameterization of the C allocation to fruits. Finally, the application of the newly developed sub-model to different geographical regions and other types of fruit trees or apple cultivars is needed to further validate the model and give more insight into the transferability of the development to different types of orchards.

Overall, our results demonstrate the ability of the newly developed CLM5-FruitTree sub-model to represent the seasonal dynamics and magnitudes of growth and ecosystem fluxes in a deciduous fruit orchard. As such, this development constitutes an important contribution to a more comprehensive representation of the agricultural land surface in CLM5 by adding a perennial, woody crop to the existing annual crop types. This will allow for a more realistic evaluation of land use and climate change effects, or water availability at regional scale such as the Mediterranean or parts of China and the US, where perennial agriculture such as fruit orchards covers large parts of the agricultural landscape.

4 Land surface modelling as a tool to explore sustainable irrigation practices in Mediterranean fruit orchards

This chapter is based on the following manuscript:

Dombrowski, O., Brogi, C., Hendricks Franssen, H. J., Bogena, H., Pisinaras, V., Panagopoulos, A., Chatzi, A., Babakos, K. & Swenson, S. (2023). Land surface modelling as a tool to explore sustainable irrigation practices in Mediterranean fruit orchards. (submitted to Water Resources Research)

Abstract

Irrigation strongly influences land-atmosphere processes from regional to global scale. Therefore, an accurate representation of irrigation is crucial to understand these interactions and address water resources issues. While irrigation schemes are increasingly integrated into land surface models, their evaluation and further development remains challenging due to data limitations, e.g. irrigation amounts and timing, and soil moisture (SM). This study assessed the representation of irrigation and its effect on crop yield in the Community Land Model version 5 (CLM5) through implementation of an irrigation data stream that allows to directly use observed irrigation data. Simulations were conducted at the point scale for two instrumented apple orchards using the CLM5 irrigation routine as well as the implemented data stream. Furthermore, irrigation requirements and the effect of deficit irrigation on crop yield and crop water use efficiency (CWUE) at the regional scale were simulated and discussed. The irrigation data stream performed better in representing observed SM dynamics compared to the standard irrigation routine that could be further improved by implementing more flexible irrigation schedules and irrigation efficiency. At the regional scale, simulated irrigation and yield showed a high sensitivity to climatic changes caused by the topographic gradient. While a 25% reduction in irrigation had negligible negative effect on simulated yield and CWUE, a reduction of 50% notably reduced both variables. These effects varied with climatic conditions, soil properties and timing of irrigation. These results showcase how CLM5 could be utilized for irrigation and water resources management.

4.1 Introduction

Irrigation plays a vital role in sustaining global food production by providing a reliable water supply to agricultural systems, especially in semi-arid or arid regions [*McLaughlin and Kinzelbach*, 2015]. With a growing global population and increasing food demands, irrigation contributes significantly to ensuring food security by enabling higher crop yields and reducing the vulnerability of agricultural systems to climate change [*McDermid et al.*, 2023; *Mueller et al.*, 2012]. On the other hand, poor management of irrigation water has led to the depletion of groundwater resources [*Dangar et al.*, 2021; *Scanlon et al.*, 2012; *Wada et al.*, 2010] and water use conflicts in many regions [*Cai et al.*, 2003; *Eshete et al.*, 2020; *Gurung et al.*, 2006]. Apart from quantitative and qualitative effects on water resources [*García-Garizábal et al.*, 2012; *Zhang et al.*, 2022], irrigation substantially impacts biogeophysical and biogeochemical processes at the land surface through alteration of the hydrological cycle or energy budget. This has subsequent effects on climate [*DeAngelis et al.*, 2010; *Erb et al.*, 2017; *Ferguson and Maxwell*, 2012; *Gordon et al.*, 2005; *Sacks et al.*, 2009]. The multidimensional role of irrigation calls for increased efforts in effective irrigation management and irrigation impact studies using large-scale approaches. This is crucial not only to meet food demands and mitigate future increases in climate change induced water stress, but also to understand its interactions and feedback mechanisms within the Earth system [*Elliott et al.*, 2014; *McDermid et al.*, 2023].

Modelling can be a powerful tool to simulate complex interactions in agricultural systems, evaluate different irrigation and climate scenarios, and provide decision support for water resources management [*Blyth et al.*, 2021; *Pongratz et al.*, 2018]. This necessitates comprehensive modelling frameworks that combine field-scale representations of crop growth and irrigation with a more holistic assessment of the impacts of irrigated agriculture on water resources and climate at larger scale [*Peng et al.*, 2020]. Process-based crop models include a range of crop parameterizations that provide a unique way to study crop growth processes in response to irrigation practices by using physical and biological principles. However, their main purpose is to simulate yield at the field scale, often over a single growing season, while lacking the interface with the land surface, soil, and climate [*Cheng et al.*, 2020]. Land surface models (LSMs), on the other hand, provide a more holistic representation of the land-atmosphere interactions to capture the feedback mechanisms between irrigation, vegetation,

hydrological processes, and climatic conditions beyond the field scale [*Blyth et al.*, 2021]. Conversely, they often lack more detailed physiological and genetic representations of crops and irrigation management [*Lombardozzi et al.*, 2020; *Peng et al.*, 2018]. This limits the ability of LSMs to reliably simulate yield and irrigation water withdrawals leading to poor model performance and biases in related processes such as carbon, energy, and water fluxes over intensively irrigated regions [*Leng et al.*, 2015; *Lombardozzi et al.*, 2020; *Ozdogan et al.*, 2010; *Zhang et al.*, 2020].

In recognition of the important role of human land management, efforts to advance the representation of crops and irrigation in LSMs are ongoing [*Pokhrel et al.*, 2016]. Various land surface models such as ORCHIDEE, the Community Land Model (CLM), and Noah-MP have since added crop modules [*Levis et al.*, 2012; *Liu et al.*, 2016; *Smith et al.*, 2010]. New crop representations have been developed to improve crop growth and management processes [*Boas et al.*, 2021; *Peng et al.*, 2018] or to add new crop types [*Dombrowski et al.*, 2022; *Fader et al.*, 2015; *Fan et al.*, 2015]. Rather simple irrigation schemes are generally incorporated based on soil moisture (SM) thresholds [*de Vrese et al.*, 2016; *Ozdogan et al.*, 2010; *Sacks et al.*, 2009], while more recent developments include the integration of irrigation techniques [*Leng et al.*, 2017; *Yao et al.*, 2022], irrigation water withdrawal from different sources [*Leng et al.*, 2017; *Xia et al.*, 2022], and water availability limitation [*Yin et al.*, 2020]. These studies, however, were performed at river basin, county, or global level with coarse spatial resolutions between 10 and 100 km. Simulated irrigation was validated against rather uncertain statistics like total yearly irrigation water withdrawals, without considering specific irrigation practices. Crop and irrigation data at higher spatial (< 5 km) and temporal (e.g. daily or sub-seasonal) resolution is needed to evaluate the representation of local irrigation schedules in LSMs and support irrigation management decisions. However, data to reliably constrain and further develop implemented irrigation schemes is often lacking, e.g. irrigation amount and timing along with continuous SM observations [*Lawston et al.*, 2017]. *Lawston et al.* [2017] first evaluated the sprinkler irrigation scheme of the NASA Land Information System LSM with point and gridded SM observations at 1 km resolution. While the model could not capture the field-scale heterogeneity and overestimated irrigation amounts, it captured well the seasonal variability and regional average SM dynamics. The authors did however use a prescribed crop phenology (green vegetation fraction) and did not examine the effect of irrigation on crop yield. A recent study examined the effect of

different irrigation setups on maize yield and two water use efficiency definitions using the dynamic crop and irrigation scheme of the Noah-MP LSM [*Huang et al.*, 2022]. They found that modelled crop yield was sensitive to irrigation quantity and timing (in which crop growth stage irrigation was applied) and based on these results recommended an optimal SM threshold to trigger irrigation. While the authors lacked data to accurately assess the irrigation amount and crop yield, their work presents a first use of a LSM to study the effects of deficit irrigation on crop growth, yield and water use efficiency.

The work presented here builds upon previous studies to continue the evaluation and improvement of irrigation representations in LSMs combining local irrigation, SM, and yield observations. In particular, this study applies CLM version 5, with a recent extension to represent deciduous fruit trees, to model irrigation and crop growth in a Mediterranean catchment. Specifically, we aim to: (1) evaluate the existing irrigation scheme of CLM5 and enhance its flexibility to account for local irrigation management practices; (2) assess whether the model can reproduce SM dynamics and crop growth in irrigated apple orchards using the enhanced model capability; (3) examine the potential to improve regional irrigation management by modelling the effect of different irrigation scenarios on crop yield and water use efficiency at the catchment scale.

4.2 Materials and Methods

4.2.1 Study area

Located in central Greece, the Pinios Hydrologic Observatory (PHO) covers an area of approximately 45 km^2 (Figure 4.1). The PHO was established in 2015 to study the Pinios catchment hydrological processes and, ultimately, to support local authorities in the sustainable management of water resources [*Pisinaras et al.*, 2018]. It is characterized by a Mediterranean climate with an annual precipitation of 500 to 1200 mm, and highest precipitation amounts in the winter months, annual potential evapotranspiration of approximately 1100 mm, and annual average air temperature of 15 °C [*Bogena et al.*, 2018]. The area displays a range of altitudes from 1500 m in the northern part down to less than 200 m in the plain. The mountainous part of the catchment features steep slopes and is covered by forests, mixed with shrubs and grassland, while the southern plain is primarily characterized by agriculture and small villages. In the plain, sandy loam soils

dominate while sandy clay loam and loamy soils also occur [*Pisinaras et al.*, 2018]. The PHO is located in one of the most productive agricultural areas in Greece owing, among other factors, to widespread irrigation practices that account for over 85% of the local freshwater consumption [*Panagopoulos et al.*, 2018]. The main cultivation are apple and cherry orchards (i.e., ~78% of agricultural area) that are irrigated between May and October. There are a few other rainfed fruit and nut tree orchards in the area with < 5% coverage. Annual crops including corn, cereal (mainly winter wheat), and potato are grown on the remaining agricultural land. They are partially irrigated, depending on precipitation occurrence, but cover a negligible part of the total irrigated area. Irrigation in the orchards is typically applied through micro sprinklers and the demand is almost entirely met by abstraction from the alluvial groundwater system through water wells, most of which are privately owned. Overexploitation of groundwater in the area due to poor irrigation management practices, amongst others, has previously been reported by *Panagopoulos et al.* [2018] and *Pisinaras et al.* [2023] resulting in the decline of groundwater levels.

Within the PHO, irrigation management in two irrigated apple orchards, hereafter referred to as S09 and S10, was studied (Figure 4.1). Both orchards have a size of around 1.2 ha, with a mild southern slope of < 5%. The soil texture is sandy loam and sandy clay loam with a high gravel content (13–29%) (Table 4.1) and many larger cobbles (> 64 mm according to *Wentworth* [1922]), especially below 30–50 cm depth. Trees are planted in rows, oriented North-South with 3.3 m distance between rows and an in-line distance of 1.5 m (approximately 2020 trees ha^{-1}). The trees in S09 and S10 were planted in 2013 and 2015 respectively, with a mixture of 3 to 5 different varieties. Trees are pruned to a height of 3.5 m throughout the winter season and residues are mulched back into the soil. Bud burst typically occurs in the second half of March while fruit development starts with the end of flowering in mid to late April. Harvest dates range from late August to mid-November depending on the harvested variety. Major leaf fall starts in late October and continues until mid-November, sometimes until early December. Trees are irrigated with a micro sprinkler system with a maximum flow rate of 60 L $hour^{-1}$ that is installed below the canopy, halfway between the tree stems of the same row. The irrigation season typically starts in May and continues until October. Orchards are fertilized with 80 kgN ha^{-1} at the end of flowering in April. Pest and fungicide treatment is applied prior to flowering and after flowering until late June. The grass in the alleys is generally mowed

once a month starting in March or April and mowing material is left on the ground. During periods of intense heat, the actively growing grass cover provides a cooling effect to protect the apples from heat damage.

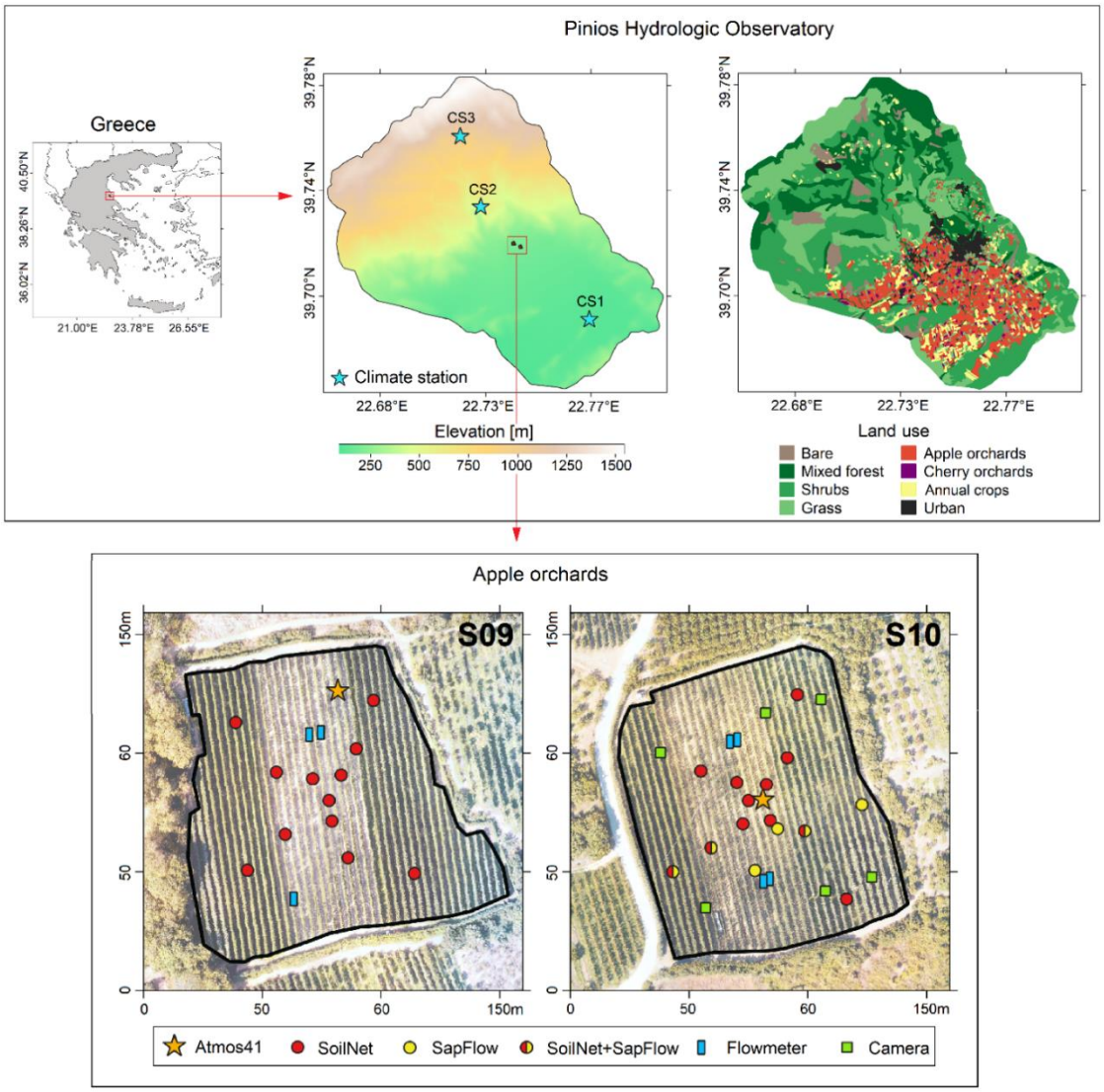

Figure 4.1 Top left: Map overview of Greece and of the study area location. Top right: Elevation and land use of Pinios Hydrologic Observatory with the locations of climate stations. Bottom: Apple orchards S09 and S10 with instrumentation.

Table 4.1 Main characteristics of the two apple orchards (S09 and S10).

Orchard ID	Altitude (m a.s.l.)	Size (ha)	Apple varieties	Soil depth (cm)	Sand content (%)	Clay content (%)	Soil organic carbon content (%)	Gravel content (%)
S09	200	1.24	3	0–30	64.5	17.8	1.5	23.3
				30–60	63.0	21.9	1.2	20.6
				60–90	59.9	24.6	0.7	13.7
S10	190	1.13	5	0–30	64.3	12.5	1.44	28.2
				30–60	65.8	12.7	0.86	28.7
				60–90	65.4	13.7	0.66	28.7

4.2.2 Data sources

The meteorological data that are necessary to drive CLM5 including precipitation, air temperature, atmospheric pressure, wind speed, relative humidity, and incoming solar radiation, were acquired from three meteorological stations located at different altitudes within the PHO (Figure 4.1) as well as two stations located in the orchards S09 and S10. For the agricultural plain, detailed soil texture and organic matter information was collected during an extensive soil sampling campaign. In total, 116 locations were sampled with one sample from the topsoil (0–50 cm) and a second sample from the subsoil (50–100 cm) (Figure 4.2). In addition to the point measurements, the LUCAS topsoil physical properties for Europe soil map [*Ballabio et al.*, 2016] and the European Soil Database (ESDB) derived data product [*Hiederer*, 2013] provide soil information for the area at a resolution of 500x500 and 1000x1000 m, respectively (Table 4.2). These data sources were combined to create soil texture (point measurements+LUCAS) and soil organic carbon (point measurements+ESDB) maps for model input (Figure 4.2). In a first step, for the unsampled regions, data points were extracted from the map products in a sampling density equal to the average density of the soil sampling locations (~580x580 m). Next, the extracted points were combined with the sampled points to a single set of data points (Figure 4.2). Then, the points were interpolated to the target resolution of 100x100 m using ordinary kriging and a spherical variogram model with a radius that included 30 measurements around an estimation point. Topographic information was available through the European Digital Elevation Model (EU-DEM) [*Copernicus*, 2016], version 1.1 at a spatial resolution of 25x25 m (Figure 4.1). Detailed maps of the

agricultural fields and orchards were provided by the Hellenic Payment and Control Agency for Guidance and Guarantee Community Aid while the land use of the remaining area was digitized from satellite imagery, using ArcGIS® software by Esri (Figure 4.1).

Orchard scale SM data were retrieved from S09 and S10, which were equipped for extensive monitoring in September 2020 (Figure 4.1). SM was monitored via a SoilNet wireless sensor network [*Bogena et al.*, 2010; *Bogena et al.*, 2022] with 12 nodes per orchard. Each node had six SMT100 SM sensors (Truebner GmbH, Neustadt, Germany) divided into two separate profiles which were installed at 5, 20, and 50 cm depth as well as two TEROS21 soil matric potential (SMP) sensors (METER Group Inc., Pullman, USA) installed at 20 cm depth. Irrigation amounts were recorded with TW-N flowmeters (TECNIDRO, Genova, Italy), installed at different irrigation sectors within the orchards. Meteorological data was collected by the cost-effective but reliable all-in-one ATMOS41 weather station (METER Group Inc., Pullman, USA) installed above the canopy in each orchard [*Dombrowski et al.*, 2021]. A more detailed description of the instrumentation and setup used to monitor SM dynamics, irrigation, and meteorological variables is given in *Brogi et al.* [2023]. Additionally, S10 was equipped with six SFM-1 sapflow sensors (ICT International Pty Ltd, Armidale, Australia) to estimate whole-tree transpiration. The sapflow sensors were installed on the trunk of six trees to represent, as much as possible, the orchards' trees in terms of height, perimeter, and vigor covering all five varieties. The installation and data correction followed the procedure outlined in *Burgess* [2018]. Phenology of the three main apple varieties was monitored using six phenocams (SnapShot Cloud 4G, Dörr GmbH, Germany) installed in S10.

Table 4.2: Main characteristics of the different soil data products used for the surface file creation of the regional case.

	European Soil Database Derived data	**LUCAS topsoil physical properties for Europe**
Underlying observational data	European Soil Database, Harmonized World Soil Database, Soil-Terrain Database	LUCAS 2009 soil survey (around 20 000 points) for EU-25
Resolution (m)	1000x1000	500x500
Soil texture	Yes	Yes
Organic matter	Yes	No
Depth ranges (cm)	0–30, 30–100	0–20

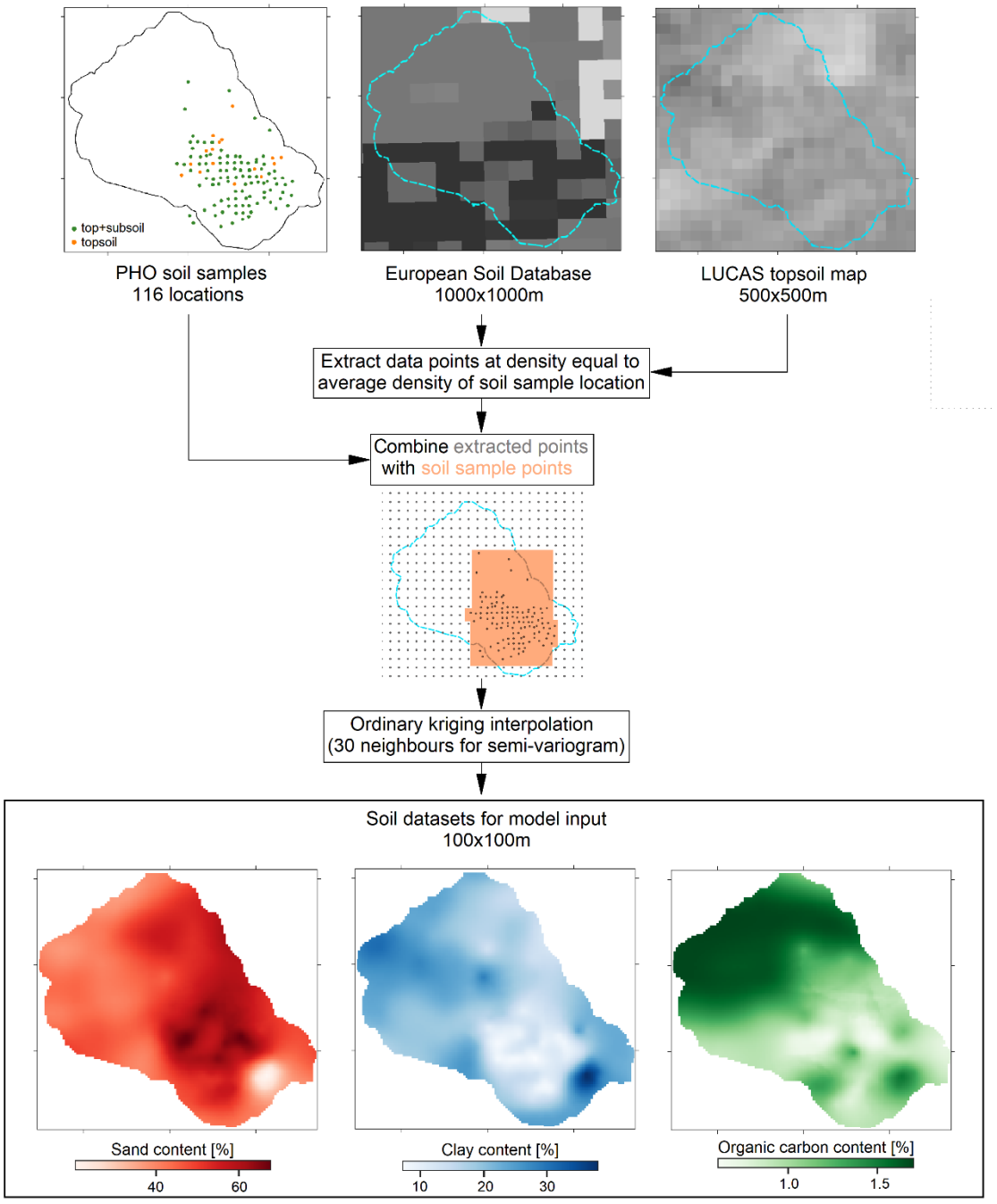

Figure 4.2 Top, from left to right: Soil sampling locations within the Pinios Hydrologic Observatory, soil data from the European soil database and the LUCAS topsoil map. Bottom: Soil texture input data sets of sand, clay, and organic carbon derived from the three data sources.

4.2.3 The land surface model

4.2.3.1 The Community Land Model

The Community Land Model v.5 (CLM5) used in this study is the latest version of the land component in the Community Earth System Model as described in detail by *Lawrence et al.* [2019]. CLM5 simulates land surface energy fluxes as well as

hydrological, biogeophysical, and biogeochemical processes that are driven by atmospheric input variables in combination with soil and vegetation states and characteristics [*Lawrence et al.*, 2018]. These processes are simulated on different subgrid units within a grid cell. Subgrid units include (1) the land unit defining the land use category (e.g., vegetated, urban, crop), (2) the column that is represented by 20 soil and 5 bedrock layers and resolves state variables and fluxes of water and energy in the soil, and (3) the patch level capturing biogeophysical and biogeochemical differences between plant functional types (PFTs) (e.g., broadleaf deciduous forest, evergreen shrub, maize, soy). The one-dimensional multilayer vertical water flow in the soil is simulated using a modified Richards equation [*Dingman*, 2015]. Soil hydraulic parameters for these calculations are derived from pedotransfer functions of sand and clay [*Clapp and Hornberger*, 1978; *Cosby et al.*, 1984] and organic properties of the soil [*Lawrence and Slater*, 2008]. With version 5 of CLM, a plant hydraulic stress routine was introduced that uses a simple hydraulic framework to model water transport along a water potential gradient from soil via plant to atmosphere [*Kennedy et al.*, 2019]. The new configuration replaces soil potential with leaf potential as the basis for plant water stress while root water potential is used to drive root water uptake. A new biogeochemistry and crop module, BGC-Crop, enhanced the representation of major crop functional types and land management practices such as irrigation and fertilization. Unlike natural vegetation that competes for water and nutrients, crops operate on separate soil columns that may be irrigated or non-irrigated, thus allowing for differences in land management [*Lawrence et al.*, 2019].

The recent development of CLM5-FruitTree enables the simulation of deciduous fruit trees and associated management practices in CLM5. The main features of the new sub-model include (1) a perennial phenology routine that allows the woody plant parts to remain on the orchard for several years, (2) carbon storage dynamics that enable the regrowth of annual plant parts, (3) an adapted carbon and nitrogen allocation, and (4) the description of typical management practices such as transplanting, pruning, and orchard rotation. Additionally, a new apple plant functional type was parameterized while fertilization and irrigation use the default CLM5 schemes. The complete model development of CLM5-FruitTree is described in *Dombrowski et al.* [2022].

4.2.3.2 Irrigation module in CLM5

Irrigation is performed individually over each irrigated soil column and responds dynamically to SM based on a daily check at 6 am. If crop leaf area is non-zero and if the available soil water over a specified irrigation depth z_{irrig} (=0.6 m by default) is below a defined threshold, irrigation is triggered. The irrigation amount is based on the SM deficit (D_{irrig}) that is calculated over z_{irrig}:

$$D_{irrig} = w_{thresh} - w_{avail} \tag{4.1}$$

where w_{avail} is the available SM (mm) and w_{thresh} is the irrigation SM threshold (mm) calculated as:

$$w_{thresh} = f_{thresh}\left(w_{target} - w_{wilt}\right) + w_{wilt} \tag{4.2}$$

where w_{target} is the irrigation target SM (mm), w_{wilt} is the SM at wilting point (mm), and f_{thresh} is a tuning parameter. If f_{thresh} = 1 (default), irrigation will be triggered once the available SM is below w_{target}. If f_{thresh} = 0, irrigation is only triggered once the available SM falls below w_{wilt}. Target SM is determined as the sum of SM at the target SM of each soil layer:

$$w_{target} = \sum_{i=1}^{n_{irr}} \theta_{target,i} * \Delta z_i \tag{4.3}$$

where n_{irr} is the index of the soil layer corresponding to z_{irrig}, Δz_i (mm) is the depth of the soil layer i and $\theta_{target,i}$ is the target volumetric SM value in a given soil layer. Similarly, w_{wilt} is calculated as the sum of SM at wilting point of each soil layer:

$$w_{wilt} = \sum_{i=1}^{n_{irr}} \theta_{wilt,i} * \Delta z_i \tag{4.4}$$

where $\theta_{wilt,i}$ is the volumetric SM value at wilting point in a given soil layer. θ_{target} and θ_{wilt} are calculated by inverting the equation for soil matric potential (SMP) (Eq. 7.53 in *Lawrence et al.* [2018]) at the respective depth. By default, the SMP parameters ψ_{target} and ψ_{wilt} are set to –34 and –1500 kPa, considered field capacity and permanent wilting point, respectively.

In addition to w_{target}, w_{wilt}, f_{thresh}, and z_{irrig}, the user can define the irrigation duration (T_{irrig}). Irrigation is applied directly to the ground surface at an intensity equal to $\frac{D_{irrig}}{T_{irrig}}$. Irrigation parameters are not spatially distributed but are defined globally for a given model domain independent of geographic location or crop type.

4.2.3.3 Irrigation data stream implementation

To study and evaluate the modelling outcomes under specific observed irrigation practices, an irrigation data stream was implemented in CLM5 to enable continuous prescription of irrigation parameters, i.e., irrigation rate, duration, and start time. These parameters are defined separately for one or multiple crop types and for each grid cell. This allows to account for differences in irrigation management depending on crop type and location to accurately reproduce local management practices. In addition, using the data stream, the applied irrigation amount can be easily adjusted, thus creating different irrigation scenarios while maintaining the same irrigation schedule. As irrigation is prescribed, the irrigation SM threshold that is calculated in the standard irrigation routine is not needed for this implementation.

4.2.4 Model implementation

4.2.4.1 Orchard scale simulations

For the simulations of S09 and S10, CLM5-FruitTree was run in single point mode and forced with hourly meteorological data from the two orchards. Fertilizer amount and soil texture were adjusted according to information provided by the farmer and soil samples. The default parameter file was adapted to account for the local climate and orchards characteristics. Crop parameters such as the different phenological stages were adjusted according to observations from the phenocam pictures, harvest information, and communication with the farmer. In the absence of observed bud break dates, parameters for the bud break prediction model were calibrated such that bud break would occur around the estimated date of 15th of March using the available local climate data. The modified crop parameters are listed in Table 4.3. Additionally, the observed irrigation time series was used as input to the irrigation data stream.

In order to balance ecosystem carbon and nitrogen pools and total water storage in CLM5 [*Lawrence et al.*, 2018], a 200 years model spin-up was performed. For this, the

CRUNCEPv7 atmospheric forcing data set from 1986 to 2016 [*Viovy*, 2018] and the parameterized apple plant functional type were used. Using the model state at the end of the spin-up, simulations were then re-initiated from planting in 2013 (S09) and 2015 (S10) using meteorological data from climate station CS1 (2016–2020) and data from the ATMOS41 sensors installed in the orchards for the years 2021 and 2022.

Table 4.3: Local crop parameters for the apple plant functional type.

Parameter	**Variable name (unit)**	**Value**
Base temperature for bud burst prediction and GDD summation	baset (°C)	8.5
Chilling requirements for bud burst	crequ (chill days)	–126
Critical temperature to initiate leaf offset	crit_temp (K)	281.15
Final root allocation coefficient until harvest	arootf2 (unitless)	0.12
GDD needed from bud break to canopy maturity	lfmat (degree days)	1350
GDD needed from bud break to harvest	hybgdd (degree days)	2100
GDD needed from bud break to the fruit ripening phase	grnrp (degree days)	640
GDD needed from bud break to the start of fruit development	grnfill (degree days)	130
Initial leaf allocation coefficient	fleafi (unitless)	0.25
Maximum canopy height	ztopmx (m)	3.65
Maximum harvest date in the northern hemisphere	max_NH_harvest_date (mmdd)	1120
Maximum LAI	laimx (m^2 m^{-2})	2.1
Maximum rooting depth	root_dmx (m)	0.6
Planting density	nstem (# m^{-2})	0.202
Ratio of height: radius at breast height	taper (unitless)	95
The slope of the relationship between leaf N per unit area (gN/m2) and Vcmax25top (umol CO2/m2/s)	s_vcad (μmol CO_2 s^{-1} gN^{-1})	30

4.2.4.2 Regional case simulations

A regional model domain, encompassing the entire PHO, was set up at a spatial resolution of 1 ha. This resolution was a compromise between accounting for the diverse, patchy landscape with small field and orchard sizes (from a few 100 m^2 to some hectares) and a reasonable computational effort. For the land use information, the database of agricultural fields and orchards was combined with the remaining land uses digitized from satellite imagery. Since CLM5 allows to define fractional land use in a single grid cell, the overall area of individual land use classes was still accurately represented.

The slope of the terrain was derived from the EU-DEM. Furthermore, the surface parameter defining the depth to bedrock was adjusted based on the minimum (0.27 m) and maximum (1.3 m) depths available to roots from the ESDB, which were linearly scaled by the slope. In the plain area, the value was set between 10 and 20 m to represent the thick alluvial deposits and prevailing free drainage conditions. Lastly, the maximum fractional saturated area (f_{max}) that controls runoff generation was set to zero for all grid cells containing crops due to the deep groundwater table, gentle sloping in the plain, and assuming that there are no large saturated areas in the fields and orchards. f_{max} was set to 0.16 in the remaining areas of the catchment as extracted from the global data set. The adjusted parameters for apple were used as described in Section 4.2.4.1 while a separate parameter set was used for cherries to account for the earlier start of the growing season and harvest, and lower productivity as compared to apples. For the sake of consistency, parameters for winter wheat and potato were also modified based on *Boas et al.* [2021] with minor adjustments to growing seasons to account for the local climate [*Dercas et al.*, 2022; *FAO*, 2023].

For the model spin-up, the available global GSWP3 v1 atmospheric forcing data set providing data from 1901 to 2010 at a 3-hourly temporal and 0.5° spatial resolution was used [*Lange and Büchner*, 2020]. The model was spun-up for 720 years until equilibrium for soil carbon and nitrogen pools, soil water storage, and other ecosystem variables was reached for all land uses in the catchment. For the remaining simulations, the model was forced with a 7-year time series obtained from the observational data of meteorological stations CS1, CS2 (2016–2022), and CS3 (2018–2022) in the study area as well as from the two ATMOS41 stations in orchard S09 and S10 (2021–2022) (Figure 4.1). The data was spatially interpolated to the same resolution as the surface data using inverse distance weighting. The interpolation of precipitation and temperature included a weighting factor for elevation variation using a linear correlation between station elevation and mean annual station precipitation and temperature, respectively, as described in *Panagoulia* [1995]. Another short spin-up period of 3 years was performed as the orchards had just reached their maximum lifespan before orchard rotation is initiated and new seedlings need a couple of years to reach the full productivity level [*Dombrowski et al.*, 2022].

4.2.5 Simulation scenarios

To assess how well CLM5-FruitTree can represent SM dynamics and crop growth in the study area, 1D simulations were first performed in orchards S09 and S10 for the growing seasons 2021 and 2022. Two model set-ups were tested: the first used the default CLM5 irrigation routine with adapted parameterization to approximate the observed irrigation schedule, while the second was prescribed with the observed irrigation through the irrigation data stream. By directly applying irrigation water to the ground surface, CLM5 assumes an irrigation efficiency of 100% which is hardly achieved in sprinkler irrigation [*Gilley and Watts*, 1977]. For the irrigation data stream, we thus assumed that only 75% of the water volume measured by the hydrometers is reaching the ground surface while the rest is lost through evaporation from leaf surfaces, transpiration of the grass cover in the orchard alleys, and leakages in the piping system. Modelling results were compared to observed SM and tree transpiration at a daily time step as well as crop yield and development. Pearson's coefficient of correlation (r), the root mean square error (RMSE) and the percent bias (%bias) were calculated for statistical model evaluation.

For the regional case, we conducted three simulation experiments to test different irrigation scenarios. Regional data on irrigation outside the instrumented orchards S09 and S10 was not available. Thus, the model was run using the default CLM5 irrigation routine with the same parameterization that was used for the point scale simulations, in the following considered the full irrigation scenario (FI). Based on this scenario, two deficit irrigation scenarios were created for both apple and cherry orchards with 75 and 50% of full irrigation (DI75 and DI50, respectively) using the irrigation data stream. All scenarios were run over the same 7-year period (2016–2022). To investigate the differences between irrigation scenarios, multi-year averages and seasonal dynamics of irrigation, SM, crop growth or yield, and crop water use efficiency (CWUE) were calculated and compared. In this study, CWUE was defined as the amount of yield produced per unit volume of water consumed [*Ibragimov et al.*, 2007]:

$$CWUE = \frac{Y}{ET} \tag{4.5}$$

where Y is crop yield in t ha^{-1} and ET is crop evapotranspiration in mm.

4.3 Results

4.3.1 Orchard scale simulations

4.3.1.1 Soil moisture and matric potential dynamics

Outside the irrigation season

Figure 4.3 and Figure 4.4 show the SM time series at 5, 20, and 50 cm depth and SMP at 20 cm depth for S09 and S10, respectively. The interquartile range (Q_{25}–Q_{75}), calculated from 24 measurements (12 nodes with two profiles each) for every depth, shows considerable variability in SM, especially in S10 and at 50 cm depth. This reflects the high heterogeneity of soil texture and gravel content that was observed during soil sampling. When comparing the observed SM dynamics in the two orchards, S09 showed 4–12 vol% higher SM on average compared to S10 throughout the measurement period. The soil textural analysis of both orchards clearly showed a higher clay and organic matter content, and lower gravel content in S09 compared to S10 (Table 4.1). Frequent rainfall during the winter months (631 and 606 mm in 2021 and 2022 respectively) kept the soil close to saturation with average SMP around –8.5 kPa in both orchards. Starting in April the soil gradually became drier causing a steep decline in SMP to around –500 kPa (S09) and –300 to –400 kPa (S10) by mid-May. The decline resulted from low rainfall amounts and increased evaporation demand along with water consumption from the grasses in the alleys and the fruit trees. In addition to the observations, the simulation results using both the standard CLM5 irrigation routine and the irrigation data stream are shown for the corresponding CLM5 soil layers in Figure 4.3 and Figure 4.4. Table 4.4 lists the model quality parameters used to evaluate the simulation results. The model simulations outside the irrigation season, using either irrigation approach, corresponded well to the observed SM in S09. However, in S10, CLM5 overestimated SM in the soil profile by on average 4.5–7.3 vol%. The observed differences in SM between both orchards were not captured by the model where SM values in S10 were only 1–2 vol% higher. In April and May, just before the start of the irrigation season, the simulations showed the strongest deviation from observed values for both orchards as the soil drying was much less pronounced in the simulations.

Irrigation season

In 2021 and 2022, the farmer irrigated every 5–7 days starting mid-May through October. Irrigation amounts per event varied strongly and averaged 14 and 25 mm in S09 and S10 respectively (upper panel of Figure 4.3 and Figure 4.4). Irrigation increased SM by up to 10 vol% in the top 5 cm and about 5 vol% at 50 cm depth. To represent the observed irrigation schedule, the CLM5 irrigation routine can be adjusted in two ways, by (1) adapting ψ_{target} or (2) tuning the f_{thresh} parameter. Figure 4.5 shows the effect that different values of these two parameters have on several aspects of the simulated irrigation (e.g., start of irrigation period, number of irrigation events, irrigation frequency) as well as on SM and crop yield. In both cases, a lower parameter value results in a later onset of irrigation, fewer irrigation events and lower total irrigation amounts. However, the parameters have different effects on irrigation frequency, whereby smaller values of f_{thresh} result in less frequent irrigation events while the irrigation volume per event increases (Figure 4.5). Changing ψ_{target}, on the other hand, has little effect on the irrigation frequency and volume. SM in the upper 50 cm of soil increases with increasing values of both parameters. The increase is exponential for ψ_{target} with values ranging between 0.195 and 0.275 $cm^3\ cm^{-3}$ and almost linear for f_{thresh} with a somewhat smaller range. Consequently, varying ψ_{target} has a more pronounced effect on yield compared to f_{thresh} for the investigated range of parameter values.

For the model run using the standard irrigation routine, we set f_{thresh} to 0.7 while leaving ψ_{target} at its default value of –34 kPa, which resulted in approximately weekly irrigation events of on average 26 mm per event, starting mid-May. This, however, could only partially reproduce the observed irrigation schedule and SM dynamics compared to using the irrigation data stream. Nevertheless, both irrigation approaches showed fluctuations of similar magnitude compared to the observed values in the upper soil. Less dynamics than observed were simulated at 50 cm depth for both irrigation approaches and both orchards. The wet bias in S10 was still persistent throughout the profile for the simulation using the irrigation data stream while simulated SM based on the default irrigation routine dropped to the range of observed values (Figure 4.4).

Simulated and observed total yearly irrigation were similar in S09 with the observed effective irrigation being 433 and 458 mm (75% of actual measured irrigation) and simulated amounts being 425 and 439 mm for 2021 and 2022, respectively. In S10,

observed effective irrigation amounts were considerably higher than in S09, which could be expected considering the lower observed SM in S10. Compared to the observed 706 and 586 mm, for 2021 and 2022, respectively, the model applied only 393 and 388 mm, which is a result of the simulated wet bias.

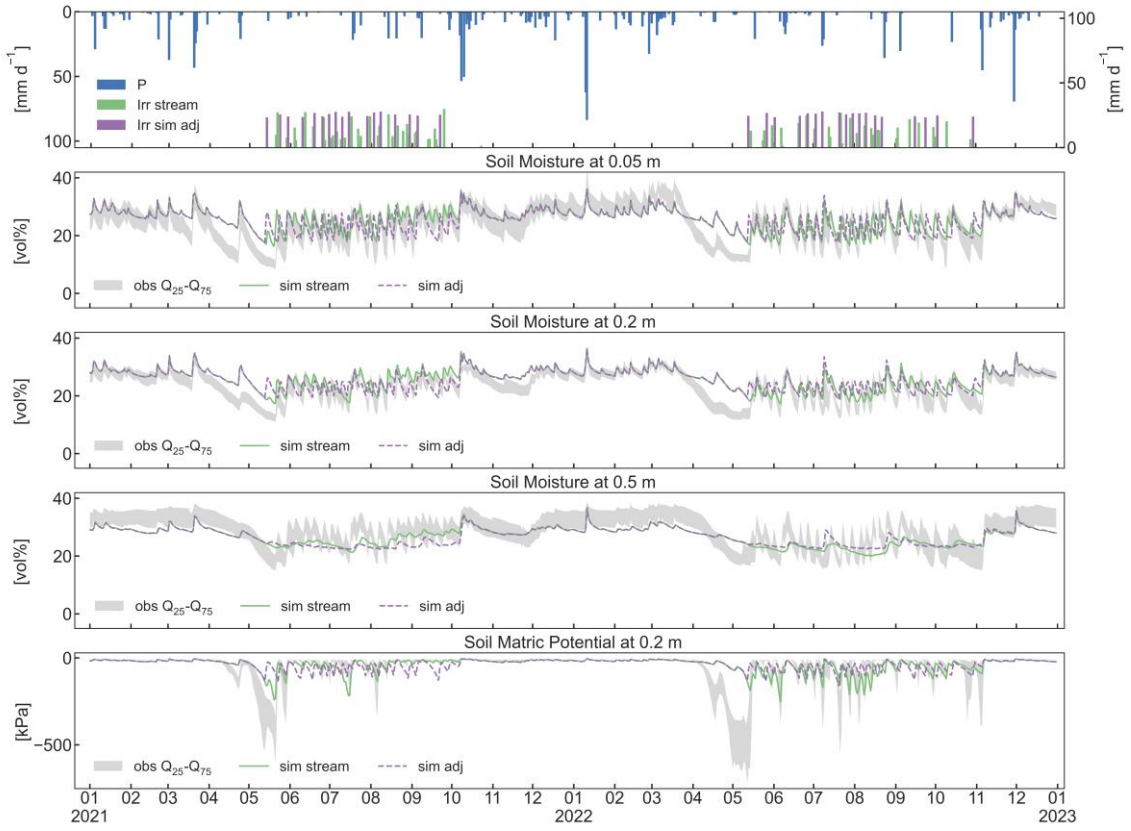

Figure 4.3 The upper panel shows precipitation, and observed and simulated irrigation for orchard S09 in mm d^{-1}. The central panels show observed soil moisture (SM) as interquartile range between the 25th and the 75th percentile from 24 measurements, simulated SM using the standard CLM5 irrigation routine and the irrigation data stream at 5, 20, and 50 cm depths. The bottom panel shows observed interquartile range and simulations using the two irrigation approaches of soil matric potential (SMP) at 20 cm depth for orchard S09 for 2021 and 2022.

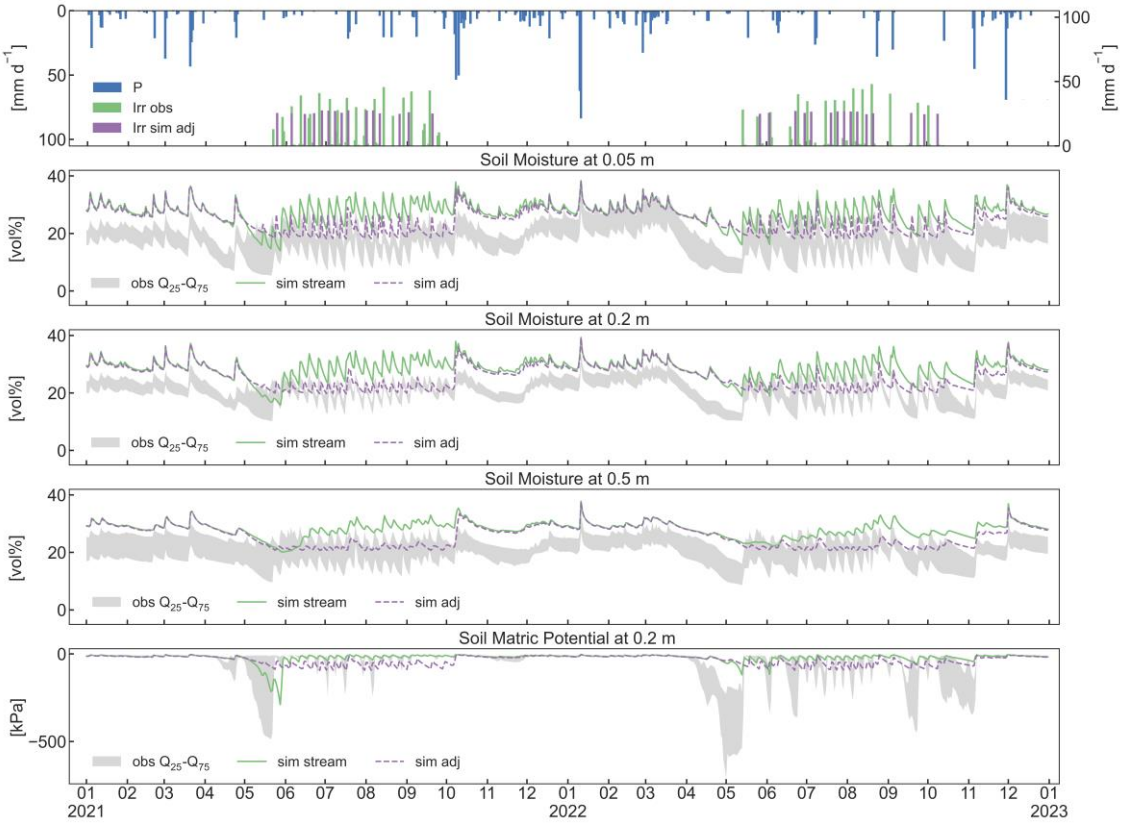

Figure 4.4 The upper panel shows precipitation, and observed and simulated irrigation for orchard S10 in mm d^{-1}. The central panels show observed soil moisture (SM) as interquartile range between the 25th and the 75th percentile from 24 measurements, simulated SM using the standard CLM5 irrigation routine and the irrigation data stream at 5, 20, and 50 cm depths. The bottom panel shows observed interquartile range and simulations using the two irrigation approaches of soil matric potential (SMP) at 20 cm depth for orchard S10 for 2021 and 2022.

Table 4.4: Pearson's coefficient of correlation (r), root mean square error (RMSE) and percent bias (%bias) for soil moisture (SM) at 5, 20 and 50 cm depth and soil matric potential (SMP) at 20 cm depth in orchards S09 and S10 simulated using the irrigation data stream. The first number refers to 2021 and the second number to 2022. Statistics were calculated for the whole year and for the irrigation season only (21th May to 25th Sep for 2021; 15th May to 10th Oct and 14th May to 2nd Oct for S09 and S10, respectively, in 2022).

			S09			S10		
		Soil depth (m)	**r**	**RMSE (vol%)**	**%bias**	**r**	**RMSE (vol%)**	**%bias**
Whole year	**2021/2022**	0.05	0.88/0.81	3.97/3.89	13.13/8.18	0.77/0.83	9.55/8.08	50.21/39.89
		0.2	0.88/0.86	3.10/3.23	10.14/9.26	0.75/0.84	8.18/7.68	37.30/35.55
		0.5	0.78/0.80	3.08/3.49	–6.60/–6.63	0.56/0.72	8.06/7.65	37.48/36.13
		SMP (kPa)	0.82/0.63	56.25/89.67	–27.54/ –37.14	0.62/0.75	41.65/122.41	–35.44/ –76.14
Irrigation season	**2021/2022**	0.05	0.86/0.74	3.85/3.02	15.47/4.30	0.70/0.83	5.13/8.43	21.13/45.60
		0.2	0.84/0.77	3.00/2.84	10.86/8.10	0.67/0.77	2.3/7.70	4.51/37.32
		0.5	0.48/0.27	3.12/3.74	–6.27/–6.14	0.25/0.45	1.73/7.10	–0.74/33.74
		SMP (kPa)	0.73/0.64	46.61/61.36	–11.08/ –7.54	0.65/0.66	52.04/98.86	–81.11/ –72.95

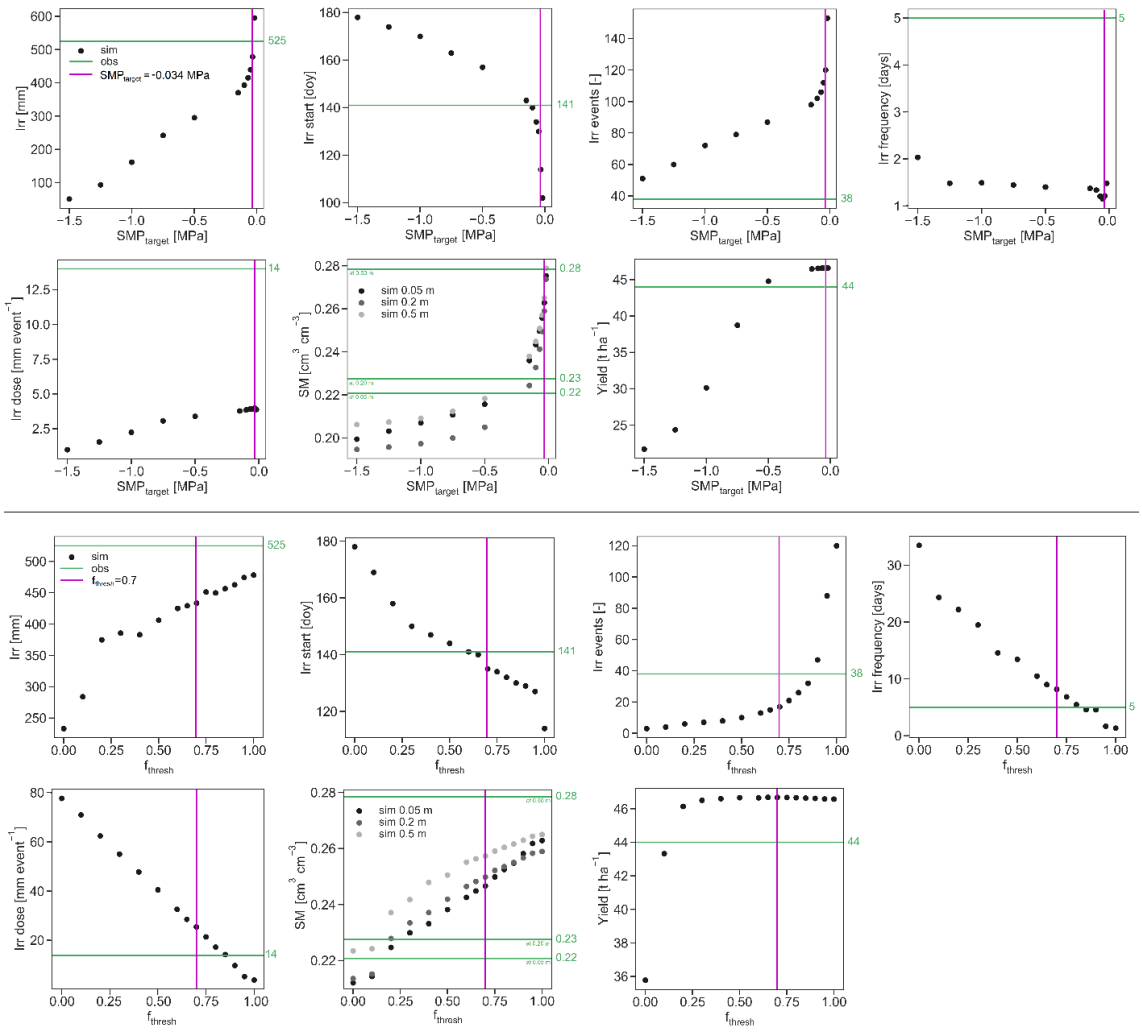

Figure 4.5 Effect of irrigation target soil matric potential (ψ_{target}) and irrigation threshold fraction (f_{thresh}) on total irrigation amount (Irr), irrigation starting date (Irr start), number of irrigation events (Irr events), irrigation frequency (Irr frequency), irrigation dose per event (Irr dose), soil moisture (SM) at 5, 20, and 50 cm depth, and yield. Shown are yearly average values for S09 and the year 2016.

4.3.1.2 Tree transpiration and fruit harvest

The comparison of measured sapflow with simulated transpiration expressed as water consumption per tree is presented in Figure 4.6. Observed sapflow varied significantly between different trees resulting in large inter-quartile ranges. The two model runs showed no difference in simulated tree transpiration despite the difference in irrigation amount and timing. In 2021, CLM5 showed higher values and a slight shift in the seasonal dynamic as a result of a too early onset of leaf development compared to the observed values (LAI_{sim} in Figure 4.6). Simulated leaf duration and total transpiration agreed well with the measurements in 2022. Tree transpiration peaked in July with a measured monthly average of 12.5 (2021) and 20.2 L tree^{-1} day^{-1} (2022) and simulated values of 25.1 (2021) and 24.5 L tree^{-1} day^{-1} (2022). The better agreement between simulated and

observed values in 2022 followed a reinstallation that was performed after partial sensor failure and unreliable measurements that resulted in data gaps for the 2021 growing season. The 2021 data should therefore be handled with care when interpreting absolute values. Simulated maximum leaf area index (LAI) was reached in early July. Full canopy cover in the orchards occurred in the second half of June, so slightly earlier, based on visual inspection of the phenocam pictures (data not shown). Simulated leaf area and hence transpiration fell to zero by December, which broadly agreed with observed sapflow and leaf senescence deduced from the phenocam images.

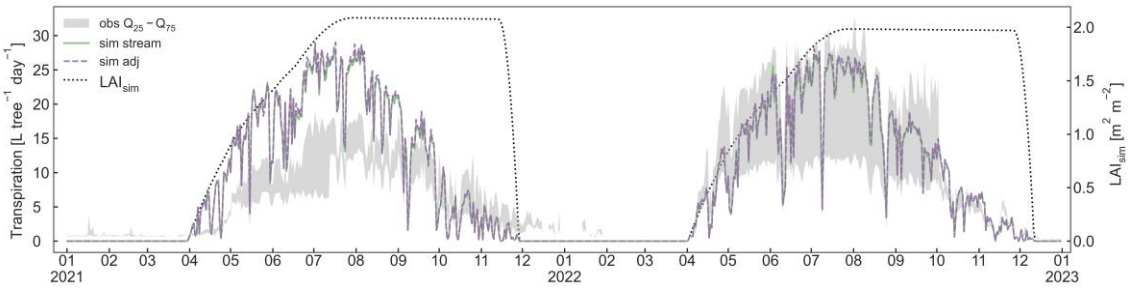

Figure 4.6 Whole tree transpiration estimated from the sapflow sensors in orchard S10 together with simulated transpiration expressed in liters per tree and day, and simulated leaf area index (LAI_{sim}) for 2021 and 2022.

Generally, fruit harvest in the orchards was performed between 17th of August and 30th of October in a first and second harvest for most varieties. Due to very low apple quantity, harvest in 2022 occurred in a single harvest between 1st Sep and 15th Nov depending on variety. Simulated harvest in 2021 occurred on 12th and 18th Sep for S09 and S10 respectively, and a few days earlier in 2022. The two simulation runs using either the adapted CLM5 irrigation routine or the irrigation data stream showed no difference in harvest amounts. In 2021, simulated yield was close to the observed values while the exceptionally low yield in 2022 was not captured by the simulations (Table 4.5). Visual inspection of the phenocam images showed significantly less flowers on the trees in 2022 compared to 2021 (data not shown). No extreme weather conditions were observed during the winter 2021/2022 that could explain the reduced flowering. Other possible reasons for the low number of flowers and hence low yield in this year may be related to alternate bearing of the varieties or other factors (e.g., plant physiology or traits, pest and disease or certain management practices) that are not included in the model.

Table 4.5: Observed and simulated apple yield in t ha^{-1} for orchards S09 and S10 for 2021 and 2022.

	Yield in S09 (t ha^{-1})		Yield in S10 (t ha^{-1})	
Year	**obs**	**sim**	**obs**	**sim**
2021	44	47	47	51
2022	16	49	11	50

4.3.2 Regional simulations

4.3.2.1 Irrigation signature in the PHO

Figure 4.7 shows simulated seasonal mean SM and sum of evapotranspiration (ET) within the PHO averaged over the 7-year period. Depicted values represent grid cell averages, meaning they are the weighted average of all land uses in a given cell. During the winter months and into spring, SM is high throughout the catchment, but with a declining gradient along the North-South axis from the mountainous part down to the plain. ET in the catchment is low during winter but starts to increase in spring, revealing a discernible pattern attributed to differences in land use (Figure 4.1). During the summer months, ET reaches its peak, displaying a distinct irrigation signature with significantly higher ET values of 293 mm on average over irrigated land, as opposed to 214 mm on average in the rest of the catchment. The pattern persists throughout autumn and is also evident in summer and autumn SM, albeit less pronounced due to the lower productivity of rainfed vegetation, resulting in reduced water uptake from the soil. The subsequent analysis will focus exclusively on the irrigated land, more specifically on apple orchards, as they account for 91% of the total irrigated area.

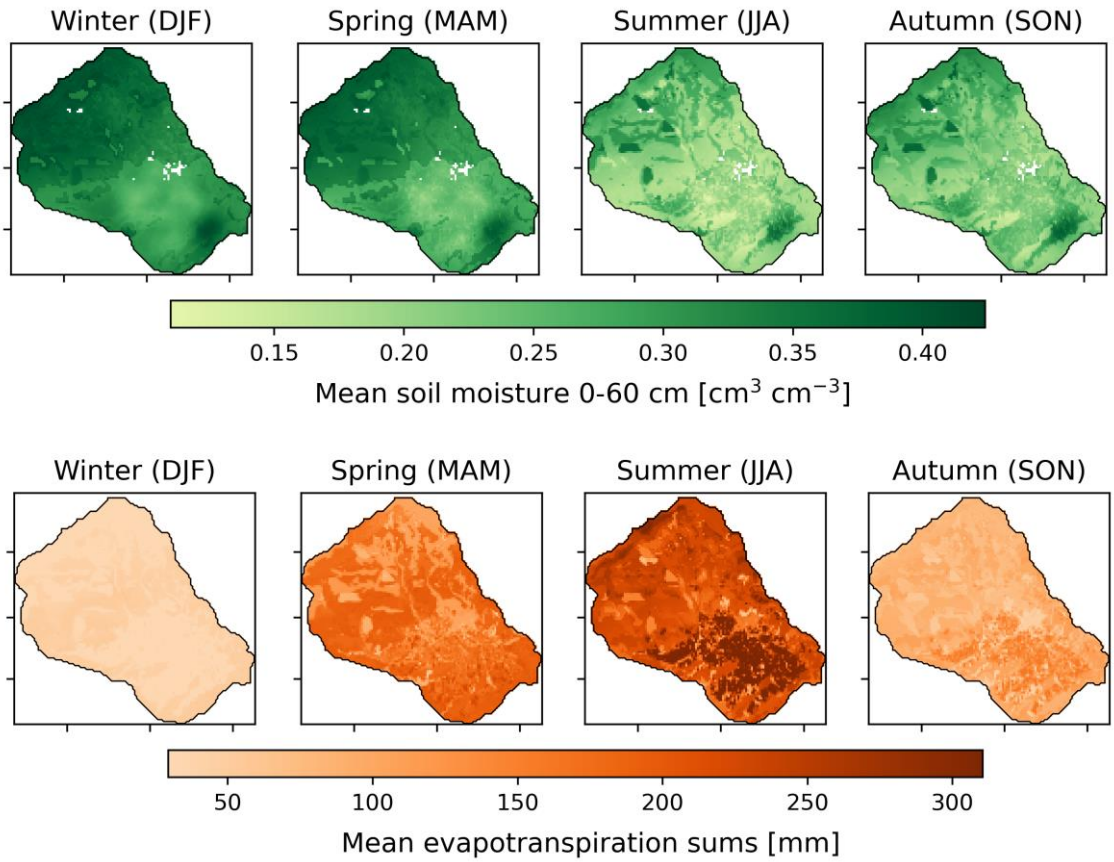

Figure 4.7 Seasonal mean soil moisture, and evapotranspiration sums in the PHO catchment, averaged over the period 2016–2022.

4.3.2.2 Simulated spatial patterns

Figure 4.8 shows average and standard deviation of the 7-year simulation period for irrigation, SM, yield, and CWUE for all apple orchards in the PHO, between 2016 and 2022. Modelling results show a clear spatial pattern that is driven by climatic conditions following the topographic gradient (Figure 4.1) on the one hand and soil characteristics on the other hand (Figure 4.2). Average yearly irrigation requirements range between 400 and 450 mm in the plain. The highest values are found in the southeast while considerably lower values occur at higher altitudes in the northern part of the catchment (< 200 mm). Harvest values show a similar pattern because cooler temperatures and lower incoming radiation in the northern part of the catchment result in lower crop productivity and thus smaller yields (16–38 t ha^{-1}) compared to the plain where yields are around 50 t ha^{-1} without much spatial variability. In addition to lower crop productivity and thus lower crop water demands, spatial variability in irrigation requirements results from the higher precipitation in the upper parts of the catchment that further reduces the need for irrigation as well as soil textural differences. The latter is most evident in the southern part of the catchment where the higher clay content and the consequently higher water holding

capacity of the soil result in increased evaporation (not shown). This in turn generates a greater irrigation demand resulting in slightly lower CWUE of orchards planted on these soils. Soil textural differences are also reflected in the SM plot where areas with a higher percentage of clay or organic matter show higher SM values than areas with sandier soils or soils that are lower in organic matter. CWUE ranges from 57–65 kg ha^{-1} mm^{-1} in the plain to 35–45 kg ha^{-1} mm^{-1} in the northern part of the catchment and largely reflects the spatial patterns of irrigation and harvest whereby high irrigation requirements and low harvest lead to low CWUE. Inter-annual variability (standard deviation plots) within the catchment shows similar patterns for irrigation, harvest, and CWUE and is higher in the northwestern part of the catchment. The higher variability was driven by local temperature differences in some years that delayed the onset of the growing season up to 14 days compared to the remaining orchards. Inter-annual variability of SM is generally low without a distinct spatial pattern.

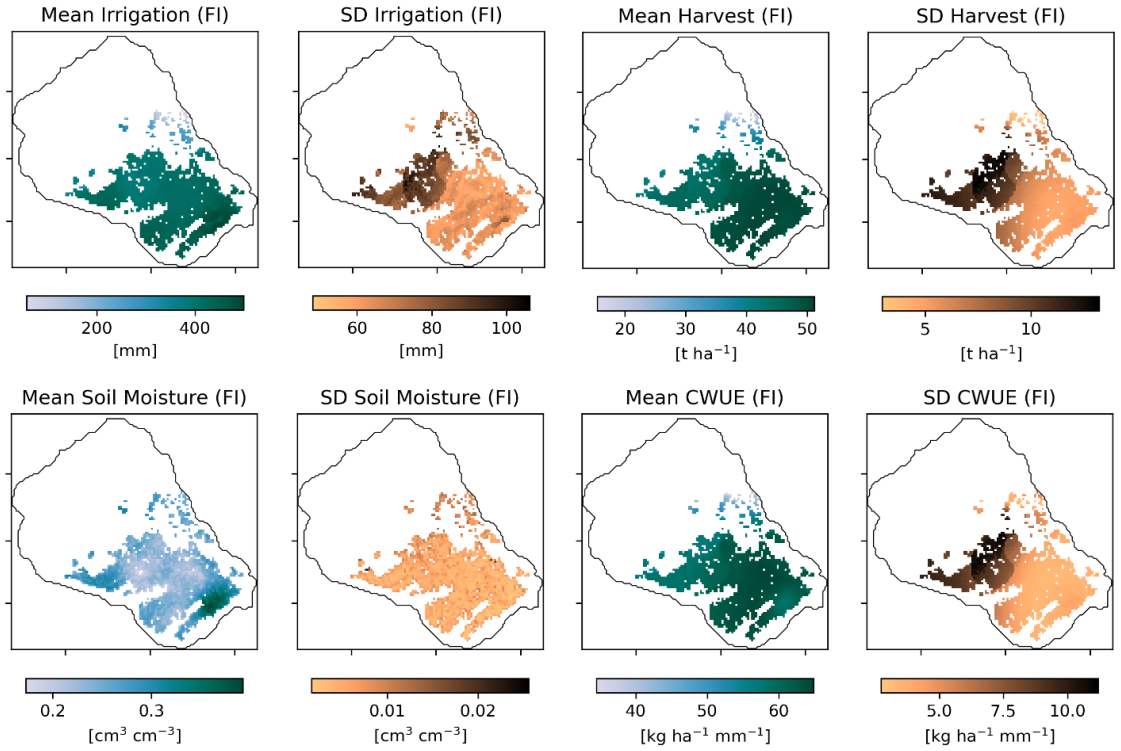

Figure 4.8 Mean and standard deviation (SD) of average yearly irrigation, soil moisture in the root zone (0–60 cm), harvest, and crop water use efficiency (CWUE) for apple orchards within the PHO between 2016–2022 under full irrigation (FI).

4.3.2.3 Effect of irrigation deficit scenarios

The effect of deficit irrigation on total irrigation amounts, harvest, and CWUE of apple orchards in the PHO for the moderate irrigation deficit scenario, DI75, and the more severe deficit scenario, DI50, are shown in Figure 4.9. Yield differences between the FI and the DI75 scenario are almost negligible, ranging from a decline of maximum 3 t ha^{-1} (5%) to even slight increases in yield. However, the DI50 scenario resulted in a clear decline of simulated yield with up to 12 t ha^{-1} corresponding to a 30% reduction in yield compared to the FI scenario. Nonetheless, orchards located at high altitudes and in the southeast on clay-rich soils are still barely affected by the higher water deficit (< 5% decline in yield). Overall, annual water savings are highest in the plain, averaging 100–125 mm for DI75 and 210–250 mm for DI50. CWUE shows a differing pattern between both scenarios. While in DI75, CWUE declines slightly in the central part of the plain by around 1 kg ha^{-1} mm^{-1} (2%), there are large areas that show an increase in CWUE of similar magnitude. The decline in CWUE is concentrated on the orchards growing on soils with a high percentage of sand. For DI50, on the other hand, CWUE is almost exclusively showing a decrease of up to 8.8 kg ha^{-1} mm^{-1} (17%), though again CWUE for orchards in the higher altitudes and the ones located on soils with higher clay content are less affected.

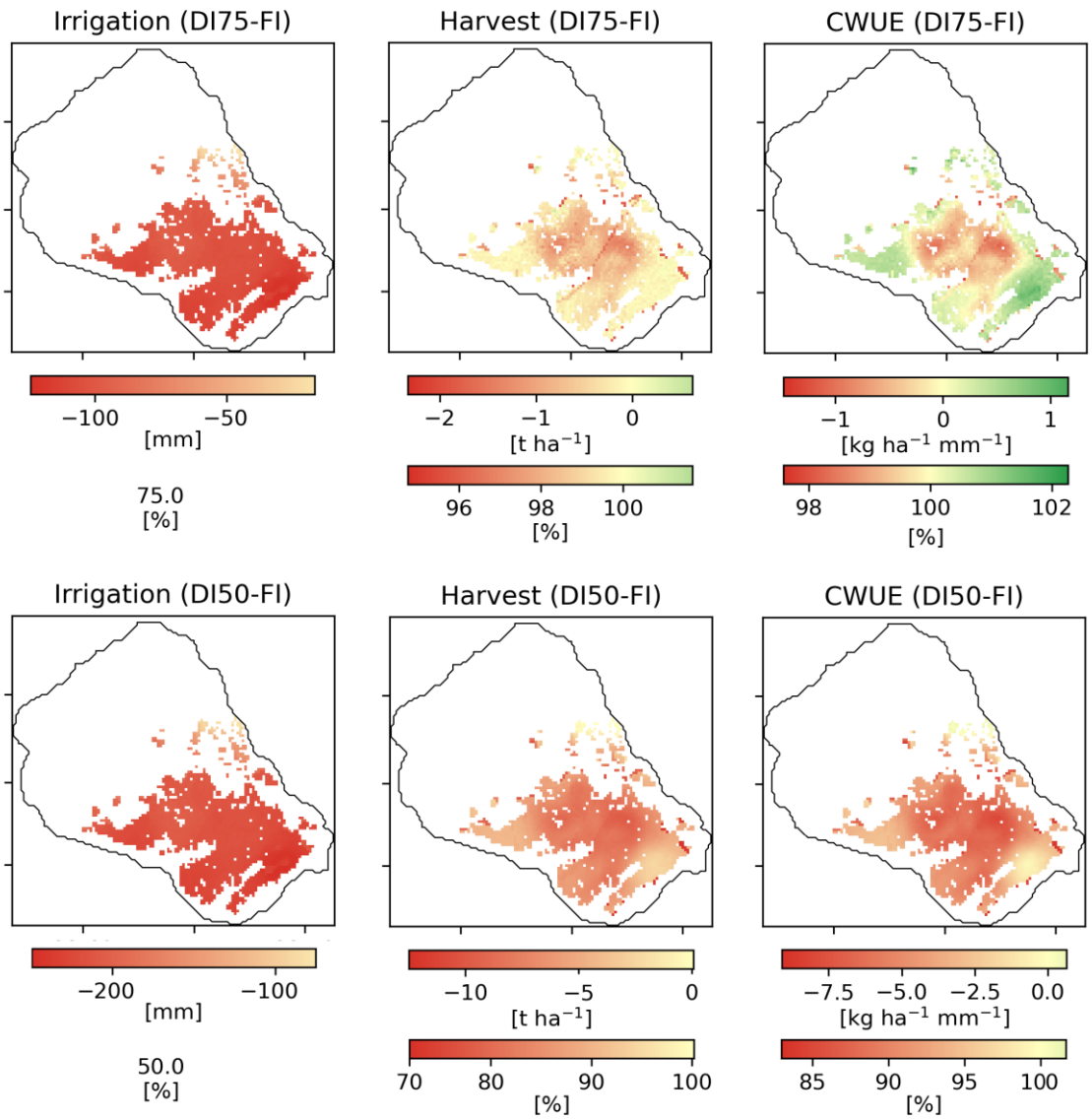

Figure 4.9 Absolute and relative differences in irrigation amount, harvest, and crop water use efficiency (CWUE) between the full and the 75% irrigation scenario (DI75-FI), and the full and 50% irrigation scenario (DI50-FI) for apple orchards within the PHO during the period 2016–2022.

4.3.2.4 Irrigation and yield at the inter-annual and monthly scale

Yearly irrigation amounts, precipitation during the main irrigation season, and harvest averaged for all apple orchards in the PHO are shown in Figure 4.10. For the investigated 7-year period, irrigation ranges between 297 and 487 mm while precipitation is around 167–322 mm from May to October. Differences in precipitation drive the inter-annual variability in irrigation requirements whereby drier summer months, such as 2019–2022, result in higher irrigation demand compared to wetter years. Yield ranges between 32 and 55 t ha^{-1}, with 2019 and 2020 being the years with the highest yields due to favourable meteorological conditions (high solar radiation and temperature). Notably, the effect of deficit irrigation on yield is strongest in these two years reducing yield by > 12 t ha^{-1} for the DI50 scenario. In contrast, both the DI75 and DI50 scenario have negligible effect on yield in the first three simulation years.

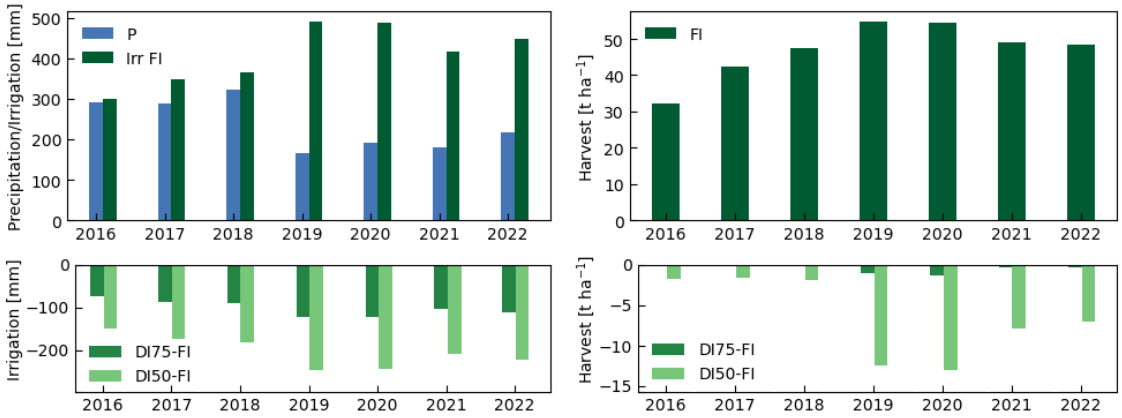

Figure 4.10 Yearly sum of precipitation during the main irrigation season (May-Oct), irrigation, and harvest averaged over all apple orchards within the PHO from 2016 to 2022, under full irrigation (FI) and the difference for the 75% and the 50% deficit irrigation scenarios (DI75 and DI50).

Figure 4.11 shows the seasonal course of irrigation, precipitation, and fruit growth in the apple orchards averaged over the PHO and the 7-year period. The simulated irrigation season starts in April or May and lasts until October with negligible amounts still applied in November for some years. Monthly irrigation requirements increase sharply between April and June until reaching their peak in August with on average 107 mm per month. Accordingly, August is also the month in which the greatest water savings occur for the deficit scenarios. After that, irrigation declines rapidly. Fruit biomass increases steadily from April to harvest in September with faster growth occurring in the earlier months. While fruit growth is barely affected by a 25% reduction in irrigation (DI75), for the DI50 scenario it decreases sharply in August and to a smaller extent in July and September.

The reduced fruit growth results in a yield loss of on average 0.5 t ha-1 for DI75 and 6.5 t ha-1 for DI50.

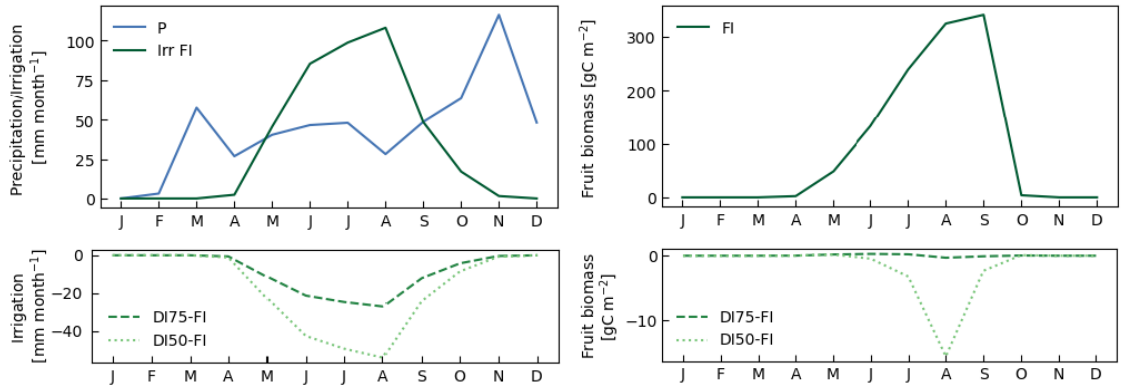

Figure 4.11 Seasonal pattern of monthly precipitation, irrigation, and fruit biomass averaged over all apple orchards within the PHO and the period 2016–2022, under full irrigation (FI) and the difference for the 75% and the 50% deficit irrigation scenarios (DI75 and DI50).

4.4 Discussion

4.4.1 Evaluation of the CLM5 irrigation routine

The direct comparison of simulated SM dynamics to observed SM from a dense sensor network in two irrigated orchards gave valuable insights into model performance. Our findings demonstrate that the standard CLM5 irrigation routine lacks the necessary flexibility to represent specific irrigation practices observed in the orchards. Simulated crop growth and transpiration at the orchard scale were not sensitive to the difference in irrigation amount and timing between the two model runs using the standard irrigation routine and the implemented irrigation data stream respectively. However, as differences between the simulated and actual irrigation practices increase, the effects may become more important especially considering runoff generation or sensible and latent heat fluxes that were not analysed in this study. Similarly, if the irrigation is limited so that the crop experiences some degree of water stress, the timing of irrigation may become more important. This could be further tested by applying different irrigation schedules under various amounts of irrigation using the irrigation data stream.

Prior studies using the irrigation module in CLM were limited to calibrating the target SM or adjusting the irrigation threshold fraction to match gross irrigation requirements reported at the country or regional level, or performed no calibration at all [*Felfelani et al.*, 2018; *Leng et al.*, 2015; *Leng et al.*, 2013; *Zhu et al.*, 2020]. The model, however,

does not currently consider restrictions on irrigation schedule, over irrigation, or irrigation efficiency that significantly affect gross irrigation requirements as our results revealed. The newly implemented irrigation data stream can be used to overcome some of these limitations by prescribing crop and farmer specific irrigation schedules and amounts. This allows investigating the irrigation-induced effects on e.g., crop yield, SM, or carbon and energy fluxes under observed irrigation practices and can help to identify existing model biases by removing one possible source of uncertainty. While the use of the irrigation data stream at larger scale is currently hampered by the limited availability of precise information on irrigation practices in most areas [*Felfelani et al.*, 2018], it can serve as a valuable tool to investigate the modelled effect of different irrigation schedules and water availability scenarios. This can offer a basis and direction for further developments of the irrigation routine that are necessary for a more realistic representation of irrigation management practices [*Yao et al.*, 2022].

4.4.2 Model uncertainties and limitations of this study

4.4.2.1 Parametric uncertainty

SM dynamics outside the growing season were well reproduced by CLM5, indicating that the model was able to capture infiltration and soil water redistribution in the studied orchards. However, the significant SM bias in S10 suggests structural and parametric uncertainty in the estimation of soil hydraulic properties, probably due to inappropriate pedotransfer functions implemented in CLM5 [*Han et al.*, 2015]. *Gao et al.* [2021] found that poor performance of CLM5 in reproducing observed root zone SM was mainly due to uncertainty in porosity estimates. In addition, a high content of rock fragments, which is typical of many Mediterranean soils [*Nijland et al.*, 2010; *Poesen and Lavee*, 1994; *Zalidis et al.*, 2002], can strongly influence the SM regime through non-linearity in soil hydraulic conductivity and by reducing the soils' effective porosity [*Angulo-Jaramillo et al.*, 1997]. For this reason, most pedotransfer functions fail to correctly reproduce the hydraulic properties of stony soils [*Nasri et al.*, 2015], which likely led to biases in simulated SM in S10. Further investigation of the results would be needed to confirm this hypothesis, e.g. data assimilation of observed soil variables could be used to optimize soil hydraulic parameters [*Strebel et al.*, 2022]. In both orchards, the simulations showed a lower simulated SM dynamic in 50 cm depth, which could be the result of uncertainties in the rooting distribution and thus root water uptake within the soil profile. The current

parameterization of the vertical discretization of root fraction results in a rather shallow profile while deeper roots may still contribute to root water uptake in the studied orchards. *Shrestha et al.* [2018] encountered a similar issue when analyzing root zone SM on a grassland site using CLM3.5 and were able to improve simulated SM dynamics by increasing the root fraction in deeper layers. This may help to improve the simulated SM dynamics at 50 cm on our study sites.

The sensitivity experiments performed using two parameters of the CLM5 irrigation routine (Figure 4.5) and the results from the irrigation scenarios revealed relatively low sensitivity of crop yield to reduced irrigation (Figure 4.9). The new plant hydraulics introduced by *Kennedy et al.* [2019] advanced the physical basis for hydraulic stress in the model, but there is large uncertainty in its parameterization and in capturing the relationship of plant water stress and SM deficit for different crops. To better quantify the model performance and find the most suitable parameters for apple orchards, comparison of simulations to observations from stressed and non-stressed crops would be necessary. Additionally, sensitivity analysis of plant hydraulic parameters, which was out of the scope for this paper, could help to better constrain these model parameters.

4.4.2.2 Crop representation

The PHO catchment is characterized by a diversity of small-scale farm holders resulting in considerable heterogeneity in management practices, which cannot be fully captured by the model. While simulated yield was close to observations during a "good" year for the point-scale simulations, according to *Mattas et al.* [2019] average Greek apple production in 2016 was only ~23 t ha^{-1}. This suggests a great variability in orchard productivity, apple cultivars, or type of end product (e.g. apples for direct consumption or for juice) which would necessitate the inclusion of additional crop types and management practices in CLM5. In striving for global applicability, CLM5 and other LSMs face constraints in computational resources and often insufficient observational data to parameterize additional crop types, which results in biases in certain regions, while others are more accurately represented [*Lombardozzi et al.*, 2020]. In our case, the model demonstrated a strong correlation of yield and irrigation with the climatic gradient induced by the topography in the PHO, indicating a high sensitivity to model forcing data. The large simulated differences in yield between orchards in the plain (~50 ton ha^{-1}) vs. the higher altitudes (as low as 16 ton ha^{-1}) may however be exacerbated, as CLM5

employs a single set of parameters for a given crop across diverse geographies and climates. In reality, various cultivars of the same crop type, along with plant physiological adaptations to their environments, can lead to comparable productivity levels despite variations in climatic conditions. This phenomenon is evident in the cultivation of numerous crops, including apples, across climates on a global scale [*Sherman and Beckman*, 2002]. The issue has been addressed by *Lombardozzi et al.* [2020] who recommended further developments in CLM5 to improve phenological triggers and agricultural management, and to include different cultivars. In the future, the incorporation of additional satellite-derived crop data, advanced parameterizations, or the use of crop calendars to constrain these models may help reduce some of the biases [*Pongratz et al.*, 2018; *Yao et al.*, 2022; *Zhang et al.*, 2020].

At the orchard scale, we found discrepancies between observed and simulated SM during the growing season that suggest limitations specific to the current representation of orchards. As CLM5 does not allow intercropping, the actively growing grass cover in the orchard alleys is not included in the CLM5-FruitTree sub-model [*Dombrowski et al.*, 2022]. Consequently, our simulations do not account for the additional root water uptake and transpiration as well as interception of the irrigation water from the grasses. The former may explain the smaller simulated decline in SM early in the season compared to the observations, while we considered the latter to some extent by assuming a reduced irrigation efficiency. In doing so, we did however neglect the additional ET flux. *Yao et al.* [2022] developed and tested different irrigation techniques in CLM5 and found an increase in canopy evaporation through increased interception for their implementation of sprinkler irrigation. However, the overall impact on ET and total applied irrigation remained small compared to the control run using the standard CLM5 irrigation. More importantly, accounting for conveyance and application losses would increase the simulated irrigation amount and could lead to more realistic irrigation values [*Yao et al.*, 2022].

Despite these limitations, and though we could not validate the simulation of crop yield and irrigation requirements in the PHO catchment due to the lack of observational data, the reasonable modelling results at the orchard scale give some confidence in the robustness of the regional simulations.

4.4.3 Implications for irrigation management

We studied the relationship between crop yield and water use efficiency, and irrigation at the regional scale, as it is determinant for a reasonable allocation of irrigation water according to crop needs. For most part of the PHO, CWUE and yield were little affected when irrigation was reduced to 75%, suggesting that this scenario lies closer to the optimal irrigation that maximizes yield while minimizing water consumption as opposed to the FI scenario. These results are similar to a study by *Li et al.* [2018] who used CLM to schedule irrigation in a citrus orchard in Spain which resulted in 24% less irrigation compared to the farmers' practices. This could indicate that farmers irrigate too much when water is available and water prices are low [*Latinopoulos*, 2005]. Simulated apple yield was sensitive to a reduction of 50% of the applied irrigation water causing up to 30% decline in yields. The effect, however, varied with different meteorological conditions and soil types within the PHO. At higher altitudes, cooler temperatures and lower incoming radiation rather than water scarcity limited crop growth. Irrigation in these orchards could thus be greatly reduced without negatively affecting yield. Moreover, under the same climatic conditions, orchards growing on soils with a higher percentage of clay (southeastern part of the catchment) could maintain similar yield and CWUE under 50% reduction in irrigation water because of the greater water holding capacity of the soil. This will make orchards growing on these soils less prone to experience water stress. The effect of deficit irrigation on fruit growth and yield varied between years and throughout the growing season. Years with high productivity and greater dependence on irrigation (due to low rainfall) showed greater yield loss under deficit irrigation (Figure 4.10). At the seasonal scale, fruit growth showed the highest reduction in August followed by July and September (Figure 4.11). This was mainly an effect of higher temperature, little rainfall, and larger leaf area that resulted in high irrigation requirements in this month. Apples, similarly to other crops, show different susceptibility to drought stress depending on their growth stages whereby flowering and fruit set as well as fruit development and maturation are highly susceptible to drought. The latter stage falls within the period July to September where the model showed the largest reduction in fruit growth. While the simulated plant water stress is currently linked to environmental conditions rather than capturing plant physiological differences in this stage of growth, it suggests that under limited water conditions, irrigation should be prioritized during these months to maintain reasonable yields.

4.4.4 Perspectives for further application and model development

The analysis performed in this study displays the current ability and potential way forward of applying CLM5 for irrigation and water resources management at various scales. Prospectively, future applications and research studies should focus on the improvement of input data sets, crop and irrigation parameterizations, and process representation. Input related improvements include the creation of high-resolution climate and land use information, especially crop types and the extent and type of irrigation. Our results clearly showed how climate and environmental heterogeneity (e.g., topography, land use, soil properties) can greatly affect total crop water requirements, emphasizing the need for spatially explicit modelling for large-scale applications. Model investigation at the orchard scale revealed the importance of soil and crop-specific parameterization to correctly represent SM and phenology dynamics, and harvest time. Extending simulations to larger scales will thus require further improving soil hydraulic parameterization through improved pedotransfer functions [*Vereecken et al.*, 2022] or parametrization of soil hydraulic properties through data assimilation approaches [*Han et al.*, 2014]. Furthermore, information on crop management and improved differentiation between different crop varieties and cultivars (e.g. different growing seasons and harvest of cherry compared to apple trees) is necessary, as these can result in distinct irrigation seasons and amounts. Concerning irrigation, this could include either crop-specific or spatially explicit values for irrigation parameters that are currently the same for all irrigated crops, hence not reflecting different management strategies or susceptibilities to water stress. Lastly, some processes could be refined or added to represent irrigation requirements more realistically. These include a parameterization of irrigation efficiency, water availability considerations and more flexible irrigation schedules that can be tailored to represent typical field practices. Conducting parallel testing and assessment of future developments covering greater spatial and temporal scales (e.g. in the form of long-term observatories) will be crucial, especially as more accurate irrigation data becomes available.

4.5 Conclusions

This study assessed the ability of the CLM5-FruitTree sub-model to represent irrigation practices in fruit orchards in a small Mediterranean catchment and explored the effects of different irrigation scenarios on simulated yield and CWUE. The standard CLM5 irrigation routine could not accurately reproduce observed irrigation practices, which motivated the implementation of an irrigation data stream that directly prescribes measured irrigation data. Using this irrigation data stream, observed SM dynamics in the two studied apple orchards were well captured by the model. We did however find some discrepancies between observed and simulated SM, transpiration, and yield that were related to uncertainties in soil hydraulic parameters and limitations in the crop representation, which does, for instance, not account for the active grass cover growing in the alleys.

To examine the potential to improve regional irrigation management using CLM5, we simulated different irrigation scenarios and analyzed their effect on crop yield and CWUE. The model showed distinct effects of deficit irrigation on yield and CWUE for scenarios with 25% and 50% reduction in irrigation (DI75 and DI50, respectively) that were tested using the irrigation data stream. While DI75 had negligible negative effect on yield and CWUE, DI50 notably reduced both yield and CWUE. Based on the modelling results, this would suggest substantial water savings of up to 125 mm $year^{-1}$ with little to no effect on apple yields and up to 250 mm $year^{-1}$ when accepting up to 30% reduction in yield (although potential effects of fruit quality need to be considered as well). These effects varied depending on climatic conditions, soil type, and timing of irrigation. Hence, under limited water availability, irrigation should primarily focus on the summer months July to September and on sandy soils with lower water holding capacity.

The outcomes of this study demonstrate the potential use of CLM5 in irrigation and water resources management research and applications. Future research efforts should focus on improving soil and crop parameterizations, and as well as process representation. Finally, we anticipate that implementing more realistic irrigation schedules in land surface models such as CLM5 will allow for better water resource management at the local and regional level.

5 Synthesis

In the face of increasing water scarcity in the Mediterranean and other arid and semi-arid regions, tools to effectively determine crop specific irrigation requirements are crucial to sustain agricultural production and to guide irrigation and water resources management decisions. To achieve this a multifaceted approach is needed that involves:

- Affordable measurement technology that can provide comprehensive, high-resolution environmental data on climate, soil, and vegetation.
- Physically-based, fully distributed predictive models that accurately represent agricultural systems and the effect of irrigation management on yield, water resources, and other components of the terrestrial system.

In the following synthesis, the contribution this thesis has made to both of these components is summarized and promising directions for further research are discussed. Lastly, potential applications for different aspects of irrigation and water resources management at the field scale and beyond are explored.

5.1 Towards high-resolution climate data using low-cost sensors

High-resolution climate data is critical to improve the resilience and sustainability of the agricultural sector. This is especially important in light of more frequent and intense weather extremes related to climate change that decision-makers will be confronted with. The evaluation of a low-cost all-in-one weather station demonstrated that this type of sensor can deliver reliable and timely observations of local microclimatic conditions. As such, it is well suited for application in precision agriculture to promote water conservation, tailor management decisions to crop needs, and reduce the risk of crop failure through early warning systems. The potential of all-in-one weather stations to increase data availability and resolution in data-scarce, remote, and heterogeneous regions, and under budget constraints will benefit the quality of local and regional

modelling and a range of applications. These include water resources management [*Jencso et al.*, 2019], weather forecasting [*Hewage et al.*, 2020], early warning systems for flood prediction [*Ibarreche et al.*, 2020; *Nikolić et al.*, 2022], and urban planning [*Bassett et al.*, 2016; *Šećerov et al.*, 2019], which are of importance not only to farmers but also to policy-makers, industries, and the general population. In any case, reliability and accuracy of the deployed sensors should meet the needs of the intended purpose, as this work also revealed that data from low-cost weather stations are associated with higher uncertainties compared to that of high-end measurement devices. This can have important implications for instance regarding their use in extreme weather research. Here, current design, size, or sensor quality may not be well fit to deliver reliable measurements under strong winds, heavy rain, or solid precipitation.

5.2 Towards improved process-based modelling of agricultural systems

In conjunction with environmental data, process-based models are increasingly being used for the simulation and sustainable management of agricultural systems. However, crops in such models are often not sufficiently differentiated or rather certain crop types are not considered at all [*Blyth et al.*, 2021; *Lombardozzi et al.*, 2020; *Peng et al.*, 2020]. Consequently, systems with diverse crops and agricultural practices, e.g. the Mediterranean that is largely characterized by permanent crops (e.g. fruit trees), are poorly represented. In this work, the widely used global LSM CLM5 was extended by a component that enables the consideration of apple orchards (CLM5-FruitTree). By capturing the prolonged growing season, permanent woody biomass, and typical management practices of fruit trees, CLM5-FruitTree offers new possibilities to address relevant research questions in Mediterranean agricultural catchments or other fruit growing regions. Particularly, the impacts of land use and climate change on crop production and crop water requirements in the Mediterranean can be investigated more reliably. This kind of analysis can reveal potential shifts in crop phenology and changes in water demand or suitable growing areas for fruit trees, which can have important implications for food security [*Fader et al.*, 2015]. Another topic that could be addressed with the model development is the potential of orchards to sequester C and help mitigate climate change impacts [*Sharma et al.*, 2021; *Wu et al.*, 2012]. This potential depends on

orchard age, biomass production, and management, as well as climatic conditions which could be jointly investigated with CLM5-FruitTree.

There is a number of additional model developments that can be envisaged to further improve the simulation of fruit orchards. Some of these improvements involve additional refinements of the new crop model routine. One model weakness that should be resolved is the failure to capture the inter-annual yield variability of fruit trees, as accurate yield prediction is essential for farmers as well as policy makers to maximize economic profit and reduce losses. This could potentially be addressed by adding parameterizations of alternate bearing and flowering, both of which greatly affect final yield. The resource budget model for alternate bearing, first introduced by *Isagi et al.* [1997], could present a possible approach in this direction. It assumes that flowers are only produced once C reserves exceed a certain threshold which could be integrated into the existing C reserve dynamics in CLM5-FruitTree. Another aspect of yield which is currently not accounted for is fruit quality, which plays an important role in fruit production. Coupling or integration of a dedicated fruit tree model such as QualiTree that includes the effect of management on fruit quality could be explored in this context [*Lescourret et al.*, 2011; *Miras-Avalos et al.*, 2013]. Moreover, the options for crop management could be further extended to include their effect on C and water fluxes in the orchard. For instance, mulching is widely used in semi-arid and arid environments for annual crops [*Chakraborty et al.*, 2008] as well as fruit orchards [*Liao et al.*, 2021; *Liu et al.*, 2014]. In CLM5-FruitTree, the effect of mulching was only crudely considered by adding more C to the soil in the form of pruned biomass but did not include its effect on soil water retention and evaporation. To account for this, two recent studies could be explored that have incorporated a (plastic) mulch layer into a surface energy balance model and a LSM, which allowed to examine its effect on surface energy fluxes and ET [*Ochege et al.*, 2022; *Yuan et al.*, 2019].

Certain other model improvements necessitate more substantial changes to the model structure or physics but could significantly advance the representation of the true land-surface heterogeneity and pave the way towards the modelling of more complex vegetation structures. One of these improvements concerns the partitioning of energy and the transfer of heat and water within different canopy structures. The current assumption of a closed canopy, typical for annual crops, needs to be revisited to reduce uncertainties in the simulation of energy balance and water cycle in fruit orchards or other

heterogeneous canopies. Under water-limited conditions this is especially important to accurately determine crop water requirements [*Gao et al.*, 2020; *Ma and Liu*, 2019]. A possible way forward may be the explicit modelling of different surfaces as proposed by *Blyth et al.* [2021] or an advanced multi-layer canopy model to improve sub-canopy processes as tested by *Ma and Liu* [2019]. Another major topic involves the types of planting systems that can be represented in CLM5. Currently, only homogenous annual cropping systems are modelled that differ significantly from orchard systems where tree rows alternate with alleys, which are often covered by weeds or cover crops. Implementing such intercropping or mixed cropping systems in CLM5 would improve the simulation of C and water fluxes and could furthermore create opportunities to extend the model towards the simulation of agro-forestry and other diversified cropping systems. Such systems could regain more relevance as they can support soil water retention, C sequestration, biodiversity, and food security [*De Stefano and Jacobson*, 2018; *Debaeke et al.*, 2017]. In their review, *Hernández-Ochoa et al.* [2022] identified several agro-ecosystem models that can represent such systems to a certain extent and which could serve as a basis for this kind of development in CLM5.

Any process-based model used to simulate the Mediterranean agricultural system needs to consider irrigation as a critical management practice to meet crop water requirements. While the land modelling community has recognized irrigation as an important driver of change in the water cycle and other processes occurring at the land surface, it is still not accurately accounted for in most LSMs. Therefore, the final part of this work focused on assessing and improving the representation of irrigation in the context of field-scale and regional irrigation management in fruit orchards using CLM5-FruitTree. Local weather data and parallel observation of SM and irrigation at the field scale were essential to quantify the model performance after making site-specific adjustments to soil, crop, and irrigation parameterizations. The models' ability to approximate observed irrigation quantities depended on how well root zone SM and water movement was simulated throughout the soil profile. Furthermore, it became evident that additional flexibility in the irrigation routine is necessary to represent farmers' irrigation practices. A confident validation of the total crop water requirements proved more challenging as only a part of ET was observed using sapflow measurements that were additionally associated with a large measurement uncertainty. At catchment scale, the explorative analysis of different irrigation scenarios gave interesting insights into expected yield and CWUE under

varying irrigation amounts, and the additional role of soil and climate in driving the magnitude of the effect of reduced irrigation. Overall, this analysis showed that CLM5 could produce relevant information to advice farmers, water authorities, and policy makers in irrigation management at different scales. Additional simulations with projections of future climate conditions can furthermore shed light on how water consumption will likely develop. Together with a more flexible irrigation routine that considers different irrigation techniques and strategies, irrigation management could be optimized to ensure high yields while minimizing water consumption.

Towards the use of CLM5 for these applications, uncertainties that are related to model processes and parameterizations need to be addressed. This is critical to ensure crop water requirements and irrigation amounts can be predicted accurately. For instance, there is large uncertainty associated with the parameters used to describe plant hydraulic stress (PHS routine) which are currently generic for all crops in CLM5. An initial assessment of the current parameterization suggested a generally low sensitivity of crops to water stress. It is, however, well established that different crops and crop varieties react differently to water stress and levels of SM depletion [*Budak et al.*, 2013; *Chaves et al.*, 2003]. Consequently, the model may not accurately represent stressed conditions for a particular crop, which limits its ability to determine optimal irrigation amounts or assess the trade-off between yield loss and water savings under various deficit irrigation scenarios. This also adds ambiguity to the calibration of the SM threshold parameter to trigger irrigation, as crop- and growth stage specific differences regarding the optimal threshold are most likely not well captured. Enhancing calibration efforts for these parameters will therefore be critical. Furthermore, some authors have suggested the implementation of more advanced approaches to better represent plant stress for different plant types. *Verhoef and Egea* [2014] suggested to combine plant and soil hydraulics with chemical signalling instead of a water stress factor that is calculated based on SMP, as it is currently used in CLM5. Another approach may be to additionally incorporate leaf water potential for an improved plant stress representation [*Kennedy et al.*, 2019]. Another issue, which was not yet discussed in this work is the simplified root profile representation in LSMs, which was found to introduce considerable uncertainty in root water uptake simulations [*Canal et al.*, 2014; *Zeng*, 2001]. For example, *Zeng* [2001] showed that the one-parameter equation used for the rooting profile in CLM5 resulted in a too shallow rooting profile, which could explain some of the observed SM biases in the

deeper soil layers. Addressing such model uncertainties will be relevant when evaluating deficit irrigation strategies or the need for irrigation in fields that are partially or entirely rainfed. In fact, under such conditions, crops can develop extensive root systems to tap deep soil water or shallow groundwater, particularly perennial crops [*Vico and Brunsell*, 2018]. Different approaches using a two-parameter equation [*Zeng*, 2001] or uniform instead of exponential root profiles [*Stevens et al.*, 2020] have been suggested next to upscaling a 3D hydraulic root architecture model [*Vanderborght et al.*, 2021], and should be further explored to improve root profile representation in CLM5.

Future model developments to improve the representation of agricultural systems and irrigation in LSMs such as CLM5 are driven by a diverse user community including crop modellers, hydrologists, climate scientists, ecologists, and many others. Such community-based model development greatly benefits from a multidisciplinary knowledge base but also faces challenges to integrate the various spatiotemporal scales that are targeted by different groups of researchers [*Blyth et al.*, 2021; *Peng et al.*, 2020]. Another difficulty comes with finding parameters for the static global parameterization that is used for crop and irrigation parameters in CLM5, as developments are often made for a specific region and dataset, and cannot be easily adapted to the global scale. The development of CLM5-FruitTree is no exception to this, as despite the comprehensive dataset, the geographic scope and timeframe were limited considering only a few seasons and a single location. *Lombardozzi et al.* [2020] therefore proposed that future model developments should focus on moving to spatially varying parameterizations instead of global parameters to better represent regional differences and crop adaptations to their environment. The crop calendar developed by *Rabin et al.* [2023] or the implementation of spatially explicit irrigation parameters could improve the models accuracy and/or flexibility to capture such differences in crop growing season and irrigation management, respectively. Either way, there is a great need for spatially continuous data concerning soils, crops, irrigation amounts, or water withdrawal for model calibration and validation across different scales [*Blyth et al.*, 2021; *Gibson et al.*, 2017; *Pongratz et al.*, 2018]. At the same time, the data should be available at a sufficient resolution (i.e. < 1 km) to produce results that are relevant for individual farmers and local authorities. Therefore, efforts to obtain the necessary data need to be continued and intensified. These may include the combined use of high-resolution satellite datasets and machine learning algorithms to retrieve irrigation extent and amount [*Dari et al.*, 2022; *Zappa et al.*, 2021],

land cover [*Li et al.*, 2022], crop phenology [*Gao and Zhang*, 2021], or yield estimates [*Hunt et al.*, 2019]. Moreover, long-term in-situ observations from new shared research infrastructures such as eLTER [*Mirtl*, 2018] and ICOS [*Heiskanen et al.*, 2022] as well as existing environmental observatories (see Section 1.1.4) are valuable sources of distributed data (e.g., atmospheric, ecosystem, biological, soil parameters). Finally, the expansion of non-traditional data sources from the rapidly developing smart farming and citizen science movements, and private sensor networks may be used for model input, calibration, and validation at improved spatiotemporal resolution in the future [*Fraisl et al.*, 2022; *Reis et al.*, 2015; *Tsai et al.*, 2021].

Such joint efforts in model development and calibration could enable the application of LSMs such as CLM5 for different aspects of irrigation and water resources management across a range of spatiotemporal scales. In the following, some possible applications in this context are explored that build on the potential of LSMs such as CLM5 as tools for research and decision-making.

5.3 Operational field-scale irrigation scheduling using CLM5

Effective irrigation scheduling is one potential way to minimize water wastage while ensuring optimal yield for the farmer. Further developing the existing model application at field scale into an operational tool for irrigation scheduling in a smart farming context could therefore be a promising extension of this work. Because irrigation in CLM5 is based on SM, determining the optimal irrigation amount necessitates, above all, an accurate representation of SM conditions.

To improve field-scale SM simulations a data assimilation framework could be applied in fields were SM is being monitored continuously. Data assimilation of SM can improve model simulations through the update of the models' SM state and the optimization of relevant model parameters, in this case, soil hydraulic parameters [*Reichle et al.*, 2007; *Strebel et al.*, 2022]. In addition, estimates of uncertainty in SM can be obtained that can be used to quantify the uncertainty in, e.g. the prediction of irrigation requirements or yield outcome [*De Lannoy et al.*, 2019]. Assimilation of SM into various LSMs has been performed previously to improve SM predictions for cropland and natural vegetation [*Hung et al.*, 2022; *Kolassa et al.*, 2017; *Mahmood et al.*, 2019; *Naz et al.*, 2019]. *Han et*

al. [2016] and *Li et al.* [2018] presented first studies using data assimilation for irrigation scheduling in drip irrigated citrus orchards in CLM4.5 with promising results and the possibility of real-time online control for the latter study. For CLM5, *Strebel et al.* [2022] recently performed and tested the coupling to PDAF (the parallel data assimilation framework) which could be applied to continue the present work and to test if the bias in simulated SM can be reduced.

The improved model simulations can further be combined with suitable short- to medium-range weather forecasts [*Hewage et al.*, 2020; *Lorite et al.*, 2015] to predict the depletion of SM within the forecasting window. Subsequently, the optimal irrigation amount and timing can be determined based on a defined target SM or SMP to avoid crop water stress while minimizing water wastage. By using ensemble weather forecasts or historical weather data as forecasts, uncertainties in the predictions could be taken into account [*Guo et al.*, 2023; *Linker and Sylaios*, 2016]. Additionally, alternative decisions of irrigation timing could be considered and the trade-off and risks between water consumption and crop stress could be communicated to the farmer to support decision-making [*Guo et al.*, 2023]. Automating the entire process, including the fetching and preparation of data for model input, starting a new model run, analysing model output, and communicating the proposed irrigation schedule to the farmer, entails the development of a web application and the necessary APIs (application programming interfaces) that allow communication between the different software applications and data portals. This is not trivial, as setting up and running CLM5 and similar models involves a multi-step process that requires a significant amount of expert knowledge and computational resources. Developing a simplified modelling infrastructure by, e.g., unifying workflows, creating templates, or building simple user interfaces can support operational use of the model. Moreover, major efforts must also be made to improve interoperability between different applications as well as for the harmonization and shared use of data [*Choi et al.*, 2021; *Maechling et al.*, 2005].

Application of the described irrigation scheduling service in combination with data assimilation necessitates the availability of continuous SM data that is representative for the target area. At present, WSNs may be the most effective solution for small, heterogeneous fields. The number of sensors and thus total costs associated with the installation of such a network will depend on several factors including the heterogeneity of soil texture, crop planting patterns, and management practices. Electromagnetic or

drone-based soil and crop surveys can be used to decide on an optimal sensor placement [*Hedley et al.*, 2012; *von Hebel et al.*, 2021]. Alternatively, non-invasive measurement techniques such as cosmic ray neutron sensing that provide an integrated SM measurement over multiple hectares could be used as the technique becomes more cost-effective. This way multiple growers could invest into a few shared sensors to lower investments for the individual and to share the benefit of improved SM simulations.

While the costs of sensing technologies are steadily decreasing, many farmers, especially in the low to middle-income countries of the Mediterranean region, lack financial assets and technical knowledge to install and maintain such extensive measurement systems. The complexity of model-based irrigation scheduling and scepticism or low confidence in this technology result in low adoption rates especially for small-scale irrigators [*Barnes et al.*, 2019; *Fernández García et al.*, 2020; *Frisvold and Deva*, 2012]. It is therefore critical that governments and water authorities support sustainable irrigation management at the farm scale through funding and training, or educational programmes based on regional and national water management plans that consider irrigation in the larger context of water resources.

5.4 Modelling frameworks for holistic irrigation and water resources management

So far, this work has considered field and regional scale irrigation under the assumption of an unrestricted supply of suitable irrigation water or hypothetical scenarios of limited water availability (deficit irrigation scenarios). It is however clear, that this does not reflect reality in the Mediterranean context, where instead, irrigation is restricted by water availability and quality, and competes with other water use sectors (e.g., agricultural, urban, industrial, environmental) [*Choukr-Allah et al.*, 2012]. Modelling for regional water resources management needs to consider this interconnectedness to ensure the responsible use and long-term sustainability of groundwater and surface water resources across sectors.

Groundwater is the main water resource in most semi-arid and arid Mediterranean catchments including the PHO [*Pisinaras et al.*, 2018; *Zagana et al.*, 2007] but also the more water rich Adige valley [*Castagna et al.*, 2015]. Taking water availability for

irrigation into account should therefore consider groundwater and the impact of irrigation activities on groundwater dynamics (depletion or recharge) in the catchment. The work of *Felfelani et al.* [2021] could be a good starting point, as they implemented a prognostic groundwater module into CLM5 that considers aquifer pumping as well as intercell lateral flow. This improved groundwater level simulations as well as the subsurface response to pumping. Apart from representing the impact of groundwater withdrawals on the surrounding areas, the implementation of intercell lateral flow will likely also improve the representation of aquifer recharge mechanisms. In the PHO but also in other Mediterranean catchments with a pronounced topographic gradient, precipitation and snow melt from the mountainous parts of the catchment contribute substantially to aquifer recharge while the lowland typically contributes little to total annual recharge [*Pisinaras et al.*, 2018; *Zagana et al.*, 2007]. Alternatively, a better representation of subsurface hydrological processes and interactions with the land surface can be achieved by coupling CLM5 with more complex hydrological models such as ParFlow or groundwater models such as MODFLOW [*Felfelani et al.*, 2022]. In this way, groundwater resources can be better assessed, and a sustainable level of water abstraction can be determined more reliably. Moreover, effective mitigation measures to avoid the overexploitation of groundwater aquifers, such as deficit irrigation strategies or the switch to less water consuming or more drought resilient crops, can be explored. *Peng et al.* [2020] argued that to reliably investigate such adaptation and mitigation strategies a much greater effort to merge agroeconomic CMs and LSMs is necessary. In this way the strength of CMs in representing the effect of environmental conditions and crop management on yield can be combined with the ability of LSMs to jointly consider agricultural systems and other land uses as well as their environmental implications on other Earth system components such as C and water cycles.

In moving towards integrated water resources management, models used as decision-making tools must reflect the multi-purpose function of water resources and the multidisciplinary nature of their management. This entails the consideration of other water use sectors including industrial, recreational, domestic, and environmental as well as artificial water reservoirs used for irrigation or other purposes [*Felfelani et al.*, 2021]. Furthermore, future model developments may also consider alternative water sources from wastewater recycling or desalination plants, since they will likely grow in importance as water scarcity in Mediterranean countries continues to worsen [*Ait-Mouheb*

et al., 2020; *Martin-Gorriz et al.*, 2014; *Martínez-Alvarez et al.*, 2019; *Moretti et al.*, 2019]. The use of such water sources comes with increased energy consumption, environmental impacts, and economic costs on top of possible health concerns that undermine their social acceptance [*Ait-Mouheb et al.*, 2020; *Martínez-Alvarez et al.*, 2019]. Therefore, the combination of environmental, economic, and social goals in the integrated approach to water resources management could be combined with the water-energy-food nexus concept to achieve higher resource efficiency and increased water, energy, and food security [*Shams and Muhammad*, 2022]. In this context a stronger integration or exchange of information between LSMs (or fully coupled Earth System Models) with models from other communities such as integrated assessment, vulnerability, and adaptation should be encouraged to create holistic modelling frameworks for water resources management [*Van Vuuren et al.*, 2012].

Appendix

Appendix I Full time series ATMOS41

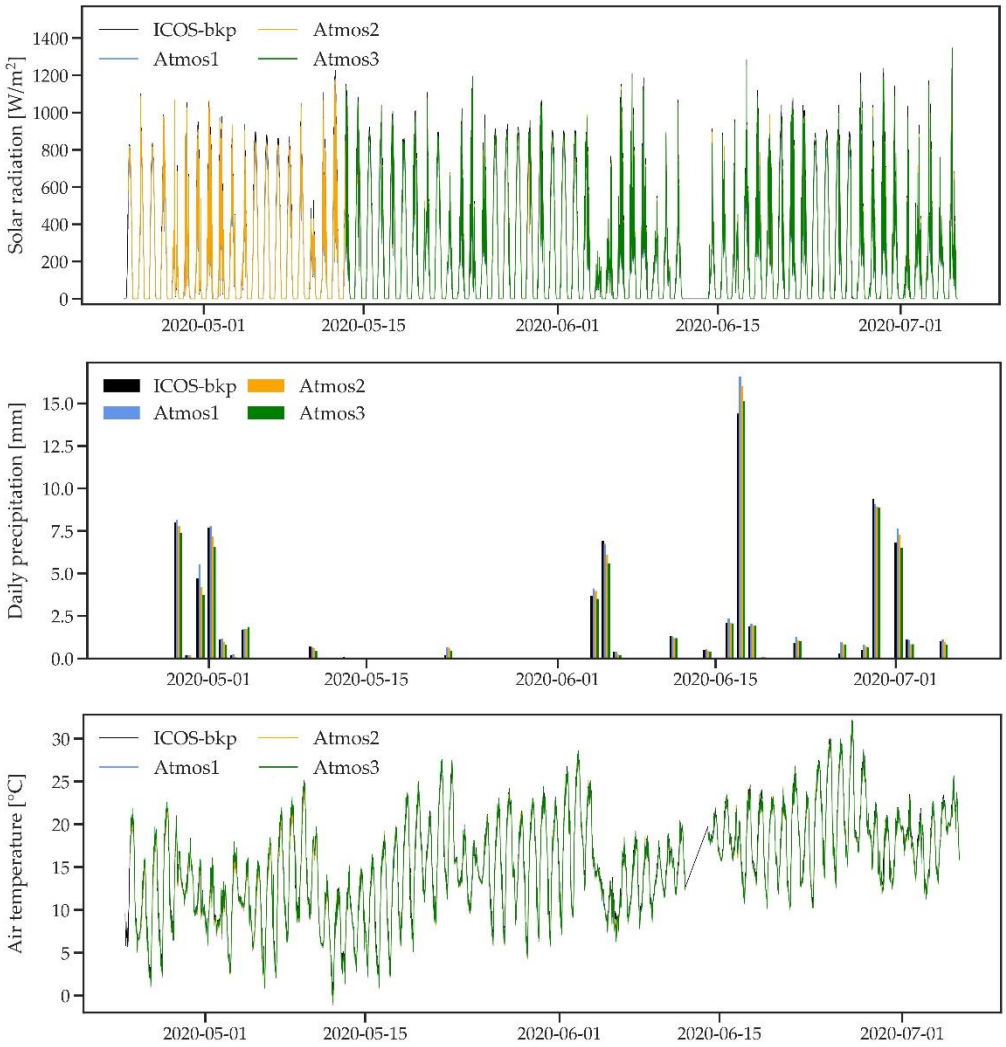

Figure A.1 *Cont.*

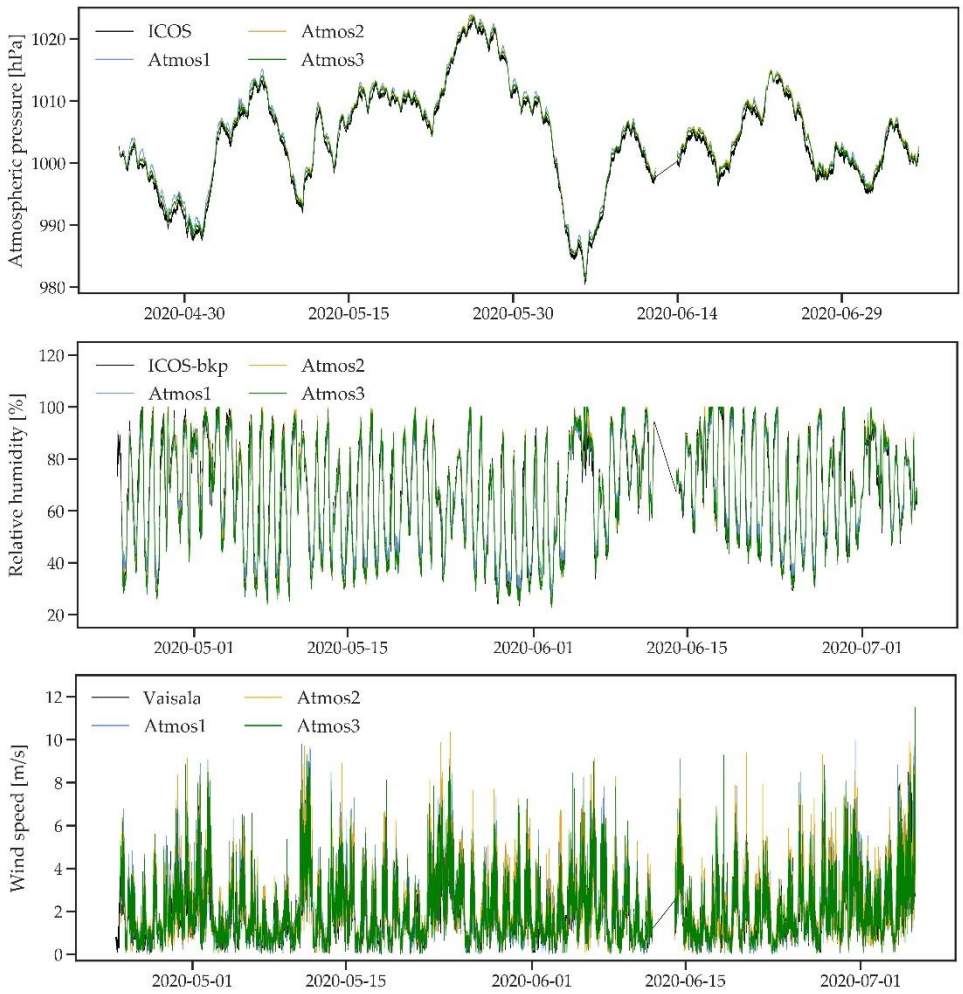

Figure A.1 Full time series for all standard weather variables measured by three ATMOS41 weather stations and the reference station.

Appendix II Linear regression ATMOS41

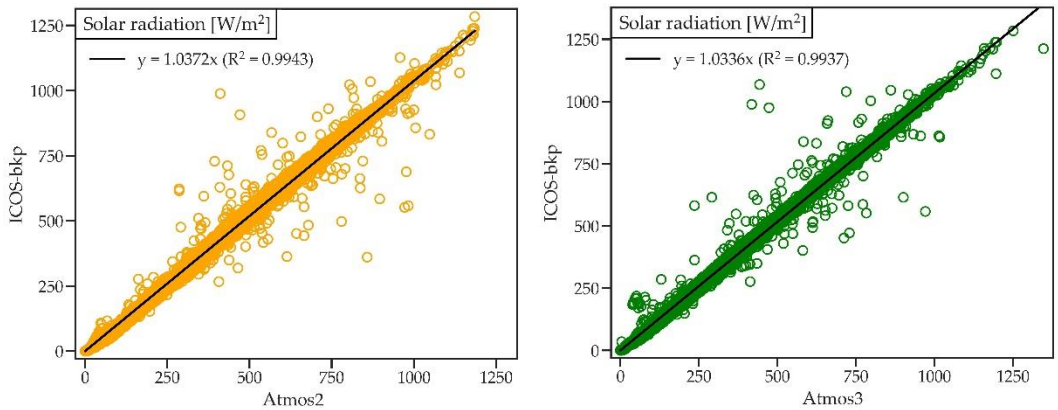

Figure A.2 Linear regression for solar radiation for Atmos2 and Atmos3 vs. ICOS-bkp station.

Appendix III Sequential model for bud break prediction

The bud break prediction in CLM5-FruitTree is based on the sequential model developed by *Cesaraccio et al.* [2004]. Negative chill days (C_d) are accumulated from the 1st of November followed by positive anti-chill days (C_a) to overcome the different stages of tree dormancy, rest and quiescence. The chilling requirement (C_R) defines the threshold for the accumulation of C_d and is reached when $\sum C_d \leq C_R$. Thereafter C_a accumulation begins until $C_R + \sum C_a \geq 0$ at which bud break occurs. The accumulation of C_d and C_a on a given day is calculated from maximum (T_x) and minimum (T_n) daily air temperature as well as a temperature threshold for chill accumulation (T_C), and varies depending on five possible temperature cases that relate T_x, T_n, T_C, and 0 °C with the daily mean air temperature (Table A.1). The optimal values for C_R and T_C were calibrated based on bud break observations from 2010–2013 for the Adige site by minimizing the RMSE between observations and predicted bud break. The optimal value for C_R was -68 while T_C was 4 °C resulting in an RMSE of 7.2 days.

Table A.1 Chill day (C_d) and anti-chill day (C_a) calculation for five different temperature cases relating maximum (T_x) and minimum (T_n) air temperature to the air temperature threshold (T_C) and 0 °C, T_M is the air mean temperature.

Temperature Cases	Chill days	Anti-chill days
$0 \leq T_C \leq T_n \leq T_x$	$C_d = 0$	$C_a = T_M - T_C$
$0 \leq T_n \leq T_C < T_x$	$C_d = -\left[(T_M - T_n) - \frac{(T_x - T_C)^2}{2(T_x - T_n)}\right]$	$C_a = \frac{(T_x - T_C)^2}{2(T_x - T_n)}$
$0 \leq T_n \leq T_x \leq T_C$	$C_d = -(T_M - T_n)$	$C_a = 0$
$T_n < 0 \leq T_x \leq T_C$	$C_d = -\left[\frac{T_x^2}{2(T_x - T_n)}\right]$	$C_a = 0$
$T_n < 0 < T_C < T_x$	$C_d = -\frac{T_x^2}{2(T_x - T_n)} - \frac{(T_x - T_C)^2}{2(T_x - T_n)}$	$C_a = \frac{(T_x - T_C)^2}{2(T_x - T_n)}$

Appendix IV Calculation of incoming longwave radiation

Incoming longwave radiation (LW_{in}) can be expressed based on the Stefan Boltzmann Law as:

$$LW_{in} = \varepsilon_{eff} * \sigma * T^4 = \varepsilon_{cs} * F * \sigma * T^4 \ , \quad \text{(A.1)}$$

where ε_{eff} is the effective emissivity that can be expressed by multiplying the clear-sky atmospheric emissivity ε_{cs} with a cloud factor F (always ≥1) that expresses the increase of LW_{in} under cloudy conditions, σ is the Stefan Boltzmann constant (5.67×10^{-8} W m^{-2} K^{-1}) and T is the 2m air temperature in K.

Clear-sky emissivity was obtained using the *Konzelmann et al.* [1994] parameterization as follows:

$$\varepsilon_{cs} = 0.23 + 0.484 * \left(\frac{e}{T}\right)^{\frac{1}{8}} \ , \quad \text{(A.2)}$$

where e is the vapour pressure in Pa at 2 m.

Equation (A.1) can be rearranged to obtain F as follows:

$$F = \frac{LW_{in}}{\varepsilon_{cs} * \sigma * T^4} \quad \text{(A.3)}$$

F was calculated at hourly interval using measured LW_{in} data from 2010 and ε_{cs} calculated using the above Eq. (A.2).

As proposed by *Sedlar and Hock* [2009], in the absence of cloud data, the cloud factor F can be parameterized as a function of the atmospheric transmissivity index τ, which is defined as follows:

$$\tau = \frac{SW_{in}}{SW_{toa}} \ , \quad \text{(A.4)}$$

where SW_{in} is the incoming shortwave radiation, and SW_{toa} is the theoretical shortwave radiation received at the top of the atmosphere.

Figure A.3 shows the linear equation that was fitted to the relationship of F and τ for the year 2010. For the calculation of clear-sky emissivity, all data where τ was greater than 0.7 (N=3863) was considered based on the suggestion by *Campbell* [1985].

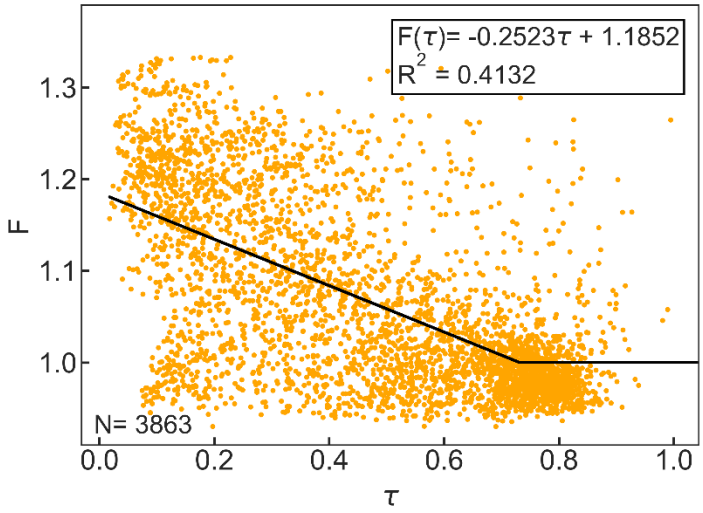

Figure A.3 Cloud factor F as a function of atmospheric emissivity τ for hourly observations. The black line represents the linear equation for F(τ) and F≥1. Clear-sky emissivity is parameterized based on *Konzelmann et al.* [1994].

For the nighttime values and for very low incoming shortwave radiation (SW_{in} < 15 W m^{-2}), τ was gap-filled with the mean of the two surrounding values to obtain a complete time series of LW_{in} data. Figure A.4 shows the results of the LW_{in} parameterization compared to LW_{in} calculated by CLM5 and to the observed data for the year 2010. As performance statistics the Pearson coefficient of correlation (r), the root mean square error (RMSE) and percent bias (%bias) are given.

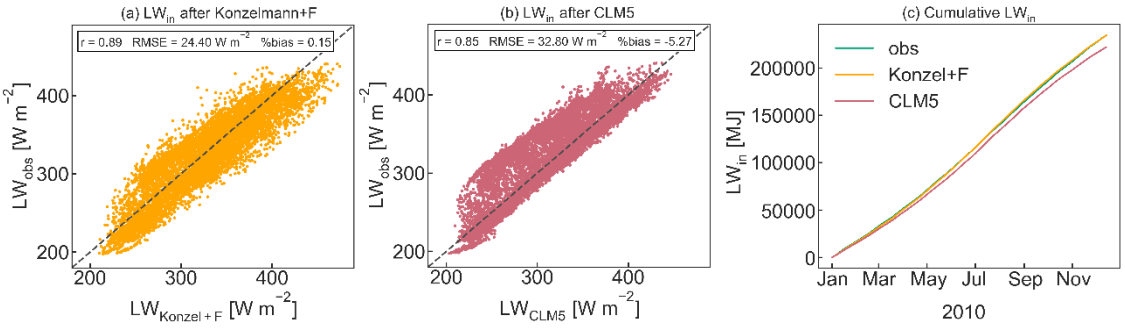

Figure A.4 Comparison of observed LW_{in} with the parameterization using (a) *Konzelmann et al.* [1994] according to Eq. (A.2) and the cloud factor parameterization F(τ), and (b) the calculation procedure used in CLM5, as well as (c) cumulative observed and calculated LW_{in} for 2010. Pearson's r, RMSE and %bias are given as performance statistics.

Appendix V Parameters used in CLM5-FruitTree and for the apple PFT

Table A.2 Parameters adapted or added in the new CLM5-FruitTree sub-model and the apple PFT including phenology, CN allocation, photosynthesis, vegetation structure as well as optical and respiration parameters. Parameters were adjusted based on field observations or literature values and are listed with their definition, unit, value, and references to the literature.

Parameter	Definition	Unit	Value	Reference
Phenological parameters				
baset	Base temperature for GDD accumulation	°C	4	Based on commonly used values for apple trees [*Díez-Palet et al.*, 2019; *Penzel et al.*, 2020; *Reyes et al.*, 2016]
crequ	Chilling requirements for bud break of fruit tree crops	unitless	-68	Calibrated using bud break dates from *Zanotelli et al.* [2013] and *Zanotelli et al.* [2015], and the sequential model [*Cesaraccio et al.*, 2004]
crit_temp	Critical temperature to initiate leaf senescence for fruit tree crops	K	278.15	Adjusted based on LAI measurements [*Zanotelli et al.*, 2013]
grnfill* (GDDfruit)	GDD needed from bud break to beginning of fruit development	degree days	400	Based on observed and commonly used values for apple trees [*Lakso et al.*, 2000; *Neumann*, 2020; *Penzel et al.*, 2020; *Zanotelli et al.*, 2013]
grnrp*(GDDripe)	GDD needed from bud break to the fruit ripening phase	degree days	1100	Based on observed and commonly used values for apple trees [*Lakso et al.*, 2000; *Neumann*, 2020; *Penzel et al.*, 2020; *Zanotelli et al.*, 2013]
huileaf (GDDleaf)	GDD accumulated at the moment of bud break (end of dormancy period)	degree days	–	Calculated based on sequential model for bud break prediction [*Cesaraccio et al.*, 2004]
hybgdd* (GDDmat)	GDD needed from bud break until fruit harvest	degree days	2880	Based on observed and commonly used values for apple trees [*Lakso et al.*, 2000; *Neumann*, 2020; *Penzel et al.*, 2020; *Zanotelli et al.*, 2013]

laimx*	Maximum leaf area index	m^2/m^2	3	Based on observed and commonly used values for apple trees [*Li et al.*, 2002; *Valancogne et al.*, 1999; *Zanotelli et al.*, 2013]
lfmat*(GDDlfmat)	GDD needed from bud break to canopy maturity	degree days	1350	Based on observed and commonly used values for apple trees [*Lakso et al.*, 2000; *Neumann*, 2020; *Penzel et al.*, 2020; *Zanotelli et al.*, 2013]
max_NH_harvest_date	maximum harvest date for northern hemisphere (NH)	date (md)	1015	Based on typical harvest dates in NH
max_NH_planting_date	maximum planting date for NH	date (md)	101	Only needed for orchard establishment and initiation of sequential model for bud break, tree is still dormant
min_NH_planting_date	minimum planting date for NH	date (md)	101	Only needed for orchard establishment and initiation of sequential model for bud break, tree is still dormant
mxmat	Maximum orchard age	days	9125	Based on common values for apple orchards [*Lakso et al.*, 2000; *Penzel et al.*, 2020; *Zanotelli et al.*, 2013]
ndays_stor	Length of period for storage growth of fruit tree crops	days	50	Based on common values for fruit orchards [*DeJong and Grossman*, 1994; *Kozlowski*, 1992; *Wünsche and Lakso*, 2000]
perennial	Binary flag for perennial crop phenology	unitless	1	
root_dmx	Maximum rooting depth of crops	m	0.8	Based on observed rooting depth [*Zanotelli et al.*, 2013]
rootprof_beta*	Rooting beta parameter, for C and N vertical discretization	unitless	0.964	Calibrated based on root sampling campaign of root mass up to 60cm (Zanotelli 2010, unpublished data)
woody	Binary flag for woody lifeform	unitless	1	

C and N allocation parameters

aleaff*	Final leaf allocation coefficient	unitless	0.01	Adjusted based on monthly biomass measurements [*Zanotelli et al.*, 2013]
aleafstor*	Leaf allocation coefficient to storage post-harvest used in CNAllocation	unitless	0.3	Adjusted based on monthly biomass measurements [*Zanotelli et al.*, 2013]
allconss*	Power to control the shape of the stem allocation curve	unitless	1.5	Adjusted based on monthly biomass measurements [*Zanotelli et al.*, 2013]
arootf*	Root allocation coefficient at start of fruit development	unitless	0.2	Adjusted based on monthly biomass measurements [*Zanotelli et al.*, 2013]
arootf2*	Final root allocation coefficient until harvest	unitless	0.08	Adjusted based on monthly biomass measurements [*Zanotelli et al.*, 2013]
arooti*	Initial root allocation coefficient	unitless	0.7	Adjusted based on monthly biomass measurements [*Zanotelli et al.*, 2013]
astemf*	Final stem allocation coefficient]	unitless	0.22	Adjusted based on monthly biomass measurements [*Zanotelli et al.*, 2013]
bfact*	Exponential factor used for fraction allocated to leaf	unitless	-0.5	Adjusted based on monthly biomass measurements [*Zanotelli et al.*, 2013]
declfact*	Decline factor to control the shape of the stem allocation curve	unitless	4	Adjusted based on monthly biomass measurements [*Zanotelli et al.*, 2013]
fcur*	Fraction of C and N allocated to the displayed pools	unitless	0.95	Tuned based on observed LAI and yield data [*Zanotelli et al.*, 2013]
fleafi*	Initial leaf allocation coefficient	unitless	0.85	Adjusted based on monthly biomass measurements [*Zanotelli et al.*, 2013]
flivewd	Fraction of new wood that is live		0.15	Same as BDT in CLM5

frootCN	Fine root C:N ratio	gC/gN	32	Average of 6 measurements (Zanotelli 2010, unpublished data)
grainCN*	Fruit C:N ratio	gC/gN	139	Average of 6 measurements (Zanotelli 2010, unpublished data)
leafCN*	Leaf C:N ratio	gC/gN	19.7	Average of 6 measurements (Zanotelli 2010, unpublished data)
lflitCN	Litter C:N ratio	gC/gN	60	Average of 4 measurements (Zanotelli 2010, unpublished data)
livewdCN	Livewood C:N ratio	gC/gN	60	Average of 6 measurements (Zanotelli 2010, unpublished data)
transplant	Initial carbon for crops transplanted from nursery	gC	5	
Photosynthetic parameters				
i_vcad*	Intercept of the relationship between leaf N per unit area and Vcmax25top	$\mu molCO_2/m^2/s$	5.2	Adjusted in between BDT and crop
medlynslope*	Medlyn slope of conductance–photosynthesis relationship	$\mu molH_2O/\mu molCO_2$	8.2	Tuned based observed GPP and ET data [*Zanotelli et al.*, 2015]
s_vcad*	Slope of the relationship between leaf N per unit area and Vcmax25top	$\mu molCO_2/s/gN$	34	Tuned based on observed LAI and yield data [*Zanotelli et al.*, 2013]
slatop*	Specific leaf area at top of canopy	m^2/gC	0.028	Mean value for the growing season based on LAI and leaf biomass measurements [*Zanotelli et al.*, 2013]
Vegetation structure and management				
displar	Ratio of displacement height to canopy top height	unitless	0.67	Same as BDT in CLM5

mulch_pruning	Binary flag for mulching (1) or export (0) of pruning material	unitless	1	Based on reported organic farming practices [*Zanotelli et al.*, 2013]
prune_fr	Fraction of dead stem that is pruned	unitless	0.85	Based on reported pruning quantity [*Zanotelli et al.*, 2015]
nstem	Planting density	#/m^2	0.33	Based on reported planting density [*Zanotelli et al.*, 2013]
taper	Ratio of stem height to radius at breast height		120	Based on reported tree allometry and height [*Zanotelli et al.*, 2013]
xl*	Leaf/stem orientation index	unitless	0.25	Same as BDT in CLM5
z0mr*	Ratio of momentum roughness length to canopy top height	unitless	0.06	Based on average values reported for apple [*la Fuente-Sáiz et al.*, 2017] and citrus [*Tanny and Cohen*, 2003] orchards
ztopmx	Maximum canopy height for crops	m	3.6	Based on reported tree heights [*Zanotelli et al.*, 2013]
Optical parameters				
rholnir*	Leaf reflectance: near-IR	fraction	0.5	Based on average values for apple trees [*Bastías and Corelli-Grappadelli*, 2012]
rholvis*	Leaf reflectance: visible	fraction	0.1	Based on average values for apple trees [*Bastías and Corelli-Grappadelli*, 2012]
rhosnir*	Stem reflectance: near-IR	fraction	0.39	Same as BDT in CLM5
rhosvis*	Stem reflectance: visible	fraction	0.16	Same as BDT in CLM5
taulnir*	Leaf transmittance: near-IR	fraction	0.3	Based on average values for apple trees [*Bastías and Corelli-Grappadelli*, 2012]

taulvis*	Leaf transmittance: visible	fraction	0.04	Based on average values for apple trees [*Bastías and Corelli-Grappadelli*, 2012]
tausnir*	Stem transmittance: near-IR	fraction	0.001	Same as BDT in CLM5
tausvis*	Stem transmittance: visible	fraction	0.001	Same as BDT in CLM5
Respiration				
FUN_fracfixers*	The maximum fraction of assimilated carbon that can be used to pay for N fixation	fraction	0.25	Same as BDT in CLM5
lmr_intercept_atkin	Intercept in the calculation of the top of canopy leaf maintenance respiration base rate.	$\mu molCO_2/m^2/s$	1.756	Same as BDT in CLM5

Bibliography

Aguilera, E., Diaz-Gaona, C., Garcia-Laureano, R., Reyes-Palomo, C., Guzmán, G. I., Ortolani, L., Sanchez-Rodriguez, M., and Rodriguez-Estevez, V. (2020). Agroecology for adaptation to climate change and resource depletion in the Mediterranean region. A review. *Agricultural Systems*, *181*, 102809.

Aguilera, E., Guzmán, G., and Alonso, A. (2015). Greenhouse gas emissions from conventional and organic cropping systems in Spain. II. Fruit tree orchards. *Agronomy for Sustainable Development*, *35*(2), 725-737.

Ait-Mouheb, N., Mayaux, P.-L., Mateo-Sagasta, J., Hartani, T., and Molle, B. (2020). Water reuse: A resource for Mediterranean agriculture. In *Water resources in the mediterranean region*, edited, pp. 107-136, Elsevier.

Akhtar, F., Awan, U. K., Tischbein, B., and Liaqat, U. W. (2018). Assessment of irrigation performance in large river basins under data scarce environment—A case of Kabul river basin, Afghanistan. *Remote Sensing*, *10*(6), 972.

Allen, M., Prusinkiewicz, P., and DeJong, T. (2005). Using L-systems for modeling source–sink interactions, architecture and physiology of growing trees: the L-PEACH model. *New phytologist*, *166*(3), 869-880.

Ammann, S. K. (1994). Ultrasonic anemometer. U.S. Patent and Trademark Office.

Anand, M., and Molnar, P. (2018). Performance of TAHMO Zurich Weather Station. Institute of Environmental Engineering, D-Baug, ETH Zurich, Switzerland.

Anderson, J., Richardson, E., and Kesner, C. (1985). Validation of chill unit and flower bud phenology models for 'Montmorency' sour cherry. In Proceedings of the I International Symposium on Computer Modelling in Fruit Research and Orchard Management, Acta Hortic.

Angelakıs, A. N., Zaccaria, D., Krasilnikoff, J., Salgot, M., Bazza, M., Roccaro, P., Jimenez, B., Kumar, A., Yinghua, W., and Baba, A. (2020). Irrigation of world agricultural lands: Evolution through the millennia. *Water*, *12*(5), 1285.

Angulo-Jaramillo, R., Thony, J., Vachaud, G., Moreno, F., Fernandez-Boy, E., Cayuela, J., and Clothier, B. (1997). Seasonal variation of hydraulic properties of soils measured using a tension disk infiltrometer. *Soil Science Society of America Journal*, *61*(1), 27-32.

Aponte-Roa, D. A., Montalvan, L. B., Velazquez, C., Espinoza, A. A., Velazquez, L. F., and Serrano, R. (2018). Evaluation of a low-cost, solar-powered weather station for small-scale wind farm site selection. *2018 IEEE International Instrumentation and Measurement Technology Conference (I2MTC)*, 1-5.

Arnell, N. W. (1999). Climate change and global water resources. *Global environmental change*, *9*, S31-S49.

Arnold, J. G., Srinivasan, R., Muttiah, R. S., and Williams, J. R. (1998). Large area hydrologic modeling and assessment part I: model development 1. *JAWRA Journal of the American Water Resources Association*, *34*(1), 73-89.

Atay, A. N., Koyuncu, F., and Atay, E. (2013). Relative susceptibility of selected apple cultivars to alternate bearing. *Journal of Biological and Environmental Sciences*, *7*(20), 81-86.

Atkin, O. K., Bloomfield, K. J., Reich, P. B., Tjoelker, M. G., Asner, G. P., Bonal, D., Bönisch, G., Bradford, M. G., Cernusak, L. A., and Cosio, E. G. (2015). Global variability in leaf respiration in relation to climate, plant functional types and leaf traits. *New phytologist*, *206*(2), 614-636.

Aureli, A., Ganoulis, J., and Margat, J. (2008). Groundwater resources in the Mediterranean region: importance, uses and sharing. *Water Mediterr*, 96-105.

Ayman, K. Email correspondance with METER Europe Support (support.europe@metergroup.com). Personal communication on 13 October 2020.

Babaeian, E., Sadeghi, M., Jones, S. B., Montzka, C., Vereecken, H., and Tuller, M. (2019). Ground, proximal, and satellite remote sensing of soil moisture. *Reviews of Geophysics*, *57*(2), 530-616.

Bach, H., and Mauser, W. (2018). Sustainable agriculture and smart farming. *Earth observation open science and innovation*, 261-269.

Ballabio, C., Panagos, P., and Monatanarella, L. (2016). Mapping topsoil physical properties at European scale using the LUCAS database. *Geoderma*, *261*, 110-123.

Balsamo, G., Beljaars, A., Scipal, K., Viterbo, P., van den Hurk, B., Hirschi, M., and Betts, A. K. (2009). A revised hydrology for the ECMWF model: Verification from field site to terrestrial water storage and impact in the Integrated Forecast System. *Journal of Hydrometeorology*, *10*(3), 623-643.

Barnes, A. P., Soto, I., Eory, V., Beck, B., Balafoutis, A., Sánchez, B., Vangeyte, J., Fountas, S., van der Wal, T., and Gómez-Barbero, M. (2019). Exploring the adoption of precision agricultural technologies: A cross regional study of EU farmers. *Land use policy*, *80*, 163-174.

Bassett, R., Cai, X., Chapman, L., Heaviside, C., Thornes, J. E., Muller, C. L., Young, D. T., and Warren, E. L. (2016). Observations of urban heat island advection from a high-density monitoring network. *Quarterly Journal of the Royal Meteorological Society*, *142*(699), 2434-2441.

Bastías, R. M., and Corelli-Grappadelli, L. (2012). Light quality management in fruit orchards: physiological and technological aspects. *Chilean Journal of Agricultural Research*, *72*(4), 574.

Batello, C., Wade, L., Cox, S., Pogna, N., Bozzini, A., and Choptiany, J. (2014). Perennial crops for food security: Proceedings of the FAO expert workshop.

Belleggia, A., Murri, G., and Neri, D. (2009). Crop load control of 'Fuji' apple in central Italy. In Proceedings of the XI International Symposium on Plant Bioregulators in Fruit Production 884.

Benyei, P., Cohen, M., Gresillon, E., Angles, S., Araque-Jiménez, E., Alonso-Roldán, M., and Espadas-Tormo, I. (2018). Pruning waste management and climate change in Sierra Mágina's olive groves (Andalusia, Spain). *Regional environmental change*, *18*(2), 595-605.

Bepete, M., and Lakso, A. (1996). Apple fruit respiration in the field: relationships to fruit growth rate, temperature, and light exposure. In Proceedings of the VI International Symposium on Integrated Canopy, Rootstock, Environmental Physiology in Orchard Systems 451.

Bernard, J. (2003). Short note on the depth of investigation of electrical methods. iris instruments.

Betts, R. A. (2005). Integrated approaches to climate–crop modelling: needs and challenges. *Philosophical Transactions of the Royal Society B: Biological Sciences*, *360*(1463), 2049-2065.

Blonquist Jr, J., Jones, S. B., and Robinson, D. (2006). Precise irrigation scheduling for turfgrass using a subsurface electromagnetic soil moisture sensor. *Agricultural Water Management*, *84*(1-2), 153-165.

Blonquist Jr, J., Jones, S. B., and Robinson, D. A. (2005). Standardizing characterization of electromagnetic water content sensors: Part 2. Evaluation of seven sensing systems. *Vadose Zone Journal*, *4*(4), 1059-1069.

Blyth, E. M., Arora, V. K., Clark, D. B., Dadson, S. J., De Kauwe, M. G., Lawrence, D. M., Melton, J. R., Pongratz, J., Turton, R. H., and Yoshimura, K. (2021). Advances in land surface modelling. *Current Climate Change Reports*, *7*(2), 45-71.

Boas, T., Bogena, H., Grünwald, T., Heinesch, B., Ryu, D., Schmidt, M., Vereecken, H., Western, A., and Hendricks Franssen, H.-J. (2021). Improving the representation of cropland sites in the Community Land Model (CLM) version 5.0. *Geoscientific Model Development*, *14*(1), 573-601.

Bogena, H., Herbst, M., Huisman, J. A., Rosenbaum, U., Weuthen, A., and Vereecken, H. (2010). Potential of wireless sensor networks for measuring soil water content variability. *Vadose Zone Journal*, *9*(4), 1002-1013.

Bogena, H., Huisman, J. A., Oberdörster, C., and Vereecken, H. (2007). Evaluation of a low-cost soil water content sensor for wireless network applications. *Journal of Hydrology*, *344*(1-2), 32-42.

Bogena, H., Huisman, J. A., Schilling, B., Weuthen, A., and Vereecken, H. (2017). Effective calibration of low-cost soil water content sensors. *Sensors*, *17*(1), 208.

Bogena, H., Weuthen, A., and Huisman, J. A. (2022). Recent Developments in Wireless Soil Moisture Sensing to Support Scientific Research and Agricultural Management. *Sensors*, *22*(24), 9792.

Bogena, H., White, T., Bour, O., Li, X., and Jensen, K. H. (2018). Toward better understanding of terrestrial processes through long-term hydrological observatories. *Vadose Zone Journal*, *17*(1), 1-10.

Bonan, G. (2019). *Climate change and terrestrial ecosystem modeling*, Cambridge University Press, Cambridge, UK, 1107043786.

Bondeau, A., Smith, P. C., Zaehle, S., Schaphoff, S., Lucht, W., Cramer, W., Gerten, D., Lotze-Campen, H., Müller, C., and Reichstein, M. (2007). Modelling the role of agriculture for the 20th century global terrestrial carbon balance. *Global change biology*, *13*(3), 679-706.

Brauer, C., van der Velde, Y., Teuling, A., and Uijlenhoet, R. (2018). The hupsel brook catchment: Insights from five decades of lowland observations. *Vadose Zone Journal*, *17*(1), 1-8.

Brito, T., Pereira, A. I., Lima, J., and Valente, A. (2020). Wireless Sensor Network for Ignitions Detection: An IoT approach. *Electronics*, *9*(6), 893.

Brocca, L., Ciabatta, L., Massari, C., Camici, S., and Tarpanelli, A. (2017). Soil moisture for hydrological applications: Open questions and new opportunities. *Water*, *9*(2), 140.

Brogi, C., Huisman, J., Pätzold, S., Von Hebel, C., Weihermüller, L., Kaufmann, M., van der Kruk, J., and Vereecken, H. (2019). Large-scale soil mapping using multi-configuration EMI and supervised image classification. *Geoderma*, *335*, 133-148.

Brogi, C., Pisinaras, V., Köhli, M., Dombrowski, O., Hendricks Franssen, H.-J., Babakos, K., Chatzi, A., Panagopoulos, A., and Bogena, H. R. (2023). Monitoring Irrigation in Small Orchards with Cosmic-Ray Neutron Sensors. *Sensors*, *23*(5), 2378.

Brogi, C., Vereecken, H., Bogena, H., and Brocca, L. (2022). Soil processes in the hydrologic cycle. In *Encyclopedia of Soils in the Environment (Second Edition)*, edited by Michael J. Goss and Oliver, M., pp. 469-481, Academic Press, 9780323951333.

Brunet, P., Clément, R., and Bouvier, C. (2010). Monitoring soil water content and deficit using Electrical Resistivity Tomography (ERT)–A case study in the Cevennes area, France. *Journal of Hydrology*, *380*(1-2), 146-153.

Brus, M., Vesala, T., Juurola, E., and Kaukolehto, M. (2013). ICOS – Integrated Carbon Observation System Stakeholders Handbook.

Bryś, K., Bryś, T., and Ojrzyńska, H. (2019). Long-wave radiation balances of grassy surface and bare soil in Wrocław. In Proceedings of the E3S Web of Conferences, EDP Sciences.

Budak, H., Kantar, M., and Yucebilgili Kurtoglu, K. (2013). Drought tolerance in modern and wild wheat. *The Scientific World Journal*, *2013*.

Buechel, M. (2021). Understanding hydrological change with land surface models. *Nature Reviews Earth & Environment*, *2*(12), 824-824.

Burgess, S. S. O. (2018). SFM1 Sap Flow Meter Manual, Version 5.1. *ICT International Pty Ltd, Armidale, NSW, Australia*.

Bwalya, J. M. (2012). Estimation of net carbon sequestration potential of citrus under different management systems using the life cycle approach. M.S. thesis, University of Zambia.

Cai, X., McKinney, D. C., and Rosegrant, M. W. (2003). Sustainability analysis for irrigation water management in the Aral Sea region. *Agricultural Systems*, *76*(3), 1043-1066.

Campbell, B. M., Beare, D. J., Bennett, E. M., Hall-Spencer, J. M., Ingram, J. S., Jaramillo, F., Ortiz, R., Ramankutty, N., Sayer, J. A., and Shindell, D. (2017). Agriculture production as a major driver of the Earth system exceeding planetary boundaries. *Ecology and society*, *22*(4).

Campbell, G. S. (1985). *Soil physics with BASIC: transport models for soil-plant systems*, Elsevier, Washington, U.S., 0080869823.

Canal, N., Calvet, J.-C., Decharme, B., Carrer, D., Lafont, S., and Pigeon, G. (2014). Evaluation of root water uptake in the ISBA-A-gs land surface model using agricultural yield statistics over France. *Hydrology and Earth System Sciences*, *18*(12), 4979-4999.

Carkoglu, A., and Eder, M. (2001). Domestic concerns and the water conflict over the Euphrates-Tigris river basin. *Middle Eastern Studies*, *37*(1), 41-71.

Carranca, C., Brunetto, G., and Tagliavini, M. (2018). Nitrogen nutrition of fruit trees to reconcile productivity and environmental concerns. *Plants*, *7*(1), 1-12.

Castagna, M., Bellin, A., and Chiogna, G. (2015). Uncertainty estimation and evaluation of shallow aquifers' exploitability: the case study of the Adige Valley Aquifer (Italy). *Water*, *7*(7), 3367-3395.

Ceccon, C., Panzacchi, P., Scandellari, F., Prandi, L., Ventura, M., Russo, B., Millard, P., and Tagliavini, M. (2011). Spatial and temporal effects of soil temperature and moisture and the relation to fine root density on root and soil respiration in a mature apple orchard. *Plant and Soil*, *342*(1), 195-206.

Ceglar, A., Zampieri, M., Toreti, A., and Dentener, F. (2019). Observed northward migration of agro-climate zones in Europe will further accelerate under climate change. *Earth's Future*, *7*(9), 1088-1101.

Cerutti, A. K., Beccaro, G. L., Bruun, S., Bosco, S., Donno, D., Notarnicola, B., and Bounous, G. (2014). Life cycle assessment application in the fruit sector: state of the art and recommendations for environmental declarations of fruit products. *Journal of cleaner production*, *73*, 125-135.

Cesaraccio, C., Spano, D., Snyder, R. L., and Duce, P. (2004). Chilling and forcing model to predict bud-burst of crop and forest species. *Agricultural and Forest Meteorology*, *126*(1-2), 1-13.

Chakraborty, D., Nagarajan, S., Aggarwal, P., Gupta, V., Tomar, R., Garg, R., Sahoo, R., Sarkar, A., Chopra, U. K., and Sarma, K. S. (2008). Effect of mulching on soil and plant water status, and the growth and yield of wheat (Triticum aestivum L.) in a semi-arid environment. *Agricultural Water Management*, *95*(12), 1323-1334.

Challinor, A., Wheeler, T., Craufurd, P., Slingo, J., and Grimes, D. (2004). Design and optimisation of a large-area process-based model for annual crops. *Agricultural and Forest Meteorology*, *124*(1-2), 99-120.

Challinor, A. J., Müller, C., Asseng, S., Deva, C., Nicklin, K. J., Wallach, D., Vanuytrecht, E., Whitfield, S., Ramirez-Villegas, J., and Koehler, A.-K. (2018). Improving the use of crop models for risk assessment and climate change adaptation. *Agricultural Systems*, *159*, 296-306.

Charrier, G., Martin-Stpaul, N., Damesin, C., Delpierre, N., Hänninen, H., Torres-Ruiz, J. M., and Davi, H. (2021). Interaction of drought and frost in tree ecophysiology: rethinking the timing of risks. *Annals of Forest Science*, *78*(40), 1-15.

Chaves, M. M., Maroco, J. P., and Pereira, J. S. (2003). Understanding plant responses to drought—from genes to the whole plant. *Functional Plant Biology*, *30*(3), 239-264.

Chen, L., and Dirmeyer, P. A. (2020). Distinct impacts of land use and land management on summer temperatures. *Frontiers in Earth Science*, *8*, 245.

Chen, M., Griffis, T. J., Baker, J. M., Wood, J. D., Meyers, T., and Suyker, A. (2018). Comparing crop growth and carbon budgets simulated across AmeriFlux agricultural sites using the Community Land Model (CLM). *Agricultural and Forest Meteorology*, *256*, 315-333.

Cheng, Y., Huang, M., Chen, M., Guan, K., Bernacchi, C., Peng, B., and Tan, Z. (2020). Parameterizing perennial bioenergy crops in Version 5 of the Community Land Model based on site-level observations in the Central Midwestern United States. *Journal of Advances in Modeling Earth Systems*, *12*(1), 1-24.

Chmielewski, F.-M., Blümel, K., and Pálešová, I. (2012). Climate change and shifts in dormancy release for deciduous fruit crops in Germany. *Climate research*, *54*(3), 209-219.

Choi, Y.-D., Goodall, J. L., Sadler, J. M., Castronova, A. M., Bennett, A., Li, Z., Nijssen, B., Wang, S., Clark, M. P., and Ames, D. P. (2021). Toward open and reproducible environmental modeling by integrating online data repositories, computational environments, and model Application Programming Interfaces. *Environmental Modelling & Software*, *135*, 104888.

Choukr-Allah, R., Ragab, R., and Rodriguez-Clemente, R. (2012). *Integrated water resources management in the Mediterranean region: dialogue towards new strategy*, Springer Science & Business Media, 9400747551.

CIHEAM (2009). Rethinking rural development in the Mediterranean. *1960-8527*, International Centre for Advanced Mediterranean Agronomic Studies and Blue Plan, Paris, France.

Clapp, R. B., and Hornberger, G. M. (1978). Empirical equations for some soil hydraulic properties. *Water Resources Research*, *14*(4), 601-604.

Colli, M., Lanza, L. G., Rasmussen, R., and Thériault, J. M. (2016). The collection efficiency of shielded and unshielded precipitation gauges. Part I: CFD airflow modeling. *Journal of Hydrometeorology*, *17*(1), 231-243.

Cook, B. I., Shukla, S. P., Puma, M. J., and Nazarenko, L. S. (2015). Irrigation as an historical climate forcing. *Climate Dynamics*, *44*, 1715-1730.

Copernicus European Digital Elevation Model (EU- DEM), version 1.1. Available online: https://land.copernicus.eu/imagery-in-situ/eu-dem/eu-dem-v1.1?tab=metadata (accessed on 13 September 2022).

Corelli-Grappadelli, L., and Lakso, A. N. (2002). Fruit development in deciduous tree crops as affected by physiological factors and environmental conditions (keynote). In Proceedings of the XXVI International Horticultural Congress: Key Processes in the Growth and Cropping of Deciduous Fruit and Nut Trees 636.

Corelli-Grappadelli, L., and Marini, R. (2008). 11 Orchard Planting Systems. In *The peach: botany, production and uses*, edited, p. 264, CABI, Pennsylvania, U.S., 1845933869.

Cosby, B. J., Hornberger, G. M., Clapp, R. B., and Ginn, T. R. (1984). A Statistical Exploration of the Relationships of Soil Moisture Characteristics to the Physical Properties of Soils. *Water Resources Research*, *20*(6), 682-690.

Cramer, W., Guiot, J., Fader, M., Garrabou, J., Gattuso, J.-P., Iglesias, A., Lange, M. A., Lionello, P., Llasat, M. C., and Paz, S. (2018). Climate change and interconnected risks to sustainable development in the Mediterranean. *Nature Climate Change*, *8*(11), 972-980.

Daccache, A., Ciurana, J., Diaz, J. R., and Knox, J. W. (2014). Water and energy footprint of irrigated agriculture in the Mediterranean region. *Environmental Research Letters*, *9*(12), 124014.

Dagon, K., Sanderson, B. M., Fisher, R. A., and Lawrence, D. M. (2020). A machine learning approach to emulation and biophysical parameter estimation with the Community Land Model, version 5. *Advances in Statistical Climatology, Meteorology and Oceanography*, *6*(2), 223-244.

Dangar, S., Asoka, A., and Mishra, V. (2021). Causes and implications of groundwater depletion in India: A review. *Journal of Hydrology*, *596*, 126103.

Dari, J., Brocca, L., Modanesi, S., Massari, C., Tarpanelli, A., Barbetta, S., Quast, R., Vreugdenhil, M., Freeman, V., and Barella-Ortiz, A. (2023). Regional data sets of high-resolution (1 and 6 km) irrigation estimates from space. *Earth System Science Data*, *15*(4), 1555-1575.

Dari, J., Brocca, L., Quintana-Seguí, P., Casadei, S., Escorihuela, M. J., Stefan, V., and Morbidelli, R. (2022). Double-scale analysis on the detectability of irrigation signals from remote sensing soil moisture over an area with complex topography in central Italy. *Advances in water resources*, *161*, 104130.

Davy, R., and Kusch, E. (2021). Reconciling high resolution climate datasets using KrigR. *Environmental Research Letters*, *16*(12), 124040.

de la Concepcion, A. R., Stefanelli, R., and Trinchero, D. (2015). Ad-hoc multilevel wireless sensor networks for distributed microclimatic diffused monitoring in precision agriculture. *2015 IEEE Topical Conference on Wireless Sensors and Sensor Networks (WiSNet)*, 14-16.

De Lannoy, G. J., Rosnay, P., and Reichle, R. H. (2019). Soil moisture data assimilation. In *Handbook of Hydrometeorological Ensemble Forecasting*, edited by Duan, Q., Pappenberger, F., Wood, A., Cloke, H. and Schaake, J., Springer, Berlin, Heidelberg, 364239924X.

De Rosnay, P., Polcher, J., Laval, K., and Sabre, M. (2003). Integrated parameterization of irrigation in the land surface model ORCHIDEE. Validation over Indian Peninsula. *Geophysical Research Letters*, *30*(19).

De Stefano, A., and Jacobson, M. G. (2018). Soil carbon sequestration in agroforestry systems: a meta-analysis. *Agroforestry Systems*, *92*, 285-299.

de Vrese, P., and Hagemann, S. (2018). Uncertainties in modelling the climate impact of irrigation. *Climate Dynamics*, *51*, 2023-2038.

de Vrese, P., Hagemann, S., and Claussen, M. (2016). Asian irrigation, African rain: Remote impacts of irrigation. *Geophysical Research Letters*, *43*(8), 3737-3745.

DeAngelis, A., Dominguez, F., Fan, Y., Robock, A., Kustu, M. D., and Robinson, D. (2010). Evidence of enhanced precipitation due to irrigation over the Great Plains of the United States. *Journal of Geophysical Research: Atmospheres*, *115*(D15).

Debaeke, P., Pellerin, S., and Scopel, E. (2017). Climate-smart cropping systems for temperate and tropical agriculture: mitigation, adaptation and trade-offs. *Cahiers Agricultures*, *26*(3), 34002.

DeJong, T. M., and Grossman, Y. L. (1994). A supply and demand approach to modeling annual reproductive and vegetative growth of deciduous fruit trees. *HortScience*, *29*(12), 1435-1442.

Demestihas, C., Plénet, D., Génard, M., Raynal, C., and Lescourret, F. (2017). Ecosystem services in orchards. A review. *Agronomy for Sustainable Development*, *37*(12), 1-21.

Dercas, N., Dalezios, N. R., Stamatiadis, S., Evangelou, E., Glampedakis, A., Mantonanakis, G., and Tserlikakis, N. (2022). AquaCrop Simulation of Winter Wheat under Different N Management Practices. *Hydrology*, *9*(4), 56.

Deryng, D., Sacks, W., Barford, C., and Ramankutty, N. (2011). Simulating the effects of climate and agricultural management practices on global crop yield. *Global Biogeochemical Cycles*, *25*(2).

Devanand, A., Huang, M., Ashfaq, M., Barik, B., and Ghosh, S. (2019). Choice of irrigation water management practice affects Indian summer monsoon rainfall and its extremes. *Geophysical Research Letters*, *46*(15), 9126-9135.

Devia, G. K., Ganasri, B. P., and Dwarakish, G. S. (2015). A review on hydrological models. *Aquatic procedia*, *4*, 1001-1007.

Dhanaraju, M., Chenniappan, P., Ramalingam, K., Pazhanivelan, S., and Kaliaperumal, R. (2022). Smart farming: Internet of Things (IoT)-based sustainable agriculture. *Agriculture*, *12*(10), 1745.

Díez-Palet, I., Funes, I., Savé, R., Biel, C., de Herralde, F., Miarnau, X., Vargas, F., Àvila, G., Carbó, J., and Aranda, X. (2019). Blooming under Mediterranean climate: Estimating cultivar-specific chill and heat requirements of almond and apple trees using a statistical approach. *Agronomy*, *9*(11), 760-781.

Diffenbaugh, N. S., and Giorgi, F. (2012). Climate change hotspots in the CMIP5 global climate model ensemble. *Climatic change*, *114*, 813-822.

Dingman, S. L. (2015). *Physical hydrology*, Waveland press, Illinois, US, 1478628073.

Doering, I., and Otto, C. (2002). *Effects of climate change and variability on agricultural production systems*, Springer Science & Business Media, 1402070284.

Döll, P. (2002). Impact of climate change and variability on irrigation requirements: a global perspective. *Climatic change*, *54*(3), 269-293.

Dombrowski, O. (2022). *odombro/CTSM: CLM5-FruitTree: A new sub-model for deciduous fruit trees* [Software]. Zenodo.

Dombrowski, O., Brogi, C., Hendricks Franssen, H.-J., Zanotelli, D., and Bogena, H. (2022). CLM5-FruitTree: a new sub-model for deciduous fruit trees in the Community Land Model (CLM5). *Geoscientific Model Development*, *15*(13), 5167-5193.

Dombrowski, O., Hendricks Franssen, H. J., Brogi, C., and Bogena, H. R. (2021). Performance of the ATMOS41 All-in-One Weather Station for Weather Monitoring. *Sensors*, *21*(3), 741.

Drewniak, B., Song, J., Prell, J., Kotamarthi, V. R., and Jacob, R. (2013). Modeling agriculture in the Community Land Model. *Geoscientific Model Development*, *6*(2), 495-515.

Dukes, M., Muñoz-Carpena, R., Zotarelli, L., Icerman, J., and Scholberg, J. (2007). Soil moisture-based irrigation control to conserve water and nutrients under drip irrigated vegetable production. *Jornada de Investigación en la Zona no Saturada*, *8*, 229-236.

DWD Deutscher Wetterdienst. Available online: https://www.dwd.de/DE/service/lexikon/Functions/glossar.html?lv2=101812&lv3=101906 (accessed on 22 October 2020).

DWD Niederschlag: vieljährige Mittelwerte 1981 - 2010 Station JUELICH (FORSCH.-ANLAGE). Available online: https://www.dwd.de/DE/leistungen/klimadatendeutschland/mittelwerte/nieder_8110_fest_html.html?view=nasPublication&nn=16102 (accessed on 11 January 2021).

El Jaouhari, N., Abouabdillah, A., Bouabid, R., Bourioug, M., Aleya, L., and Chaoui, M. (2018). Assessment of sustainable deficit irrigation in a Moroccan apple orchard as a climate change adaptation strategy. *Science of The Total Environment*, *642*, 574-581.

Elliott, J., Deryng, D., Müller, C., Frieler, K., Konzmann, M., Gerten, D., Glotter, M., Flörke, M., Wada, Y., and Best, N. (2014). Constraints and potentials of future irrigation water availability on agricultural production under climate change. *Proceedings of the National Academy of Sciences*, *111*(9), 3239-3244.

Elliott, J., Müller, C., Deryng, D., Chryssanthacopoulos, J., Boote, K., Büchner, M., Foster, I., Glotter, M., Heinke, J., and Iizumi, T. (2015). The global gridded crop model intercomparison: data and modeling protocols for phase 1 (v1. 0). *Geoscientific Model Development*, *8*(2), 261-277.

Environmental XPRT WeatherHawk - Model 620 - Wireless Weather Station. Available online: https://www.environmental-expert.com/products/weatherhawk-model-620-wireless-weather-station-302957 (accessed on 02 November 2020).

Erb, K. H., Luyssaert, S., Meyfroidt, P., Pongratz, J., Don, A., Kloster, S., Kuemmerle, T., Fetzel, T., Fuchs, R., and Herold, M. (2017). Land management: data availability and process understanding for global change studies. *Global change biology*, *23*(2), 512-533.

Eshete, D. G., Sinshaw, B. G., and Legese, K. G. (2020). Critical review on improving irrigation water use efficiency: Advances, challenges, and opportunities in the Ethiopia context. *Water-Energy Nexus*, *3*, 143-154.

Estévez, J., Gavilán, P., and Giráldez, J. V. (2011). Guidelines on validation procedures for meteorological data from automatic weather stations. *Journal of Hydrology*, *402*(1-2), 144-154.

Fader, M., Shi, S., von Bloh, W., Bondeau, A., and Cramer, W. (2016). Mediterranean irrigation under climate change: more efficient irrigation needed to compensate for increases in irrigation water requirements. *Hydrology and Earth System Sciences*, *20*(2), 953-973.

Fader, M., von Bloh, W., Shi, S., Bondeau, A., and Cramer, W. (2015). Modelling Mediterranean agro-ecosystems by including agricultural trees in the LPJmL model. *Geoscientific Model Development*, *8*(11), 3545-3561.

Fan, Y., Roupsard, O., Bernoux, M., Le Maire, G., Panferov, O., Kotowska, M. M., and Knohl, A. (2015). A sub-canopy structure for simulating oil palm in the Community Land Model (CLM-Palm): phenology, allocation and yield. *Geoscientific Model Development*, *8*(11), 3785-3800.

FAO FAO Crops and livestock products. Available online: https://www.fao.org/faostat/en/#data/QCL (accessed on 22 December 2021).

FAO Land Use. Available online: https://www.fao.org/faostat/en/#data/RL (accessed on 08 September 2023).

FAO (2022). *World Food and Agriculture – Statistical Yearbook 2022*, FAO, Rome, 9251369305.

FAO Crop Information - Potato. Available online: https://www.fao.org/land-water/databases-and-software/crop-information/potato/en/ (accessed on 19 June 2023).

Farquhar, G. D., von Caemmerer, S. v., and Berry, J. A. (1980). A biochemical model of photosynthetic CO 2 assimilation in leaves of C 3 species. *planta*, *149*, 78-90.

Faust, M., Erez, A., Rowland, L. J., Wang, S. Y., and Norman, H. A. (1997). Bud dormancy in perennial fruit trees: physiological basis for dormancy induction, maintenance, and release. *HortScience*, *32*(4), 623-629.

Felfelani, F., Chen, F., Dugger, A. L., Gochis, D., Schneider, T., Traylor, J., Hughes, J. D., and Essaid, H. (2022). Effects of Coupling MODFLOW with Land Surface Models to Reduce Bias in Groundwater-flow Simulations. In Proceedings of the AGU Fall Meeting Abstracts.

Felfelani, F., Lawrence, D. M., and Pokhrel, Y. (2021). Representing intercell lateral groundwater flow and aquifer pumping in the community land model. *Water Resources Research*, *57*(1), e2020WR027531.

Felfelani, F., Pokhrel, Y., Guan, K., and Lawrence, D. M. (2018). Utilizing SMAP soil moisture data to constrain irrigation in the Community Land Model. *Geophysical Research Letters*, *45*(23), 12,892-812,902.

Ferguson, I. M., and Maxwell, R. M. (2012). Human impacts on terrestrial hydrology: climate change versus pumping and irrigation. *Environmental Research Letters*, *7*(4), 044022.

Fernández García, I., Lecina, S., Ruiz-Sánchez, M. C., Vera, J., Conejero, W., Conesa, M. R., Domínguez, A., Pardo, J. J., Léllis, B. C., and Montesinos, P. (2020). Trends and challenges in irrigation scheduling in the semi-arid area of Spain. *Water*, *12*(3), 785.

Fisher, R. A., and Koven, C. D. (2020). Perspectives on the future of land surface models and the challenges of representing complex terrestrial systems. *Journal of Advances in Modeling Earth Systems*, *12*(4), 1-24.

Fraisl, D., Hager, G., Bedessem, B., Gold, M., Hsing, P.-Y., Danielsen, F., Hitchcock, C. B., Hulbert, J. M., Piera, J., and Spiers, H. (2022). Citizen science in environmental and ecological sciences. *Nature Reviews Methods Primers*, *2*(1), 64.

Frisvold, G. B., and Deva, S. (2012). Farm size, irrigation practices, and conservation program participation in the US Southwest. *Irrigation and Drainage*, *61*(5), 569-582.

Gaitani, N., Spanou, A., Saliari, M., Synnefa, A., Vassilakopoulou, K., Papadopoulou, K., Pavlou, K., Santamouris, M., Papaioannou, M., and Lagoudaki, A. (2011). Improving the microclimate in urban areas: a case study in the centre of Athens. *Building Services Engineering Research and Technology*, *32*(1), 53-71.

Gao, F., and Zhang, X. (2021). Mapping crop phenology in near real-time using satellite remote sensing: Challenges and opportunities. *Journal of Remote Sensing*.

Gao, L., Zhao, P., Kang, S., Li, S., Tong, L., Ding, R., and Lu, H. (2020). Comparison of evapotranspiration and energy partitioning related to main biotic and abiotic controllers in vineyards using different irrigation methods. *Frontiers of Agricultural Science and Engineering*, *7*(4), 490-504.

Gao, X., Avramov, A., Saikawa, E., and Schlosser, C. A. (2021). Emulation of Community Land Model version 5 (CLM5) to quantify sensitivity of soil moisture to uncertain parameters. *Journal of Hydrometeorology*, *22*(2), 259-278.

García-Garizábal, I., Causapé, J., and Abrahão, R. (2012). Nitrate contamination and its relationship with flood irrigation management. *Journal of Hydrology*, *442*, 15-22.

García-Tejero, I. F., Durán-Zuazo, V. H., and Muriel-Fernández, J. L. (2014). Towards sustainable irrigated Mediterranean agriculture: implications for water conservation in semi-arid environments. *Water international*, *39*(5), 635-648.

Gibson, J., Franz, T. E., Wang, T., Gates, J., Grassini, P., Yang, H., and Eisenhauer, D. (2017). A case study of field-scale maize irrigation patterns in western Nebraska: implications for water managers and recommendations for hyper-resolution land surface modeling. *Hydrology and Earth System Sciences*, *21*(2), 1051-1062.

Gill Instruments Limited MaxiMet GMX600 Compact Weather Station. Available online: https://gillinstruments.com/compare-weather-stations/maximet-weather-station/ (accessed on 01 November 2023).

Gilley, J. R., and Watts, D. G. (1977). Energy reduction through improved irrigation practices. In *Agriculture and Energy*, edited, pp. 187-203, Elsevier, 978-0-12-454250-1.

Glover, J. D., Reganold, J., Bell, L., Borevitz, J., Brummer, E., Buckler, E. S., Cox, C., Cox, T. S., Crews, T., and Culman, S. (2010). Increased food and ecosystem security via perennial grains. *Science*, *328*(5986), 1638-1639.

Göhler, M., Mai, J., and Cuntz, M. (2013). Use of eigendecomposition in a parameter sensitivity analysis of the Community Land Model. *Journal of Geophysical Research: Biogeosciences*, *118*(2), 904-921.

Goldschmidt, E. E., and Lakso, A. N. (2005). Fruit tree models: scope and limitations. *Information and Communication Technology (ICT) Development and Adoption: Perspectives of Technological Innovation*, 1-19.

Gordon, L. J., Steffen, W., Jönsson, B. F., Folke, C., Falkenmark, M., and Johannessen, Å. (2005). Human modification of global water vapor flows from the land surface. *Proceedings of the National Academy of Sciences*, *102*(21), 7612-7617.

Gornott, C., and Wechsung, F. (2015). Level normalized modeling approach of yield volatility for winter wheat and silag emaize on different scales within Germany. *Journal für Kulturpflanzen*, *67*(6), 205-223.

Grechi, I., Sauge, M. H., Sauphanor, B., Hilgert, N., Senoussi, R., and Lescourret, F. (2008). How does winter pruning affect peach tree–Myzus persicae interactions? *Entomologia Experimentalis et Applicata*, *128*(3), 369-379.

Greer, D. H., Wünsche, J. N., and Halligan, E. A. (2002). Influence of postharvest temperatures on leaf gas exchange, carbohydrate reserves and allocations, subsequent budbreak, and fruit yield of 'Braeburn'apple (Malus domestica) trees. *New Zealand Journal of Crop and Horticultural Science*, *30*(3), 175-185.

Gruber, A., De Lannoy, G., Albergel, C., Al-Yaari, A., Brocca, L., Calvet, J.-C., Colliander, A., Cosh, M., Crow, W., and Dorigo, W. (2020). Validation practices for satellite soil moisture retrievals: What are (the) errors? *Remote Sensing of Environment*, *244*, 111806.

Gu, Z., Qi, Z., Burghate, R., Yuan, S., Jiao, X., and Xu, J. (2020). Irrigation scheduling approaches and applications: A review. *Journal of Irrigation and Drainage Engineering*, *146*(6), 04020007.

Gunawardena, N., Pardyjak, E. R., Stoll, R., and Khadka, A. (2018). Development and evaluation of an open-source, low-cost distributed sensor network for environmental monitoring applications. *Measurement Science and Technology*, *29*(2), 024008.

Guo, D., Wang, Q. J., Ryu, D., Yang, Q., Moller, P., and Western, A. W. (2023). An analysis framework to evaluate irrigation decisions using short-term ensemble weather forecasts. *Irrigation science*, *41*(1), 155-171.

Gurung, T. R., Bousquet, F., and Trébuil, G. (2006). Companion modeling, conflict resolution, and institution building: sharing irrigation water in the Lingmuteychu Watershed, Bhutan. *Ecology and society*, *11*(2).

Haddeland, I., Heinke, J., Biemans, H., Eisner, S., Flörke, M., Hanasaki, N., Konzmann, M., Ludwig, F., Masaki, Y., and Schewe, J. (2014). Global water resources affected by human interventions and climate change. *Proceedings of the National Academy of Sciences*, *111*(9), 3251-3256.

Hall, D. O., and Rao, K. (1999). *Photosynthesis*, Cambridge University Press, 0521644976.

Hammad, H. M., Nauman, H. M. F., Abbas, F., Ahmad, A., Bakhat, H. F., Saeed, S., Shah, G. M., Ahmad, A., and Cerdà, A. (2020). Carbon sequestration potential and soil characteristics of various land use systems in arid region. *Journal of environmental management*, *264*, 110254.

Han, X., Franssen, H.-J. H., Rosolem, R., Jin, R., Li, X., and Vereecken, H. (2015). Correction of systematic model forcing bias of CLM using assimilation of cosmic-ray Neutrons and land surface temperature: a study in the Heihe Catchment, China. *Hydrology and Earth System Sciences*, *19*(1), 615-629.

Han, X., Franssen, H. J. H., Montzka, C., and Vereecken, H. (2014). Soil moisture and soil properties estimation in the Community Land Model with synthetic brightness temperature observations. *Water Resources Research*, *50*(7), 6081-6105.

Han, X., Hendricks Franssen, H.-J., Jiménez Bello, M. Á., Rosolem, R., Bogena, H., Alzamora, F. M., Chanzy, A., and Vereecken, H. (2016). Simultaneous soil moisture and properties estimation for a drip irrigated field by assimilating cosmic-ray neutron intensity. *Journal of Hydrology*, *539*, 611-624.

Harmanny, K. S., and Malek, Ž. (2019). Adaptations in irrigated agriculture in the Mediterranean region: an overview and spatial analysis of implemented strategies. *Regional environmental change*, *19*, 1401-1416.

Hart, J. K., and Martinez, K. (2006). Environmental sensor networks: A revolution in the earth system science? *Earth-Science Reviews*, *78*(3-4), 177-191.

He, Y., Wang, C., Hu, J., Mao, H., Duan, Z., Qu, C., Li, R., Wang, M., and Song, X. (2023). Discovering Optimal Triplets for Assessing the Uncertainties of Satellite-Derived Evapotranspiration Products. *Remote Sensing*, *15*(13), 3215.

Hedley, C., Ekanayake, J., and Roudier, P. (2012). Wireless soil moisture sensor networks for precision irrigation scheduling. In Proceedings of the Workshop abstracts, advanced nutrient management: Gains from the past-goals for the future.

Heide, O. M., and Prestrud, A. K. (2005). Low temperature, but not photoperiod, controls growth cessation and dormancy induction and release in apple and pear. *Tree physiology*, *25*(1), 109-114.

Heinrich, I., Balanzategui, D., Bens, O., Blasch, G., Blume, T., Böttcher, F., Borg, E., Brademann, B., Brauer, A., and Conrad, C. (2018). Interdisciplinary geo-ecological research across time scales in the Northeast German Lowland Observatory (TERENO-NE). *Vadose Zone Journal*, *17*(1), 1-25.

Heiskanen, J., Brümmer, C., Buchmann, N., Calfapietra, C., Chen, H., Gielen, B., Gkritzalis, T., Hammer, S., Hartman, S., and Herbst, M. (2022). The integrated carbon observation system in Europe. *Bulletin of the American Meteorological Society*, *103*(3), E855-E872.

Hernández-Ochoa, I. M., Gaiser, T., Kersebaum, K.-C., Webber, H., Seidel, S. J., Grahmann, K., and Ewert, F. (2022). Model-based design of crop diversification through new field arrangements in spatially heterogeneous landscapes. A review. *Agronomy for Sustainable Development*, *42*(4), 74.

Hewage, P., Behera, A., Trovati, M., Pereira, E., Ghahremani, M., Palmieri, F., and Liu, Y. (2020). Temporal convolutional neural (TCN) network for an effective weather forecasting using time-series data from the local weather station. *Soft Computing*, *24*, 16453-16482.

Hiederer, R. (2013). Mapping soil properties for Europe—spatial representation of soil database attributes, *47*, 1831-9424.

Hla, A. K., and Scherer, T. F. (2003). Introduction to micro-irrigation. North DakotaState University Extension Service, Fargo, N.D., USA.

Hoblyn, T., Grubb, N., Painter, A., and Wates, B. (1937). Studies in biennial bearing.—I. *Journal of pomology and horticultural science*, *14*(1), 39-76.

Holzkämper, A. (2017). Adapting agricultural production systems to climate change—what's the use of models? *Agriculture*, *7*(10), 86.

Hou, T., Wang, Y., Guo, F., Jia, Q., Wu, X., Wang, E., and Hong, J. (2021). Soil Respiration Characteristics and Influencing Factors for Apple Orchards in Different Regions on the Loess Plateau of Shaanxi Province. *Sustainability*, *13*(9), 1-21.

Houdret, A. (2012). The water connection: Irrigation, water grabbing and politics in southern Morocco. *Water Alternatives*, *5*(2), 284-303.

Huang, Y., Zhang, Z., Li, Z., Dai, D., and Li, Y. (2022). Evaluation of water use efficiency and optimal irrigation quantity of spring maize in Hetao Irrigation District using the Noah-MP Land Surface Model. *Agricultural Water Management*, *264*, 107498.

Hung, C. P., Schalge, B., Baroni, G., Vereecken, H., and Hendricks Franssen, H. J. (2022). Assimilation of Groundwater Level and Soil Moisture Data in an Integrated Land Surface-Subsurface Model for Southwestern Germany. *Water Resources Research*, *58*(6), e2021WR031549.

Hunt, M. L., Blackburn, G. A., Carrasco, L., Redhead, J. W., and Rowland, C. S. (2019). High resolution wheat yield mapping using Sentinel-2. *Remote Sensing of Environment*, *233*, 111410.

Ibarreche, J., Aquino, R., Edwards, R., Rangel, V., Pérez, I., Martínez, M., Castellanos, E., Álvarez, E., Jimenez, S., and Rentería, R. (2020). Flash flood early warning system in colima, mexico. *Sensors*, *20*(18), 5231.

Ibragimov, N., Evett, S. R., Esanbekov, Y., Kamilov, B. S., Mirzaev, L., and Lamers, J. P. (2007). Water use efficiency of irrigated cotton in Uzbekistan under drip and furrow irrigation. *Agricultural Water Management*, *90*(1-2), 112-120.

ICOS Selhausen (C1). Available online: http://www.icos-infrastruktur.de/en/icos-d/komponenten/oekosysteme/beobachtungsstandorte/selhausen-c1/ (accessed on 06 November 2020).

Idso, S. B. (1981). A set of equations for full spectrum and 8-to 14-μm and 10.5-to 12.5-μm thermal radiation from cloudless skies. *Water Resources Research*, *17*(2), 295-304.

Iglesias, A., and Garrote, L. (2015). Adaptation strategies for agricultural water management under climate change in Europe. *Agricultural Water Management*, *155*, 113-124.

Ioannou, K., Karampatzakis, D., Amanatidis, P., Aggelopoulos, V., and Karmiris, I. (2021). Low-cost automatic weather stations in the internet of things. *Information*, *12*(4), 146.

IPCC (2012). Summary for policymakers: managing the risks of extreme events and disasters to advance climate change adaptation. In *Planning for Climate Change*, edited by Field, C. B., Barros, V., Stocker, T. F., Dahe, Q., Dokken, D. J., Ebi, K. L., Mastrandrea, M. D., Mach, K. J., Plattner, G.-K. and Allen, S. K., pp. 111-128, Routledge.

IPCC (2022). Climate Change 2022: Impacts, Adaptation and Vulnerability. Contribution of Working Group

II to the Sixth Assessment Report of the Intergovernmental Panel on Climate Change [H.-O. Pörtner, D.C.

Roberts, M. Tignor, E.S. Poloczanska, K. Mintenbeck, A. Alegría, M. Craig, S. Langsdorf, S. Löschke, V.

Möller, A. Okem, B. Rama (eds.)]. *Cambridge University Press, Cambridge, UK and New York, NY, USA*, 3056 pp.

Irmak, S. (2008). Plant growth and yield as affected by wet soil conditions due to flooding or over-irrigation. Lincoln City, OR, USA.

Isagi, Y., Sugimura, K., Sumida, A., and Ito, H. (1997). How does masting happen and synchronize? *Journal of Theoretical Biology*, *187*(2), 231-239.

Jackson, D. (2011). Flowers and fruit. In *Temperate and subtropical fruit production.*, edited, pp. 34-43, CABI, Cambridge, U.K.

Jakobi, J., Huisman, J. A., Vereecken, H., Diekkrüger, B., and Bogena, H. R. (2018). Cosmic Ray Neutron Sensing for Simultaneous Soil Water Content and Biomass Quantification in Drought Conditions. *Water Resources Research*, *54*(10), 7383-7402.

Jencso, K., Hyde, K., Bocinsky, K., and Hoylman, Z. H. (2019). The Montana Mesonet - a Nascent Wireless Network in the Upper Missouri River Basin. *AGU Fall Meeting Abstracts*, *2019*, PA11C-0955.

Jensen, K. H., and Illangasekare, T. H. (2011). HOBE: A hydrological observatory. *Vadose Zone Journal*, *10*(1), 1-7.

Jensen, M. E. (1968). Water consumption by agricultural plants. In *Water Deficits and Plant Growth*, edited by Kozlowski, T. T., pp. 1-22, Academic Press, New York, NY, USA.

Jiang, Y., Kim, J. B., Still, C. J., Kerns, B. K., Kline, J. D., and Cunningham, P. G. (2018). Inter-comparison of multiple statistically downscaled climate datasets for the Pacific Northwest, USA. *Scientific data*, *5*(1), 1-18.

Joffre, R., and Rambal, S. (2001). Mediterranean ecosystems. *Encyclopedia of Life Sciences*, 1-7.

Jones, C. A., Kiniry, J. R., and Dyke, P. (1986). *CERES-Maize: A simulation model of maize growth and development*, Texas A&M University Press, College Station, USA, 0890962693.

Jones, J., Hoogenboom, G., Porter, C., Boote, K., Batchelor, W., Hunt, L., Wilkens, P., Singh, U., Gijsman, A., and Ritchie, J. (2003). The DSSAT cropping system model. *European Journal of Agronomy*, *18*(3-4), 235-265.

Katyal, A., Yadav, R., and Pandey, M. (2016). Wireless arduino based weather station. *International Journal of Advanced Research in Computer and Communication Engineering*, *5*(4), 274-276.

Kazimierski, P., Hercel, P., Suchocki, T., Smoliński, J., Pladzyk, A., Kardaś, D., Łuczak, J., and Januszewicz, K. (2021). Pyrolysis of Pruning Residues from Various Types of Orchards and Pretreatment for Energetic Use of Biochar. *Materials*, *14*(11), 1-14.

Keating, B. A., Carberry, P. S., Hammer, G. L., Probert, M. E., Robertson, M. J., Holzworth, D., Huth, N. I., Hargreaves, J. N., Meinke, H., and Hochman, Z. (2003). An overview of APSIM, a model designed for farming systems simulation. *European Journal of Agronomy*, *18*(3-4), 267-288.

Kennedy, D., Swenson, S., Oleson, K. W., Lawrence, D. M., Fisher, R., Lola da Costa, A. C., and Gentine, P. (2019). Implementing plant hydraulics in the community land model, version 5. *Journal of Advances in Modeling Earth Systems*, *11*(2), 485-513.

Kephe, P. N., Ayisi, K. K., and Petja, B. M. (2021). Challenges and opportunities in crop simulation modelling under seasonal and projected climate change scenarios for crop production in South Africa. *Agriculture & Food Security*, *10*(1), 1-24.

Khan, S., Tariq, R., Yuanlai, C., and Blackwell, J. (2006). Can irrigation be sustainable? *Agricultural Water Management*, *80*(1-3), 87-99.

Kochendorfer, J., Rasmussen, R., Wolff, M., Baker, B., Hall, M. E., Meyers, T., Landolt, S., Jachcik, A., Isaksen, K., and Brækkan, R. (2017). The quantification and correction of wind-induced precipitation measurement errors. *Hydrology and Earth System Sciences*, *21*(4), 1973.

Köhli, M., Schrön, M., Zreda, M., Schmidt, U., Dietrich, P., and Zacharias, S. (2015). Footprint characteristics revised for field-scale soil moisture monitoring with cosmic-ray neutrons. *Water Resources Research*, *51*(7), 5772-5790.

Kolassa, J., Reichle, R., and Draper, C. S. (2017). Merging active and passive microwave observations in soil moisture data assimilation. *Remote Sensing of Environment*, *191*, 117-130.

Konzelmann, T., van de Wal, R. S., Greuell, W., Bintanja, R., Henneken, E. A., and Abe-Ouchi, A. (1994). Parameterization of global and longwave incoming radiation for the Greenland Ice Sheet. *Global and Planetary change*, *9*(1-2), 143-164.

Koyama, C. N., Liu, H., Takahashi, K., Shimada, M., Watanabe, M., Khuut, T., and Sato, M. (2017). In-situ measurement of soil permittivity at various depths for the calibration and validation of low-frequency SAR soil moisture models by using GPR. *Remote Sensing*, *9*(6), 580.

Kozlowski, T. T. (1992). Carbohydrate sources and sinks in woody plants. *The botanical review*, *58*(2), 107-222.

Krinner, G., Viovy, N., de Noblet-Ducoudré, N., Ogée, J., Polcher, J., Friedlingstein, P., Ciais, P., Sitch, S., and Prentice, I. C. (2005). A dynamic global vegetation model for studies of the coupled atmosphere-biosphere system. *Global Biogeochemical Cycles*, *19*(1), 1-33.

Krysanova, V., Wechsung, F., Arnold, J., Srinivasan, R., and Williams, J. (2000). SWIM (soil and water integrated model). *PIK-69*, 239 pp, Potsdam-Institut für Klimafolgenforschung (PIK), Potsdam, Germany.

Kueppers, L. M., and Snyder, M. A. (2012). Influence of irrigated agriculture on diurnal surface energy and water fluxes, surface climate, and atmospheric circulation in California. *Climate Dynamics*, *38*, 1017-1029.

Kueppers, L. M., Snyder, M. A., Sloan, L. C., Cayan, D., Jin, J., Kanamaru, H., Kanamitsu, M., Miller, N. L., Tyree, M., and Du, H. (2008). Seasonal temperature responses to land-use change in the western United States. *Global and Planetary change*, *60*(3-4), 250-264.

Kumar, D. N., and Reshmidevi, T. (2013). Remote sensing applications in water resources. *Journal of the Indian Institute of Science*, *93*(2), 163-188.

Kurunc, A., Ersahin, S., Sonmez, N. K., Kaman, H., Uz, I., Uz, B. Y., and Aslan, G. E. (2016). Seasonal changes of spatial variation of some groundwater quality variables in a large irrigated coastal Mediterranean region of Turkey. *Science of The Total Environment*, *554*, 53-63.

la Fuente-Sáiz, D., Ortega-Farías, S., Fonseca, D., Ortega-Salazar, S., Kilic, A., and Allen, R. (2017). Calibration of METRIC model to estimate energy balance over a drip-irrigated apple orchard. *Remote Sensing*, *9*(7), 1-18.

Lakso, A., White, M., and Tustin, D. (2000). Simulation modeling of the effects of short and long-term climatic variations on carbon balance of apple trees. In Proceedings of the VII International Symposium on Orchard and Plantation Systems 557.

Lakso, A., Wunsche, J., Palmer, J., and Grappadelli, L. C. (1999). Measurement and modeling of carbon balance of the apple tree. *HortScience*, *34*(6), 1040-1047.

Lange, S., and Büchner, M. (2020). ISIMIP2a atmospheric climate input data (v1.0).

Lasslop, G., Migliavacca, M., Bohrer, G., Reichstein, M., Bahn, M., Ibrom, A., Jacobs, C., Kolari, P., Papale, D., and Vesala, T. (2012). On the choice of the driving temperature for eddy-covariance carbon dioxide flux partitioning. *Biogeosciences*, *9*(12), 5243-5259.

Latinopoulos, P. (2005). Valuation and pricing of irrigation water: An analysis in Greek agricultural areas. *Global NEST Journal*, *7*(3), 323-335.

Laurent, O. (2017). ICOS Atmospheric Station Specifications. ICOS.

Lawrence, D. M., Fisher, R., Koven, C., Oleson, K., Swenson, S., Vertenstein, M., Andre, B., Bonan, G., Ghimire, B., and van Kampenhout, L. (2018). Technical description of version 5.0 of the Community Land Model (CLM). *National Center Atmospheric Research (NCAR)*. Available online: http://www.cesm.ucar.edu/models/cesm2/land/CLM50_Tech_Note.pdf (accessed on 02 May 2021).

Lawrence, D. M., et al. (2019). The Community Land Model Version 5: Description of New Features, Benchmarking, and Impact of Forcing Uncertainty. *Journal of Advances in Modeling Earth Systems*, *11*(12), 4245-4287.

Lawrence, D. M., and Slater, A. (2008). Incorporating organic soil into a global climate model. *Climate Dynamics*, *30*, 145-160.

Lawston, P. M., Santanello, J. A., Hanson, B., and Arsensault, K. (2020). Impacts of irrigation on summertime temperatures in the Pacific Northwest. *Earth Interactions*, *24*(1), 1-26.

Lawston, P. M., Santanello Jr, J. A., Franz, T. E., and Rodell, M. (2017). Assessment of irrigation physics in a land surface modeling framework using non-traditional and human-practice datasets. *Hydrology and Earth System Sciences*, *21*(6), 2953-2966.

Le Roux, X., Lacointe, A., Escobar-Gutiérrez, A., and Le Dizès, S. (2001). Carbon-based models of individual tree growth: a critical appraisal. *Annals of Forest Science*, *58*(5), 469-506.

Ledo, A., Smith, P., Zerihun, A., Whitaker, J., Vicente-Vicente, J. L., Qin, Z., McNamara, N. P., Zinn, Y. L., Llorente, M., and Liebig, M. (2020). Changes in soil organic carbon under perennial crops. *Global change biology*, *26*(7), 4158-4168.

Leng, G., Huang, M., Tang, Q., and Leung, L. R. (2015). A modeling study of irrigation effects on global surface water and groundwater resources under a changing climate. *Journal of Advances in Modeling Earth Systems*, *7*(3), 1285-1304.

Leng, G., Huang, M., Tang, Q., Sacks, W. J., Lei, H., and Leung, L. R. (2013). Modeling the effects of irrigation on land surface fluxes and states over the conterminous United States: Sensitivity to input data and model parameters. *Journal of Geophysical Research: Atmospheres*, *118*(17), 9789-9803.

Leng, G., Leung, L. R., and Huang, M. (2017). Significant impacts of irrigation water sources and methods on modeling irrigation effects in the ACME Land Model. *Journal of Advances in Modeling Earth Systems*, *9*(3), 1665-1683.

Lescourret, F., Moitrier, N., Valsesia, P., and Génard, M. (2011). QualiTree, a virtual fruit tree to study the management of fruit quality. I. Model development. *Trees*, *25*(3), 519-530.

Levis, S., Bonan, G. B., Kluzek, E., Thornton, P. E., Jones, A., Sacks, W. J., and Kucharik, C. J. (2012). Interactive crop management in the Community Earth System Model (CESM1): Seasonal influences on land–atmosphere fluxes. *Journal of Climate*, *25*(14), 4839-4859.

Levis, S., and Sacks, W. (2011). Technical descriptions of the interactive crop management (CLM4CNcrop) and interactive irrigation models in version 4 of the Community Land Model. *National Center Atmospheric Research (NCAR)*. Available online: https://www2.cesm.ucar.edu/models/cesm1.0/clm/CLMcropANDirrigTechDescriptions.pdf (accessed on 01 November 2023).

Li, D., Franssen, H.-J. H., Han, X., Jiménez-Bello, M. A., Alzamora, F. M., and Vereecken, H. (2018). Evaluation of an operational real-time irrigation scheduling scheme for drip irrigated citrus fields in Picassent, Spain. *Agricultural Water Management*, *208*, 465-477.

Li, F., Cohen, S., Naor, A., Shaozong, K., and Erez, A. (2002). Studies of canopy structure and water use of apple trees on three rootstocks. *Agricultural Water Management*, *55*(1), 1-14.

Li, Z., Zhang, H., Lu, F., Xue, R., Yang, G., and Zhang, L. (2022). Breaking the resolution barrier: A low-to-high network for large-scale high-resolution land-cover mapping using low-resolution labels. *ISPRS Journal of Photogrammetry and Remote Sensing*, *192*, 244-267.

Liao, Y., Cao, H.-X., Liu, X., Li, H.-T., Hu, Q.-Y., and Xue, W.-K. (2021). By increasing infiltration and reducing evaporation, mulching can improve the soil water environment and apple yield of orchards in semiarid areas. *Agricultural Water Management*, *253*, 106936.

Licker, R., Johnston, M., Foley, J. A., Barford, C., Kucharik, C. J., Monfreda, C., and Ramankutty, N. (2010). Mind the gap: how do climate and agricultural management explain the 'yield gap'of croplands around the world? *Global ecology and biogeography*, *19*(6), 769-782.

Linker, R., and Sylaios, G. (2016). Efficient model-based sub-optimal irrigation scheduling using imperfect weather forecasts. *Computers and Electronics in Agriculture*, *130*, 118-127.

Lionello, P., Malanotte-Rizzoli, P., Boscolo, R., Alpert, P., Artale, V., Li, L., Luterbacher, J., May, W., Trigo, R., and Tsimplis, M. (2006). The Mediterranean climate: an overview of the main characteristics and issues, *4*, 1-26.

Liu, X., Chen, F., Barlage, M., Zhou, G., and Niyogi, D. (2016). Noah-MP-Crop: Introducing dynamic crop growth in the Noah-MP land surface model. *Journal of Geophysical Research: Atmospheres*, *121*(23), 13,953-913,972.

Liu, Y., Wang, J., Liu, D., Li, Z., Zhang, G., Tao, Y., Xie, J., Pan, J., and Chen, F. (2014). Straw mulching reduces the harmful effects of extreme hydrological and temperature conditions in citrus orchards. *PloS one*, *9*(1), e87094.

Lobell, D. B., Bonfils, C. J., Kueppers, L. M., and Snyder, M. A. (2008a). Irrigation cooling effect on temperature and heat index extremes. *Geophysical Research Letters*, *35*(9).

Lobell, D. B., Burke, M. B., Tebaldi, C., Mastrandrea, M. D., Falcon, W. P., and Naylor, R. L. (2008b). Prioritizing climate change adaptation needs for food security in 2030. *Science*, *319*(5863), 607-610.

Lobianco, A., and Roberto, E. (2006). The regional model for Mediterranean agriculture. Munich Personal RePEc Archive (MPRA), Munich, Germany.

Loescher, W. H., McCamant, T., and Keller, J. D. (1990). Carbohydrate reserves, translocation, and storage in woody plant roots. *HortScience*, *25*(3), 274-281.

Lokupitiya, E., Denning, A. S., Schaefer, K., Ricciuto, D., Anderson, R., Arain, M., Baker, I., Barr, A., Chen, G., and Chen, J. (2016). Carbon and energy fluxes in cropland ecosystems: a model-data comparison. *Biogeochemistry*, *129*, 53-76.

Lombardozzi, D. L., Lu, Y., Lawrence, P. J., Lawrence, D. M., Swenson, S., Oleson, K. W., Wieder, W. R., and Ainsworth, E. A. (2020). Simulating agriculture in the Community Land Model version 5. *Journal of Geophysical Research: Biogeosciences*, *125*(8), 1-19.

López-Olivari, R., Ortega-Farías, S., and Poblete-Echeverría, C. (2016). Partitioning of net radiation and evapotranspiration over a superintensive drip-irrigated olive orchard. *Irrigation science*, *34*(1), 17-31.

Lopez, J. C. B., and Villaruz, H. M. (2015). Low-cost weather monitoring system with online logging and data visualization. *2015 International Conference on Humanoid, Nanotechnology, Information Technology, Communication and Control, Environment and Management (HNICEM)*, 1-6.

Lorite, I., Ramírez-Cuesta, J., Cruz-Blanco, M., and Santos, C. (2015). Using weather forecast data for irrigation scheduling under semi-arid conditions. *Irrigation science*, *33*, 411-427.

Luo, Q., Wen, J., Hu, Z., Lu, Y., and Yang, X. (2020). Parameter sensitivities of the Community Land Model at two alpine sites in the three-river source region. *Journal of Meteorological Research*, *34*(4), 851-864.

Lytos, A., Lagkas, T., Sarigiannidis, P., Zervakis, M., and Livanos, G. (2020). Towards smart farming: Systems, frameworks and exploitation of multiple sources. *Computer Networks*, *172*, 107147.

Ma, Y., and Liu, H. (2019). An advanced multiple-layer canopy model in the WRF model with large-eddy simulations to simulate canopy flows and scalar transport under different stability conditions. *Journal of Advances in Modeling Earth Systems*, *11*(7), 2330-2351.

Maechling, P., Chalupsky, H., Dougherty, M., Deelman, E., Gil, Y., Gullapalli, S., Gupta, V., Kesselman, C., Kim, J., and Mehta, G. (2005). Simplifying construction of complex workflows for non-expert users of the southern california earthquake center community modeling environment. *ACM SIGMOD Record*, *34*(3), 24-30.

Maestre-Valero, J. F., Testi, L., Jiménez-Bello, M. A., Castel, J. R., and Intrigliolo, D. S. (2017). Evapotranspiration and carbon exchange in a citrus orchard using eddy covariance. *Irrigation science*, *35*(5), 397-408.

Maharjan, B., Venterea, R. T., and Rosen, C. (2014). Fertilizer and irrigation management effects on nitrous oxide emissions and nitrate leaching. *Agronomy Journal*, *106*(2), 703-714.

Mahmood, T., Xie, Z., Jia, B., Habib, A., and Mahmood, R. (2019). A Soil Moisture Data Assimilation System for Pakistan Using PODEn4DVar and CLM4. 5. *Journal of Meteorological Research*, *33*(6), 1182-1193.

Malaguti, D., Millard, P., Wendler, R., Hepburn, A., and Tagliavini, M. (2001). Translocation of amino acids in the xylem of apple (Malus domestica Borkh.) trees in spring as a consequence of both N remobilization and root uptake. *Journal of Experimental Botany*, *52*(361), 1665-1671.

Manivasagam, V., and Rozenstein, O. (2020). Practices for upscaling crop simulation models from field scale to large regions. *Computers and Electronics in Agriculture*, *175*, 105554.

Maréchal, J.-C., Selles, A., Dewandel, B., Boisson, A., Perrin, J., and Ahmed, S. (2018). An observatory of groundwater in crystalline rock aquifers exposed to a changing environment: Hyderabad, India. *Vadose Zone Journal*, *17*(1), 1-14.

Marshall-Colon, A., Long, S. P., Allen, D. K., Allen, G., Beard, D. A., Benes, B., Von Caemmerer, S., Christensen, A., Cox, D. J., and Hart, J. C. (2017). Crops in silico: generating virtual crops using an integrative and multi-scale modeling platform. *Frontiers in plant science*, *8*, 786.

Martin-Gorriz, B., González-Real, M. M., Egea, G., and Baille, A. (2020). Ecosystem respiration of old and young irrigated citrus orchards in a semiarid climate. *Agricultural and Forest Meteorology*, *280*, 1-15.

Martin-Gorriz, B., Soto-García, M., and Martínez-Alvarez, V. (2014). Energy and greenhouse-gas emissions in irrigated agriculture of SE (southeast) Spain. Effects of alternative water supply scenarios. *Energy*, *77*, 478-488.

Martínez-Alvarez, V., Maestre-Valero, J. F., González-Ortega, M. J., Gallego-Elvira, B., and Martin-Gorriz, B. (2019). Characterization of the agricultural supply of desalinated seawater in Southeastern Spain. *Water*, *11*(6), 1233.

Martinez, K., Hart, J. K., and Ong, R. (2004). Environmental sensor networks. *Computer*, *37*(8), 50-56.

Mattas, K., Tsakiridou, E., Karelakis, C., Kallirroi, N., Gatsikos, A., and Papadopoulos, I. (2019). PDO Zagora and PGI Kastoria Apples in Greece. *Sustainability of European Food Quality Schemes: Multi-Performance, Structure, and Governance of PDO, PGI, and Organic Agri-Food Systems*, 231-264.

Maurer, E. P., and Hidalgo, H. G. (2008). Utility of daily vs. monthly large-scale climate data: an intercomparison of two statistical downscaling methods. *Hydrology and Earth System Sciences*, *12*(2), 551-563.

McDermid, S., Nocco, M., Lawston-Parker, P., Keune, J., and Yadu Pokhrel, M. J., Jonas Jägermeyr, Luca Brocca, Christian Massari, Andrew D. Jones, Pouya Vahmani, Wim Thiery, Yi Yao, Andrew Bell, Liang Chen, Wouter Dorigo, Naota Hanasaki, Scott Jasechko, Min-Hui Lo, Rezaul Mahmood, Vimal Mishra, Nathaniel D. Mueller, Dev Niyogi, Sam S. Rabin, Lindsey Sloat, Yoshihide Wada, Luca Zappa, Fei Chen, Benjamin I. Cook, Hyungjun Kim, Danica Lombardozzi, Jan Polcher, Dongryeol Ryu, Joe Santanello, Yusuke Satoh, Sonia Seneviratne, Deepti Singh & Tokuta Yokohata (2023). Irrigation in the Earth System. *Nature Reviews Earth & Environment*, *4*, 435-453.

McLaughlin, D., and Kinzelbach, W. (2015). Food security and sustainable resource management. *Water Resources Research*, *51*(7), 4966-4985.

Mendelsohn, R., Kurukulasuriya, P., Basist, A., Kogan, F., and Williams, C. (2007). Climate analysis with satellite versus weather station data. *Climatic change*, *81*(1), 71-83.

Mengen, D., Montzka, C., Jagdhuber, T., Fluhrer, A., Brogi, C., Baum, S., Schüttemeyer, D., Bayat, B., Bogena, H., and Coccia, A. (2021). The SARSense campaign: Air-and space-borne C-and L-band SAR for the analysis of soil and plant parameters in agriculture. *Remote Sensing*, *13*(4), 825.

Met One Instruments Inc. Weather Sensor AIO 2 Sonic. Available online: https://metone.com/products/aio-2-sonic-weather-sensor/ (accessed on 01 November 2023).

METER Group, I. U. (2017). ATMOS41 User Manual. METER Group, Pullman, WA, USA.

METER Group, I. U. METER: Scientific weather station performance data and weather sensor comparisons. Available online: https://www.metergroup.com/environment/articles/weather-sensor-comparison-scientific-weather-station-performance-data-2/ (accessed on 04 December 2020).

Michaelides, S. (2019). *Remote Sensing of Precipitation*, MDPI, 978-3-03921-285-9.

Millán, S., Casadesús, J., Campillo, C., Moñino, M. J., and Prieto, M. H. (2019). Using soil moisture sensors for automated irrigation scheduling in a plum crop. *Water*, *11*(10), 2061.

Millard, P. (1996). Ecophysiology of the internal cycling of nitrogen for tree growth. *Zeitschrift für Pflanzenernährung und Bodenkunde*, *159*(1), 1-10.

Millard, P., Wendler, R., Grassi, G., Grelet, G.-A., and Tagliavini, M. (2006). Translocation of nitrogen in the xylem of field-grown cherry and poplar trees during remobilization. *Tree physiology*, *26*(4), 527-536.

Miller, G., Farahani, H., Hassell, R., Khalilian, A., Adelberg, J., and Wells, C. (2014). Field evaluation and performance of capacitance probes for automated drip irrigation of watermelons. *Agricultural Water Management*, *131*, 124-134.

Miras-Avalos, J. M., Alcobendas, R., Alarcón, J. J., Valsesia, P., Genard, M., and Nicolas, E. (2013). Assessment of the water stress effects on peach fruit quality and size using a fruit tree model, QualiTree. *Agricultural Water Management*, *128*, 1-12.

Mirtl, M. (2018). eLTER, european long-term ecosystem and socio-ecological research infrastructure, h2020. *Impact*, *2018*(8), 30-32.

Mohamed, A. Z., Osroosh, Y., Peters, T. R., Bates, T., Campbell, C. S., and Ferrer-Alegre, F. (2019). Morning crop water stress index as a sensitive indicator of water status in apple trees. *2019 ASABE Annual International Meeting*, 1900577.

Molénat, J., Raclot, D., Zitouna, R., Andrieux, P., Coulouma, G., Feurer, D., Grunberger, O., Lamachère, J.-M., Bailly, J.-S., and Belotti, J.-L. (2018). OMERE: A long-term observatory of soil and water resources, in interaction with agricultural and land management in Mediterranean hilly catchments. *Vadose Zone Journal*, *17*(1), 1-18.

Monselise, S., and Goldschmidt, E. (1982). Alternate bearing in fruit trees. *Horticultural reviews*, *4*(1).

Montagnani, L., Zanotelli, D., Tagliavini, M., and Tomelleri, E. (2018). Timescale effects on the environmental control of carbon and water fluxes of an apple orchard. *Ecology and evolution*, *8*(1), 416-434.

Montanaro, G., Celano, G., Dichio, B., and Xiloyannis, C. (2010). Effects of soil-protecting agricultural practices on soil organic carbon and productivity in fruit tree orchards. *Land Degradation & Development*, *21*(2), 132-138.

Montzka, C., Bogena, H. R., Zreda, M., Monerris, A., Morrison, R., Muddu, S., and Vereecken, H. (2017). Validation of spaceborne and modelled surface soil moisture products with cosmic-ray neutron probes. *Remote Sensing*, *9*(2), 103.

Moretti, M., Van Passel, S., Camposeo, S., Pedrero, F., Dogot, T., Lebailly, P., and Vivaldi, G. (2019). Modelling environmental impacts of treated municipal wastewater reuse for tree crops irrigation in the Mediterranean coastal region. *Science of The Total Environment*, *660*, 1513-1521.

Moriondo, M., and Bindi, M. (2007). Impact of climate change on the phenology of typical Mediterranean crops. *Italian Journal of Agrometeorology*, *3*, 5-12.

Moysiadis, V., Sarigiannidis, P., Vitsas, V., and Khelifi, A. (2021). Smart farming in Europe. *Computer science review*, *39*, 100345.

Mueller, N. D., Gerber, J. S., Johnston, M., Ray, D. K., Ramankutty, N., and Foley, J. A. (2012). Closing yield gaps through nutrient and water management. *Nature*, *490*(7419), 254-257.

Muller, B., and Martre, P. (2019). Plant and crop simulation models: powerful tools to link physiology, genetics, and phenomics, *70*(9), 2339-2344.

Muller, C. L., Chapman, L., Johnston, S., Kidd, C., Illingworth, S., Foody, G., Overeem, A., and Leigh, R. R. (2015). Crowdsourcing for climate and atmospheric sciences: current status and future potential. *International Journal of Climatology*, *35*(11), 3185-3203.

Musacchi, S., and Serra, S. (2018). Apple fruit quality: Overview on pre-harvest factors. *Scientia horticulturae*, *234*, 409-430.

Mutuku, E. A., Roobroeck, D., Vanlauwe, B., Boeckx, P., and Cornelis, W. M. (2020). Maize production under combined Conservation Agriculture and Integrated Soil Fertility Management in the sub-humid and semi-arid regions of Kenya. *Field Crops Research*, *254*, 107833.

Myers, N., Mittermeier, R. A., Mittermeier, C. G., Da Fonseca, G. A., and Kent, J. (2000). Biodiversity hotspots for conservation priorities. *Nature*, *403*(6772), 853-858.

Nasri, B., Fouché, O., and Torri, D. (2015). Coupling published pedotransfer functions for the estimation of bulk density and saturated hydraulic conductivity in stony soils. *Catena*, *131*, 99-108.

Naz, B. S., Kurtz, W., Montzka, C., Sharples, W., Goergen, K., Keune, J., Gao, H., Springer, A., Hendricks Franssen, H.-J., and Kollet, S. (2019). Improving soil moisture and runoff simulations at 3 km over Europe using land surface data assimilation. *Hydrology and Earth System Sciences*, *23*(1), 277-301.

Nešpor, V., and Sevruk, B. (1999). Estimation of wind-induced error of rainfall gauge measurements using a numerical simulation. *Journal of Atmospheric and Oceanic Technology*, *16*(4), 450-464.

Neumann, L. (2020). Improving the apple carbon balance model MaluSim by integrating and testing water deficit and fruit drop effects. M.A. thesis, 147 pp, Hannover: Institutionelles Repositorium der Leibniz Universität Hannover, Hannover, Germany.

Nijland, W., Van der Meijde, M., Addink, E. A., and De Jong, S. M. (2010). Detection of soil moisture and vegetation water abstraction in a Mediterranean natural area using electrical resistivity tomography. *Catena*, *81*(3), 209-216.

Nikolić, Ž., Srzić, V., Lovrinović, I., Perković, T., Šolić, P., and Kekez, T. (2022). Coastal Flooding Assessment Induced by Barometric Pressure, Wind-Generated Waves and Tidal-Induced Oscillations: Kaštela Bay Real-Time Early Warning System Mobile Application. *Applied Sciences*, *12*(24), 12776.

Noilhan, J., and Mahfouf, J.-F. (1996). The ISBA land surface parameterisation scheme. *Global and Planetary change*, *13*(1-4), 145-159.

Nsabagwa, M., Byamukama, M., Kondela, E., and Otim, J. S. (2019). Towards a robust and affordable Automatic Weather Station. *Development Engineering*, *4*, 100040.

NSF (2007). Cyberinfrastructure vision for 21st century discovery. National Science Foundation, Cyberinfrastructure Council.

Ntshidi, Z., Dzikiti, S., Mazvimavi, D., and Mobe, N. (2021). Contribution of understorey vegetation to evapotranspiration partitioning in apple orchards under Mediterranean climatic conditions in South Africa. *Agricultural Water Management*, *245*, 1-11.

O'Connell, M., and Scalisi, A. (2019). Sensing fruit and tree performance under deficit irrigation in 'September Bright' nectarine. In Proceedings of the International Symposium on Precision Management of Orchards and Vineyards 1314.

Obaideen, K., Yousef, B. A., AlMallahi, M. N., Tan, Y. C., Mahmoud, M., Jaber, H., and Ramadan, M. (2022). An overview of smart irrigation systems using IoT. *Energy Nexus*, 100124.

Ochege, F. U., Luo, G., Yuan, X., Owusu, G., Li, C., and Justine, F. M. (2022). Simulated effects of plastic film-mulched soil on surface energy fluxes based on optimized TSEB model in a drip-irrigated cotton field. *Agricultural Water Management*, *262*, 107394.

Okafor, N. U., Alghorani, Y., and Delaney, D. T. (2020). Improving data quality of low-cost IoT sensors in environmental monitoring networks using data fusion and machine learning approach. *ICT Express*, *6*(3), 220-228.

Oliveira, C. M., and Priestley, C. A. (1988). Carbohydrate reserves in deciduous fruit trees. *Horticultural reviews*, *10*, 403-430.

Oorthuis, R., Vaunat, J., Hürlimann, M., Lloret, A., Moya, J., Puig-Polo, C., and Fraccica, A. (2021). Slope orientation and vegetation effects on soil thermo-hydraulic behavior. An experimental study. *Sustainability*, *13*(1), 1-14.

Osborne, T., Gornall, J., Hooker, J., Williams, K., Wiltshire, A., Betts, R., and Wheeler, T. (2014). JULES-crop: a parametrisation of crops in the Joint UK Land Environment Simulator. *Geoscientific Model Development Discussions*, *7*(5), 6773-6809.

Overpeck, J. T., Meehl, G. A., Bony, S., and Easterling, D. R. (2011). Climate data challenges in the 21st century. *Science*, *331*(6018), 700-702.

Ozdogan, M., Rodell, M., Beaudoing, H. K., and Toll, D. L. (2010). Simulating the effects of irrigation over the United States in a land surface model based on satellite-derived agricultural data. *Journal of Hydrometeorology*, *11*(1), 171-184.

Pacific Institute Water Conflict Chronology. Available online: https://www.worldwater.org/water-conflict/ (accessed on 11 October 2023).

Pallas, B., Da Silva, D., Valsesia, P., Yang, W., Guillaume, O., Lauri, P.-E., Vercambre, G., Génard, M., and Costes, E. (2016). Simulation of carbon allocation and organ growth variability in apple tree by connecting architectural and source–sink models. *Annals of Botany*, *118*(2), 317-330.

Panagopoulos, A., Herrmann, F., Pisinaras, V., and Wendland, F. (2018). Impact of climate change on irrigation need and groundwater resources in pinios basin. In Proceedings of the Proceedings, MDPI AG.

Panagoulia, D. (1995). Assessment of daily catchment precipitation in mountainous regions for climate change interpretation. *Hydrological sciences journal*, *40*(3), 331-350.

Pasa, M. d. S., Carra, B., Brighenti, A. F., Pinto, F. A. M. F., Mello-Farias, P. C. d., and Herter, F. G. (2021). Ethephon as a potential tool to manage alternate bearing of 'Fuji' apple trees. *Revista Ceres*, *68*, 180-184.

Payraudeau, S., and van der Werf, H. M. (2005). Environmental impact assessment for a farming region: a review of methods. *Agriculture, Ecosystems & Environment*, *107*(1), 1-19.

Peng, B., Guan, K., Chen, M., Lawrence, D. M., Pokhrel, Y., Suyker, A., Arkebauer, T., and Lu, Y. (2018). Improving maize growth processes in the community land model: Implementation and evaluation. *Agricultural and Forest Meteorology*, *250*, 64-89.

Peng, B., Guan, K., Tang, J., Ainsworth, E. A., Asseng, S., Bernacchi, C. J., Cooper, M., Delucia, E. H., Elliott, J. W., and Ewert, F. (2020). Towards a multiscale crop modelling framework for climate change adaptation assessment. *Nature plants*, *6*(4), 338-348.

Peng, J., Albergel, C., Balenzano, A., Brocca, L., Cartus, O., Cosh, M. H., Crow, W. T., Dabrowska-Zielinska, K., Dadson, S., and Davidson, M. W. (2021). A roadmap for high-resolution satellite soil moisture applications–confronting product characteristics with user requirements. *Remote Sensing of Environment*, *252*, 112162.

Penzel, M., Lakso, A. N., Tsoulias, N., and Zude-Sasse, M. (2020). Carbon consumption of developing fruit and the fruit bearing capacity of individual RoHo 3615 and Pinova apple trees. *Int. Agrophys.*, *34*, 409-423.

Pereira, L., Paredes, P., and Jovanovic, N. (2020). Soil water balance models for determining crop water and irrigation requirements and irrigation scheduling focusing on the FAO56 method and the dual Kc approach. *Agricultural Water Management*, *241*, 106357.

Perkins, J. H. (1990). The Rockefeller Foundation and the green revolution, 1941–1956. *Agriculture and Human Values*, *7*, 6-18.

Pietrosemoli, E., Rainone, M., and Zennaro, M. (2019). On Extending the Wireless Communications Range of Weather Stations using LoRaWAN. *GoodTechs '19: EAI International Conference on Smart Objects and Technologies for Social Good*, 78-83.

Pisinaras, V., Herrmann, F., Panagopoulos, A., Tziritis, E., McNamara, I., and Wendland, F. (2023). Fully Distributed Water Balance Modelling in Large Agricultural Areas—The Pinios River Basin (Greece) Case Study. *Sustainability*, *15*(5), 4343.

Pisinaras, V., Panagopoulos, A., Herrmann, F., Bogena, H. R., Doulgeris, C., Ilias, A., Tziritis, E., and Wendland, F. (2018). Hydrologic and geochemical research at Pinios Hydrologic Observatory: Initial results. *Vadose Zone Journal*, *17*(1), 1-16.

Pisinaras, V., Tsihrintzis, V., Petalas, C., and Ouzounis, K. (2010). Soil salinization in the agricultural lands of Rhodope District, northeastern Greece. *Environmental monitoring and assessment*, *166*, 79-94.

Poesen, J., and Lavee, H. (1994). Rock fragments in top soils: significance and processes. *Catena*, *23*(1-2), 1-28.

Pokhrel, Y., Hanasaki, N., Koirala, S., Cho, J., Yeh, P. J.-F., Kim, H., Kanae, S., and Oki, T. (2012). Incorporating anthropogenic water regulation modules into a land surface model. *Journal of Hydrometeorology*, *13*(1), 255-269.

Pokhrel, Y., Koirala, S., Yeh, P. J. F., Hanasaki, N., Longuevergne, L., Kanae, S., and Oki, T. (2015). Incorporation of groundwater pumping in a global Land Surface Model with the representation of human impacts. *Water Resources Research*, *51*(1), 78-96.

Pokhrel, Y. N., Hanasaki, N., Wada, Y., and Kim, H. (2016). Recent progresses in incorporating human land–water management into global land surface models toward their integration into Earth system models. *Wiley Interdisciplinary Reviews: Water*, *3*(4), 548-574.

Pongratz, J., Dolman, H., Don, A., Erb, K. H., Fuchs, R., Herold, M., Jones, C., Kuemmerle, T., Luyssaert, S., and Meyfroidt, P. (2018). Models meet data: Challenges and opportunities in implementing land management in Earth system models. *Global change biology*, *24*(4), 1470-1487.

Portmann, F. T., Siebert, S., and Döll, P. (2010). MIRCA2000—Global monthly irrigated and rainfed crop areas around the year 2000: A new high-resolution data set for agricultural and hydrological modeling. *Global Biogeochemical Cycles*, *24*(1).

Prentice, I. C., Liang, X., Medlyn, B. E., and Wang, Y.-P. (2015). Reliable, robust and realistic: the three R's of next-generation land-surface modelling. *Atmospheric Chemistry and Physics*, *15*(10), 5987-6005.

Prusinkiewicz, P., and Runions, A. (2012). Computational models of plant development and form. *New phytologist*, *193*(3), 549-569.

Rabin, S. S., Sacks, W. J., Lombardozzi, D. L., Xia, L., and Robock, A. (2023). Observation-based sowing dates and cultivars significantly affect yield and irrigation for some crops in the Community Land Model (CLM5). *Geoscientific Model Development Discussions*, *2023*, 1-29.

Rai, A. C., Kumar, P., Pilla, F., Skouloudis, A. N., Di Sabatino, S., Ratti, C., Yasar, A., and Rickerby, D. (2017). End-user perspective of low-cost sensors for outdoor air pollution monitoring. *Science of The Total Environment*, *607*, 691-705.

Ramankutty, N., Mehrabi, Z., Waha, K., Jarvis, L., Kremen, C., Herrero, M., and Rieseberg, L. H. (2018). Trends in global agricultural land use: implications for environmental health and food security. *Annual review of plant biology*, *69*, 789-815.

Rappin, E., Mahmood, R., Nair, U., and Pielke Sr, R. (2022). Land–atmosphere interactions during GRAINEX: planetary boundary layer evolution in the presence of irrigation. *Journal of Hydrometeorology*, *23*(9), 1401-1417.

Reichle, R. H., Koster, R. D., Liu, P., Mahanama, S. P., Njoku, E. G., and Owe, M. (2007). Comparison and assimilation of global soil moisture retrievals from the Advanced Microwave Scanning Radiometer for the Earth Observing System (AMSR-E) and the Scanning Multichannel Microwave Radiometer (SMMR). *Journal of Geophysical Research: Atmospheres*, *112*(D9).

Reichstein, M., Falge, E., Baldocchi, D., Papale, D., Aubinet, M., Berbigier, P., Bernhofer, C., Buchmann, N., Gilmanov, T., and Granier, A. (2005). On the separation of net ecosystem exchange into assimilation and ecosystem respiration: review and improved algorithm. *Global change biology*, *11*(9), 1424-1439.

Reis, S., Seto, E., Northcross, A., Quinn, N. W., Convertino, M., Jones, R. L., Maier, H. R., Schlink, U., Steinle, S., and Vieno, M. (2015). Integrating modelling and smart sensors for environmental and human health. *Environmental Modelling & Software*, *74*, 238-246.

Reyes, F., DeJong, T., Franceschi, P., Tagliavini, M., and Gianelle, D. (2016). Maximum growth potential and periods of resource limitation in apple tree. *Frontiers in plant science*, *7*, 1-12.

Ritchie, J., and Otter, S. (1985). *Description and performance of CERES wheat: A user-oriented wheat yield model*, 159-175 pp., Natl Tech Info Serv, Springfield, Missouri, USA.

Romano, N., Nasta, P., Bogena, H., De Vita, P., Stellato, L., and Vereecken, H. (2018). Monitoring hydrological processes for land and water resources management in a Mediterranean ecosystem: The Alento River Catchment Observatory. *Vadose Zone Journal*, *17*(1), 1-12.

Rosa, L. (2022). Adapting agriculture to climate change via sustainable irrigation: Biophysical potentials and feedbacks. *Environmental Research Letters*, *17*(6), 063008.

Ruiz, G., and Bandera, C. (2017). Validation of Calibrated Energy Models: Common Errors. *Energies*, *10*(10), 1587.

Sabatini, F. (2017). Setting up and Managing Automatic Weather Stations for Remote Sites Monitoring: From Niger to Nepal. In *Renewing Local Planning to Face Climate Change in the Tropics*, edited by Tiepolo, M., Pezzoli, A. and Tarchiani, V., pp. 21-39, Green Energy and Technology; Springer International Publishing, Cham, Switzerland, 978-3-319-59096-7.

Sacks, W. J., Cook, B. I., Buenning, N., Levis, S., and Helkowski, J. H. (2009). Effects of global irrigation on the near-surface climate. *Climate Dynamics*, *33*, 159-175.

Saini, H., Thakur, A., Ahuja, S., Sabharwal, N., and Kumar, N. (2016). Arduino based automatic wireless weather station with remote graphical application and alerts. *2016 3rd International Conference on Signal Processing and Integrated Networks (SPIN)*, 605-609.

Sanchez, E. E., Khemira, H., Sugar, D., and Righetti, T. L. (1995). Nitrogen management in orchards. In *Nitrogen Fertilization in the Environment*, edited, Marcel Dekker, Inc., New York, U.S.

Scandellari, F., Caruso, G., Liguori, G., Meggio, F., Palese, A. M., Zanotelli, D., Celano, G., Gucci, R., Inglese, P., and Pitacco, A. (2016). A survey of carbon sequestration potential of orchards and vineyards in Italy. *European Journal of Horticultural Science*, *81*, 106-114.

Scanlon, B. R., Faunt, C. C., Longuevergne, L., Reedy, R. C., Alley, W. M., McGuire, V. L., and McMahon, P. B. (2012). Groundwater depletion and sustainability of irrigation in the US High Plains and Central Valley. *Proceedings of the National Academy of Sciences*, *109*(24), 9320-9325.

Schaphoff, S., von Bloh, W., Rammig, A., Thonicke, K., Biemans, H., Forkel, M., Gerten, D., Heinke, J., Jägermeyr, J., and Knauer, J. (2018). LPJmL4–a dynamic global vegetation model with managed land–Part 1: Model description. *Geoscientific Model Development*, *11*(4), 1343-1375.

Schmidt, M., Reichenau, T. G., Fiener, P., and Schneider, K. (2012). The carbon budget of a winter wheat field: An eddy covariance analysis of seasonal and inter-annual variability. *Agricultural and Forest Meteorology*, *165*, 114-126.

Schoof, J. T. (2013). Statistical downscaling in climatology. *Geography Compass*, *7*(4), 249-265.

Schwamback, D., Persson, M., Berndtsson, R., Bertotto, L. E., Kobayashi, A. N. A., and Wendland, E. C. (2023). Automated Low-Cost Soil Moisture Sensors: Trade-Off between Cost and Accuracy. *Sensors*, *23*(5), 2451.

Šećerov, I. B., Savić, S. M., Milošević, D. D., Arsenović, D. M., Dolinaj, D. M., and Popov, S. B. (2019). Progressing urban climate research using a high-density monitoring network system. *Environmental monitoring and assessment*, *191*, 1-19.

Sedlar, J., and Hock, R. (2009). Testing longwave radiation parameterizations under clear and overcast skies at Storglaciären, Sweden. *The Cryosphere*, *3*(1), 75-84.

Segovia-Cardozo, D. A., Franco, L., and Provenzano, G. (2022). Detecting crop water requirement indicators in irrigated agroecosystems from soil water content profiles: An application for a citrus orchard. *Science of The Total Environment*, *806*.

Semple, E. C. (1929). Irrigation and reclamation in the ancient Mediterranean region. *Annals of the Association of American Geographers*, *19*(3), 111-148.

Sevruk, B., and Klemm, S. (1989). *Catalogue of national standard precipitation gauges*, 11-17 pp., World Meteorological Organization.

Shams, A. K., and Muhammad, N. S. (2022). Toward sustainable water resources management: critical assessment on the implementation of integrated water resources management and water–energy–food nexus in Afghanistan. *Water Policy*, *24*(1), 1-18.

Sharma, S., Rana, V. S., Prasad, H., Lakra, J., and Sharma, U. (2021). Appraisal of carbon capture, storage, and utilization through fruit crops. *Frontiers in Environmental Science*, *9*, 700768.

Sheets, K. R., and Hendrickx, J. M. (1995). Noninvasive soil water content measurement using electromagnetic induction. *Water Resources Research*, *31*(10), 2401-2409.

Sheng, M., Liu, J., Zhu, A.-X., Rossiter, D. G., Zhu, L., and Peng, G. (2018). Evaluation of CLM-Crop for maize growth simulation over Northeast China. *Ecological Modelling*, *377*, 26-34.

Sherman, W., and Beckman, T. (2002). Climatic adaptation in fruit crops. In Proceedings of the XXVI International Horticultural Congress: Genetics and Breeding of Tree Fruits and Nuts 622.

Shrestha, P., Kurtz, W., Vogel, G., Schulz, J. P., Sulis, M., Hendricks Franssen, H. J., Kollet, S., and Simmer, C. (2018). Connection between root zone soil moisture and surface energy flux partitioning using modeling, observations, and data assimilation for a temperate grassland site in Germany. *Journal of Geophysical Research: Biogeosciences*, *123*(9), 2839-2862.

Sieck, L. C., Burges, S. J., and Steiner, M. (2007). Challenges in obtaining reliable measurements of point rainfall. *Water Resources Research*, *43*(1), W01420.

Skuras, D., and Psaltopoulos, D. (2012). A broad overview of the main problems derived from climate change that will affect agricultural production in the Mediterranean area. In Proceedings of the Joint FAO/OECD Workshop: Building resilience for adaptation to climate change in the agriculture sector, FAO, Rome, Italy.

Smith, P., De Noblet-Ducoudré, N., Ciais, P., Peylin, P., Viovy, N., Meurdesoif, Y., and Bondeau, A. (2010). European-wide simulations of croplands using an improved terrestrial biosphere model: Phenology and productivity. *Journal of Geophysical Research: Biogeosciences*, *115*(G1).

Song, J., Miller, G. R., Cahill, A. T., Aparecido, L. M. T., and Moore, G. W. (2020). Modeling land surface processes over a mountainous rainforest in Costa Rica using CLM4. 5 and CLM5. *Geoscientific Model Development*, *13*(11), 5147-5173.

Steduto, P., Hsiao, T. C., Raes, D., and Fereres, E. (2009). AquaCrop—The FAO crop model to simulate yield response to water: I. Concepts and underlying principles. *Agronomy Journal*, *101*(3), 426-437.

Stehfest, E., Heistermann, M., Priess, J. A., Ojima, D. S., and Alcamo, J. (2007). Simulation of global crop production with the ecosystem model DayCent. *Ecological Modelling*, *209*(2-4), 203-219.

Stevens, D., Miranda, P. M., Orth, R., Boussetta, S., Balsamo, G., and Dutra, E. (2020). Sensitivity of surface fluxes in the ECMWF land surface model to the remotely sensed leaf area index and root distribution: Evaluation with tower flux data. *Atmosphere*, *11*(12), 1362.

Steyn, D., Oke, T., Hay, J., and Knox, J. (1981). On scales in meteorology and climatology. *Climatological Bulletin*, *39*, 1-8.

Stöckle, C. O., Donatelli, M., and Nelson, R. (2003). CropSyst, a cropping systems simulation model. *European Journal of Agronomy*, *18*(3-4), 289-307.

Strebel, L., Bogena, H. R., Vereecken, H., and Hendricks Franssen, H.-J. (2022). Coupling the Community Land Model version 5.0 to the parallel data assimilation framework PDAF: description and applications. *Geoscientific Model Development*, *15*(2), 395-411.

Sun, Q., Miao, C., Duan, Q., Ashouri, H., Sorooshian, S., and Hsu, K. L. (2018). A review of global precipitation data sets: Data sources, estimation, and intercomparisons. *Reviews of Geophysics*, *56*(1), 79-107.

Sweetlove, L. J., Williams, T. C., Cheung, C. M., and Ratcliffe, R. G. (2013). Modelling metabolic CO2 evolution–a fresh perspective on respiration. *Plant, cell & environment*, *36*(9), 1631-1640.

TAHMO Trans-African Hydro-Meteorological Observatory. Available online: https://tahmo.org/ (accessed on 01 November 2020).

Tanny, J., and Cohen, S. (2003). The effect of a small shade net on the properties of wind and selected boundary layer parameters above and within a citrus orchard. *Biosystems Engineering*, *84*(1), 57-67.

Tavakolifar, H., Shahghasemi, E., and Nazif, S. (2017). Evaluation of climate change impacts on extreme rainfall events characteristics using a synoptic weather typing-based daily precipitation downscaling model. *Journal of Water and Climate Change*, *8*(3), 388-411.

Tenzin, S., Siyang, S., Pobkrut, T., and Kerdcharoen, T. (2017). Low cost weather station for climate-smart agriculture. *2017 9th International Conference on Knowledge and Smart Technology (KST)*, 172-177.

TERENO TERrestrial ENvironmental Observatories. Available online: https://www.tereno.net/ (accessed on 01 November 2020).

Thomas, B. F., and Famiglietti, J. S. (2019). Identifying climate-induced groundwater depletion in GRACE observations. *Scientific reports*, *9*(1), 4124.

Thornton, P. E., Law, B. E., Gholz, H. L., Clark, K. L., Falge, E., Ellsworth, D. S., Goldstein, A. H., Monson, R. K., Hollinger, D., and Falk, M. (2002). Modeling and measuring the effects of disturbance history and climate on carbon and water budgets in evergreen needleleaf forests. *Agricultural and Forest Meteorology*, *113*(1-4), 185-222.

Tilse, M., Stockmann, U., and Filippi, P. (2023). Proximal soil sensing in the field. In *Encyclopedia of Soils in the Environment (Second Edition)*, edited by Michael J. Goss, M. O., Academic Press, 9780323951333.

Tomè, E., Ventura, M., Folegot, S., Zanotelli, D., Montagnani, L., Mimmo, T., Tonon, G., Tagliavini, M., and Scandellari, F. (2016). Mycorrhizal contribution to soil respiration in an apple orchard. *Applied Soil Ecology*, *101*, 165-173.

Tomlinson, C. J., Chapman, L., Thornes, J. E., and Baker, C. (2011). Remote sensing land surface temperature for meteorology and climatology: A review. *Meteorological Applications*, *18*(3), 296-306.

Tomlinson, C. J., Prieto-Lopez, T., Bassett, R., Chapman, L., Cai, X.-M., Thornes, J. E., and Baker, C. J. (2013). Showcasing urban heat island work in Birmingham - measuring, monitoring, modelling and more. *Weather*, *68*(2), 44-49.

Touil, S., Richa, A., Fizir, M., Argente Garcia, J. E., and Skarmeta Gomez, A. F. (2022). A review on smart irrigation management strategies and their effect on water savings and crop yield. *Irrigation and Drainage*, *71*(5), 1396-1416.

Tramblay, Y., Llasat, M. C., Randin, C., and Coppola, E. (2020). Climate change impacts on water resources in the Mediterranean. *Regional environmental change*, *20*(3), 83.

Tromp, J. (1983). Nutrient reserves in roots of fruit trees, in particular carbohydrates and nitrogen. *Plant and Soil*, *71*(1), 401-413.

Tsai, W.-P., Feng, D., Pan, M., Beck, H., Lawson, K., Yang, Y., Liu, J., and Shen, C. (2021). From calibration to parameter learning: Harnessing the scaling effects of big data in geoscientific modeling. *Nature communications*, *12*(1), 5988.

Tuel, A., and Eltahir, E. A. (2020). Why is the Mediterranean a climate change hot spot? *Journal of Climate*, *33*(14), 5829-5843.

Tuinenburg, O., Hutjes, R., Jacobs, C., and Kabat, P. (2011). Diagnosis of local land–atmosphere feedbacks in India. *Journal of Climate*, *24*(1), 251-266.

Turrini, A., Caruso, G., Avio, L., Gennai, C., Palla, M., Agnolucci, M., Tomei, P. E., Giovannetti, M., and Gucci, R. (2017). Protective green cover enhances soil respiration and native mycorrhizal potential compared with soil tillage in a high-density olive orchard in a long term study. *Applied Soil Ecology*, *116*, 70-78.

Valancogne, C., Dayau, S., Pieri, P., Ferreira, M. I., Silvestre, J., and Angelocci, L. (1999). Influence of orchard and vineyard characteristics on maximal plant transpiration. In Proceedings of the 3. International symposium on irrigation of Horticultural crops, ISHS, Lisbonne, Portugal.

Valente, A., Silva, S., Duarte, D., Cabral Pinto, F., and Soares, S. (2020). Low-Cost LoRaWAN Node for Agro-Intelligence IoT. *Electronics*, *9*(6), 987.

van de Giesen, N., Hut, R., and Selker, J. (2014). The Trans-African Hydro-Meteorological Observatory (TAHMO): The Trans-African Hydro-Meteorological Observatory. *Wiley Interdisciplinary Reviews: Water*, *1*(4), 341-348.

Van Dijk, M., Morley, T., Rau, M. L., and Saghai, Y. (2021). A meta-analysis of projected global food demand and population at risk of hunger for the period 2010–2050. *Nature Food*, *2*(7), 494-501.

Van Laar, H., Goudriaan, J. v., and Van Keulen, H. (1997). SUCROS97: Simulation of crop growth for potential and water-limited production situations. As applied to spring wheat. (Quantitative Approaches in Systems Analysis; No. 14). AB-DLO, TPE.

Van Vliet, M. T., Jones, E. R., Flörke, M., Franssen, W. H., Hanasaki, N., Wada, Y., and Yearsley, J. R. (2021). Global water scarcity including surface water quality and expansions of clean water technologies. *Environmental Research Letters*, *16*(2), 024020.

Van Vuuren, D. P., Bayer, L. B., Chuwah, C., Ganzeveld, L., Hazeleger, W., van den Hurk, B., Van Noije, T., O'Neill, B., and Strengers, B. J. (2012). A comprehensive view on climate change: coupling of earth system and integrated assessment models. *Environmental Research Letters*, *7*(2), 024012.

Vanderborght, J., Couvreur, V., Meunier, F., Schnepf, A., Vereecken, H., Bouda, M., and Javaux, M. (2021). From hydraulic root architecture models to macroscopic representations of root hydraulics in soil water flow and land surface models. *Hydrology and Earth System Sciences*, *25*(9), 4835-4860.

Venäläinen, A., and Heikinheimo, M. (2002). Meteorological data for agricultural applications. *Physics and Chemistry of the Earth, Parts A/B/C*, *27*(23-24), 1045-1050.

Vereecken, H., Amelung, W., Bauke, S. L., Bogena, H., Brüggemann, N., Montzka, C., Vanderborght, J., Bechtold, M., Blöschl, G., and Carminati, A. (2022). Soil hydrology in the Earth system. *Nature Reviews Earth & Environment*, *3*(9), 573-587.

Vereecken, H., Huisman, J., Bogena, H., Vanderborght, J., Vrugt, J., and Hopmans, J. (2008). On the value of soil moisture measurements in vadose zone hydrology: A review. *Water Resources Research*, *44*(4).

Vereecken, H., Pachepsky, Y., Bogena, H., and Montzka, C. (2019). Upscaling issues in ecohydrological observations. *Observation and Measurement of Ecohydrological Processes, edited by: Li, X. and Vereecken, H., Springer, Berlin, Heidelberg*, 435-454.

Vereecken, H., Schnepf, A., Hopmans, J. W., Javaux, M., Or, D., Roose, T., Vanderborght, J., Young, M., Amelung, W., and Aitkenhead, M. (2016). Modeling soil processes: Review, key challenges, and new perspectives. *Vadose Zone Journal*, *15*(5).

Verhoef, A., and Egea, G. (2014). Modeling plant transpiration under limited soil water: Comparison of different plant and soil hydraulic parameterizations and preliminary implications for their use in land surface models. *Agricultural and Forest Meteorology*, *191*, 22-32.

Vico, G., and Brunsell, N. A. (2018). Tradeoffs between water requirements and yield stability in annual vs. perennial crops. *Advances in water resources*, *112*, 189-202.

Viovy, N. (2018). *CRUNCEP Version 7 - Atmospheric Forcing Data for the Community Land Model* [Dataset]. Research Data Archive at the National Center for Atmospheric Research, Computational and Information Systems Laboratory.

von Hebel, C., Reynaert, S., Pauly, K., Janssens, P., Piccard, I., Vanderborght, J., van der Kruk, J., Vereecken, H., and Garré, S. (2021). Toward high-resolution agronomic soil information and management zones delineated by ground-based electromagnetic induction and aerial drone data. *Vadose Zone Journal*, *20*(4), e20099.

Wada, Y., Van Beek, L. P., Van Kempen, C. M., Reckman, J. W., Vasak, S., and Bierkens, M. F. (2010). Global depletion of groundwater resources. *Geophysical Research Letters*, *37*(20).

Walter, A., Finger, R., Huber, R., and Buchmann, N. (2017). Smart farming is key to developing sustainable agriculture. *Proceedings of the National Academy of Sciences*, *114*(24), 6148-6150.

Walther, B. A., and Moore, J. L. (2005). The concepts of bias, precision and accuracy, and their use in testing the performance of species richness estimators, with a literature review of estimator performance. *Ecography*, *28*(6), 815-829.

Wang, Y., Long, S. P., and Zhu, X.-G. (2014). Elements required for an efficient NADP-malic enzyme type C4 photosynthesis. *Plant Physiology*, *164*(4), 2231-2246.

Warne, J. (2017). Guidelines on economical alternative AWS. In Proceedings of the Commission for Instruments and Methods of Observation: Joint Session of the Expert Team on Operational In Situ Technologies (ET-OIST) and the Expert Team on Developments in In Situ Technologies (ET-DIST), WMO, Geneva, Switzerland.

Watthanawisuth, N., Tuantranont, A., and Kerdcharoen, T. (2009). Microclimate real-time monitoring based on ZigBee sensor network. *2009 IEEE Sensors*, 1814-1818.

Wentworth, C. K. (1922). A scale of grade and class terms for clastic sediments. *The journal of geology*, *30*(5), 377-392.

Western, A. W., Grayson, R. B., and Blöschl, G. (2002). Scaling of soil moisture: A hydrologic perspective. *Annual review of earth and planetary sciences*, *30*(1), 149-180.

Wheaton, T., Castle, W., Whitney, J., Tucker, D., and Muraro, R. (1990). A high density citrus planting. In Proceedings of the Florida State Horticultural Society, Florida State Horticultural Society, Lake Alfred, etc, Florida, U.S.

White, J. W., Hoogenboom, G., Kimball, B. A., and Wall, G. W. (2011). Methodologies for simulating impacts of climate change on crop production. *Field Crops Research*, *124*(3), 357-368.

Wiebe, K. (2001). The Nile River: potential for conflict and cooperation in the face of water degradation. *Natural Resources Journal*, 731-754.

Wilkerson, G., Jones, J., Boote, K., Ingram, K., and Mishoe, J. (1983). Modeling soybean growth for crop management. *Transactions of the ASAE*, *26*(1), 63-0073.

Williams, J., Jones, C., Kiniry, J., and Spanel, D. A. (1989). The EPIC crop growth model. *Transactions of the ASAE*, *32*(2), 497-0511.

WMO (2008). Guide to Instruments and Methods of Observation. *978-92-63-10008-5*, 65-90 pp, WMO, Geneva, Switzerland.

WMO Progress/Activity reports presented at CBS-XIV (unedited). Available online: https://library.wmo.int/doc_num.php?explnum_id=5515 (accessed on 15 November 2020).

WMO The Global observing system for climate: Implementation needs. Available online: https://library.wmo.int/doc_num.php?explnum_id=3417 (accessed on 10 November 2020).

World Bank Agriculture, forestry, and fishing, value added (% of GDP). Available online: https://datacatalog.worldbank.org/search/dataset/0037712/World-Development-Indicators (accessed on 29 May 2023).

Wu, T., Wang, Y., Yu, C., Chiarawipa, R., Zhang, X., Han, Z., and Wu, L. (2012). Carbon sequestration by fruit trees-Chinese apple orchards as an example. *PloS one*, *7*(6), 1-13.

Wu, X., Vuichard, N., Ciais, P., Viovy, N., de Noblet-Ducoudré, N., Wang, X., Magliulo, V., Wattenbach, M., Vitale, L., and Di Tommasi, P. (2016). ORCHIDEE-CROP (v0), a new process-based agro-land surface model: model description and evaluation over Europe. *Geoscientific Model Development*, *9*(2), 857-873.

Wünsche, J. N., and Lakso, A. N. (2000). Apple tree physiology-implications for orchard and tree management. *Compact Fruit Tree*, *33*(3), 82-88.

WWAP (2012). The United Nations world water development report 4: knowledge base. UNESCO, Paris, France.

WWAP (2019). Leaving No One Behind: The United Nations World Water Development Report. UNESCO, Paris, France.

Xia, Q., Liu, P., Fan, Y., Cheng, L., An, R., Xie, K., and Zhou, L. (2022). Representing Irrigation Processes in the Land Surface-Hydrological Model and a Case Study in the Yangtze River Basin, China. *Journal of Advances in Modeling Earth Systems*, *14*(7), e2021MS002653.

Xie, W., Kimura, M., Iida, T., and Kubo, N. (2020). Simulation of water temperature in paddy fields by a heat balance model using plant growth status parameter with interpolated weather data from weather stations. *Paddy and Water Environment*.

Xu, X., Huang, G., Sun, C., Pereira, L. S., Ramos, T. B., Huang, Q., and Hao, Y. (2013). Assessing the effects of water table depth on water use, soil salinity and wheat yield: Searching for a target depth for irrigated areas in the upper Yellow River basin. *Agricultural Water Management*, *125*, 46-60.

Xu, X., Jiang, Y., Liu, M., Huang, Q., and Huang, G. (2019). Modeling and assessing agro-hydrological processes and irrigation water saving in the middle Heihe River basin. *Agricultural Water Management*, *211*, 152-164.

Yang, Z., Qian, Y., Liu, Y., Berg, L. K., Hu, H., Dominguez, F., Yang, B., Feng, Z., Gustafson Jr, W. I., and Huang, M. (2019). Irrigation impact on water and energy cycle during dry years over the United States using convection-permitting WRF and a dynamical recycling model. *Journal of Geophysical Research: Atmospheres*, *124*(21), 11220-11241.

Yao, Y., Vanderkelen, I., Lombardozzi, D., Swenson, S., Lawrence, D., Jägermeyr, J., Grant, L., and Thiery, W. (2022). Implementation and evaluation of irrigation techniques in the Community Land Model. *Journal of Advances in Modeling Earth Systems*, *14*(12).

Yasin, G., Farrakh Nawaz, M., Zubair, M., Qadir, I., Saleem, A. R., Ijaz, M., Gul, S., Amjad Bashir, M., Rehim, A., and Rahman, S. U. (2021). Assessing the Contribution of Citrus Orchards in Climate Change Mitigation through Carbon Sequestration in Sargodha District, Pakistan. *Sustainability*, *13*(22), 1-10.

Yick, J., Mukherjee, B., and Ghosal, D. (2008). Wireless sensor network survey. *Computer Networks*, *52*(12), 2292-2330.

Yin, Z., Wang, X., Ottlé, C., Zhou, F., Guimberteau, M., Polcher, J., Peng, S., Piao, S., Li, L., and Bo, Y. (2020). Improvement of the irrigation scheme in the ORCHIDEE land surface model and impacts of irrigation on regional water budgets over China. *Journal of Advances in Modeling Earth Systems*, *12*(4), e2019MS001770.

Yuan, X., Bai, J., Li, L., Kurban, A., and De Maeyer, P. (2019). Modeling the effects of drip irrigation under plastic mulch on vapor and energy fluxes in oasis agroecosystems, Xinjiang, China. *Agricultural and Forest Meteorology*, *265*, 435-442.

Zagana, E., Kuells, C., Udluft, P., and Constantinou, C. (2007). Methods of groundwater recharge estimation in eastern Mediterranean—a water balance model application in Greece, Cyprus and Jordan. *Hydrological Processes: An International Journal*, *21*(18), 2405-2414.

Zagaria, C., Schulp, C. J., Malek, Ž., and Verburg, P. H. (2023). Potential for land and water management adaptations in Mediterranean croplands under climate change. *Agricultural Systems*, *205*, 103586.

Zalidis, G., Stamatiadis, S., Takavakoglou, V., Eskridge, K., and Misopolinos, N. (2002). Impacts of agricultural practices on soil and water quality in the Mediterranean region and proposed assessment methodology. *Agriculture, Ecosystems & Environment*, *88*(2), 137-146.

Zanchi, C., and Cecchi, S. (2010). Soil salinisation in the grosseto plain (Maremma, Italy): An environmental and socio-economic analysis of the impact on the agro-ecosystem. In *Coastal Water Bodies: Nature and Culture Conflicts in the Mediterranean*, edited by Scapini, F., Ciampi, G., pp. 79-90, Springer, 9048188539.

Zanotelli, D., Montagnani, L., Andreotti, C., and Tagliavini, M. (2019). Evapotranspiration and crop coefficient patterns of an apple orchard in a sub-humid environment. *Agricultural Water Management*, *226*, 1-11.

Zanotelli, D., Montagnani, L., Manca, G., Scandellari, F., and Tagliavini, M. (2015). Net ecosystem carbon balance of an apple orchard. *European Journal of Agronomy*, *63*, 97-104.

Zanotelli, D., Montagnani, L., Manca, G., and Tagliavini, M. (2013). Net primary productivity, allocation pattern and carbon use efficiency in an apple orchard assessed by integrating eddy covariance, biometric and continuous soil chamber measurements. *Biogeosciences*, *10*(5), 3089-3108.

Zappa, L., Schlaffer, S., Bauer-Marschallinger, B., Nendel, C., Zimmerman, B., and Dorigo, W. (2021). Detection and quantification of irrigation water amounts at 500 m using sentinel-1 surface soil moisture. *Remote Sensing*, *13*(9), 1727.

Zavalloni, C., Andresen, J. A., and Flore, J. (2006). Phenological Models of Flower Bud Stages and Fruit Growth ofMontmorency'Sour Cherry Based on Growing Degree-day Accumulation. *Journal of the American Society for Horticultural Science*, *131*(5), 601-607.

Zehe, E., Becker, R., Bárdossy, A., and Plate, E. (2005). Uncertainty of simulated catchment runoff response in the presence of threshold processes: Role of initial soil moisture and precipitation. *Journal of Hydrology*, *315*(1-4), 183-202.

Zeng, X. (2001). Global vegetation root distribution for land modeling. *Journal of Hydrometeorology*, *2*(5), 525-530.

Zeng, Y., Xie, Z., and Liu, S. (2017). Seasonal effects of irrigation on land–atmosphere latent heat, sensible heat, and carbon fluxes in semiarid basin. *Earth System Dynamics*, *8*(1), 113-127.

Zhang, Y., Hou, K., Qian, H., Gao, Y., Fang, Y., Xiao, S., Tang, S., Zhang, Q., Qu, W., and Ren, W. (2022). Characterization of soil salinization and its driving factors in a typical irrigation area of Northwest China. *Science of The Total Environment*, *837*, 155808.

Zhang, Z., Barlage, M., Chen, F., Li, Y., Helgason, W., Xu, X., Liu, X., and Li, Z. (2020). Joint modeling of crop and irrigation in the central United States using the Noah-MP land surface model. *Journal of Advances in Modeling Earth Systems*, *12*(7), e2020MS002159.

Zhou, J., Cheng, G., Li, X., Hu, B. X., and Wang, G. (2012). Numerical modeling of wheat irrigation using coupled HYDRUS and WOFOST models. *Soil Science Society of America Journal*, *76*(2), 648-662.

Zhu, B., Huang, M., Cheng, Y., Xie, X., Liu, Y., Zhang, X., Bisht, G., Chen, X., Missik, J., and Liu, H. (2020). Effects of irrigation on water, carbon, and nitrogen budgets in a semiarid watershed in the Pacific northwest: A modeling study. *Journal of Advances in Modeling Earth Systems*, *12*(9), e2019MS001953.

Zotarelli, L., Dukes, M., Scholberg, J., Femminella, K., and Munoz-Carpena, R. (2011). Irrigation scheduling for green bell peppers using capacitance soil moisture sensors. *Journal of Irrigation and Drainage Engineering*, *137*(2), 73-81.

Zreda, M., Desilets, D., Ferré, T. P. A., and Scott, R. L. (2008). Measuring soil moisture content non-invasively at intermediate spatial scale using cosmic-ray neutrons. *Geophysical Research Letters*, *35*(21), L21402.